UNIVERSITY OF CAPE TOWN

DOCTORAL DISSERTATION

---

# An assessment of four decades of wave power variability - a critical requirement for coastal resilience.

---


*Author:*

**Candice Hall**

*Supervisors:*

**Prof. Isabelle Ansorge**

**Dr. Robert E. Jensen**

**Dr. David W. Wang**


*A dissertation submitted in fulfilment of the requirements*
*for the degree of Doctor of Philosophy*
*in the*

Department of Oceanography

# Declaration of Authorship

I, Candice Hall, declare that this dissertation titled, **An assessment of four decades of wave power variability - a critical requirement for coastal resilience**, and the work presented in it is my own. I confirm that:

- This work was done wholly while in candidature for a research degree at the University of Cape Town.
- Where I have consulted the published work of others, this is clearly attributed.
- I have acknowledged all main sources of assistance.
- Where the dissertation is based on work done by myself in conjunction with others, I have made clear exactly who contributed what portion of the work.
- I confirm that I have been granted written permission by the Dean of the Science Faculty, who is head of the University of Cape Town Doctoral Degrees Board, to include the following publications in my PhD dissertation, and where co-authorships are involved, my co-authors have agreed that I may include the publications.

  **Chapter 2: Hall, C., Jensen, R.E. & Wang, D.W. 2022**. Performance evaluation of the newly operational NDBC 2.1-m hull. *Journal of Atmospheric and Oceanic Technology*. https://doi.org/10.1175/JTECH-D-21-0172.1

  **Contributions:**

  - Study idea: C.H. (90 %), R.E.J., D.W.W.
  - Study design: C.H. (90 %), R.E.J., D.W.W.
  - Data collection: C.H. (100 %)
  - Data analysis: C.H. (100 %)
  - Manuscript writing: C.H. (100 %)
  - Manuscript revision: C.H. (90 %), R.E.J., D.W.W.

**Chapter 3: Hall, C. & Jensen, R.E. 2022.** United States Army Corps of Engineers Coastal and Hydraulics Laboratory Quality Controlled, Consistent Measurement Archive. *Scientific Data*. http://dx.doi.org/10.1038/s41597-022-01344-z

**Contributions:**

- Study idea: C.H. (90 %), R.E.J.
- Study design: C.H. (95 %), R.E.J.
- Data collection: C.H. (100 %)
- Data analysis: C.H. (100 %)
- Manuscript writing: C.H. (100 %)
- Manuscript revision: C.H. (95 %), R.E.J.

**Chapter 3 & 4: Hall, C., Jensen, R.E., & Wang, D.W. 2022**. Wave Power Trends along the U.S. Coastline: In situ Measurements and Model Hindcasts Estimates. *Ocean Dynamics*. https://doi.org/10.1007/s10236-022-01515-x

**Contributions:**

- Study idea: C.H. (95 %), R.E.J., D.W.W.
- Study design: C.H. (95 %), R.E.J., D.W.W.
- Data collection: C.H. (100 %)
- Data analysis: C.H. (100 %)
- Manuscript writing: C.H. (100 %)
- Manuscript revision: C.H. (95 %), R.E.J., D.W.W.

Signed: Signed by candidate

Date: 10 October 2022

*For Mom*

# Abstract

**An assessment of four decades of wave power variability - a critical requirement for coastal resilience.**

**Candice Hall**

Wave power estimates and trend assessments are crucial for coastal management and resilience, as increases in wave power introduces significant risks of flooding and shoreline erosion. This study evaluates wave power trends at 29 National Oceanic and Atmospheric Administration (NOAA) National Data Buoy Center (NDBC) moored buoy sites with associated U.S. Army Corps of Engineers (USACE) Wave Information Study model estimates within the North Pacific Ocean, Hawaiian Islands, Gulf of Mexico and North Atlantic Ocean. This work is the first conclusive study to show spatially and temporally comparative observational and model wave power results, providing new information on the accuracy of model estimates using wave power as a proxy. Wave power data were interpolated to augment missing values and detrended for seasonality to facilitate testing of interannual and interdecadal trends in wave power. Results show that the majority of the eastern Pacific Ocean and Hawaii wave power trends are downward, with mixed slope wave power trends apparent within the Atlantic Ocean and Gulf of Mexico. Observational and model results show that wave power peaks in long term inter-annual trends are similar with respect to timing, but not magnitude. Variability in the wave power trend direction within each region suggests that site specific wave power trends should not be generalised to represent a large region, with regionally grouped annual maximum $90^{th}$ percentiles obscuring the variability of individual site results.

Prior to the calculation of these wave power estimates, a thorough interrogation of the quality of the observational wave data was conducted. Three tasks achieved confidence in these observational datasets: a) an evaluation of the effects of changing NDBC instrumentation technologies on data quality; b) the development of an independent, self-describing, archive that mitigates for historical data storage issues; and c) the subsequent removal of identified discontinuities within the time series datasets.

Instrumented buoy intercomparisons within the Pacific Ocean and U.S. Great Lakes prove that the recently deployed NDBC 2.1-m hulls show an increased wave data accuracy when compared to the legacy NDBC 3-m hulls for significant wave height, average wave period, and spectral signal-to-noise ratio, which allows for an increase in swell energy retention in the lower frequency spectral range. With confidence in the newly deployed NDBC platforms, this work then addressed NDBC data accessibility issues, as data are stored in multiple archives with unique storage, metadata, and quality control protocols. Known storage and quality control inconsistencies were removed and the validated data for all NDBC moored buoy stations are stored within a USACE Quality Controlled, Consistent (QCC) Measurement Archive, which is now a public database of best available historical NDBC data with verified metadata.

Spectral wave data from this USACE QCC Archive were interpolated for frequency equivalency and used to recalculate the required wave power input parameters to ensure consistency through the historical datasets, successfully removing a number of previously identified time series discontinuations. With these data discontinuity corrections, uncertainties and inaccuracies are removed from the estimated wave power trends.

Overall, this study highlights the undeniable need for accurate and consistent observational data that are essential for a realistic estimation of local wave climate studies, a vital requirement for all coastal risk management considerations. Although these observational and model wave power trends are U.S. specific, the methodologies developed within this work are applicable to datasets in any region.

# Dissertation publications at a glance

**Please note: While every effort was made to avoid repetition within the dissertation, overlaps exist when describing wave theory, agency collection methodologies and processing techniques, and data preparation. These overlaps were necessary to allow for comprehension of the key question investigations within each chapter.**

**Paper 1 (Chapter 2): Performance evaluation of the newly operational NDBC 2.1-m hull.**

**Aim**: Evaluate wave observations collected using a newly operational, smaller and more lightweight NDBC 2.1-m hull.
**Method**: Statistical comparisons of 2.1-m hull test data and data collected using a larger, operational 3-m hull against a nearby reference buoy. Expectations are that the 2.1-m hull test data will show higher correlations with the reference data than data collected using the larger, 3-m hull.

**Conclusions**:

- Statistical analyses and wave spectral comparisons confirm that the wave measurements reported from the NDBC 2.1-m hulls show an increased accuracy when compared to the previously collected NDBC 3-m hull wave data for significant wave height and average wave period.
- Results show that the NDBC 2.1-m hull retains consistent accuracy for directional results, purporting that hull size does not impact NDBC directional data estimates.
- Spectrally, the NDBC 2.1-m hulls show an improved signal-to-noise ratio, allowing for increase in energy retention in the lower frequency spectral range, with an improved high frequency spectral accuracy above 0.25 Hz within the short seas and wind chop wave spectral components.
- These improvements in both NDBC bulk and spectral data accuracy provide confidence for the wave community's use of NDBC wave data to drive wave model technologies, improvements and validations.

**<u>Paper 2 (Chapter 3)</u>: United States Army Corps of Engineers Coastal and Hydraulics Laboratory Quality Controlled, Consistent Measurement Archive.**

**Aim**: Develop an independent, self-describing, USACE Quality Controlled, Consistent (QCC) Measurement Archive that captures the best available NDBC observations with verified metadata.

**Method**: Methodology requires the merging of manually quality controlled data that are stored on the NDBC website with the lower quality netCDF data and metadata files for the same stations that are stored at the NOAA National Centers for Environmental Information (NCEI). The data archive routine involves a six step process for each buoy station: (1) data download, (2) individual source concatenation, (3) metadata verification, (4) comparison of data from the two sources; geographically quality assure/quality control (QA/QC) the data; and attach verified metadata to the NDBC datasets, (5) create best available dataset from the two sources, and (6) create Thredds netCDF data files that contain the best available data with associated metadata.

**Conclusions**:

- This USACE QCC Measurement Archive provides a database of best available, consistently stored, QA/QC data for the accurate evaluation of long-term trends in wave climates.
- Note that this methodology only removes data that are known to be in error using QC methods and could not be verified for quality from an alternate source.

**<u>Paper 3 (Chapters 3&4)</u>: Wave Power Trends along the U.S. Coastline: In situ Measurements and Model Hindcasts Estimates.**

**Aim**: This study tested for shifting observational inter-annual wave power trends at sites within the North Pacific Ocean, Hawaiian Islands, Gulf of Mexico and North Atlantic Ocean, using the above newly developed, unique, USACE QCC Measurement Archive (chapter 4).

**Method**: A viable methodology was developed to remove the observational time series data discontinuations that were highlighted by previous studies. Once time series data homogeneity was established, tests were conducted to investigate interannual and interdecadal shifting trends in wave power using measurement data that are interpolated for missing values and detrended for seasonality, allowing for a continuous time series of moored buoy data with no gaps or background seasonality variance bias.

**Conclusions**:

- This study is one of the first to show spatially and temporally comparative observational and model wave power results, providing new information on the accuracy of model wave power estimates, while showcasing in situ wave power trends at 29 sites around the U.S. coastline.
- This work offers a viable methodology to remove documented observational time series data discontinuities.
- The majority of the eastern Pacific Ocean and Hawaii wave power trends are downward, with mixed slope wave power trends apparent within the Atlantic Ocean and Gulf of Mexico.
- Observational and model results are similar with respect to timing, but not magnitude, of wave power peaks in long term inter-annual trends, with the moored buoy data presenting smaller wave power ranges for two (eastern Pacific Ocean and Hawaii) of the four regions.
- The detection of a noticeable variability in the wave power trend direction within each region suggests that site specific wave power trends should not be generalised to represent a large region, with regionally grouped annual maximum $90^{th}$ percentiles obscuring the variability of individual site results.
- This work demonstrates that observational data are essential in local wave climate studies to accurately estimate wave power.

# Acknowledgements

Massive thanks go to my supervisors and co-authors, Professor Isabelle Ansorge, Drs Robert Jensen and David Wang, and my unofficial editor, David Hall. Without your support and guidance, this work would not be possible!

I would also like to thank the examiners, as well as the journal paper reviewers for their invaluable comments and suggestions that improved the quality of this dissertation and the included journal papers. Appreciation goes to the NOAA National Data Buoy Center, U.S. Army Corps of Engineers Wave Information Study program, and the Scripps Institute of Oceanography Coastal Data Information Program for collecting decades of wave data.

Finally, thank you to my long-suffering family and friends, especially David, Richard, Kathy and Tim, who have kept me sane and well fed during this effort. Mom, this is for you.

# Contents

# List of Figures

# List of Tables

# List of Abbreviations

| | |
|---|---|
| ACT | Alliance for Coastal Technologies |
| alpha$_1$ | $\alpha_1(f)$: mean frequency-dependent wave direction (degrees from North) |
| alpha$_2$ | $\alpha_2(f)$: primary frequency-dependent wave direction (degrees from East) |
| AMPS | Advance Modular Payload System |
| AMS | American Meteorological Society |
| ARES | Acquisition and Reporting Environmental System (payload) |
| $C_{11}(f)$ | spectral wave energy |
| CDIP | Coastal Data Information Program |
| CFOSAT | Chinese-French Oceanic SATellite |
| CHL | USACE ERDC Coastal Hydraulic Laboratory |
| CMEMS | Copernicus Marine Environment Monitoring Service |
| CMS | Coastal Modeling System |
| DACT | Data Acquisition Control and Telemetry (payload) |
| DBCP | Data Buoy Cooperation Panel |
| DDWM | Digital Directional Wave Module |
| DODS | NOAA NDBC Distributed Oceanographic Data Systems framework |
| DWDA | Directional Wave Data Analyzer |
| DWPM | Directional Wave Processing Module |
| DWR | Datawell® Directional Waverider MkIII |
| ECCC | Environment and Climate Change Canada |
| ECMWF | The European Centre for Medium-Range Weather Forecasts |
| ECWAM | ECMWF Ocean Wave Model |
| ENSO | El Niño Southern Oscillation |
| ERDC | USACE Engineering and Research Development Center |
| ESA | European Space Agency |
| FFT | fast Fourier transform |
| FLOSSIE | Field Laboratory for Ocean Sea State Investigation and Experimentation |
| FRF | USACE ERDC CHL Field Research Facility |
| GOW | Global Ocean Wave |
| GPS | Global Positioning Satellite |
| GSBP | General Service Buoy Payload |
| GWP | global wave power |
| $H_m$ | individual wave height (m) |
| $H_{m0}$ | significant wave height (m). Also known as $H_s$, $H_{sig}$, $H_{1/3}$, WVHT |
| $H_{max}$ | Maximum wave height (m) |
| $H_{rms}$ | root-mean-square wave heights (m) |
| $H_s$ | significant wave height (m). Also known as $H_{m0}$, $H_{sig}$, $H_{1/3}$, WVHT |
| Hz | hertz |
| IOC | Intergovernmental Oceanographic Commission |
| ICOADS | International Comprehensive Ocean-Atmosphere Data Set |
| IOOS | U.S. Integrated Ocean Observing System |
| IPCC | Intergovernmental Panel on Climate Change |
| JCOMM | Joint Technical Commission for Oceanography and Marine Meteorology |
| $k$ | wave number (m/radians) |

| | |
|---|---|
| $L$ | wavelength |
| m | metres |
| MARS | Multifunction Acquisition and Reporting System |
| MEI | Multivariate ENSO Index |
| NAO | North Atlantic Oscillation |
| NCEI | NOAA National Center for Environmental Information |
| NCEP | NOAA NWS National Centers for Environmental Prediction |
| NDBC | NOAA National Data Buoy Center |
| NHC | NOAA NWS National Hurricane Center |
| NOAA | U.S. National Oceanic and Atmospheric Administration |
| NOMAD | Navy Oceanographic Meteorological Automatic Device |
| NPI | North Pacific Index |
| NWS | NOAA National Weather Service |
| OISST | Optimal Interpolation Sea Surface Temperature |
| OWL | Ocean Wave Linux |
| PDI | Pacific Decadal Index |
| PDO | Pacific Decadal Oscillation |
| POT | Peak over threshold |
| PP-WET | Pilot Project on Wave measurement Evaluation and Testing |
| $r_1$, $r_2$ | frequency dependent spreading parameter function (unitless) |
| RMSE | root mean square errors |
| SAR | synthetic aperture radar |
| SCOOP | Self-Contained Ocean Observing Payload |
| SKIM | Sea surface Kinematics Multiscale |
| SST | sea surface temperatures |
| STWAVE | Steady State Spectral Wave |
| SWAN | Simulating Waves Nearshore |
| SWIM | Surface Wave Investigation and Monitoring |
| $T_a$ | mean or average wave period (s). Also known as $T_m$ or APD. |
| $T_p$ | peak or dominant wave period (s). Also known as DPD. |
| UNESCO | United Nations Educational, Scientific and Cultural Organization |
| USACE | U.S. Army Corps of Engineers |
| USF | University of South Florida |
| VEEP | Value Engineered Environmental Payload |
| WAM | The Wave Model |
| WA | Wave Analyzer |
| WavEval | WavEval Wave Spectra Comparison Tool |
| WIS | USACE ERDC CHL Wave Information Study |
| WMO | World Meteorological Organization |
| WPM | wave processor module |
| WRA | Wave Record Analyzer |
| WW3 | WAVEWATCH III® |
| WW3DG | WAVEWATCH III Development Group |

## Chapter 1

# 1 General Introduction

### 1.1 Introduction

Waves are found in water bodies across the globe. “In the simplest case, waves transport energy without transporting mass” (Maul, 2005:1049). Understanding this transfer of energy, or wave power, across the planet is vital due to its impact on shoreline movement and sand dispersal; forces on coastal structures and offshore exploration (harbours, sea-walls, oil and gas exploration), global and localised research purposes, and possible threats to commercial and recreational water usage (fishing, shipping, boating, beach-users).

In the northern hemisphere, the United States (U.S.) Census Bureau (2019a) estimates that approximately 40 % of the U.S. population live within coastal areas. These regions “produce more than $8.6 trillion in goods and services, employ 56.8 million people, and pay $3.5 trillion in wages” (U.S. Census Bureau, 2019b). The U.S. Global Change Research Program’s Climate Resilience Toolkit states an estimated $500 million per year in property loss due to coastal erosion (U.S. Federal Government, 2019), requiring beach nourishment and shoreline erosion mitigation efforts that annually average $150 million (U.S. Census Bureau, 2013). “In addition to beach erosion, more than 80,000 acres [323.75 $km^2$] of coastal wetlands are lost annually - the equivalent of seven football fields disappearing every hour of every day” (Dahl and Stedman, 2013:46), with Conathan et al. (2014) describing the 1998 – 2009 wetland loss as exceeding 3144 $km^2$ (the size of Rhode Island, U.S.).

These staggering dollar amounts demonstrate the importance of understanding long-term coastal wave climate variability to facilitate accurate, life-saving wave forecasting, as well as comprehensive implementation of effective and sustainable coastal management plans to mitigate coastal erosion. To fully achieve these essential tasks, forecasters and planners

require reliable real-time and historical observational wave measurements that allow for confidence in future wave climate predictions.

Therefore, using wave power variability as a proxy for coastal wave climate, this work assesses four decades of wave power variability to investigate changing trends over time. However, numerous entities collect these observational wave measurements via multiple platforms, various sensors and several methodologies. If all wave measurement systems returned identical results, then any differences in these platforms, sensors and methodologies would be immaterial. Unfortunately, they do not (Livermont et al., 2015; 2017; Bouchard et al., 2018), and the returned differences highlight the undeniable realisation that achieving accurate and consistent observational wave measurements requires a) standardisation between agency, measurement and instrumentation platforms; and b) documented transparency in methodologies is required to facilitate unbiased user decision making.

While agency standardisation and transparency are beyond the scope of a research project, this study tackles consistencies between wave instruments and buoy platforms, with a view of ultimately detecting whether coastal wave power has changed over the last four decades. In short, this work investigates whether a) measurements from different wave measurement systems are comparable, b) whether it is possible to correct for bias between different wave measurement systems to produce long-term time series records, and finally c) whether wave power has increased over time.

Therefore, wave power estimates and trends are evaluated from observational and modelled hindcast wave data at 29 indicator sites within the North Pacific Ocean, around the Hawaiian Islands, and within the Gulf of Mexico and the North Atlantic Ocean (Figure 1.1). These locations were chosen due to the longevity of the time series data collected at those sites by the U.S. National Oceanic and Atmospheric Administration (NOAA) National Weather Service (NWS) National Data Buoy Center (NDBC) and the U.S. Army Corps of Engineers (USACE) Wave Information Study (WIS) model wave estimates.

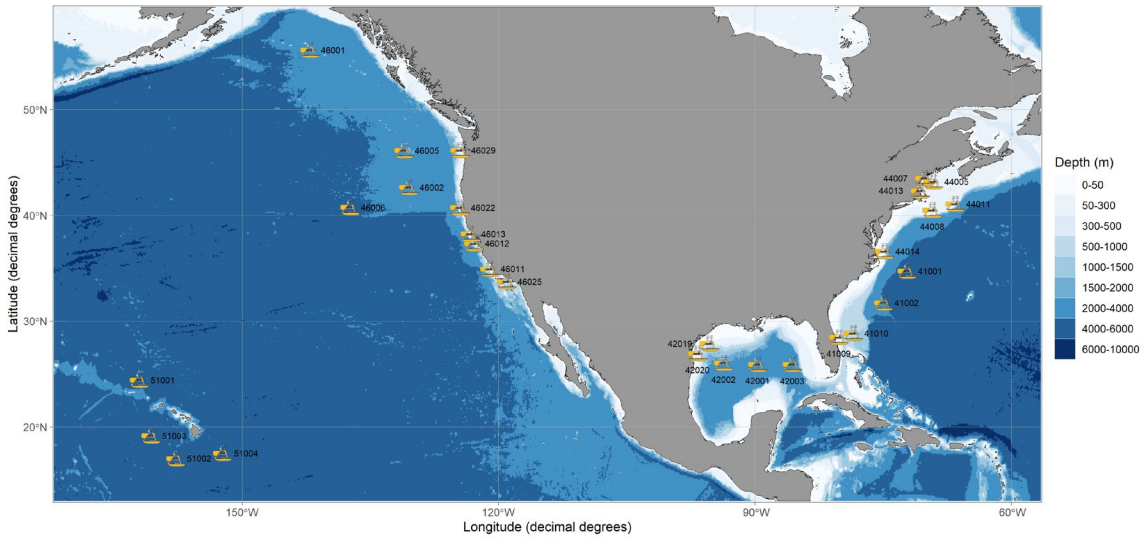


Figure 1.1. Reviewed NDBC and WIS locations (Hall et al., 2022a).

In summary, this study is first to combine spatially and temporally comparable observational and model wave power estimates, providing new information on the accuracy of model bulk wave estimates, while showcasing in situ wave power trends around the U.S. coastline (Chapter 4). This work is also the first to use a newly available, self-describing archive of observational data with verified metadata to calculate these wave power estimates (Chapter 3). Additionally, this is the first study to combine comparison results between wave instrument systems (Chapter 2) with a viable methodology to correct for documented time series discontinuities within observational data sets (Chapter 3), providing the best available, site-specific wave power estimates to date. Of note is that these methodologies are applicable to observational data from any source or location around the world.

The paper is organised as follows. Chapter 1 reviews previous wave climate studies and known wave theory related to these key questions. Chapter 2 proves that different observational wave instrumentations are statistically comparable and are sufficient for the analysis of long term time series trends. Chapter 3 describes and applies a viable methodology for removing known discontinuities within these observational time series data. Finally, Chapter 4 details wave power calculations, including methods to mitigate

for missing observational data and isolate historical trends by removing seasonal effects within the observational and model data, before offering overall wave power trend summaries and comparisons for the North Pacific Ocean, Hawaiian Islands, Gulf of Mexico, and the North Atlantic Ocean.

## 1.2 Literature Review

This literature review outlines available wave data sources, reiterates the need for accurate wave measurements and outlines how researchers are using these wave data. It showcases the body of work that is currently available for determining wave climates and ultimately wave power trends over time.

### *1.2.1 Wind Generated Ocean Waves*

"Ocean waves may be defined as periodic undulations about an interfacial reference level, and as such can move horizontally, vertically, or at angles inclined to the horizontal" (Maul, 2005:1049). Although this classification includes many types of oceanic waves (e.g. internal, Rossby, Kelvin, tidal), this work focuses on surface gravity waves that are created by the transfer of energy from winds blowing across the ocean surface. Prior to delving into the focus of this work, it is important to introduce concepts and variables that are used in the estimation of wave power trends.

Wind generated ocean waves and their development are described (Figure 1.2) by the measurement of their wavelength, height (wave amplitude = ½ wave height), steepness and period (or the reciprocal of frequency). From these measurements, researchers can determine a wave's speed (celerity), energy and power. Wavelength ($L, l, \lambda$) can be defined as the distance between two consecutive crests or troughs of a wave (Short, 2005). Wave height ($H$), the vertical distance from crest to trough (Figure 1.2), depends directly on the air-sea energy transfer. There are multiple ways to define wave height. The most commonly used metrics are individual ($H_m$), maximum ($H_{max}$), significant ($H_s$; $H_{m0}$, $H_{sig}$; $H_{1/3}$; $WVHT$), and root-mean-square ($H_{rms}$) wave heights. However, significant wave

height is the most commonly used as it closely correlates with the wave height that a human observer would typically estimate (Kinsman, 1965). Significant wave height is the "average of the highest one-third of the waves" that occur within a set time period (NDBC, 2020a). Units for wave heights are typically metres (m). Steepness is defined by Short (2005) as the ratio of wave height to wavelength. Wave breaking and energy dissipation occurs when the individual wave steepness exceeds 1/7 (or a height to depth limit in shallow water.

Wave period ($T$) is the time it takes for one wavelength (Figure 1.2), or "two successive crests or troughs to pass a fixed point, the reciprocal of which is frequency" ($f, \omega$) (Short, 2005:1049). NDBC (2020a) defines swells as waves with longer wavelengths (i.e., longer wave periods or lower frequencies) and wind-waves as waves with shorter wavelengths (i.e., shorter wave periods or higher frequencies).

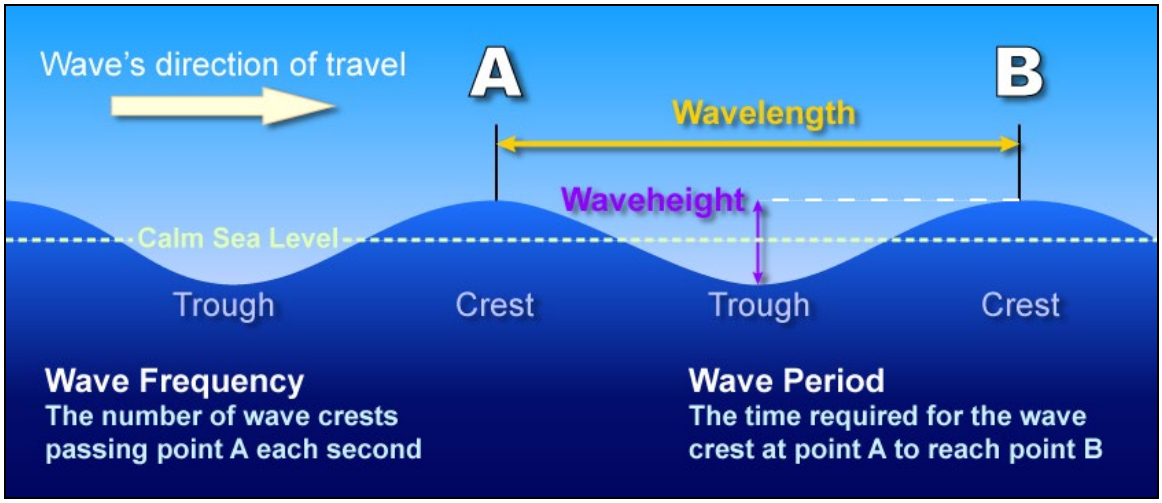

Figure 1.2. Anatomy of a wave (Reprinted from NWS, 2021).

Wave period (Figure 1.2) can be articulated in terms of its reciprocal (or more accurately: multiplicative inverse): radial frequency $\omega = 2(\pi)/T$, just as wavelength is the reciprocal of wave number $k = 2(\pi)/L$ (Kinsman, 1965). In other words, "the frequency is the measurement of the number of repeating units of a propagating wave per unit of time, and wave number is the measurement of the number of repeating units of a propagating wave per unit of space"(University of South Florida [USF], 2005). Again, a number of wave

periods statistically describe the sea state within a given time interval: peak or dominant wave period ($T_p$, DPD) and mean (average) wave period ($T_m$, $T_a$, APD). The peak period is the wave period with the highest energy observed during the sampling period (reciprocal of the peak frequency, $f_p$), while the mean wave period is the mean of all the wave periods as calculated during the sampling period. Both are important for understanding the sea state at a fixed location. The unit for the time domain, period, is seconds (s).

Another useful wave characteristic is wave speed, or celerity ($C$ in metres per second [m/s]), which is the ratio of the wavelength over the wave period; $L/T = \omega/k$ (American Meteorological Society [AMS], 2021). Wave celerity is influenced by only wavelength ($L$) and water depth ($d$) (USF, 2005). Waves with longer wavelengths travel more quickly than waves with shorter wavelengths. These waves are subjected to dispersion as they travel through the water, where the dispersion relationship relates wave period and wavelength as $\omega^2 = gk(tanh(kd))$. Deep water waves are considered to have a wavelength that is shorter than twice the water depth ($d > L/2$), so are not influenced by the ocean bottom. Shallow water waves are considered to be waves with wavelengths that are greater than 20 times the water depth ($d < L/20$), and are therefore influenced by mechanisms dependent on the water depth (advection, refraction and shoaling) and source/sink terms as in the case of bottom friction (USF, 2005). Hence waves of a given period travel slower in shallow water than deeper water because the wavelength decreases with decreasing water depth. For more information on wave types, wave spectra and statistics, and bulk wave parameter calculations, please see Appendix A1.

Of interest to coastal communities is wave power defined as the rate at which wave energy of wave trains is transferred (per metre of wave-crest length in kW/m; Resio, 2003). Wave power is computed as the product of wave energy ($E$) and the wave group velocity ($C_g$) is related to wave celerity ($C$) as $C_g = nC$, where $n = 0.5 * (1 + \frac{2kd}{sinhkd})$. The factor $n$ has deep-water and shallow waters asymptotes of 0.5 and 1, respectively (Dean and Dalrymple, 1991).

Ultimately wave power contained within incident waves as they reach the shoreline is of most relevance when predicting extreme wave events or damage to coastal structures, and is therefore the focus of this work. For deep water waves (water depth > ½ wavelength), using bulk wave parameters of significant wave height ($H_{m0}$) and peak period ($T_p$), Resio et al. (2003) approximated wave power ($P$) of a random wave field as the product of total wave energy, $E = \frac{1}{16}\rho g H_{m0}^2$, and wave group velocity of peak period, $C_g = \frac{1}{4\pi} g T_p$, which is expressed as

$$P = \frac{\rho g^2}{64\pi} H_{m0}^2 T_p,$$

where water density $\rho$ = 998 kg/m$^3$, and gravitational acceleration, $g$ = 9.81 m/s (Appendix A1). This dissertation utilises these equations to convert published spectral data at predetermined locations into bulk parameters for the calculation of wave power time series datasets. Trends in these wave power estimates are ultimately tested to determine if power is significantly increasing in the wave systems over time.

### *1.2.2 Wave climate and coastal protection*

In an effort to mitigate coastal erosion costs, the NWS participates in a national "Weather-Ready Nation" program, which requires accurate, observational wave climate data. This program aims to build a resilient nation and prepare coastal communities for extreme weather, water and climate events; from the use of the most advanced science and technology for data collection and modelling, to social science and emergency management information delivery systems (NWS, 2020). Every six hours, the NWS's National Hurricane Center (NHC), the Ocean Prediction Center, and the Honolulu Weather Forecast Office issue High Seas Forecasts for relevant portions of the North Atlantic and North Pacific Ocean. These bulletins describe current wind and wave conditions, and 24- and 48- hour forecasts. For transiting mariners, NHC's Tropical Analysis and Forecast Branch disseminate five day Offshore Waters Forecasts for the Gulf of Mexico, Caribbean Sea, and portions of the Atlantic Ocean. These forecasts cover large scale environmental conditions such as weather systems, winds, and sea state as

determined by significant wave height (NHC, 2020). For all of these products, the NWS needs accurate, real-time and historical wave data for large ocean regions, for both now- and forecasts, and to initiate and validate their weather prediction models.

Closer inshore, the USACE is one of the agencies responsible for sustainable coastal planning across the U.S. states and territories. Understanding coastal wave climates is acknowledged as vital to USACE planning. In fact, the USACE Coastal Engineering Manual highlights this need: "Knowledge of these waves and the forces they generate is essential for the design of coastal project since they are the major factor that determines the geometry of beaches, the planning and design of marinas, waterways, shore protection measures, hydraulic structures, and other civil and military coastal works. Estimates of wave conditions are needed in almost all coastal engineering studies" (USACE CECW-CE, 2002: EM1110-2-1100: II-1-1). Not only do they need to know the heights of these waves, but they need to know the probability and direction that these waves hit the coastline. To this end, in 1977, USACE's Coastal and Hydraulics Laboratory constructed a coastal Atlantic Ocean observatory at the Field Research Facility (FRF) in North Carolina, U.S. Since then, the FRF has provided waves, winds, tides and current information (USACE, 2020a) for the USACE Engineer Research and Development Center (ERDC) and public use. However, USACE is responsible for coastal planning in all U.S. domains, requiring accurate wave climate data from many more locations than just North Carolina.

### *1.2.3 Sources of wave data*

#### *1.2.3.1 Observational wave buoys*

To answer these various wave questions, a number of agencies and organisations collect in situ observational lake and ocean wave measurements. Arguably the most extensive network of weather buoys is operated by NDBC. NDBC's mission is to "provide quality observations in the marine environment in a safe and sustainable manner to support the understanding of and predictions to changes in weather, climate, oceans and coast"

(NDBC, 2020b). To this point, NDBC was originally formed in 1967 (as the National Data Buoy Development Program [NDBDP]), and was managed by the U.S. Coast Guard, who needed accurate meteorological, wave and current data to aid in search and rescue operations. In 1970, that NOAA National Ocean Service inherited and rebranded the NDBDP as the NOAA Data Buoy Center (NDBO). Finally, in 1982, NOAA renamed and transferred NDBO to the NWS as NDBC.


Figure 1.3. NDBC Legacy DDWM (top) and the new OWL (bottom) (Reprinted from Hall, 2018a).

Since the 1970's NDBC and their partners have deployed approximately 140 weather and climate buoys with wave measurement instrumentation within U.S. waters of interest. Initially NDBC's wave measurement technologies were only adept at measuring non-directional wave energy data on their weather buoys. However, in 1984, NDBC increased their non-directional wave measurement system capabilities to include a Directional Wave Data Analyzer (DWDA) system on a 10-m diameter discus hull that was deployed at an operational NDBC station (Steele et al., 1985). Since the 1970's, NDBC has deployed at least eight types of directional wave instruments for operational or experimental use (Steele et al., 1985; NDBC, 1996; Teng et al., 2007; Crout et al., 2008, Teng et al., 2009,

Riley et al., 2011; Hall et al., 2018a, 2018b; Riley et al., 2019). Figure 1.3 highlights NDBC's latest wave technology: the legacy Digital Directional Wave Module (DDWM) and new Ocean Wave Linus (OWL) module (Hall, 2018a).

As of April 2022, NDBC and their partners collect weather and climate data from 1327 stations deployed across the globe (NDBC, 2022), which include a standard meteorological suite of significant wave height ($H_{m0}$), dominant wave period ($T_p$), average wave period ($T_a$), mean wave direction ($\theta$), spectral wave energy ($C_{11}$) and direction variables ($alpha_1$, $alpha_2$, $r_1$ and $r_2$), wind direction, wind speed, wind gust, barometric pressure, air temperature, sea water temperature and dew point temperature (Appendix A1.1; NDBC, 2020c).

Another U.S. wave measurement program is the Coastal Data Information Program (CDIP), which is managed by the Scripps Institution of Oceanography's Ocean Engineering Research Group (CDIP, 2020). CDIP has been operating dedicated wave data collection systems around the U.S. coastline and within the Great Lakes since their first wave buoy was deployed in 1975 (CDIP, 2020). In 1977, due to the USACE's need for wave climate data, they began partially funding CDIP, and now provide the major share of CDIP's operating budget (CDIP, 2020). The majority of CDIP's early wave measurement systems were non-directional buoys. However, CDIP started deploying directional buoys that collected wave height, period and direction, as well as sea surface temperature, in the 1990's (CDIP, 2020).

As of April 2022, CDIP have 67 active Datawell® Directional Waveriders (Datawell BV, 2020) deployed across the Gulf of Mexico, Pacific and Atlantic Oceans (CDIP, 2022), and collect a standard suite of significant wave height ($H_s$), dominant wave period ($T_p$), mean wave direction ($\theta$), spectral energy ($c_{11}$) and directional coefficients ($a_1$, $a_2$, $b_1$, $b_2$) data, as well as sea surface temperature (CDIP, 2020). CDIP is currently upgrading their fleet with newly developed Datawell® Directional Waveriders Mk4 (Datawell BV, 2020) that have surface current measurement capabilities (CDIP, 2020).

#### *1.2.3.2 Observational satellites*

Since the 70's, satellite radar altimeters and synthetic aperture radar (SAR) have provided other sources of wave data. In 1978, Seasat's SAR instrument enabled initial measurements of wavenumber (number of waves per a specific distance) and directional wave spectra from space. One benefit of SAR instrumentation is that the collection of data is not affected by sunlight or cloudy weather conditions (Jinsong et al., 2004). In 1982, Thomas published the first methodology for estimating wave height from these SAR images. Thomas (1982) was able to compare images from two Seasat passes with concurrent waverider buoy measurements and a shipborne wave recorder. He found that his SAR calculation method overestimated wave height by approximately 20 %, but this methodology relied on an untypical tilt assumption (Jinsong et al., 2004).

After multiple rounds of methodology development and validations against observational data – both buoy and satellite altimetry data (e.g. Brüning et al., 1994; Plant and Zurk, 1997; Chapron et al., 2001; Ardhuin et al., 2004; Jinsong et al., 2004; Jinsong et al., 2008; Shao et al., 2016; Pleskachevsky et al., 2019), bulk wave parameters (significant wave height, wave period and wave direction) can be retrieved from SAR platforms on a global scale. SAR data have been and still are available from an array of satellites, e.g. ERS-1/-2 and Envisat satellites, the Radarsat-1/-2 satellites, the COSMOSkyMed constellation, TerraSAR-X and TanDEM-X, ALOS-2, the Gaofen-3, Sentinel-1A and Sentinel-1B (Shao et al., 2016; Yang et al., 2018). However, Pramudya et al. (2019) report that significant wave height estimation accuracy is still affected by high wind speeds and wind-wave dominant conditions when validated against NDBC buoy data.

Since 1985 (Ribal and Young, 2019), satellite radar altimeters have also measured significant wave height data. Of interest to this study is the validation of satellite altimetry wave height data with in situ buoy wave data. Just recently, Yang and Zhang (2019) validated the Sentinel-3A/3B SAR Altimeter wave height data against NDBC buoy wave data to show that the SAR Altimeter data are accurate and stable, although still exhibited a root mean square error (RMSE) of 0.20 - 0.30 m for Sentinel 3A (March 2016 – February

2019) and 0.18 - 0.31 m for Sentinel 3B (November 2018 – March 2019). These RMSE's are higher than NDBC standard accuracy of ± 0.20 m for significant wave heights (NDBC, 2017), possibly due to spatial and temporal difference in records between the satellites and the NDBC buoys. However, the importance of accurate, in situ buoy measurements is evident as they are used for satellite product validation; and these satellite data are subsequently used in countless environmental studies.

For example, Young et al. (2011) used 23 years of satellite altimeter wind speed and wave height data to investigate climate changes in ocean wind speed and wave heights. They found that both were increasing globally. Of interest is their estimation that high latitude extreme significant wave heights are increasing at a greater rate than the mean significant wave height conditions (Young et al., 2011). This increase in mean and extreme event wave heights adds impact to Vinent and Moore's (2014) prediction that the natural recovery of barrier islands after extreme events will slow exponentially with the added pressures from a changing climate.

In 2017, Copernicus Marine Environment Monitoring Service (CMEMS) published the first real-time global Significant Wave Height that is derived from Sentinel-3A and Jason-3 satellite altimeter data (Copernicus, 2017). Dr. Romain Husson (responsible for this wave product), said the following when interviewed in 2017: "These satellite wave products … often offer a better description of extreme events, which numerical models tend to under-estimate. In situ wave data, typically provided by buoys, are similarly very helpful but in many areas of open water, there are no such buoys available" (Copernicus, 2017). However, these data are still calibrated and validated against in situ buoy data.

Ribal and Young (2019) also reviewed 33 years of significant wave height and wind speed data that was collected via the GEOSAT, ERS-1, TOPEX, ERS-2, GFO, JASON-1, ENVISAT, JASON-2, CRYOSAT-2, HY-2A, SARAL, JASON-3 and SENTINEL-3A satellite radar altimeters. They found that each altimeter and subsequent dataset are calibrated differently and are available in different data formats. To remove variability, Ribal and Young (2019) calibrated and validated those 13 altimeter datasets against

NDBC buoy data, and then confirmed those calibrations with cross-validation between the altimetry datasets. Their aim was to provide a single consistent, calibrated and cross validated global dataset (Ribal and Young, 2019). Again, NDBC data played an important role in the calibration and validation of these datasets.

One major drawback of these satellite altimetry products is that only significant wave height is available; wave period and direction are not yet attainable. CMEMS is hoping to provide directional, cross sea conditions by including data from the Synthetic Aperture Radar instrument (Copernicus, 2017). Due to this resource gap, for Hemer et al. (2010) to ultimately investigate longshore sediment flux along south-western Australia, they had to include global numerical wave model products (significant wave height, mean wave period and mean wave direction) with their satellite altimetry (significant wave height) data. They used these products to investigate seasonal variability in the directional wave climate of the vast Southern Hemisphere and relatively inaccessible Southern Ocean, where few in situ buoy observations are available for these large areas.

However, the future of satellite exploration of ocean surface currents and waves is looking bright. In 2018, the Chinese-French Oceanic SATellite (CFOSAT) project planned the launch of a Surface Wave Investigation and Monitoring (SWIM) radar to measure the direction, amplitude and wavelength of surface waves (Hauser et al., 2017). Secondly, the European Space Agency (ESA) is hoping to launch a Sea surface Kinematics Multiscale (SKIM) monitoring satellite this decade (Ardhuin et al., 2019a). This satellite will be able to measure ocean current and wave interaction from space.

#### *1.2.3.3 Numerical wave models*

As Dr. Husson noted above, observationally measuring the wave climate over statistically significant time periods, at sufficient resolutions to satisfy weather predictions and coastal planning needs around the globe, is unrealistic from a cost and logistical perspective. Instead, numerous numerical wave models have been developed to provide wave estimates for waters around the world. In 1992, European wave modellers launched the discrete

spectral Wave Model (WAM; Komen et al., 1994) that predicted waves based on "the physics of wind-wave generation, nonlinear interactions and dissipation by wave breaking" (The European Centre for Medium-Range Weather Forecasts [ECMWF], 2012). The ECMWF globally forecasts wave height, period, and direction using the ECMWF Ocean Wave Model (ECWAM) version of WAM (ECMWF, 2020).

The U.S. Navy uses the numerical wave model, WAVEWATCH III® (WAVEWATCH III Development Group [WW3DG], 2019) to predict wind-generated surface gravity waves over the world's oceans (Rogers et al., 2014). Closer inshore, the U.S. Navy uses the nearshore wave model, Simulating WAves Nearshore (SWAN; Delft University of Technology, 2020), to "provide support for planning and operation missions concentrating on littoral waters, which require small-scale high-resolution forecasts" (Rogers et al., 2014:63). WAVEWATCH III® (WW3) is managed by the NOAA NWS National Centers for Environmental Prediction (NCEP) Environmental Modeling Center (NCEP, 2019; Tolman et al., 2014), and used within their operational forecasts.

In 2015, Zieger et al., tested the newly developed third-generation numerical wave model WW3 that used the latest input and dissipation source parameterisations (wind wave interaction and white-capping dissipation source terms) against a) academic duration-limited test results, b) buoy measurements for wind-sea dominated conditions, c) Hurricane Katrina extreme wind conditions, and d) altimeter data. WW3 results showed "agreement by means of growth curves as well as bulk and spectral parameters in the simulations and hindcast" (Zieger et al., 2015:2). Of note is that Zieger et al. (2015) used NDBC buoy observations in their comparison analyses, showing their reliance on accurate NDBC buoy wave data.

To satisfy the USACE requirement for risk-based designs, in the 1970's they developed the Wave Information Study (WIS) that calculates hourly wave conditions for the US coastlines, Great Lakes and US island territories (USACE, 2020b). WIS generates "hindcast wave estimates (height, wave period, and direction) and directional spectral

estimates for pre-select[ed] output locations along the coast" (USACE, 2020b). WIS uses WW3 for the Pacific and Atlantic Ocean, and WAM for the Western Alaska region, the Gulf of Mexico and the Great Lakes (USACE, 2020b).

As sophisticated as ocean numerical wave models and satellite instrumentation become, as shown they both require in situ buoy wave climate data for calibration and validation. Many studies support the necessity of these in situ buoy wave climate data validations (e.g. Ortiz-Royero and Mercado-Irizarry, 2008; Reguero et al., 2012; Rusu and Guedes Soares, 2012; Van Nieuwkoop et al., 2013; Stopa and Cheung, 2014; Stopa and Mouche, 2016). For example, even though SWAN is designed as a nearshore wave model, Ortiz-Royero and Mercado-Irizarry (2008) tested oceanic scale SWAN and WW3 model results against NDBC buoy data. They determined that WW3 performs better than SWAN in deep water when validated with buoy observations, which is to be expected due to the individual models' parametric designs. In 2013, Van Nieuwkoop el al. also validated 23 years of hindcast SWAN wave climate data against buoy measurements to investigate the validity of two proposed wave energy sites for the United Kingdom. Of importance in this study are the errors in the model that the authors detected. They noticed that although the SWAN model computed realistic significant wave heights and periods for standard wave conditions, the significant wave heights and periods reported during extreme conditions were often underestimated. As this study aimed to select the most viable wave power candidate site, these underestimations introduce uncertainty into the reliability of the numerical wave model results and could have significant logistical impacts to the selected wave energy site.

These numerical wave models versus observational data inconsistencies are to be expected – the probability of mathematically predicting the complexities of ocean movement accurately are not presently realistic. There are still too many unknown or complicated physical interactions to account for during model parameterisation. However, numerical wave models are convenient when there is a scarcity of observational data for use. One

method to address this model uncertainty is to create reanalysis datasets that recalibrate numerical wave model hindcast data with instrument satellite altimetry and in situ buoy wave measurements.

Reguero el al. (2012) did just that. With a goal to enable global climate variability analyses and coastal engineering applications, they developed a Global Ocean Wave (GOW) reanalysis for 1948 – 2008. They recalibrated and revalidated a WW3 dataset using buoy wave measurements (from NDBC, the Environment and Climate Change Canada [ECCC] and Puertos del Estado) and satellite altimetry wave data (from TOPEX, Jason 1, Jason 2, Envisat, ERS-2 and GFO altimetry sensors).

Stopa and Cheung (2014) compared wave and wind data from both the ECMWF Reanalysis Interim and the NCEP Climate Forecast System Reanalysis. In addition to their comprehensive analyses of the datasets' accuracies, they hoped to "provide a template and a benchmark for evaluation of improved or future reanalysis datasets" (Stopa and Cheung, 2014:82). In 2016, Stopa, along with three other researchers (Stopa et al., 2016), continued this comparison work by assessing significant wave height and frequency spectra of four parameterisation options within the WW3 modelling framework with three observational wave data sources (buoy, altimeter and SAR derived wave data) to investigate the models strengths and weaknesses. They determined that certain spectral wave parameterisations perform better for others, but that the "directional spread within the wave spectra performs poorly and needs improvement" (Stopa et al., 2016:2).

These different methods of obtaining bulk and spectral wave parameters all have one thing in common – they require accurate and consistent in situ observational buoy wave measurements for their calibration (whether it is satellite based or model derived) and their output validation. However, as noted by Swail et al. (2009), these observational systems require continuous data quality testing and evaluation to allow for integrated data use across measurement platforms (Figure 1.4).

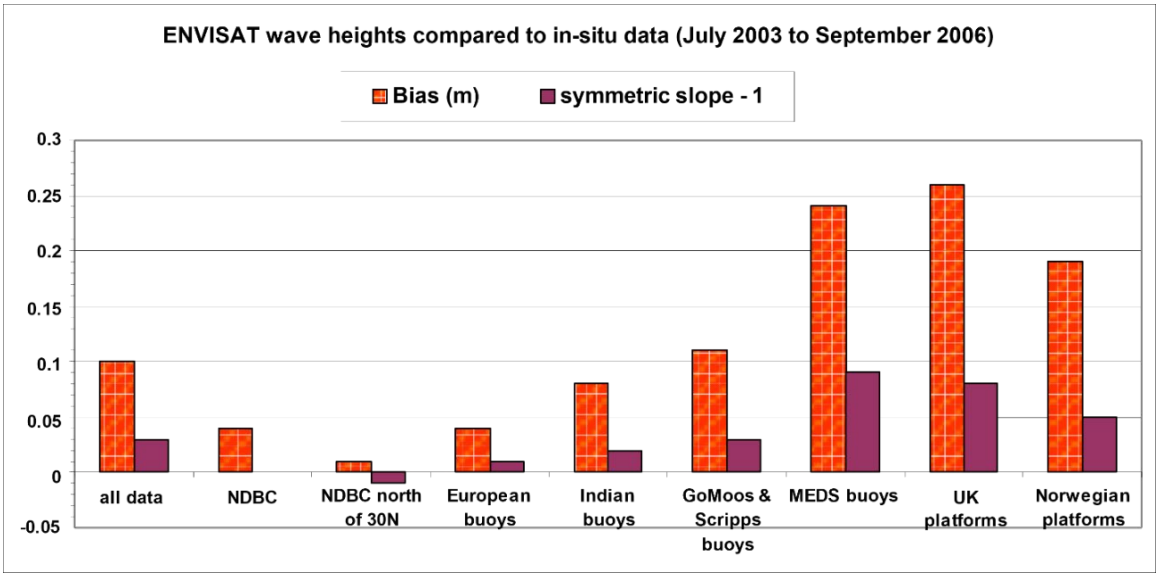


Figure 1.4. Instrumentation wave height inconsistencies (Altimeter vs. in situ bias, and slope ratio of variance altimeter to variance in situ) between Envisat wave heights and global in situ platforms (Reprinted from Swail et al., 2009).

### *1.2.4 Who is supporting the need for accurate wave data?*

Wave measurement protocols are considered so important to the wave community that multiple national and international workshops and conferences are held to discuss the subject. Since 1986 a biennial international wave workshop has been held to deliberate on ocean wave measurements, modelling and prediction, from basic research to the end user community. In 2017, these workshops logically expanded to include storm surge and coastal hazards, becoming the International Workshop on Waves, Storm Surges and Coastal Hazards (http://waveworkshop.org/).

Within the coastal engineering realm, engineers use the Hudson Formula (USACE CECW-CE, 2002), amongst others, to size armour units for hardened coastal structures. The Hudson Formula incorporates wave height, the medium mass and mass density of the rocks (amongst other parameters). An offset of 10% in wave height would translate to an uncertainty in rock size of 33%. Coastal engineers also use wave height to calculate longshore sediment transport. The CERC formula (USACE CECW-CE, 2002) incorporates significant wave height and wave angle at breaking. For this equation, if there

is a 10% uncertainty in the wave height, it translates to an uncertainty in the longshore sediment transport rate of $(1.1)^{5/2}$ or ~ 27%. Note that this percentage does not incorporate any errors inherited from the wave angle.

This undeniable need for accurate and consistent observational wave climate data necessitates two more requirements: standardisation between agency, measurement and instrumentation platforms; and transparency in methodologies for user decision making. Numerous agencies agree with this standardisation requirement and multiple attempts have been made to recommend collection standards.

In 2008, the Joint Technical Commission for Oceanography and Marine Meteorology (JCOMM) intergovernmental body (a combination of experts from the World Meteorological Organization [WMO] and UNESCO's Intergovernmental Oceanographic Commission [IOC]), developed a Pilot Project on Wave measurement Evaluation and Testing (IOC, 2010) that was managed by the JCOMM Data Buoy Cooperation Panel (DBCP). Due to the success of this pilot project, in 2016 the DBCP evolved this project into a fully-fledged Task Team on Wave Measurement. The Task Team was charged with developing standards and best practice for drifting and stationary measurements of waves (DBCP, 2019). These requirements include data quality for "reliable, high-quality spectral wave measurements, including directional spectra" (DBCP, 2020:11).

In 2009, the U.S. Integrated Ocean Observing System (IOOS), a collaboration of national and regional organisations that combine data and tools to cohesively improve forecasts and data accessibility (IOOS, 2020a), published a National Operational Wave Observation Plan. This plan was a combined effort from IOOS, USACE and NOAA NDBC (IOOS, 2020b). This plan was updated in 2012 and included a new partner, the U.S. Naval Meteorology and Oceanography Command. An important recommendation from this effort was the strategic placement of directional wave sensors to optimise the distribution, and hence effectiveness, of data collection around the U.S. coastline (IOOS, 2020b).

In 2013, IOOS added a Quality Assurance/Quality Control of Real-Time Oceanographic Data (QARTOD) Manual for Real-Time Quality Control of In-Situ Surface Wave Data (IOOS, 2020c), with a revision in 2019, to the growing list of wave measurement documentation. However, these procedures are not strictly enforced or employed uniformly by U.S. wave data collection agencies.

In 2019, the WMO and the IOC's DBCP Task Team on Wave Measurement initiated an international Wave Measurement Workshop, to be held in October 2022. This workshop is by invitation only, to include those who collect and utilise wave measurement data on a daily basis, as well as those in authority to facilitate their understanding of the need for accurate in situ wave data measurements. The necessity for continued meetings of this nature highlight the community's universally accepted standard for quality in the currently disseminated in situ buoy data.

### *1.2.5 Bulk wave data studies*

The accuracy of consistent in situ observational buoy data is vital for use by researchers and coastal planners around the globe. Inaccurate data collection or storage practices may skew study outcomes, resulting in inaccurate conclusions that could have ripple effects. One such consideration that has been raised in the wave community is whether wave conditions are changing over time (Allan and Komar, 2000; Allan and Komar, 2006; Méndez et al., 2006; Menéndez et al., 2008; Gemmrich et al., 2011 and Livermont et al., 2015 and 2017).

Based on proof of an increase of wave heights in the North Atlantic (Carter and Draper, 1988; Bacon and Carter, 1991; Kushnir et al, 1997; Gulev and Hasse, 1999), Allan and Komar (2000) postulated that they would find similar results when investigating wave conditions along the U.S. North Pacific coastline. They focused on two NDBC products: significant wave height, and derived spectral-peak period (the period with the most wave energy), from six deep-water buoys stationed between Alaska and California (Allan and Komar, 2000). They discovered that "wave heights have increased during the past 20-30

years, and the greatest increase has occurred offshore from the Washington coast. Slightly smaller increases are found offshore from Oregon and northern California, while no significant increase has occurred off the coast of southern-central California or in the Gulf of Alaska. Associated with the rise in wave heights has been an increase in the periods of the waves. Unlike the wave heights, there is little systematic variation in the wave-period trends along the west coast" (Allan and Komar, 2000:561). However, they only looked at data from six stations along the Pacific Ocean coastline. Their wave height vs hurricane work published in 2007 (Komar and Allan, 2007) adds that they believe that an increase in hurricane intensity (Emanuel, 2005), not necessarily frequency, when combined with increasing climate-change induced sea water temperatures, is contributing to the observed increasing wave heights in the Atlantic Ocean.

Gulev and Grigorieva (2004, 2006) tried to answer this wave height trend over time question by avoiding buoy wave data altogether. Instead they used a much longer 100 year period of visually observed wave height data that were collected along major shipping routes and homogenised in the International Comprehensive Ocean-Atmosphere Data Set (ICOADS, 2019). Their results "demonstrate positive trends in significant wave height over the North Pacific with a maximum of 8–10 cm/decade in the northeast Pacific. In the North Atlantic and other basins significant upward changes (up to 14 cm/decade) are observed only for the last 50 years and not for centennial records" (Gulev and Grigorieva, 2004:1).

Of interest to the North Atlantic and North Pacific wave climate mechanisms is that their 2006 work showcased that "variability in wind sea is closely associated with the local wind speed, while swell changes can be driven by the variations in the cyclone counts, implying the importance of forcing frequency for the resulting changes in significant wave height. This mechanism of differences in variability patterns of wind sea and swell is likely more realistic than the northeastward propagation of swells from the regions from which the wind sea signal originates" (Gulev and Grigorieva, 2006:5667). Although Gulev and Grigorieva (2004) were able to use a much longer dataset to investigate trends, visual data are notoriously biased to the recorder's opinion; and these wave height data were collected

by a myriad of different mariners over vastly different shipping routes. Add in mariners' behaviour to avoid storms at all costs, and these considerations are likely to result in inconsistent data coverage and bias towards calm weather.

Méndez et al. (2006) used only a single NDBC buoy significant wave height dataset (46005) to investigate extreme wave conditions using a time-dependent peak over threshold (POT) methodology. Upon a successful result using this POT model, Méndez continued this work with Menéndez et al. (2008) to include significant wave height datasets from 26 NOAA and ECCC buoys from 1985 to 2007. Using their POT model they show that there are "significant positive longterm trends in extreme wave height between 30–45°N near the western coast of the US averaging 2.35 cm/yr" (Menéndez et al., 2008:1). Ruggiero and Allan (2010) conducted a similar investigation and assessed multiple methodologies to project significant wave height and period estimates for the U.S. West Coast over the next 25- to 100-years. They used significant wave height data from one NDBC buoy (46005) that was collected between 1976 and 2007. They determined that all modelling approaches have caveats and rely on the complete understanding of ocean processes. "Until more is known about how variations in Earth's climate affect the Pacific North West deep-water wave climate, projected extreme values should be considered as uncertain and care should be used when applying these various techniques to real-world coastal engineering and management problems" (Ruggiero and Allan, 2010:551).

*Extreme versus background wave conditions*

The 2020 Atlantic hurricane season yielded "30 named storms (top winds of 39 mph or greater), of which 13 became hurricanes (top winds of 74 mph or greater), including six major hurricanes (top winds of 111 mph or greater). This is the most storms on record, surpassing the 28 from 2005, and the second-highest number of hurricanes on record" (NOAA, 2020). Figure 1.5 shows all the tropical storms and their tracks between 1848 and 2013 (NOAA Digital Coast GeoZone – IBTracs Archive; Eslinger, 2014). While conceptually an increase of hurricane occurrences should raise the wave power values, in

reality that population of very large events is relatively small so there is only an incremental departure from the mean trend. This suggests that using the mean value to track climate trends is not a good indicator. Additionally, a reasonable storm event with a duration of hours or days could cause more damage to a coastline than a fast moving extreme event.

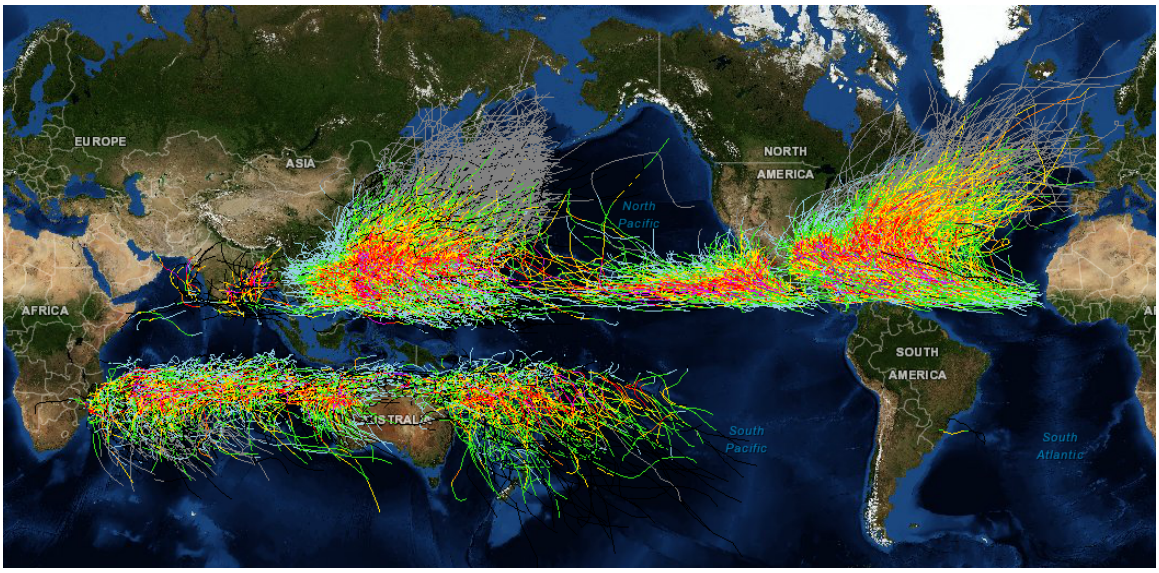


Figure 1.5. Global Tropical Storms, 1848 – 2013. Warmer colours indicate stronger winds (Reprinted from NOAA Digital Coast GeoZone – IBTracs Archive; Eslinger, 2014).

Panchang et al. (2013) reviewed a 51-year database of $H_s$ that was developed using wind and wave models, and validated with in situ buoy measurements. Their objective was to determine whether the 2004-2008 Gulf of Mexico hurricane season's exceedance of the then recognized 100-year $H_s$ levels were significant, due to the damage and disruptions that those hurricanes caused to the offshore Gulf of Mexico oil and gas platforms and ultimately the U.S. energy supply. They discovered an "increasing trend in the annual maximum SWHs ($H_s$) in the eastern part of the Gulf of Mexico; the maximum trend is approximately 5.6 cm/year, which is of the same magnitude as that reported for the U.S. west coast. The western part; on the other hand, shows a decreasing trend" (Panchang et al., 2013:031104-1). They determined the frequency of larger waves had increased significantly, even if the maximum $H_s$ had not.

Therefore, extreme wave conditions and wave heights are no longer the only incidences to consider when concerned with the impacts of waves. Appendini et al. (2018) investigated the effects of anticyclonic cold surges (*Nortes*) that produce less energetic but more frequent increased wave conditions in the Gulf of Mexico. Vinent and Moore (2014) modelled barrier island responses to the expected increase in both extreme events and sea level rise as predicted by climate scientists (Sallenger et al., 2012; Emanuel, 2013; Losada, I.J., 2013; IPCC, 2014; Vinent and Moore, 2014; IPCC, 2022). Although only 10 % of the world's coastline are barrier islands (Stutz and Pilkey, 2011), they are important as they protect inner coastlines and vulnerable populations from severe storm damage. For example, a census in 2000 estimated that 1.4 million people live on barrier islands in the U.S., and populations were increasing exponentially (Zang and Leatherman, 2011). Adding to a growing population and anthropogenic effects on erosion, Vinent and Moore (2014) found that if barrier islands were subjected to frequent storms and rising seas, they would become trapped in a perpetual state of susceptibility, becoming unstable and possibly collapse. Hence, understanding the background wave climate is essential to determine the baseline stress levels of barrier islands, in an effort to predict responses to extreme storm events.

Inshore, Leonardi et al. (2015) postulate that variations in background or mean wave power appear to have a greater effect on salt marsh erosion than extreme wave conditions across eight locations in the U.S., Australia and Italy. They discovered a universally linear relationship between wave power and salt marsh deterioration, and determined that, unlike with beach dunes (Vinent and Moore, 2014), there is no significant tipping point for salt marsh collapse during extreme wave power events. Their 20 year dataset showed that salt marshes sustained higher erosion rates from variable mean wave energy caused by moderate storms with 2.5 month return rates, and only a 1 % long-term erosion rate due to extreme storms. This is significant as recent conservation practices have focused on developing living shorelines and vegetated surfaces due to their propensity to reduce storm surge and wave power (Currin et al., 2010; Temmerman et al., 2013; Fagherazzi, 2014; Moller et al., 2014; Leonardi et al., 2015). Of interest is that Leonardi et al. (2015) used

wave climate equations developed by Young and Verhagen (1996), which were derived from studies conducted in Lake George, Australia (a lake with almost constant depth of 2m) and not in an open ocean wave climate. Regardless, this study emphasises the consequences of mean wave power and not just incident wave power impacts during extreme events, especially for compound (wave and storm) erosion investigations.

Allan and Komar revisited their 2000 work in 2006 (Allan and Komar, 2006) to investigate erosion along the U.S. West Coast. When attempting to use a combination of NDBC and CDIP wave data, they found "systematic differences between the reported wave heights and periods derived from the two buoy networks, so it is best not to mix the data sets in analyses" (Allan and Komar, 2006:512). These results clearly highlight the differences in wave collection protocols. They were informed that NDBC had changed their analysis procedures in 1984, affecting the derived NDBC significant wave heights and periods. Earle et al. (1984) had reported at the Institute for Electrical and Electronic Engineers (IEEE) Oceans 1984 conference that NDBC had developed a sea-state independent correction function (noise correction) to remove spurious energy from the acceleration spectra that was introduced by the use of a fixed accelerometer. This newly operational correction removes introduced low frequency noise and improves NDBC swell measurements (Earle et al., 1984). This noise correction was further improved in 1987 (Lang, 1987) and again in 2011 (Riley et al., 2011).

Continuing their coastal erosion study, Allan and Komar (2006) used regression analyses to test for shifts before and after 1984 on wave data from ten NDBC buoys. Finding little difference, they continued with NDBC significant wave height, average wave period, wave energy spectra, and the peak spectral wave period data to investigate climate controlled "processes [which] act together to produce the extreme total water levels that have resulted in major episodes of property losses experienced along the West Coast" (Allan and Komar, 2006:527). After considering decadal changes in wave climate; storm size and latitude; run-up elevations on beaches; as well as monthly and annual mean sea levels; and climate processes such as the multivariate El Niño Southern Oscillation index

and the North Pacific index, they concluded that considerable increases in wave height have occurred along the U.S. West Coast over their 25 year time series (Allan and Komar, 2006).

Of note is that above studies by Allan and Komar (2000); Méndez et al. (2006); Menéndez et al. (2008) and Ruggiero and Allan (2010), did not take into account the effects of instrumentation and data analyses changes on wave measurements collected over the 20-30 year data period. Gemmrich et al. (2011) attempted to do that by adjusting their seven Meteorological Service of Canada and NDBC buoy wave measurement datasets (~1970-2011) to account for step changes in the mean monthly significant wave heights (changes in instrumentation usage over time, as well as data collection while equipment was faulty). Gemmrich et al. (2011) results showed a regional pattern of wave height increases that were smaller than that described by Allan and Komar (2000), regardless of data collection instrumentation. They noticed "positive trends for some of the southern locations and negative trends at the northern buoys" (Gemmrich et al., 2011:1). However, this Gemmrich et al. (2011) study only investigated a small number of observational buoys.

### *1.2.6 Instrumentation effects on wave measurements*

Overall, these studies show the need to carefully evaluate in situ observational buoy wave data before use, especially if the wave data have been collected at the same site for decades. Long term data time series are expected to have experienced multiple instrumentation upgrades that have occurred with technological advances over their collection periods. For example, Gemmrich et al. (2011) listed three hull types of different sizes, six payloads (main on-board computer system, does not include wave sensors) and five wave processing systems (includes wave sensors and on-board wave processor to convert raw time series wave data) for NDBC station 46001 between 1974 and 2010. NDBC Station 46006 experienced six hull types of different sizes, seven payload changes during service visits, and four wave processing systems between 1977 and 2010 (Gemmrich et al., 2011).

Therefore, users need to be familiar with the instrumentation employed to collect their in situ observational wave data, including caveats and potential errors that are present in these data. At the 14th International Workshop on Wave Hindcasting and Forecasting & 5th Coastal Hazard Symposium, Key West, FL, USA, Livermont et al. (2015) presented results of their NDBC wave record corrections for ten buoys located off of the U.S. East Coast. They applied analysis of covariance (ANCOVA) and Tukey-Kramer statistical tests to identify hull and platform type effects on the significant wave height data. They discovered that "both hull and platform type resulted in significant changes to the time series, with the hull type as the more significant contributor" (Livermont et al., 2015:31). After correcting their time series data, they found that "long-term coefficient estimates for the trend were significant for sixteen of the twenty-one buoy, [but] there was not a spatial pattern in the long-term trends" (Livermont et al., 2015:31). Livermont et al. (2017) continued their work with the use of trend analyses and Probability Density Functions (PDF's) to correct for changes in NDBC buoy wave records. They concluded that quantile normalisation did not change observed trends (Figure 1.6) in their data, but did lessen the magnitude of their trends (Livermont et al., 2017).

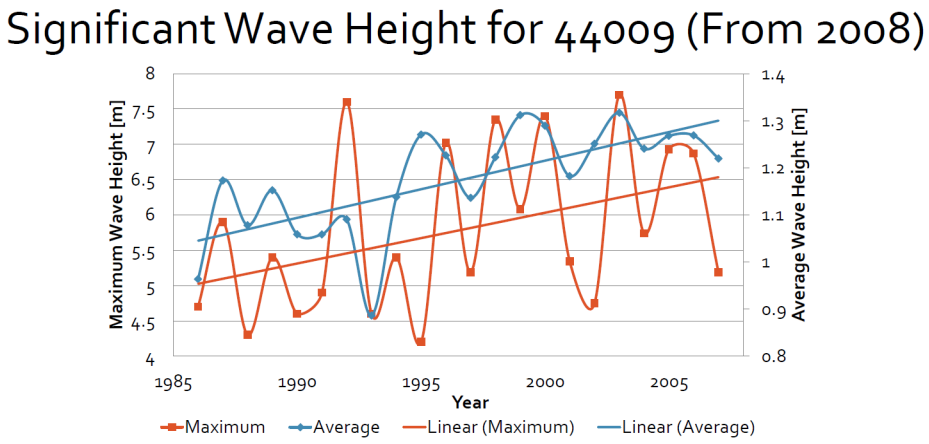


Figure 1.6. Significant wave height for NDBC station 44009 from 1985 – 2008 (Reprinted from Livermont et al., 2017).

To investigate these instrumentation, platform and hull effects on NDBC wave data collection, in 2015 USACE ERDC CHL funded a collaborative project with NDBC to deploy a single hull and payload with multiple legacy and newly developed wave sensors.

They deployed a 6-m NOMAD (Navy Oceanographic Meteorological Automatic Device) hull that NDBC has utilised operationally since October 1977 (Jensen et al., 2015; Bouchard et al., 2016; Bouchard et al., 2018). They deployed this test system, called the FLOSSIE Project (Field Laboratory for Ocean Sea State Investigation and Experimentation), at the Wave Evaluation and Testing area off of Monterey Bay, California, which is in close proximity to an operational NDBC 3-m hull with a Digital DDWM and a reference standard in a Datawell Waverider buoy. Wave measurement systems installed on the FLOSSIE Project included the NDBC 1) Wave Analyzer (WA) system (which utilised a Inclinometer), deployed by NDBC between 1984 and 2011, and 2) the Directional Wave Processing Module (DWPM) Hippy (which utilised a magnetometer), which was operated by NDBC 2003 until 2016, and 3) the DDWM (which utilised a 3DMG), and is presently the standard system deployed by NDBC. Two additional ECCC sensors, a presently deployed Axys-Triaxys Next Wave II Directional Wave Sensor/Wave Module and a historically deployed Axys-Watchman (strapped down accelerometer), completed the FLOSSIE instrumentation set (Jensen et al., 2015).

Bouchard et al., (2016) documented a plan to investigate the differences between the wave measurement systems at a spectral frequency level, by investigating the energy and directional distribution variances between the systems. At the 2nd International Workshop on Waves, Storm Surges, and Coastal Hazards, Melbourne, Victoria, Australia, Bouchard and Jensen (2019) showcased trend analysis and error statistics for FLOSSIE Project's three DWR, WA and DDWM significant wave height datasets. Jensen et al. (2021) documented the final, 5 year-long FLOSSIE Project's results that ultimately showed a good agreement between bulk parameter comparisons amongst the wave sensors. Jensen et al. (2015); Bouchard et al. (2016); Bouchard et al. (2018); and Bouchard and Jensen (2019) all stressed the usefulness of the FLOSSIE Project, in that the research provides an in-depth understanding of historical NDBC wave data system differences, and that these results should be used to develop a more homogeneous and useful historical NDBC wave dataset.

Since then, NDBC has introduced additional, newly-developed instrumentation: a new wave system called the Ocean Wave Linux (OWL); a new, advanced Self-Contained Ocean Observing Payload (SCOOP; Figure 1.7); and a newly developed 2.1-m foam hull (Hall et al., 2018a). “The OWL system uses a Linux-based processor to reduce computational time, but retains existing NDBC wave system data processing techniques and algorithms, as well as the pitch and roll angle method to calculate wave direction. This configuration allows NDBC to retain data continuity, reduce development costs, and avoid problems associated with changing data message formats. The 2.1-m foam hull reduces the superstructure area, which improves operational efficiency.” (Hall et al., 2018a:1).

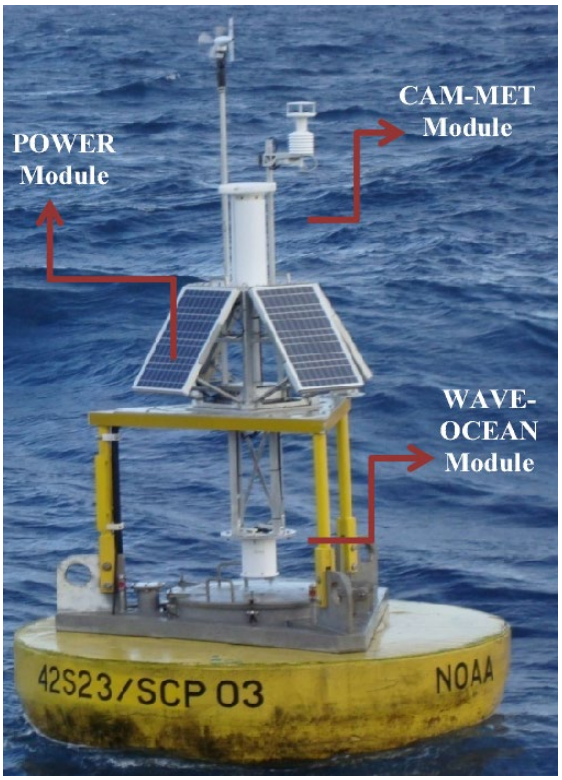


Figure 1.7. SCOOP - NDBC's new ocean observing system (Reprinted from Kohler et al., 2015).

Hall et al. (2018b) evaluated the performance of NDBC's newly developed SCOOP (Figure 1.7) that were deployed on modified 3-m foam hulls and nearby operational systems. “Small biases between the three SCOOP systems deployed on modified 3-m foam hulls and their operational counterparts’ show that the new systems are in good

agreement. Observed variance in the systems is likely due to spatial effects of the comparative buoy locations" (Hall et al., 2018b). Recommendations from Hall et al. (2018a) and Hall et al. (2018b) included further analyses of the differences in directional and non-directional spectral frequency data collected on the newly operational NDBC 2.1-m foam hull and the newly developed NDBC OWL system.

*Motivations for key questions 1 and 2:*

These recommendations lead directly into this dissertation's first key question, which asks if measurements from different wave systems are comparable. Although recent studies have investigated differences between NDBC legacy wave measurement systems, no published studies have investigated NDBC's newly operational 2.1-m foam hull.

This first key question builds from recent studies undertaken by Jensen et al. (2015); Bouchard et al. (2016); Bouchard et al. (2018), and Hall et al. (2018b) who investigated significant wave heights collected using NDBC's legacy wave measurement systems. Jensen et al. (2015) considered dissimilarities in peak spectral wave period and the vector mean wave direction at the peak frequency, while Bouchard et al. (2018) showcased wave steepness and wave power differences. To answer this key question concerning newly operational NDBC instrumentation accuracies, the author plans to test bulk and spectral wave data variance between NDBC's newly operational 2.1-m foam hulls and NDBC's legacy 3-m aluminium discus hulls against collocated and concurrent reference CDIP Datawell Directional Waverider MkIII (DWR) wave measurement systems.

If these different wave measurement systems prove to be comparable, key question two of this dissertation asks whether it is possible to correct for bias between different wave measurement systems to produce long-term time series records. As shown above, many studies have attempted to correct NDBC time series wave data (Gemmrich et al., 2011; Livermont et al., 2015; and Livermont et al., 2017). However, those authors only corrected significant wave height trends for a limited number of buoys. This dissertation work corrects the complete historical bulk and spectral NDBC wave datasets. Not only are these

corrected NDBC buoy wave datasets essential for accurate validation and calibration of satellite altimeter and SAR datasets and instruments, as well as for the validation and initiation of numerous wave model datasets, they are essential for investigating wave climate changes with time.

### *1.2.7 Inclusive bulk parameter use*

Once these spectral dataset for all the buoys in the NDBC network are corrected, new significant wave heights and periods may be calculated. With these data, a definitive answer to the question of increasing wave heights over time is achievable. However, while wave height is an obvious and visible factor when considering the impact of wave conditions on coasts and structures, variations in wave period and direction are just as important. Harley et al. (2017) highlighted a case of misidentified wave direction, where an extratropical cyclone of average intensity for southeast Australia resulted in their largest beach erosion event in forty years (11.5 million $m^3$ of sand from above mean sea level was transferred offshore along the 177 km that were surveyed). Sopkin et al. (2014) reported on the devastation of Hurricane Sandy in 2012 along the U.S. East Coast, and Harley et al. (2017) determined that the cause for this extraordinary damage was due to the storm's unusual wave direction. Therefore it was the intensity and direction of wave energy striking the shoreline that led to the extensive damage, not just the height of waves during the storm.

Comola et al. (2014) also noticed the impacts of wave period and direction, in conjunction with wave heights. They studied the effects of incremental damage to a rock armoured breakwater roundhead when subjected to varying significant wave heights, peak wave periods, directional spreading and spectral width. They created a physical model within a basin that was able to produce 3-D wave fields with specified directional wave spectra, including oblique wave trains. To investigate mean wave direction, they divided their roundhead into sectors that equated to incident wave angles. After a series of tests with multidirectional waves of varying heights and periods, Comola et al. (2014) concluded that wave period and significant wave height both influenced the distribution of damage

to the roundhead, although initial damage was reliant on significant wave height. However, once degradation had begun, they found similar results to Maciñeira and Burcharth (2008), that "under short wave periods, the damage is more uniform over the roundhead, and a slightly higher damage level appears in the frontal sectors. Under longwave periods, the damage is almost totally concentrated in the last two sectors" (Comola et al., 2014:29). They did note that wave spreading and spectral width of the incident waves did not appear to influence the pattern of damage to the roundhead. Most importantly, they determined that the critical sector of roundhead damage shifts leeward with increasing peak wave period (Comola et al., 2014).

These studies highlight the importance of mean wave direction and peak period when considering the impact of the wave climate on our coasts. Users require more information than just significant wave height; they ultimately need to know the intensity of the wave power that will intersect with the coastline. For example, Moghim and Alizadeh (2014) developed a new berm recession formula that is "derived from the relation of the wave force with maximum wave momentum flux" (Moghim and Alizadeh, 2014:63).

Hence, the transport rate of wave power are far more informative tools for determining the effects of high seas and wave conditions on shoreline movement, pressure on coastal and offshore structures, and commercial or recreational water usage. In fact, as late as 2019, Reguero et al. berated the fact that "most studies have focused on studying parameters such as wave heights, but a systematic, global and long-term signal of climate change in global wave behavior remains undetermined" (Reguero et al., 2019:1). An inclusive indicator of wave behaviour, such as wave power (calculated using wave height and period), should be investigated to understand coastal changes.

### *1.2.8 Wave power trends*

If significant wave heights are increasing over time (as shown above by Allan and Komar, 2000; Allan and Komar, 2006; Méndez et al., 2006; Menéndez et al., 2008; Gemmrich et al., 2011 and Livermont et al., 2015 and 2017), then we expect an associated increase in

wave power. Increases in shoreline wave power introduces significant risks of flooding and erosion, eliciting major repercussions for ocean engineering applications and disaster risk management.

As an example, in 1997, after witnessing property loss from shoreline damage that cost approximately $170 million, Meadows et al. (1997) used long-term wave climate hindcast data (1956 - 1987) from the USACE WIS model for Lake Michigan, with historical NOAA lake level data (1918 - 1994), to investigate the relationship between increasing coastal high water levels and incident wave energy. This WIS model dataset was calibrated and verified with NDBC buoy data. Meadows et al. (1997) found strong correlations between total wave energy and high lake water levels that were recorded during 1959 to 1990. Of interest was their evidence that "relative changes in incident wave energy have a greater effect on damage expectation than do changes in water elevation" (Meadows et al, 1997:681). Meadows et al. (1997) postulated that these increasing wave energies are caused partly by the climatological, northward shift in cyclone tracks, allowing for greater fetch for wave growth over Lake Michigan, and partly by an increase in local storm patterns.

Overall, multiple studies have employed numerical wave models to corroborate these increasing wave power hypotheses (e.g. Mackay, 2012; Reguero et al., 2015; Thomson et al., 2016; Mentaschi et al., 2017; Ulazia et al., 2017; Morim et al., 2019). Others have used wave models to quantify mean global wave energy estimates (e.g. Cornett, 2008; Mork et al., 2010; Gunn and Stock-Williams, 2012; Arinaga and Cheung, 2012). However, these studies only review a relatively short, six to ten year period.

Reguero et al. (2015) developed a calibrated and validated 61-yr wave reanalysis (which was calibrated with altimetry data and validated with buoys data) to calculate a global assessment of the variability of deep water wave power. Accounting for temporal variability, they estimated a global wave power of "32 GW h/yr, or 16 GW h/yr considering the direction of the energy" (Reguero et al., 2015:366). Mentaschi et al. (2017) used the WW3 (version 4.18; Tolman, 2014) numerical model to demonstrate a

substantial ~30% increase in wave power over the next 100 years for the Southern Hemisphere's coastal areas, with a substantial negative trend in the Northern Hemisphere. They highlighted the impact of the increasing wave power and projected sea level rise on low-lying Southern Hemisphere coastal areas.

On a regional scale, Thomson et al. (2016) investigated the impact of intensified sea state and therefore wave power on the longer, seasonal extent of open waters of the Beaufort and Chukchi seas. They used the WW3 wave model hindcast data; sea ice concentration data from the Earth Observing System Distributed Active Archive Center (at the National Snow and Ice Data Center, University of Colorado at Boulder, http://nsidc.org); as well as the ECMWF ERA-Interim wind reanalysis product (Dee et al., 2011). Their results show that the Arctic's lengthening open water season is lending to the increase in sea state, with larger wave heights and longer peak wave periods. Interestingly, they noted that the added wave power is mainly directed at the coast, not the ice (Thomson et al., 2016).

While Meadows et al. (1997) realised that increasing wave power in the land-locked Great Lakes are due to shifting extreme weather events and opportunities for increasing wind fetch, others such as Seymour (2011) and Reguero et al. (2019) believe that the anthropogenically-induced global warming phenomenon is contributing to an increase in wave intensity. Seymour (2011) used deep water wave buoy measurements ($H_{m0}$ from NDBC and CDIP stations) to investigate correlations with three global scale climate indices – the North Pacific Index (NPI) showed strong correlations, with the Multivariate ENSO Index (MEI) and Pacific Decadal Index (PDI) less correlated. However, century-scale correlations between the indices and $H_{m0}$ showed significant linear trends in NPI and MEI, causing the authors to postulate that global warming is increasing mean wave power and therefore wave intensity in the North Pacific.

Reguero et al. (2019) investigated their theory that global warming is heating up the surface layers of the ocean by correlating sea surface temperatures (SST) and wave power. To build their global SST grid, they used two SST anomaly products: a) the Optimal Interpolation Sea Surface Temperature (OISST) dataset (0.25º global grid of observations

from satellites, ships, buoys; Reynolds et al., 2007), and b) a recent ERSSTv3b dataset (International Comprehensive Ocean-Atmosphere Data Set that interpolates in situ SST measurements to construct a global 2˚grid for the period of record from1854 to the present; Reguero et al., 2019). Of note is that the OISST data were used to calibrate the ERSSTv3b dataset.

To calculate wave power for each cell in their global grid, Reguero et al. (2019) used their previous GOW reanalysis numerical wave model outputs (Reguero et al., 2012) of significant wave heights, mean wave periods and mean wave direction. As a reminder, their reanalysis was based on WW3 model outputs, and both these satellite altimetry data and WW3 outputs are calibrated and validated using NDBC and other in situ buoy wave data. After cross-checking their results against two independent sources (a more recent high-resolution global reanalysis – Rascle and Ardhuin, 2013, and AVISO satellite altimetry significant wave height results), Reguero et al. (2019) grouped their gridded global wave power (GWP) and SST time series data by season and year to calculate regional and globally averaged wave power and SST anomalies for latitudes, ocean basins, and wind-wave generation regions.

In total, Reguero et al. (2019) computed a 0.4% increase in GWP since 1948. They found that "oceanic warming in the different basins has likely led to an increase in GWP through the influence of SST on wind patterns" (Reguero et al., 2019:10), particularly in the tropical Atlantic and in the high south latitudes. "Consequently, the effect of climate change in oceanic warming has been increasing the global energy transferred from winds to the waves represented in the GWP. The impact of climate warming on the wave climate can therefore be seen in the energy transported by the waves, measured through the GWP as a long-term signal of climate change" (Reguero et al., 2019:10).

*Motivations for key question 3:*

However, all of these studies utilise observational buoy wave measurements, either directly via self-validation, or indirectly via the use of model or satellite products that are

calibrated and validated against buoy wave measurement data. With the acknowledgment of inherent wind field estimates and numerical wave model uncertainties, the need for accurate buoy wave measurements becomes even more critical when calculating not only bulk wave parameters, but deriving wave power trends over time. Without intimate knowledge of in situ buoy wave data collection methods, users have been unable to correct these data over the past decades, introducing uncertainty into the very fabric of their investigations. Therefore, once this study has removed the known inconsistencies (key question 2) within the historical NDBC wave data, this work will use these data to definitively address whether wave power is increasing with time (key question 3).

### *1.2.9 Study area wave environments*

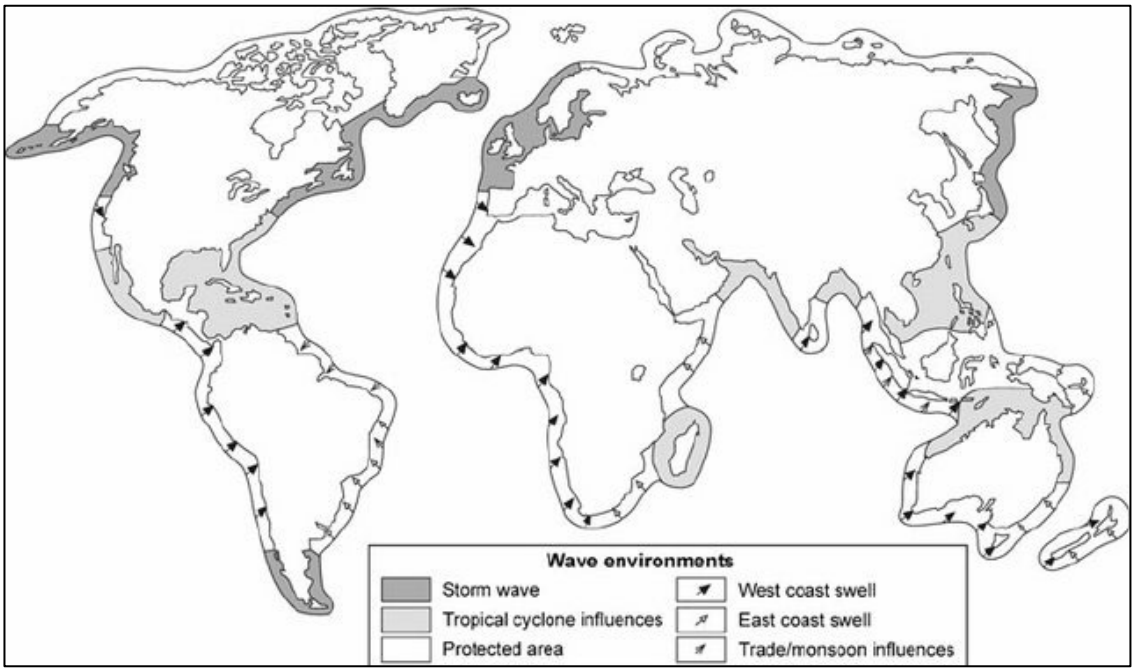


Figure 1.8. Global wave climates (Reprinted from Davies, 1980; 1982, modified by Masselink and Hughes, 2003).

Before commencement of this wave trends work, an overview of the wave environments found within the reviewed study areas provides context to the results uncovered during this dissertation's key question investigations. As has been established, the surface gravity waves that are under discussion in this dissertation are generated by wind stress on the

ocean surface. Davies (1980) defines three wave characteristics that are correlated to the zonal influences of winds as storm waves, swells and protected sea environments. Davies (1982) correlates these characteristics to four global, deepwater wave environments: a) upper mid-latitudes high-energy storm waves; b) west coast swells; c) east coast swells; and d) low-energy protected polar and tropical coastal regions (Figure 1.8). One exception to Davies' (1982) protected polar region classification would be the Southern Ocean, where storms circle the uninterrupted stretch of oceans surrounding Antarctica with little or no islands or reef barriers to slow the generation of storm and swell waves.

Short (1999) outlined the geographical locations of these wave environments, from storms waves between 40 – 60 ° North (N) and South (S); to west and east coast swells between 0 – 40 ° N and S; and east coast cyclones between 25 – 35° N and S. Trade wind waves are associated with 0 – 20 ° N and S; and protected coastlines are found between 0 – 10 ° and 70 – 90 ° N and S, where waves are dampened by their proximity to the doldrums, coral reefs and islands in the tropics, and sea ice and low velocity polar easterlies in the poles (Short, 2005).

As this dissertation is primarily concerned with long term wave measurements collected at the NDBC stations (Figure 1.1), the wave environmental conditions affecting the wave climates along the North Pacific Ocean, Hawaiian Islands, Gulf of Mexico, North Atlantic Ocean and Great Lakes will be discussed here. These wave environments include storm waves for the northern latitudes along both U.S. coastlines; west and east coast waves along the North Pacific Ocean and North Atlantic Ocean coastlines to the south of 40 ˚N; east coast cyclone wave conditions within the Gulf of Mexico and North Atlantic Ocean; and locally-driven wind seas within the Great Lakes.

#### *1.2.9.1 North Pacific Ocean and Hawaii*

Due to the size of the Pacific Ocean, and therefore the significant fetch potential, the reviewed moored buoy North Pacific Ocean sites (located along the U.S. West Coast) experience seasonal (winter) west coast swell waves (long persistent waves) that are

generated by storms in other regions. These west coast swell waves are sufficiently well developed when they arrive at the North Pacific Ocean sites, typically from a northwest direction (Short, 2005). Short (1999) typifies these waves as moderate to high (1.5 – 3 m), long period (8 – 12 s), uniform swells.

The North Pacific Ocean and Hawaiian sites are also subjected to storm waves, which are considered to be the most energetic of the wave systems (Short, 2005). These wave conditions are typically found between 40 – 60 ° North (and South), and are driven by the strong westerly wind belt. These sites are subjected to sub-polar low storms, which may produce long (10 – 14 s) waves of 2 – 3 m for 90% of the year, and waves reaching 5 – 6 m for 10% of the year (Young and Holland, 1996; Short, 1999). Southern Hemisphere swells also contribute to the North Pacific wave climate, and are more noticeable in the summer months when storms from the North Pacific are at their lowest level (Jensen, personal communication 2021, May 20).

In essence, the North Pacific Ocean and Hawaiian sites are subjected to both swell and wind sea waves throughout the year. However, well sorted swell waves dominate the wave environments due to the Pacific Ocean basin's large fetch potential and frequent storm occurrences.

#### *1.2.9.2 North Atlantic Ocean*

The reviewed North Atlantic Ocean sites (located along the U.S. East Coast) are also affected by winter east coast swells that develop from distant storms. Wave conditions consist of a mixture of locally generated wind-seas and swell conditions, especially in the fall when Northeasters dominate the meteorological conditions (Jensen, personal communication 2021, May 20). Short (1999) describes east coast waves as moderate in height (1 – 2 m), with moderate to long periods (8 – 12 s).

The North Atlantic Ocean sites are subjected to frequent summer tropical cyclone activity (Komar and Allan, 2007), which falls into the storm wave category (Figure 1.5; Figure

1.8). The impact of hurricanes along the Atlantic seaboard are likely to increase the frequency of long period swells. At the time of this dissertation, the highest confirmed wave height during an Atlantic tropical storm (Hurricane Luis), at 30 m, was experienced in September 1995 aboard the Queen Elizabeth II in the North Atlantic Ocean (The Canadian Atlas, 2004). Short (1999) describes these east coast cyclonic waves as high in height (2 – 5 m), with moderate to long periods (8 – 12 s).

Ultimately, although the North Atlantic Ocean sites are subjected to both swell and wind sea waves throughout the year, wind sea waves dominate the wave environments. Locally generated wind-seas tend to erode the coastline during spring, fall and winter, while the persistent swells occurring in the summer tend to return the sand to the beaches (Jensen, personal communication 2021, May 20).

#### *1.2.9.3 U.S. Gulf of Mexico*

The reviewed Gulf of Mexico sites fall within the protected wave environment category, as the environment is reliant on "local winds for generation of short, low seas, interspersed with long calms" (Short, 2005). Short (1999) describes these protected coastline (Figure 1.8) waves as low in height (< 0.5 m), with short periods (< 5 s). However, the Gulf of Mexico sites also experience east coast swells that enter the basin from the Atlantic Ocean.

The Gulf of Mexico shoreline also has the dubious honour of being the coastline (along with the U.S. Southeast coastline, Australia, and Eastern Asia and Africa) to experience the most hurricane landfalls across the globe (Figure 1.5). Researchers from the U.S. Naval Research Laboratory at the Stennis Space Center in Mississippi (Wang et al., 2005) measured a Gulf of Mexico wave during Hurricane Ivan (September 2004) that was 27.7 m in height ($H_{max}$). Unfortunately their sensors missed the eye of the storm, although they postulated that Hurricane Ivan may have generated $H_s$ and $H_{max}$ waves reaching 21 m and 40 m high, respectively (Wang et al., 2005). As the Gulf of Mexico is not very deep, these waves push large amounts of water inshore as storm surge, causing a significant amount of damage to coastal communities.

#### *1.2.9.4 U.S. Great Lakes*

The U.S. Great Lakes (Great Lakes) are a chain of lakes found within the northeastern U.S. They provide a unique study environment as their waves are only produced by local wind driven seas (Hubertz et al., 1991), due to short fetches and the speed of the meteorological events that do not permit long-period swells from forming. However, these wind seas can cause significant shoreline damage – Meadows et al. (1997) listed that Great Lakes shoreline protection measures cost approximately $170 million between 1972 and 1976.

#### *1.2.9.5 Study site overview*

The three key questions investigated within this work use a variety of NDBC buoy stations within the North Pacific Ocean, Hawaiian Islands, Gulf of Mexico, Great Lakes and Atlantic Ocean. Key question one reviews sites that capture a swell-dominated wave climate within the North Pacific Ocean, and wind driven seas with no swell within the Great Lakes, therefore covering the complete frequency range of surface gravity waves.

Key question two removes inconsistencies within the NDBC time series data across all available NDBC stations, therefore encompassing open and closed U.S. wave environments.

Finally, the work that examines wave power trends (key question 3) uses the corrected NDBC time series data and WIS model estimates from 29 sites. These sites are selected to sample across the open ocean U.S. wave environments: the North Pacific Ocean, the Hawaiian Islands, the Gulf of Mexico and the North Atlantic Ocean.

## 1.3 Key Questions Overview

Using the wave measurements obtained from one of the longest available time series data sets, this dissertation addresses the following key questions:

1.3.1 Are measurements from different wave measurement systems comparable?

1.3.2 Is it possible to correct for bias between different wave measurement systems to produce homogeneous long-term time series records?

1.3.3 Is wave power increasing over time?

This dissertation is organised as follows:

- Chapter 2 showcases previous comparison studies and incorporates a peer-reviewed journal paper that investigates whether measurements from different wave systems are comparable.
- Chapter 3 incorporates work from two peer reviewed journal papers that offer a correction methodology for mitigating wave measurement discontinuities that are produced from different wave measurement systems.
- Chapter 4 presents a peer reviewed journal paper that postulates that wave power is variable over time (no site-specific mean trend).
- Chapter 5 provides a general discussion and concluding remarks for chapters 2–4.

## Chapter 2

# 2. Are measurements from different wave measurement systems comparable?

### Preface:

This chapter discusses the equivalence of dissimilar wave measurement systems that allow for the spatial and temporal intercomparisons of wave measurements. Portions of this chapter have been published in a peer-reviewed journal, and are included within this chapter in the Journal of Atmospheric and Oceanic Technology format:

**Hall, C., Jensen, R.E. & Wang, D.W. 2022.** Performance evaluation of the newly operational NDBC 2.1-m hull. *Journal of Atmospheric and Oceanic Technology*. https://doi.org/10.1175/JTECH-D-21-0172.1

This chapter addresses the second key question listed in Section 1.3.1.

### 2.1 Introduction

Wave measurement systems consist of multiple components that can affect the quality of the final wave data product: the wave instrument, the hull platform, and the combination of on-board and shore-side wave data processing protocols. Theoretical and laboratory tests allow collection agencies to investigate any variance between different wave instrumentation and wave data processing protocols (Earle et al., 1984; Steele et al., 1985; Teng et al., 2009; Riley et al., 2011; Hall et al., 2018b; Riley et al., 2019). These theory and laboratory studies report that there are little variations in integral wave properties when calculated from data collected via different wave instruments and processing protocols.

Jensen et al. (2015; 2021) specifically tested wave instrumentation during a comprehensive field experiment dubbed FLOSSIE (Field Laboratory for Ocean Sea State Investigation and Experimentation). This work fundamentally tested the agreement between the majority of the wave sensors utilised by NDBC and ECCC over the previous decades. The experiment required the deployment of three NDBC sensors (a historically deployed NDBC-Inclinometer, a historically deployed NDBC-HIPPY/magnetometer, and the standard NDBC-DDWM-3DMG) and two ECCC (Canadian) sensors (a Axys-Triaxys Next Wave II Directional Wave Sensor/Wave Module and a Axys-Watchman, which is essentially a strapped down accelerometer) for five years on a single 6-m NOMAD buoy that was stationed near a reference CDIP Datawell® Directional Waverider (DWR) buoy.

Although a number of instrumentation conclusions were drawn from Jensen et al. (2021), of importance here is that they determined that there was a general agreement in concurrent bulk parameter values between the six sensors (Inclinometer, HIPPY/magnetometer, DDWM-3DMG, Axys-Triaxys, Axys-Watchman and DWR), with the historical sensors returning comparable results to the more modern wave sensors that are currently deployed by the collection agencies. Interestingly this study showcased that, when using the DWR directional data as a reference, the 6-m NOMAD buoy produced directional wave estimates with bias of 6 to 9 degrees, and RMSE of approximately 30 degrees. This is important as NOMAD hulls are boat-shaped, and oscillate to ride the waves in a bow-first direction, a motion that this author expected would introduce a larger directional bias.

Of note is that upon review of the spectral frequency data collected during the FLOSSIE project, Jensen et al. (2021) noticed that the wave sensors deployed on the 6-m NOMAD under estimated the energy captured within the high frequency wave bands in comparison with the reference DWR high frequencies. These high frequency ranges correspond to smaller wind waves and capillary waves (> 0.35 Hz), and are important considerations for model wave generation and satellite roughness validations. As these wave sensors utilised

standard processing protocols, this high frequency variability is likely due to the hull platform itself. Hence the investigation of different hull sizes on wave data estimates is an integral part of the evaluation of a wave measurement system package.

As NDBC data are used within this dissertation to investigate changes in wave power over time, the following chapter will focus entirely on the accuracy of NDBC wave measurement systems. The above studies showcase the good agreements between historical and deployed NDBC wave instruments and the 6-m NOMAD buoy platform and reference DWR stations. The following studies investigate the newly-operational NDBC 2.1-m buoy hull that is expected to become NDBC standard platform.

## 2.2 Performance evaluation of the newly operational NDBC 2.1-m hull

*The following work is published in Hall, Jensen & Wang (2022b): 'Performance evaluation of the newly operational NDBC 2.1-m hull', as cited at the top of this chapter.*

### *2.2.1 Abstract*

The importance of quantifying the accuracy in wave measurements is critical to not only understand the complexities of wind-generated waves, but imperative for the interpretation of implied accuracy of the prediction systems that use these data for verification and validation. As wave measurement systems have unique collection and processing attributes that result in large accuracy ranges, this work quantifies bias that may be introduced into wave models from the newly operational NOAA National Data Buoy Center (NDBC) 2.1-m hull. Data quality consistency between the legacy NDBC 3-m aluminium hulls and the new 2.1-m hull is compared to a relative reference, and provides a standardised methodology and graphical representation template for future intra-measurement evaluations. Statistical analyses and wave spectral comparisons confirm that the wave measurements reported from the NDBC 2.1-m hulls show an increased accuracy from previously collected NDBC 3-m hull wave data for significant wave height and average wave period, while retaining consistent accuracy for directional results,

purporting that hull size does not impact NDBC directional data estimates. Spectrally, the NDBC 2.1-m hulls show an improved signal-to-noise ratio, allowing for increase in energy retention in the lower frequency spectral range, with an improved high frequency spectral accuracy above 0.25 Hz within the short seas and wind chop wave component regions. These improvements in both NDBC bulk and spectral data accuracy provide confidence for the wave community's use of NDBC wave data to drive wave model technologies, improvements and validations.

### *2.2.2 Introduction*

Many researchers and engineers who are concerned with ocean conditions for construction, navigation, sediment transport, climate change, community resilience, and risk assessment studies, use the National Oceanic and Atmospheric Administration (NOAA) National Data Buoy Center (NDBC) in situ operational buoy wave and wind measurements for validation and interpretation of their air-ocean-wave prediction systems (e.g. Rogers et al., 2002; Rogers and Wang, 2006; Ortiz-Royero and Mercado-Irizarry, 2008; Hanson et al., 2009; Jensen et al., 2012; Rogers et al., 2014; Stopa and Cheung, 2014; Stopa and Mouche, 2016; Bryant and Jensen, 2017; Jensen et al., 2017; Rogowski et al., 2021; Jensen et al., 2021). In particular, the U.S. Army Corps of Engineers (USACE) use site specific NDBC buoy measurements to validate and verify their model and prediction products, including their long-standing Wave Information Study (WIS), their Steady State Spectral Wave (STWAVE), and their Coastal Modeling System (CMS). In addition, the USACE use NDBC wave measurements as boundary conditions to drive all offshore and nearshore wave model technologies, and as drivers for model improvements. However, all wave measurement systems have unique collection and processing attributes that result in large accuracy ranges (Cavaleri et al., 2018; Ardhuin et al., 2019b). In fact, Gemmrich et al. (2011) identified buoy instrumentation and platform modifications as introducers of variability in wave measurements. Therefore, to correctly estimate the long-term U.S. wave climate, analogous wave measurements from in situ observation platforms are essential for the continued and accurate assessment of wave and ocean modelling estimates.

Since the 1980's, NDBC have routinely deployed their ocean observing systems on legacy NDBC 3-m aluminium hulls (NDBC, 2016; Bouchard and Jensen, 2019; NDBC, 2020d). Recently, Kohler et al. (2015), Bouchard et al. (2017) and Hall et al. (2018a) introduced NDBC's new modular Self-Contained Ocean Observing Payload (SCOOP). To house this new instrumentation package, NDBC developed a 2.1-m foam hull that is specifically designed to contain the "plug and play" SCOOP (Hall et al., 2018b). In 2019 NDBC commissioned this 2.1-m foam hull into operational use, and it is this smaller, lighter hull (~492 kg vs ~1,720 kg 3-m aluminium hull) that is evaluated by proxy within these wave parameter analyses.

The USACE mission is primarily concerned with the impacts of the wave climate on coastal flooding and navigation, which is critical for risk-based management, climate change and community resilience. To ensure wave data quality consistency between the legacy NDBC 3-m aluminium hulls and the newly operational NDBC 2.1-m hull, we evaluate and validate the performance of wave measurements of the newly operational NDBC 2.1-m hull, in particular, the wave energy spectra data of long-period swells (important in Pacific and Atlantic Ocean) and short-period wind seas (especially vital within the Great Lakes). Of the available 2.1-m hull evaluation sites, two were chosen to broadly highlight distinct wave environments that cover the entire frequency range of wind generated surface gravity waves. A Great Lakes site (NDBC station 45001) showcases locally generated wind sea conditions, while a Pacific Ocean site (NDBC station 46029) captures west coast swell waves with large fetch. The paper is organised as follows. Section 2 gives a description of the evaluation methodology and statistical analyses, including a brief overview of NDBC and CDIP wave spectral parameters. In Section 3, the results of the evaluation are discussed, with an overall performance determination summary in Section 4.

### *2.2.3 Performance evaluation methods*

Figure 2.1 depicts the hull types under evaluation: the newly operational NDBC 2.1-m foam hull; the legacy NDBC 3-m aluminium hull; and an independent reference, the

Scripps Institution of Oceanography's (SIO) Coastal Data Information Program (CDIP, http://cdip.ucsd.edu/) Datawell WaveRiders® (DWR). Due to nonuniformity in periods of records, as per O'Reilly et al. (1996) we evaluate the non-concurrent NDBC 2.1-m and 3-m hull performances in relation to an independent reference buoy, the CDIP DWR (ACT, 2007, 2012; Luther et al., 2013; Jensen et al., 2021).

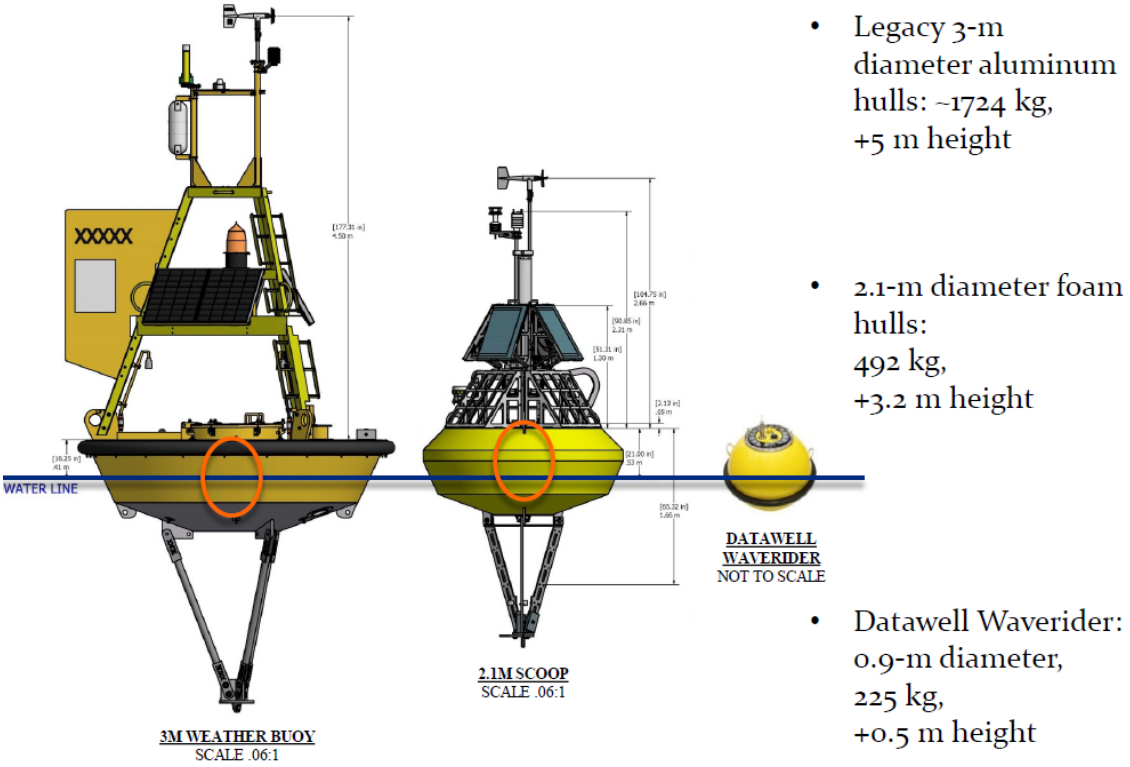


Figure 2.1. NDBC platform comparisons for a 3-m aluminium discus buoy, a 2.1-m foam hull SCOOP buoy and a Datawell Waverider®. The orange circles highlight the location of the DDWM 3D wave measurement system (Hall et al, 2018a; with schematic credit to Eric Gay, NDBC).

Of note is the weight and superstructure height differences between the hulls (3-m aluminium hull: ~1724 kg and ~5 m height; 2.1-m foam hull: ~492 kg and ~3.2 m height; and DWR: ~225 kg and ~0.5 m height). The size and shape of the buoy hull may determine the primary response nature of the buoy as either a surface-following or particle-following buoy. CDIP's smaller size and shape results in a wave particle-following response for wave measurements, as it follows and measures the wave orbital motions (x, y, z). On the other hand, NDBC 3-m and 2.1-m hulls are processed as surface-following buoys (i.e. heave,

and two slopes). In an effort to isolate the hull effects, evaluation sites were selected where the target NDBC 2.1-m hull and earlier 3-m hull wave data were collected using the same directional wave measurements system, the NDBC Digital Directional Wave Module (DDWM) version 3.04 and a tri-axial MicroStrain® 3DM-GX1 motion sensor (herewith referred to as DDWM; Teng et al., 2009, Riley et al., 2011).

Of the available 2.1-m hull evaluation sites, two were chosen to broadly highlight distinct wave environments that cover the entire frequency range of wind generated surface gravity waves. A Great Lakes site (NDBC station 45001 and CDIP DWR 230/WMO 45180) showcases locally generated wind sea conditions, while a Pacific Ocean site (NDBC station 46029 and CDIP DWR 179/WMO 46248) captures west coast swell waves with large fetch potential. Evaluation site details are listed in Table 2.1.

Table 2.1. Evaluation sites

| Site | Station | Location (DD) | Depth (m) | Distance from co-located station | 3-m hull comparison data dates | 2.1-m hull comparison data dates |
|---|---|---|---|---|---|---|
| Great Lakes (Lake Superior) | NDBC 45001 | 48.061 N 87.793 W | 247 | 3 nm NW of 230 | May-Oct 2017<br>May, Sept-Oct 2018 | May-Nov 2019<br>Aug-Oct 2020<br>Jun-Jul 2021 |
| | CDIP 230 | 48.034 N 87.730 W | 239 | 3 nm SE of 45001 | May-Oct 2017<br>May-Oct 2018<br>Aug-Oct 2020<br>Jun-Jul 2021 | |
| Pacific Ocean (west of the Columbia River Mouth) | NDBC 46029 | 46.143 N 124.485 W | 134 | 7 nm E of 179 | Aug 2012–Aug 2015<br>Sep 2015-Feb 2017<br>May 2017-Aug 2018<br>Aug 2018-May 2020 | May, Sep-Oct 2020<br>May-Jun 2021 |
| | CDIP 179 | 46.133 N 124.644 W | 181 | 7 nm W of 46029 | Apr 2011-Dec 2012<br>Feb-Nov 2013<br>Jan-Oct 2014<br>Aug 2017-Oct 2019<br>Dec 2019-Aug 2020<br>Sep 2020-Jun 2021 | |

NDBC deployed a 2.1-m foam hull at NDBC 45001 in May 2019, replacing the previously deployed NDBC 3-m aluminium hull. For the Pacific site, in May 2020 NDBC exchanged the 3-m aluminium hull at NDBC station 46029 with a 2.1-m foam hull, both with a seal cage adaptation, which is standard for all NDBC Pacific ocean buoys. Co-located and concurrent Great Lakes NDBC 45001 and CDIP 230 data are available for 2017 – 2018

for the 3-m aluminium hull, pre-2.1-m hull comparison datasets, and 2020 – 2021 for the 2.1-m hull deployed dataset comparisons (Table 2.1). Similarly, 3-m aluminium hull, pre-2.1-m hull comparison datasets are available for 2011 – 2020 for the Pacific Ocean NDBC 46029 and CDIP 179, and 2020 – 2021 for the 2.1-m hull comparison datasets (Table 2.1).

Table 2.2. Wave measurement system characteristics (adapted from Jensen et al., 2021)

| Wave system | Sensor type | Sample freq. (Hz) | Sample duration (s) | Samples | No. freq. bands | Freq. min (Hz) | Freq. max (Hz) | Transmit minute | Time stamp (min) |
|---|---|---|---|---|---|---|---|---|---|
| DDWM | Tri-Axial Motion 3DMG | 1.7066 | 1200 / 600 | 2048 / 1024 | 46 | 0.0200 | 0.485 | 50 | 00 |
| DWR | Datawell HIPPY | 1.28 | 1600 | 2048 | 64 | 0.0250 | 0.5800 | 30 | 24/25 |

As mentioned, the 2.1-m hull and earlier 3-m hull wave data at each NDBC site were collected using only the DDWM. The CDIP reference buoys compared within these analyses employ a DWR MkIII, which contain a gimballed Datawell HIPPY. The NDBC DDWM and CDIP DWR systems have different sampling strategies (Table 2.2). NDBC systems transmit wave messages on the hour for wave measurement data that are collected between minutes 20 and 40. DWR systems report wave messages every 30 minutes with wave calculations that cover a 28 minute sample length. The institutional time stamps of CDIP and NDBC also differ as CDIP's time stamp is the start of the sampling period and NDBC is the end. The DDWM utilises 46 frequency bands (0.0325 – 0.4850 Hz; the 0.02 Hz frequency is not used for calculating any wave parameters), while the DWR MkIII exploits 64 (0.0250 – 0.5800 Hz). Due to the different frequency ranges, low and high DWR non-directional spectral energy frequency bands were truncated (to match 0.0325 – 0.4850 Hz) and the remaining spectrum linearly interpolated (using the function interp1 in the R pracma v1.9.9 package) to remain consistent with the NDBC data.

Earle et al. (1984, 1999), along with Steele et al. (1985, 1992), NDBC (2003), Riley et al. (2011), and Riley and Bouchard (2015) comprehensively described NDBC's methodology, applied calibration techniques and processing protocols for non-directional and directional wave measurements. While NDBC develops and maintains their own wave

measurement systems, calibration techniques and processing protocols, CDIP utilises inherent Datawell methodology. Of interest here are differences in the calculation of NDBC and CDIP Datawell data products, as detailed by Earle et al. (1999) and Jensen et al. (2021).

NDBC and CDIP deliver wave elevation spectral variances, *S(f)*, as non-directional spectral frequency *E(f)* (*C11(f)* in NDBC nomenclature) and the four Fourier directional parameters. CDIP estimates and publishes non-directional ($a_0$, where $a_0 = \frac{E(f)}{\pi}$ ) and directional Fourier coefficients ($a_1$, $a_2$, $b_1$ and $b_2$) directly for public use, while NDBC wave measurement systems convert these Fourier coefficients into directional functions ($\alpha_1, \alpha_2$) and spreading functions ($r_1, r_2$) before transmitting wave messages to shore (NDBC, 2003). In this study, CDIP $a_0$ , $a_{1,2}$ and $b_{1,2}$ data were converted into NDBC standard non-directional spectral energy, $C_{11}(f)$, $\alpha_1(f)$ and $\alpha_2(f)$ (mean and principal wave directions in clockwise degrees from true North), and directional spectral spreading, $r_1(f)$ and $r_2(f)$ (non-dimensional first and second normalised polar coordinates of the Fourier coefficients, respectively).

On shore, both NDBC and CDIP derive significant wave height ($H_{m0}$) from the zeroth moment ($m_0$) of the energy spectrum, $H_{m0} = 4\sqrt{m_0}$, to approximate the average of the highest 1/3 of the waves from trough to crest. NDBC and CDIP define $m_0 = \sum_{f_1}^{f_u}\big(E(f) \cdot d(f)\big)$, where spectral density *E(f)* is summed "over all frequency bands, from the lowest frequency $f_l$ to the highest frequency, $f_u$, of the nondirectional wave spectrum and *d(f)* is the bandwidth of each band" (NDBC, 2018a; CDIP, 2021a). Average wave period, $T_a = \sqrt{\frac{m_0}{m_2}}$ (NDBC, 2018a) is the square root of the zeroth moment divided by the second moment of the reported energy spectrum, where NDBC (2018a) defines $m_2 = \sum_{f_1}^{f_u}(E(f) \cdot d(f) \cdot f^2)$. Conversely, CDIP derives the average wave period from the "zeroth moment divided by the first moment of the reported energy spectrum" (CDIP, 2021a). For comparative purposes during these analyses, these data were recalculated using the same NDBC moment methodology for consistency.

CDIP also publishes peak directional spread, $\sigma(f_m)$, where $f_m = \frac{1}{T_p}$. $T_p$ is the "period corresponding to the frequency band with the maximum value of spectral density in the nondirectional wave spectrum" (NDBC, 2018a) and mean wave direction at peak frequency ($\alpha_m(f_m)$), where $\sigma(f_m) = \sqrt{2\left\{\left(1 - \left(a_1^2(f_m) + b_1^2(f_m)\right)^{\frac{1}{2}}\right)\right\}}$ and $\alpha_m(f_m) = \left\{\frac{b_1(f_m)}{a_1(f_m)}\right\}$ (adapted from O'Reilly et al., 1996; Jensen et al., 2021). From these equations, we calculate comparative NDBC peak spread using $r_1$ at the peak frequency: $\sigma(f_m) = \sqrt{2\left(1 - r_1(f_m)\right)}$, converted to sigma from alpha, i.e. from counter-clockwise from the east to the WMO (1988) convention of direction measured from true north (Earle et al., 1999; NDBC, 2003). To remove shore-side processing effects and remain consistent with NDBC peak directional spread ($\sigma_p$) and mean wave direction at peak frequency ($\alpha_m$), CDIP $\sigma_p$ and $\alpha_m$ were recalculated as follows: $\alpha = \tan^{-1}\left(\frac{b_1}{a_1}\right)$ and $\sigma = [2(1 - M_1)]^{\frac{1}{2}}$, where $M_1 = (a_1^2 + b_1^2)^{\frac{1}{2}}$ (adapted from O'Reilly et al, 1996).

Although the majority of these definitions and equations are equivalent, the number of frequencies utilized by both systems are different. To remove bias, $H_{m0}$ and $T_a$ bulk parameters were recalculated (using the formulas above) from NDBC and CDIP frequency spectral estimates, where CDIP frequencies were truncated and interpolated to match the available NDBC frequencies. To account for directional energy captured within the higher CDIP frequencies (> 0.485), directional peak spreading and mean direction ($\sigma$, $\theta_{mean}$) were recalculated utilising the original frequency ranges provided by the individual NDBC and CDIP sensors (Table 2.2). Directional peak spreading was converted from radians to degrees for plotting purposes. Outliers were removed using limits and quality controls (QC), adapted from NDBC QC protocols (NDBC, 2003).

The following goodness of fit statistical analyses tested the relationship between the co-located 3-m, 2.1-m and DWR datasets: root mean square errors, $RMSE = \sqrt{\frac{1}{2}\sum_{r=1}^{R}\left(\hat{\psi}_r - \psi\right)^2}$ and bias, $bias = \frac{1}{R}\sum_{r=1}^{R}\left(\hat{\psi}_r - \psi\right)$, where "$R$ is the number of replications, $\psi$ is the true population parameters, and $\hat{\psi}_r$ is the sample estimate for the $r$th dataset analyzed" (Sigal and Chalmers, 2016). Relationship strength between the co-located samples are estimated by means of Pearson correlation coefficients, $r = \frac{\sum xy}{\sqrt{\sum x^2 \sum y^2}}$ (Zar, 1984), where 1.0 indicates a strong positive correlation. A simple linear regression method tests the trends of the datasets, $Y_i = A + BX_i$, where $X$ is the independent variable, $Y$ is the dependent variable, $A$ is the intercept, and $B$ is the slope, including an associated $R^2$ to quantify regression variability (Zar, 1984), while locally weighted scatterplot smoothing (LOWESS) regressions visually showcase a smooth curve that fits the data points, $\sum_k w(x_k)\, G(x_k)(y_k - A - Bx_k)^2$ for $k$ = 1,…,$N$, where the robust weighting functions, $w(x_k)G(x_k)$ and regression smoothing, $y_k - A - Bx_k$, are calculated for each data point (Cleveland, 1979).

When considering directional results, mean wave direction at peak frequency vectors were separated into their respective north and east vector components, $X = cos\ \alpha_1(f_m)$ and $Y = sin\ \alpha_1(f_m)$ (NDBC, 2003) before bias and RMSE amplitude and direction statistical calculations. Similarly for comparison plotting purposes, possible heading variations in mean wave direction at peak frequency ($\alpha_m$) around the 0-360 modulo cut points were also accounted for by remapping the data using their X and Y components and inferring the angles (Kelley, 2018).

### *2.2.4 Results and Discussion*

Intercomparisons between systems form the basis of NDBC published accuracy standards and sensors (Bouchard et al., 2017). NDBC reported accuracy readings (NDBC, 2003; NDBC, 2017) are listed as ± 0.2 metres (m) for $H_{m0}$, ± 1.0 seconds (s) for $T_a$, and ± 10 degrees for mean wave direction ($\theta_m$). Analyses were performed using R software (R Core Team, 2021; RStudio Team, 2021) and the WavEval Wave Spectra Comparison Tool,

v2.0 (WavEval), a spectral comparison tool co-developed by CDIP and the U.S. Army Corps of Engineers, Engineer Research & Development Center, Coastal and Hydraulics Laboratory (ACT, 2007; Jensen et al., 2011).

For comparison purposes, Great Lakes NDBC 45001 data were subset to isolate 3-m and 2.1-m hull data with their co-located and concurrent CDIP 230 DWR data (Table 2.1). Pacific Ocean NDBC 46029 3-m and 2.1-m hull data with associated CDIP DWR 179 data were treated in the same manner (Table 2.1).

#### *2.2.4.1 Wave height and period*

Historically significant wave height ($H_{m0}$) and average wave period ($T_a$) results are typically robust for NDBC wave data collection (e.g. O'Reilly et al., 1996; Bouchard et al., 2017; Hall et al., 2018a; Jensen et al., 2021). That pattern is evident within the results from this study (Table 2.3) as the statistical comparisons meet published NDBC accuracy standards of ± 0.2 m for $H_{m0}$ and ± 1.0 seconds (s) for $T_a$ (NDBC, 2003; NDBC, 2017). Following the practice of O'Reilly et al. (1996), comparison $H_{m0}$ datasets return stable Pearson correlation coefficients ($r_{hull\text{-}size}$) of $r_{3\text{-}m}$ and $r_{2.1\text{-}m}$ = 0.993 and reduced 2.1-m hull bias for the Great Lakes site (3-m hull observations [$Obs_{3\text{-}m}$] = 4284; $Obs_{2.1\text{-}m}$ = 2173) when compared to co-located CDIP DWR data. The Pacific Ocean site (Table 2.3) also shows stable correlation coefficients with $r_{3\text{-}m}$ = 0.982 and $r_{2.1\text{-}m}$ = 0.973 and improved RMSE and bias for the 2.1-m deployment ($Obs_{3\text{-}m}$ = 20543; $Obs_{2.1\text{-}m}$ = 2645). Similarly matching Pearson correlations estimates are visible in $T_a$ evaluations of $r_{3\text{-}m}$ = 0. 962 and 0.960 and $r_{2.1\text{-}m}$ 0.969 and 0.959 for the same Great Lakes and Pacific Ocean datasets, respectively (Table 2.3).

Of interest is the slight improvement in bias and linear regression between the $H_{m0}$ and $T_a$ 3-m hull and subsequent 2.1-m hull analyses (Table 2.3; Figure 2.2; Figure 2.3) when compared to co-located CDIP DWR data at both sites. The Great Lakes $H_{m0}$ bias decreased from 0.073 m to 0.060 m (Table 2.3), and the linear regression intercept changes from -0.051 to -0.039 (slope change of 0.969 to 0.971). Variability is well explained using this

linear regression model ($R^2$ of 0.99 for both 3-m and 2.1-m hull datasets). The Pacific Ocean site returns improvements in $H_{m0}$ bias from 0.070 m to 0.016 m (Table 2.3), and $H_{m0}$ linear regression intercept of 0.966 to 0.986 (Table 2.3).

Table 2.3. Goodness of fit statistical results between the NDBC data and the concurrent, co-located DWR data for the Great Lakes and Pacific Ocean sites. NDBC* refers to NDBC published accuracy standards (NDBC, 2003; NDBC, 2017)

| Variable | Hull | No. Obs. | Correlation coefficient (r) | RMSE | Bias | Mean | Intercept | Slope | $R^2$ |
|---|---|---|---|---|---|---|---|---|---|
| $H_{m0}$ (m) NDBC*: ± 0.2 m | Great Lakes (NDBC 45001 vs CDIP DWR 230) | | | | | | | | |
| | 3-m /DWR | 4284 | 0.993 | 0.097 | 0.073 | 0.644 | -0.051 | 0.969 | 0.986 |
| | 2.1-m /DWR | 2173 | 0.993 | 0.091 | 0.060 | 0.709 | -0.039 | 0.971 | 0.985 |
| | Pacific Ocean (NDBC 46029 vs CDIP DWR 179) | | | | | | | | |
| | 3-m /DWR | 20543 | 0.982 | 0.246 | 0.070 | 2.323 | 0.010 | 0.966 | 0.964 |
| | 2.1-m /DWR | 2645 | 0.973 | 0.153 | 0.016 | 1.683 | 0.008 | 0.986 | 0.948 |
| $T_a$ (s) NDBC*: ± 1.0 s | Great Lakes (NDBC 45001 vs CDIP DWR 230) | | | | | | | | |
| | 3-m /DWR | 4284 | 0.962 | 0.296 | 0.203 | 3.494 | 0.682 | 0.859 | 0.926 |
| | 2.1-m /DWR | 2173 | 0.969 | 0.244 | 0.117 | 3.482 | 0.547 | 0.874 | 0.939 |
| | Pacific Ocean (NDBC 46029 vs CDIP DWR 179) | | | | | | | | |
| | 3-m /DWR | 20543 | 0.960 | 0.686 | 0.464 | 7.258 | 0.716 | 0.843 | 0.922 |
| | 2.1-m /DWR | 2645 | 0.959 | 0.516 | 0.354 | 6.383 | 0.591 | 0.856 | 0.920 |
| $\sigma_p$ (degrees) | Great Lakes (NDBC 45001 vs CDIP DWR 230) | | | | | | | | |
| | 3-m /DWR | 4666 | 0.600 | 13 | 4 | NA | NA | NA | 0.360 |
| | 2.1-m /DWR | 2398 | 0.544 | 14 | 5 | NA | NA | NA | 0.296 |
| | Pacific Ocean (NDBC 46029 vs CDIP DWR 179) | | | | | | | | |
| | 3-m /DWR | 20699 | 0.229 | 18 | 13 | NA | NA | NA | 0.053 |
| | 2.1-m /DWR | 2646 | 0.241 | 16 | 13 | NA | NA | NA | 0.058 |
| $\alpha_p$ (degrees) NDBC*: ± 10˚ | Great Lakes (NDBC 45001 vs CDIP DWR 230) | | | | | | | | |
| | 3-m /DWR | 4666 | 0.772 | 45 | 52 | NA | NA | NA | 0.597 |
| | 2.1-m /DWR | 2398 | 0.724 | 45 | 26 | NA | NA | NA | 0.524 |
| | Pacific Ocean (NDBC 46029 vs CDIP DWR 179) | | | | | | | | |
| | 3-m /DWR | 20699 | 0.708 | 45 | 14 | NA | NA | NA | 0.501 |
| | 2.1-m /DWR | 2646 | 0.577 | 45 | 58 | NA | NA | NA | 0.332 |

Figure 2.2 shows that the Great Lakes 3-m and 2.1-m hull $H_{m0}$ both register as slighter lower than the co-located and concurrent CDIP DWR wave measurements (both integrated directly from spectral data to negate any institutional processing and quality controls edits). However, as this does not occur at the Pacific Ocean site (Figure 2.2), this causation is not due to on-board sensor differences between the DWR HIPPY vs NDBC 3D-MG. As the Great Lakes is a wind-wave dominated climate, this offset is due to a hull-size sensitivity variations between the smaller 0.9-m CDIP DWR buoys and the larger NDBC 3-m and 2.1-m hulls. Additionally, these effects are amplified by the NDBC processing protocols that remove any spurious energy identified in frequencies below the

sampling period specific noise frequency cut-off (approximately 0.18 Hz, ~ 5 seconds; NDBC, 2011). This protocol is implemented due to the amplitude of low-frequency noise after integral conversion of acceleration to displacement. In fact, as a rule NDBC does not publish any peak wave period and mean wave direction data that are associated with significant wave heights below 0.25 m (NDBC, 2003).

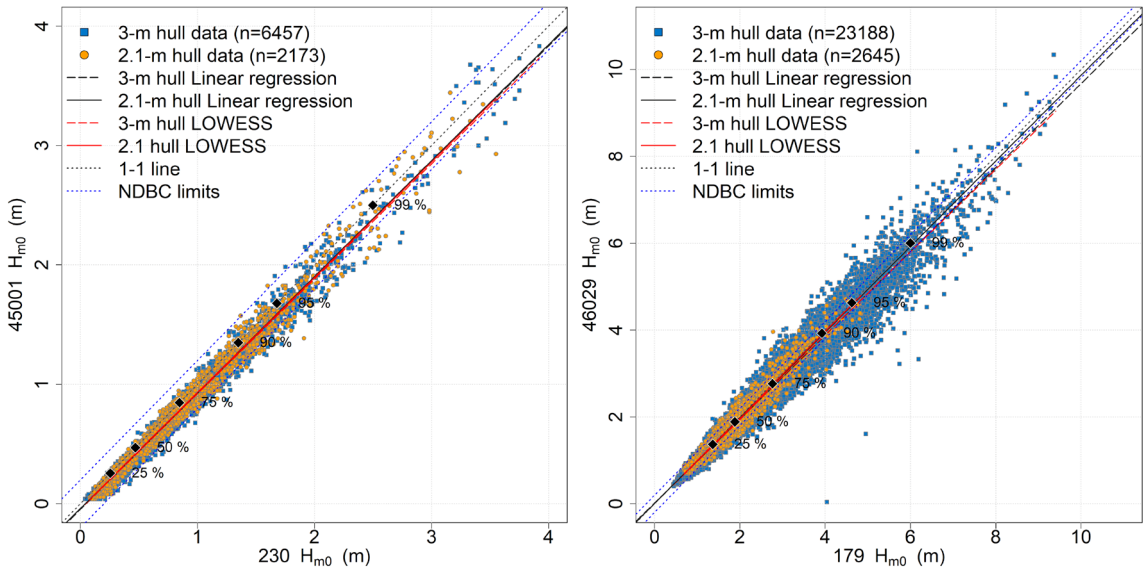


Figure 2.2. Scatter diagrams of the 3-m (blue points) vs 2.1-m hull (orange points) $H_{m0}$ data for the Great Lakes NDBC station 45001 and CDIP 230 (left) and Pacific Ocean NDBC station 46029 and CDIP 179 (right). 3-m (dashed) vs 2.1-m (solid) hull linear (grey) and locally weighted scatterplot smoothing (red LOWESS) regressions highlight trends. Black diamonds indicate 2.1-m hull data percentiles, and sit on a dashed, grey one-to-one line for alignment reference. Blue dotted lines represent the NDBC $H_{m0}$ accuracy limits of ±0.2 m.

Figure 2.2 shows that in the Pacific Ocean, the NDBC 2.1-m and 3-m $H_{m0}$ data match well to their concurrent, collocated CDIP DWR $H_{m0}$ data. Delving deeper into the $H_{m0}$ datasets collected during the 2.1-m hull deployments (Table 2.1), Figure 2.3 shows the 3-m and 2.1-m hull vs. the CDIP DWR $H_{m0}$ difference vs. sea state (top) and $T_a$ difference vs. average period (bottom), where both are normalised by the CDIP DWR data. The 3-m hull and 2.1-m hull vs their respective CDIP DWR datasets show similar LOWESS regression trends in both Great Lakes and the Pacific Ocean for both $H_{m0}$ and $T_a$, with a slight improvement in the Great Lakes $T_a$ trend for wave periods less than 5 s. The Great Lakes

$H_{m0}$ and $T_a$ both show an increase in data scatter during low wave height and period conditions, regardless of hull type deployed. These low wave sea states are not found within the Pacific Ocean's swell-dominated wave climate.

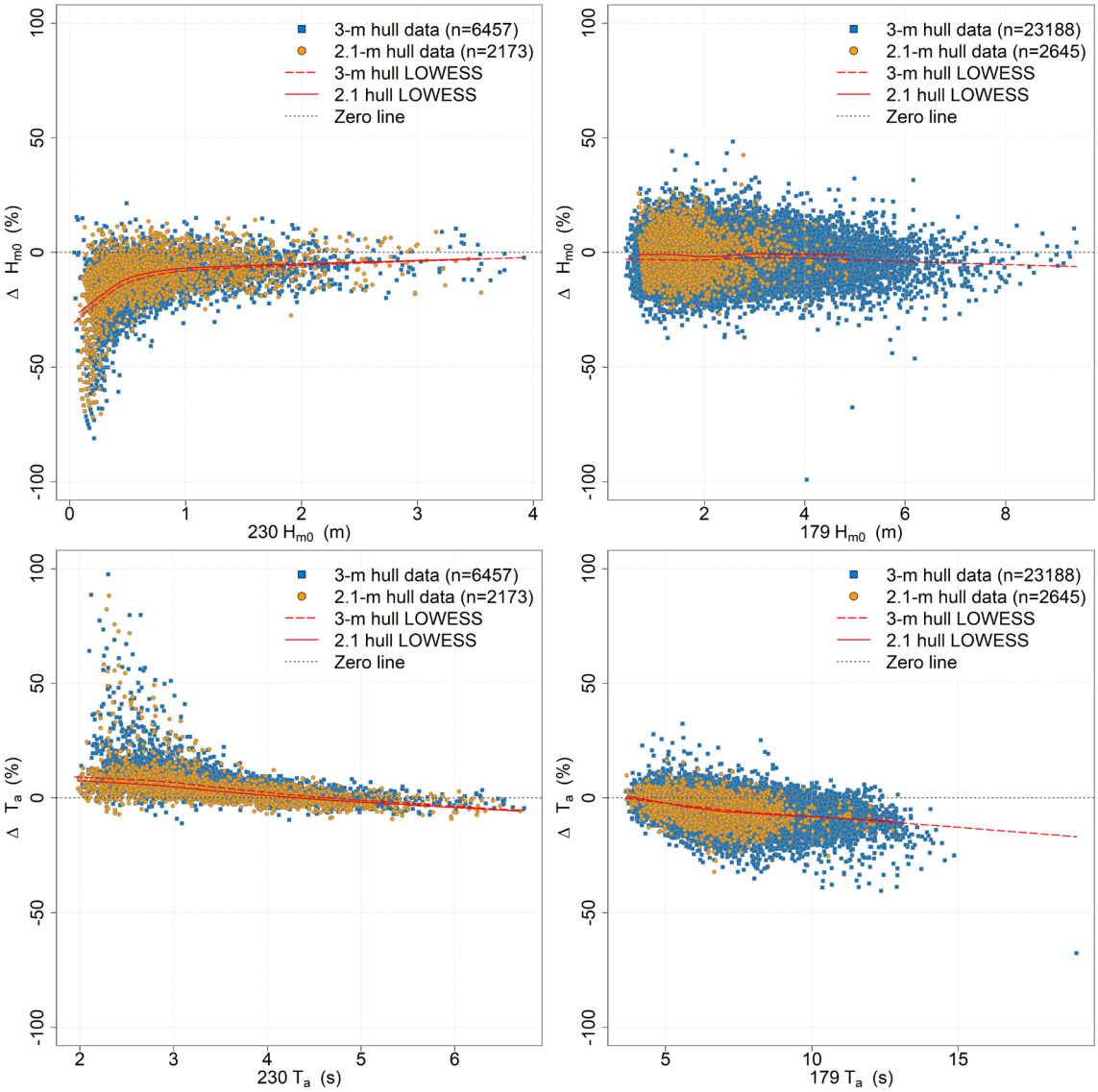


Figure 2.3. Scatter diagrams of the 3-m (blue points) vs 2.1-m hull (orange points) $H_{m0}$ (top) and $T_a$ (bottom) percent difference between concurrent NDBC and CDIP data, when compared to CDIP data for the Great Lakes NDBC 45001 and CDIP 230 (left) and Pacific Ocean NDBC 46029 and CDIP 179 (right). 3-m (dashed) vs 2.1-m (solid) hull locally weighted scatterplot smoothing (LOWESS; red) regressions highlight trends. All plots include a dotted grey zero line.

Figure 2.3 confirms that the previously identified good $H_{m0}$ correlations (Figure 2.2) are associated with relatively small wave height conditions. During these sampling periods, the majority of the significant wave heights ranged between 0 – 1.5 m (~2 – 5 s $T_a$) within the Great Lakes and 0 – 2.5 m (~4 – 8 s $T_a$) in the Pacific Ocean (Figures 3).

Figure 2.3 highlights the importance of 2.1-m hull evaluations across multiple regions that represent different wave conditions. However, as USACE are concerned with wave development in modelling scenarios, of particular interest is the NDBC 2.1-m hull data performance when compared to the previous 3-m hull and reference CDIP DWR data across the full range of spectral frequencies. Investigating this offset further on a spectral level, bias and RMSE of average wave height as a function of wave frequency and energy on the co-located binned spectral $C_{11}(f)$ data (Figure 2.4 and Chapter 2's Appendix 2.2.6.1: Figure 2.14) are considered.

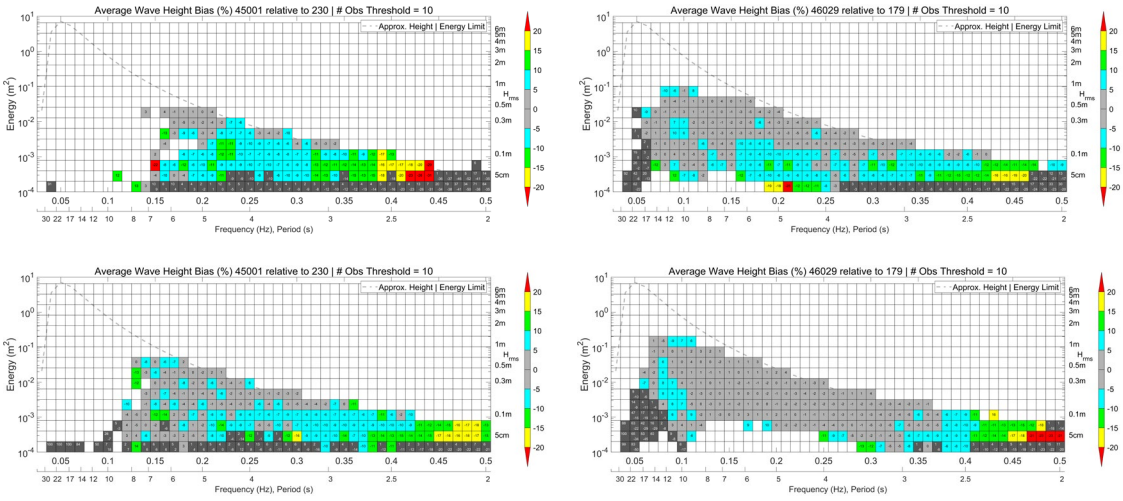


Figure 2.4. One month of CDIP DWR versus NDBC 3-m hull (top left: August 2017 for the Great Lakes, and top right: August 2019 for the Pacific Ocean) and 2.1-m hull data (bottom left: September 2020 for the Great Lakes, and bottom right: June 2021 for the Pacific Ocean) average wave height bias (in %) binned per CDIP frequency bands. Colours represent categorised bias values, where grey = ± 0-5 %; blue = ± 5-10 %; green = ± 10-15 %; yellow = ± 15-20 %; and red = > ± 20 %. White bins indicate no comparable data.

Average percent wave height bias and RMSE are binned per NDBC frequency bands, where colours represent categorised bias and RMSE values. In essence, an increase in the number of grey colour bins between the 3-m and 2.1-m bias plots indicates an improvement between hull types. One month's worth of 3-m hull (August 2017 for the Great Lakes and August 2019 for the Pacific Ocean) and 2.1-m hull data (September 2020 for the Great Lakes and June 2021 for the Pacific Ocean) were subset with their concurrent, co-located CDIP DWR data samples for testing.

These plots were created using the WavEval Wave Spectra Comparison Tool (WavEval), v2.0 (ACT, 2007; Jensen et al., 2011). WavEval applies its own interpolation process to the NDBC data to match the CDIP frequencies, which is opposite to all of the other results shown here, where CDIP frequencies were matched to the NDBC frequency data for NDBC, not CDIP, evaluation purposes.

Of note is the improvement in bias values across the spectral range between the 3-m hull and 2.1-m hull data vs their co-located and concurrent CDIP DWR values for both the Great Lakes and Pacific Ocean sites (Figure 2.4). Between 0.18 Hz (the approximate frequency below which NDBC low-frequency noise filters are applied) and 0.485 (the highest frequency of NDBC data collection), the percentage of bias bins above 5 % reduces from 60 % to 53 % in the Great Lakes (Figure 2.4, left), and 51 % to 32 % in the Pacific Ocean (Figure 2.4, right). The scattered, higher than 5% bias throughout the frequencies are related to slight temporal and spatial variations in the co-located datasets. The Great Lakes WavEval results highlight the increase in low frequency energy evident within the 2.1-m hull dataset than in the 3-m hull datasets (Figure 2.4). Again these results indicate a better signal-to-noise response of the 2.1-m hull. Also evident is the Pacific Ocean wave climate, where the swell energy is dominant, and the 2.1-m data matches the CDIP DWR data over a broader frequency range than the 3-m data. Considering wave height RMSE, with bias removed (Chapter 2's Appendix 2.2.6.1: Figure 2.14), highlights the low frequency noise (below 0.18 Hz) disparity between the NDBC and CDIP protocols, as discussed above.

Another good test to evaluate hull performance is the agreements and deviations from unity (zero in this case) of the spectral wave energy densities ($C_{11}$) and uncorrected acceleration values ($C_{11}^m$) across the standard NDBC 0.020 - 0.485 Hz frequencies. Delving deeper into the spectral signals, mean $C_{11}$ and $C_{11}^m$ data, with their associated ratios (red lines in the top plots, and again replotted against each other as blue and orange lines in the bottom left plots to visually showcase the 2.1-m hull ratio improvements) were examined for August 2017 (3-m hull data) and September 2020 (2.1-m hull data) in the Great Lakes (Figure 2.5), and August 2019 (3-m hull data) and June 2021 (2.1-m hull data) in the Pacific Ocean (Figure 2.6). These dates were selected to incorporate a full month of data into each analysis (~717-745 hourly samples).

While deviations between the co-located low frequency signals (less than 0.18 Hz) may be attributed to noise (NDBC, 2011), the high frequency tail of the NDBC $c_{11}$ spectra (indicated by orange lines in the top plots in Figure 2.5 and Figure 2.6) at both locations show more agreement with the concurrent CDIP DWR frequency values (blue lines within the top plot in the figures). As these improvements are mainly evident in the short sea and wind chop spectral wave components (denoted by 'e' and 'f' in the figures), they indicate that the small, more lightweight 2.1-m hull is able to detect higher frequency wave signals than the previous 3-m and larger NDBC hulls. This determination is supported by the improved ratios between the 2.1-m NDBC and CDIP DWR data (bottom left plots in the figures), and is particularly enhanced in the high frequency tail deviations within the 3-m and 2.1-m hull $C_{11}^m$ comparison plots (bottom right plots in the figures). Of interest is that both sites show a 2.1-m hull $C_{11}^m$ data improvement across the spectrum, even though these NDBC 3-m and 2.1-m data are from different time periods. Of particular note is the reduction of noise in the lower frequencies ranges below 0.05 Hz, indicating that the 2.1-m hull is introducing less hull and sensor noise into the spectral signals. This indicates that the lighter and small 2.1-m buoy hull has a better heave acceleration response and thus has a better signal to noise ratio of acceleration data for low-frequency waves.

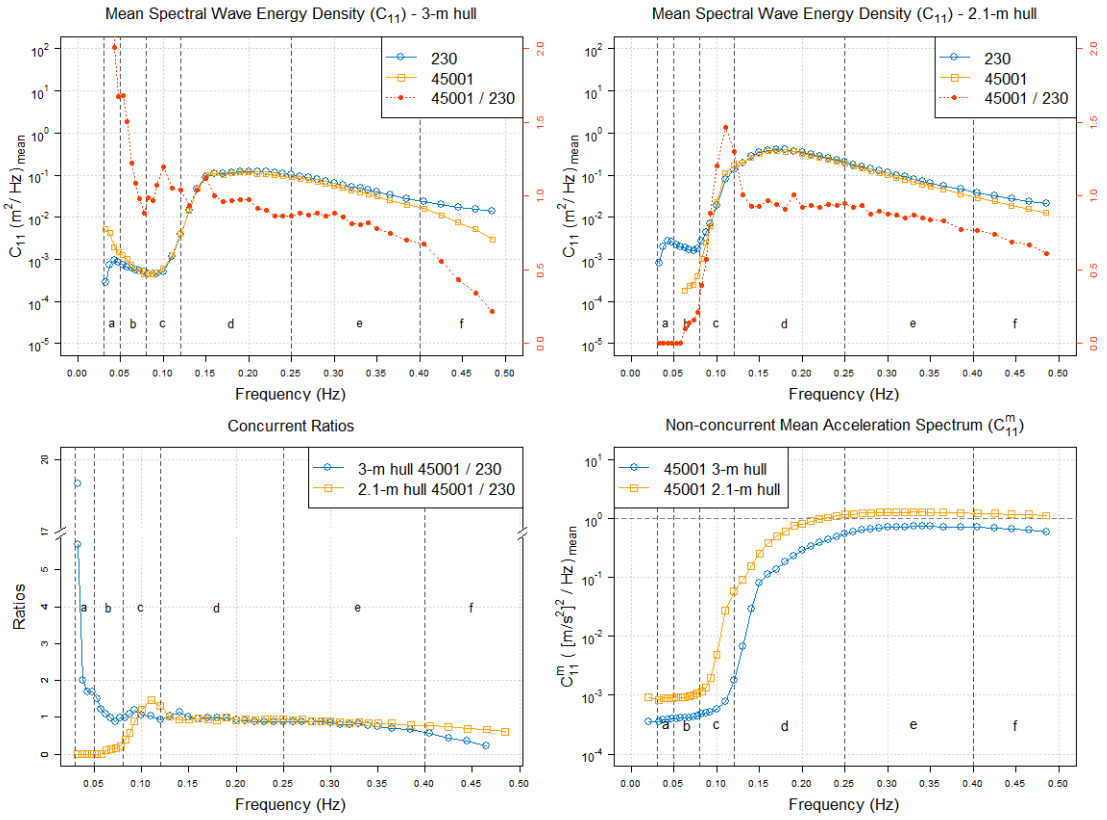


Figure 2.5. Concurrent 3-m and 2.1-m hull mean spectral wave energy density ($C_{11}$) on the top, concurrent 3-m and 2.1-m hull mean spectral wave energy density ($C_{11}$) ratios on the bottom left, and non-concurrent mean acceleration spectra ($C_{11}^{m}$) on the bottom right for the Great Lakes NDBC 45001 (orange lines) and CDIP 230 (blue lines) frequency spectra (August 2017 vs September 2020). Vertical black dotted lines delineate the six spectral wave components, where a) forerunners, b) long swell, c) short swell, d) long sea, e) short seas, and f) wind chop.

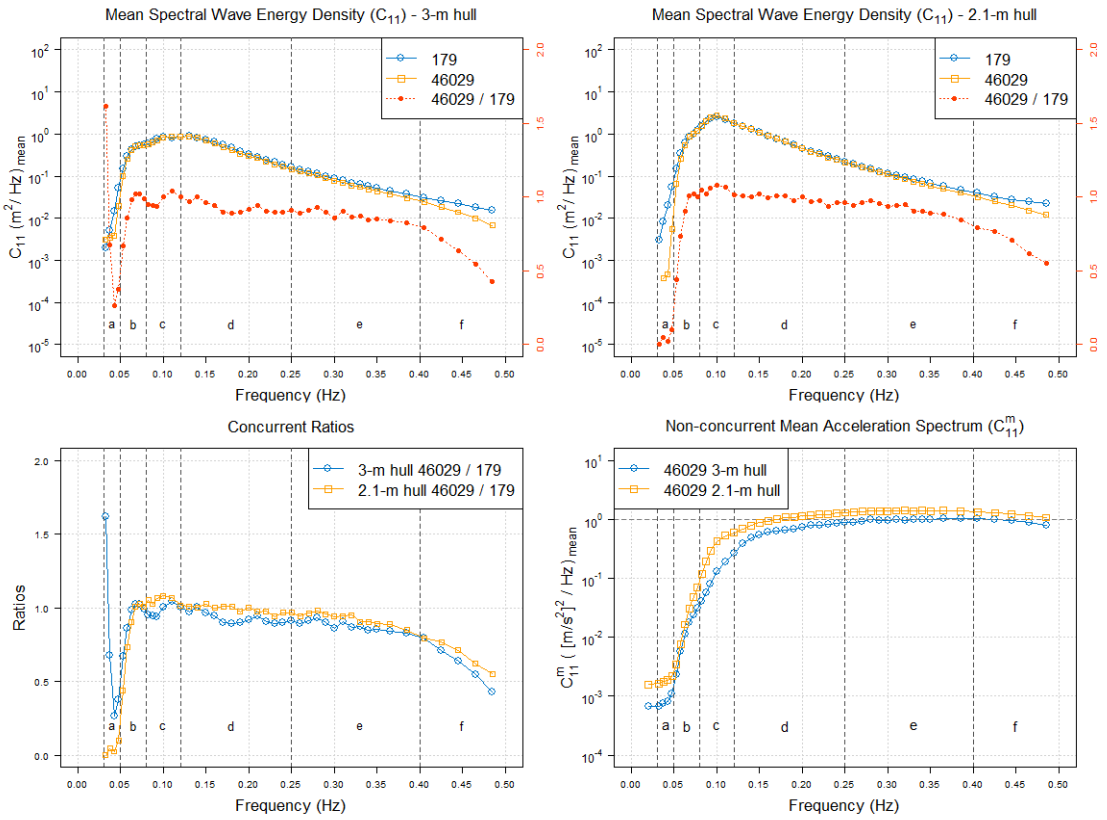


Figure 2.6. Concurrent 3-m and 2.1-m hull mean spectral wave energy density ($C_{11}$) on the top, concurrent 3-m and 2.1-m hull mean spectral wave energy density ($C_{11}$) ratios on the bottom left, and non-concurrent mean acceleration spectra ($C_{11}^{m}$) on the bottom right for the Pacific Ocean NDBC 46029 (orange lines) and CDIP 179 (blue lines) frequency spectra (August 2019 vs June 2021). Vertical black dotted lines delineate the six spectral wave components, where a) forerunners, b) long swell, c) short swell, d) long sea, e) short seas, and f) wind chop.

Table 2.4. Goodness of fit statistical wave component results between NDBC 3-m and 2.1-m hull data and concurrent, co-located DWR data for the Great Lakes and Pacific Ocean sites

| Variable | Hull | No. Obs. | Correlation coefficient (r) | RMSE (m) | Bias (m) | Mean (m) | Intercept | Slope | $R^2$ |
|---|---|---|---|---|---|---|---|---|---|
| Forerunners (0.03 – 0.05 Hz) | Great Lakes (NDBC 45001 vs CDIP DWR 230) | | | | | | | | |
| | 3-m /DWR | 395 | 0.610 | 0.104 | 0.090 | 0.065 | 0.065 | 2.245 | 0.371 |
| | 2.1-m /DWR | 4 | Sample size too small for evaluation | | | | | | |
| | Pacific Ocean (NDBC 46029 vs CDIP DWR 179) | | | | | | | | |
| | 3-m /DWR | 6362 | 0.897 | 0.123 | 0.038 | 0.220 | -0.004 | 0.856 | 0.804 |
| | 2.1-m /DWR | 172 | 0.645 | 0.061 | 0.045 | 0.097 | 0.003 | 0.602 | 0.412 |
| Long Swell (0.05 – 0.08 Hz) | Great Lakes (NDBC 45001 vs CDIP DWR 230) | | | | | | | | |
| | 3-m /DWR | 524 | 0.420 | 0.043 | 0.027 | 0.046 | 0.046 | 0.437 | 0.175 |
| | 2.1-m /DWR | 49 | Sample size too small for evaluation | | | | | | |
| | Pacific Ocean (NDBC 46029 vs CDIP DWR 179) | | | | | | | | |
| | 3-m /DWR | 20530 | 0.975 | 0.208 | 0.028 | 0.974 | 0.006 | 0.966 | 0.950 |
| | 2.1-m /DWR | 2607 | 0.950 | 0.103 | 0.042 | 0.441 | -0.024 | 0.960 | 0.902 |
| Short Swell (0.08 – 0.12 Hz) | Great Lakes (NDBC 45001 vs CDIP DWR 230) | | | | | | | | |
| | 3-m /DWR | 841 | 0.975 | 0.066 | 0.001 | 0.168 | 0.001 | 0.998 | 0.950 |
| | 2.1-m /DWR | 497 | 0.982 | 0.060 | 0.001 | 0.174 | -0.005 | 1.022 | 0.963 |
| | Pacific Ocean (NDBC 46029 vs CDIP DWR 179) | | | | | | | | |
| | 3-m /DWR | 20543 | 0.976 | 0.208 | 0.025 | 1.451 | 0.044 | 0.953 | 0.953 |
| | 2.1-m /DWR | 2646 | 0.971 | 0.147 | 0.001 | 1.027 | 0.029 | 0.973 | 0.942 |
| Long Seas (0.12 – 0.25 Hz) | Great Lakes (NDBC 45001 vs CDIP DWR 230) | | | | | | | | |
| | 3-m /DWR | 1326 | 0.945 | 0.086 | 0.021 | 0.160 | 0.030 | 0.939 | 0.893 |
| | 2.1-m /DWR | 628 | 0.978 | 0.061 | 0.025 | 0.171 | -0.022 | 0.985 | 0.957 |
| | Pacific Ocean (NDBC 46029 vs CDIP DWR 179) | | | | | | | | |
| | 3-m /DWR | 20543 | 0.981 | 0.232 | 0.037 | 1.673 | 0.030 | 0.960 | 0.963 |
| | 2.1-m /DWR | 2646 | 0.975 | 0.129 | 0.022 | 1.014 | 0.006 | 0.972 | 0.950 |
| Short Seas (0.25 – 0.40 Hz) | Great Lakes (NDBC 45001 vs CDIP DWR 230) | | | | | | | | |
| | 3-m /DWR | 4232 | 0.983 | 0.049 | 0.035 | 0.356 | -0.003 | 0.914 | 0.966 |
| | 2.1-m /DWR | 2096 | 0.982 | 0.045 | 0.027 | 0.389 | 0.001 | 0.929 | 0.964 |
| | Pacific Ocean (NDBC 46029 vs CDIP DWR 179) | | | | | | | | |
| | 3-m /DWR | 20532 | 0.949 | 0.062 | 0.033 | 0.472 | 0.006 | 0.922 | 0.901 |
| | 2.1-m /DWR | 2646 | 0.927 | 0.062 | 0.027 | 0.431 | 0.034 | 0.864 | 0.859 |
| Wind Chop (0.40 – 0.50 Hz) | Great Lakes (NDBC 45001 vs CDIP DWR 230) | | | | | | | | |
| | 3-m /DWR | 3661 | 0.932 | 0.065 | 0.060 | 0.168 | -0.009 | 0.740 | 0.869 |
| | 2.1-m /DWR | 2022 | 0.932 | 0.039 | 0.032 | 0.186 | 0.007 | 0.805 | 0.869 |
| | Pacific Ocean (NDBC 46029 vs CDIP DWR 179) | | | | | | | | |
| | 3-m /DWR | 19794 | 0.782 | 0.066 | 0.052 | 0.199 | 0.004 | 0.752 | 0.611 |
| | 2.1-m /DWR | 2566 | 0.848 | 0.049 | 0.036 | 0.193 | 0.023 | 0.717 | 0.720 |

The detected shifts in the higher frequencies are clearly highlighted in 3-m and 2.1-m hull deployment spectral wave components (CDIP, 2021b) comparisons (Table 2.4; Figure 2.7 and Figure 2.8 for the Great Lakes and Pacific Ocean, respectively). Short seas (0.25 – 0.40 Hz) and wind chop (0.40 – 0.50 Hz) comparisons show a visual correction in regression (grey lines) slopes after deployment of the 2.1-m hull. These trends are quantifiable in the wind-sea driven Great Lakes as stable correlation coefficients and improved bias of 0.027 from 0.035 for short seas and 0.032 from 0.060 for wind chop (Table 2.4).

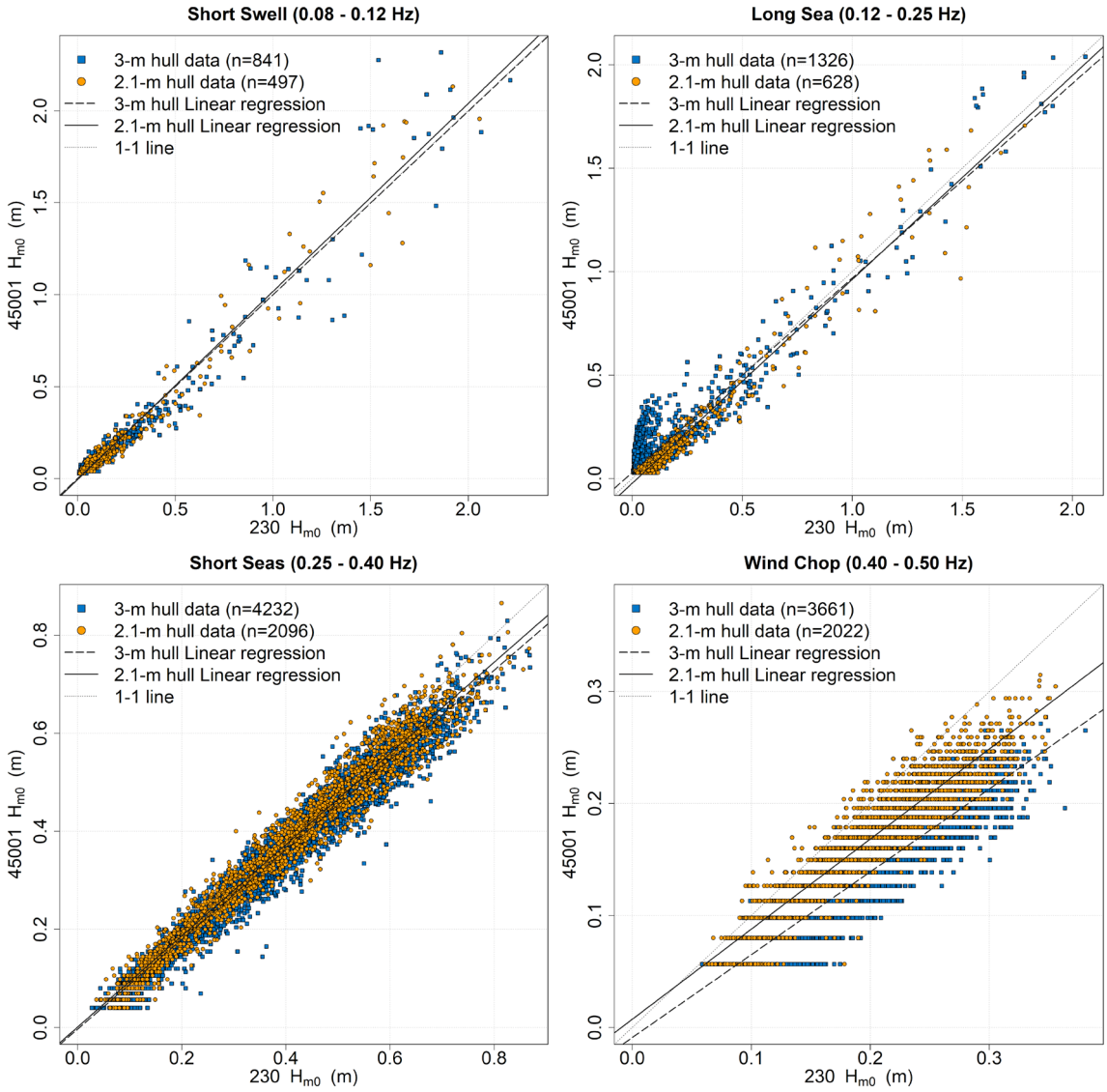


Figure 2.7. 3-m and 2.1-m hull wave component significant wave height as calculated from spectral energy density for the Great Lakes NDBC 45001 versus CDIP DWR 230 for short swell (top left), long sea (top right), short seas (bottom left), and wind chop (bottom right). Forerunners and long swell sample sizes were too small to include here (less than 50 2.1-m hull samples). Solid grey lines represent linear regressions for the 2.1-m hull deployment data, while dashed grey lines represent linear regressions for the 3-m hull deployment data.

Increased agreements are evident in the Great Lakes (Table 2.4; Figure 2.7) short swell (0.08 – 0.12 Hz) and long sea (0.12 – 0.25 Hz) correlation coefficients of 0.982 from 0.975 and of 0.978 from 0.975, respectively. As the Great Lakes wave climate does not include low frequency swell data due to short fetch lengths, the Great Lakes 2.1-m evaluation data samples were not sufficient in size to evaluate forerunner (0.03 – 0.05 Hz) and long swell (0.05 – 0.08 Hz) 2.1-m hull performance (Table 2.4). However, the 2.1-m hull vs CDIP DWR long sea data appear more consistent than the earlier 3-m hull vs CDIP DWR long sea correlations (Figure 2.8), as the 2.1-m vs DWR data show less scatter within the low wave heights (< 0.25 m) than those observed within the 3-m vs DWR data. Of interest is that the Great Lakes wave component 3-m and 2.1-m hull bias and RMSE results are within NDBC reported accuracy requirements of ± 0.2 m for $H_{m0}$ (NDBC, 2003; NDBC, 2017).

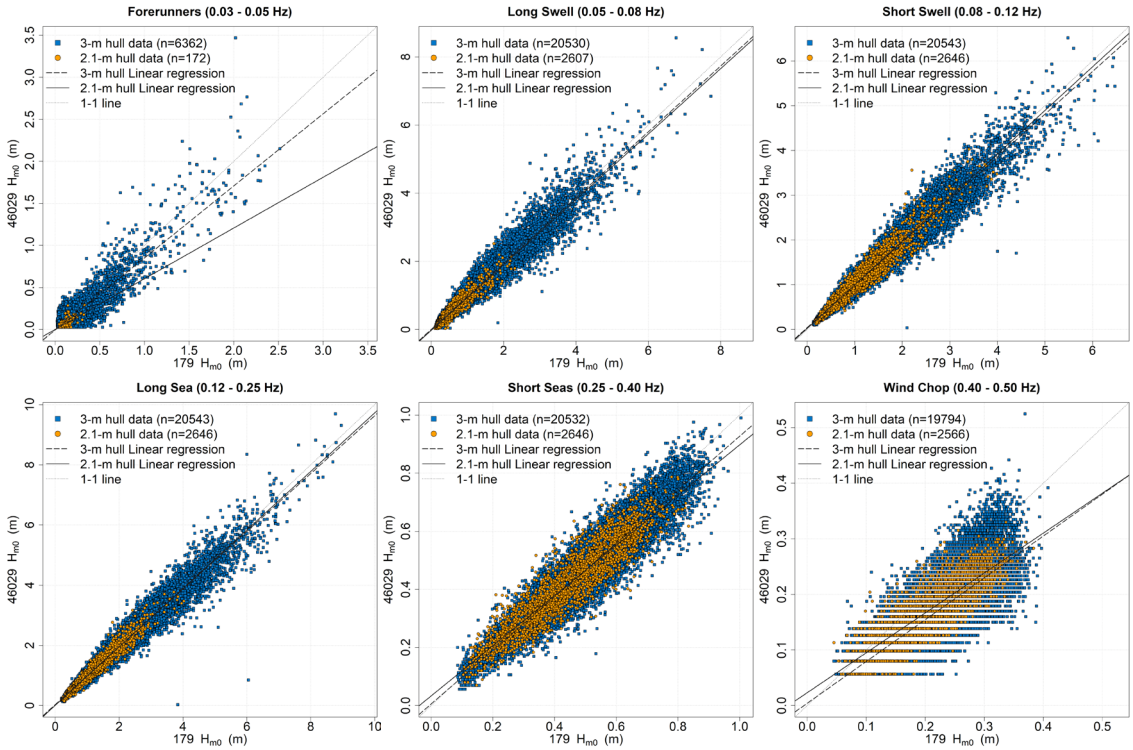


Figure 2.8. 3-m and 2.1-m hull wave component significant wave height as calculated from spectral energy density for the Pacific Ocean NDBC 46029 versus CDIP DWR 179 for forerunners (top left), long swells (top middle), short swell (top right), long sea (bottom left), short seas (bottom middle), and wind chop (bottom right). Solid grey lines represent linear regressions for the 2.1-m hull deployment data, while dashed grey lines represent linear regressions for the 3-m hull deployment data.

However this is not true for the Pacific Ocean wave components (Table 2.4; Figure 2.8). RMSE results for 3-m hull long swell, short swell, and long seas vs co-located DWR tests show an exceedance of the ± 0.2 m requirement at 0.208 m; 0.208 m and 0.232 m, respectively. However, the NDBC requirement is for total significant wave height, so this is a slightly unfair assessment. In comparison, the 2.1-m hull vs CDIP DWR results do meet this NDBC requirement, with improved long swell, short swell, and long seas RMSEs of 0.103 m; 0.147 m; and 0.129 m, respectively (Table 2.4).

Delving into the higher frequency wave components shows a 2.1-m deployment improvement from the 3-m hull data within both correlation coefficients and bias with the co-located CDIP DWR data at the Pacific Ocean site (Table 2.4). Wind chop correlation coefficient results (Table 2.4) increased from 0.782 to 0.848, with a reduced RMSE of 0.049 m from 0.066 m, and an improved bias of 0.036 m from 0.052 m. Short seas show similar 2.1-m hull results (Table 2.4), with stable correlation coefficients and bias improvements of 0.027 m from 0.033 m. Reviewing the low frequency swell data in the Pacific Ocean forerunner results (Table 2.4) show an improved RMSE of 0.061 m vs 0.123 m after 2.1-m hull deployment. However, a larger 2.1-m hull sample size (n = 172) is required to definitely confirm this improvement ($R^2_{2.1\text{-m}} = 0.412$).

To ultimately summarise NDBC bulk parameter results as a whole, percentile non-exceedance curves show improved trends across NDBC bulk parameters ($H_{m0}$: Figure 2.9; and $T_a$: Chapter 2's Appendix 2.2.6.2: Figure 2.17) across both evaluation sites. Within the Pacific Ocean, the 2.1-m hull $H_{m0}$ data reaches 95 % at approximately 0.38 m, while the 3-m hull data exceeds 95 % at 0.5 m. $H_{m0}$ remains stable within the Great Lakes, where both the 3-m and 2.1-m hull $H_{m0}$ data reach 95 % at approximately 0.24 m (Figure 2.9). This is because fetch distances within the Great Lakes are bounded by the size of the lakes, constraining wave height maxima and ultimately limiting the high end of the wave height distribution, as no large storm events were observed in the two datasets. Therefore inter-annual wave height variations within the Great Lakes are stable and there is consistency between the non-concurrent 2.1-m and 3-m buoy data. This is not true for the Pacific Ocean, where inter-annual variations are based on multiple wave measurement systems

that are associated with larger fetch lengths, and thus the high end of the wave height distributions will be affected by differences in the wave conditions from year to year. $T_a$ data show a very slight improvement with exceedance curves crossing the 95 % threshold at approximately 0.48 s when compared to the previous 3-m hull results of 0.52 s, which is similar to the improvement within the Pacific Ocean's $T_a$ curves where the 95 % values improves from 1.8 s to 1.1 s between the hull deployments (Chapter 2's Appendix 2.2.6.2: Figure 2.17). These exceedance curve results suggest less confidence in validations based on smaller datasets (2.1-m hull in this case), supporting an argument that any evaluation of a new buoy should be treated as a long-term project, allowing time for the capture of a large range of wave conditions.

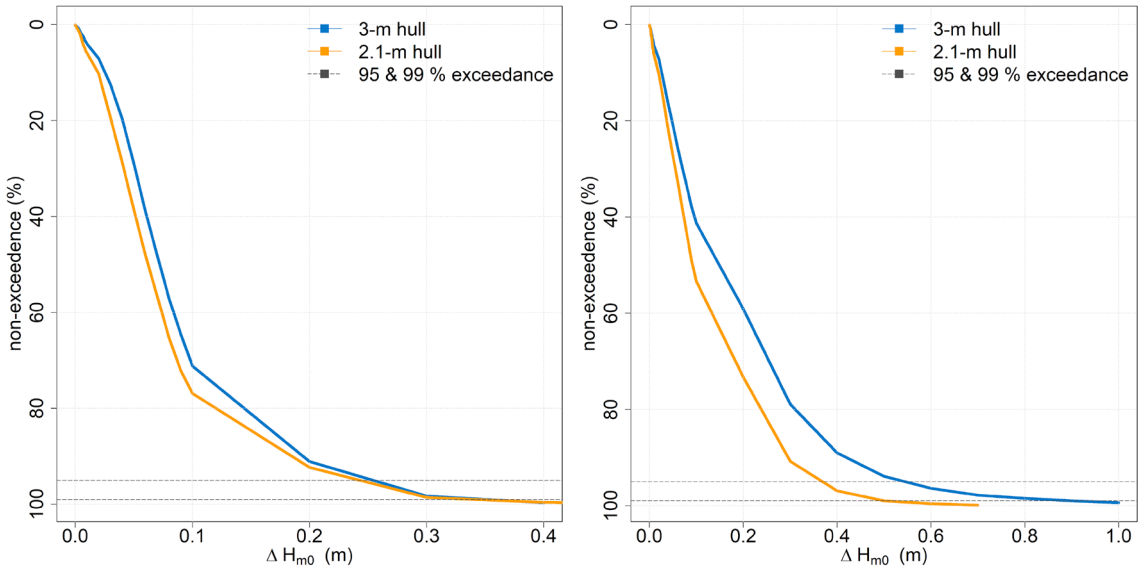


Figure 2.9. Exceedance curves for the absolute difference in $H_{m0}$ between the 3-m vs 2.1-m hulls and their concurrent DWR data at the Great Lakes NDBC station 45001 (left) and Pacific Ocean NDBC station 46029 (right). The grey dotted lines represent the 95 % and 99 % exceedance limits.

### *2.2.4.2 Wave direction and spread*

The Great Lakes wave climate has been directly correlated to the wind directions as wind-generated seas normally are, and are spatially coherent, or follow the outline of the neighbouring coastline (Lin and Resio, 2001). In addition, the winds in the regions of the Great Lakes are temporally variable, which can result in translatory storm systems and

shifts in wind directions between 90 ˚ and 180 ˚. Hence the wind-driven Great Lakes wave climate typically echoes these wind shifts with oscillating wave directions, due to a strong dependency between winds and waves. This trend is evident within these reviewed Great Lakes mean wave directions ($\alpha_p$) as both the 3-m and 2.1-m hull deployments (Table 2.1) have similar lobe distributions to the co-located CDIP DWR stations (Figure 2.10, left). Isolating the 2.1-m hull data in Figure 2.10 shows mean wave directions at peak frequency within the SE and SW quadrants, with the majority of the waves approaching from 100 - 180 ˚ and from 210 - 260 ˚. These results are consistent with Lin and Resio (2001), and the directional lobes found at the buoy site are aligned to the primary axes for the longest fetch lengths contained in Lake Superior relative to the buoy site. Density sampling highlights the predominant Lake Superior mean wave direction at peak frequency at approximately 235 ˚ (Figure 2.10) for the 2398 comparative samples collected during the 2020-2021 summer and fall sampling periods (Table 2.1).

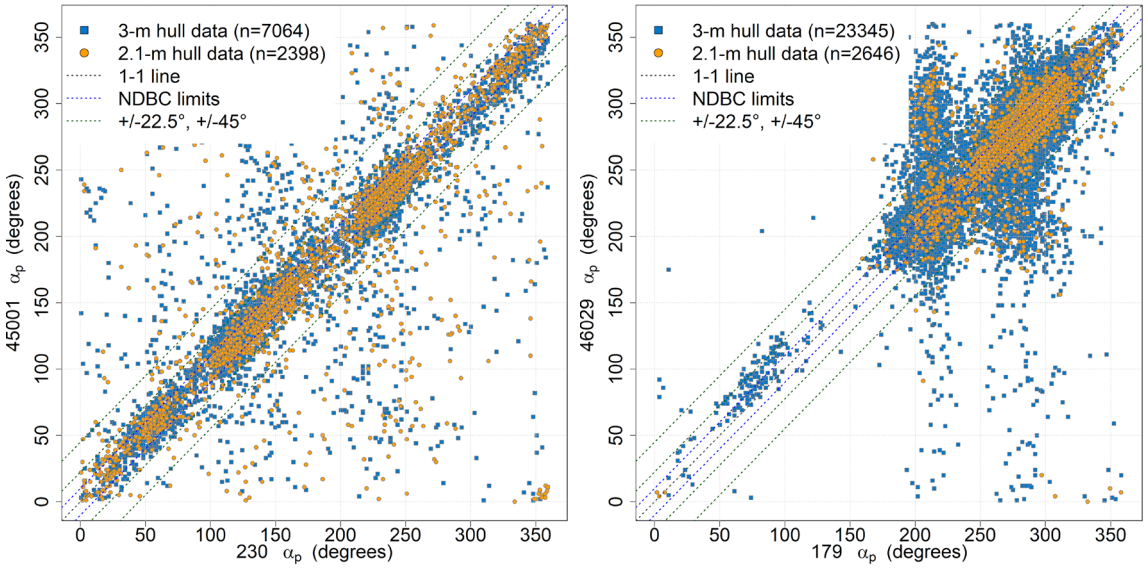


Figure 2.10. Scatter diagrams of the 3-m (blue points) vs 2.1-m hull (orange points) $\alpha_p$ data for the Great Lakes NDBC station 45001 and CDIP 230 (left) and Pacific Ocean NDBC station 46029 and CDIP 179 (right). Blue dotted lines represent the NDBC ±10 ˚ accuracy limits for direction. Green dotted lines indicate ±22.5 ˚ and ±45 ˚ limits. Both plots include a dotted grey 1-1 line.

The Pacific Ocean evaluation site, on the other hand, is dominated by swells that originate from storms that translate across the vast expanse of the ocean basin. As expected, density sampling shows that the predominant NDBC station 46029 mean wave direction at peak frequency is from the west around 280 ˚ for the 2646 comparative samples collected during the 2020-2021 sampling periods (Table 2.1; Figure 2.10, right). Of note is that the Pacific Ocean results show NDBC and CDIP processing differences when measuring multiple wave systems that contain similar peak energies in different frequency bands (Jensen et al., 2021). The offsets around 200 ˚ are primary South Pacific Ocean, low frequency swells that are well measured by the CDIP DWR system. However, NDBC's wave measurement system may not be able to fully detect the low-frequency swell peaks of the multiple wave systems, meaning that this spectrum peak frequency direction may be associated with rotating high-frequency wind sea peaks. Further evaluations of the peak wave direction bias between the two systems would require isolation of the wave trains from differing sources, which is beyond the scope of this work.

Reviewing the directional $\alpha_p$ results (Table 2.3) shows an improved directional bias of 26 ˚ for the 2.1-m hull vs CDIP DWR data, from the bias calculated using the 3-m hull vs CDIP DWR data of 52 ˚ ($Obs_{3\text{-m}}$ = 4666; $Obs_{2.1\text{-m}}$ = 2398) for the Great Lakes. Although the Pacific Ocean site does not present an improved $\alpha_p$ bias estimate ($bias_{3\text{-m}}$ = 14 ˚; $bias_{2.1\text{-m}}$ = 58 ˚; $Obs_{3\text{-m}}$ = 20699; $Obs_{2.1\text{-m}}$ = 2646) after the deployment of the 2.1-m hull (Table 2.3), both sites show RMSE results (Table 2.3) as 45 ˚ across the board (Great Lakes: $r_{3\text{-m}}$ = 0.772; $r_{2.1\text{-m}}$ = 0.724; Pacific Ocean: $r_{3\text{-m}}$ = 0.708; $r_{2.1\text{-m}}$ = 0.577). The directional statistical results exceed NDBC's accuracy limits of ± 10 ° (NDBC, 2003; NDBC, 2017) for wave directional data at both the peak frequency and for the directional spread around the vector mean wave direction defined at the peak frequency. The majority of the mean wave directional results remain within the ± 22.5 ° and ± 45 ° boundaries, designated as dashed green lines with the plots. These ± 45 ° boundaries represent the eight primary compass directions, while the ± 22.5 ° boundaries represent half of the eight. These directional results are consistent with other reviews of directional NDBC data (Hall et al., 2018a, 2018b; Jensen et al., 2021).

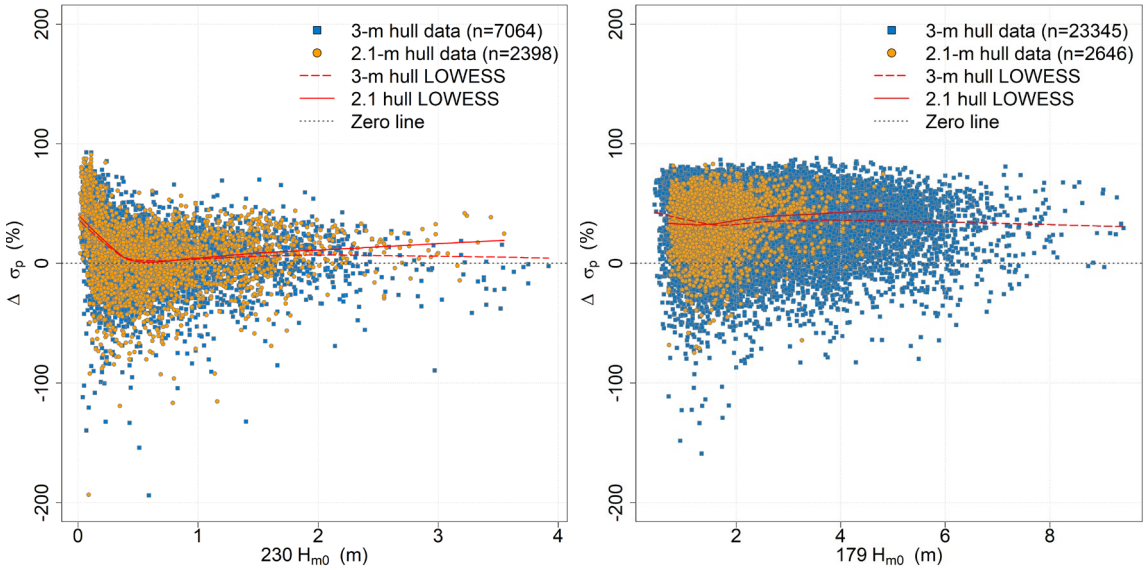


Figure 2.11. Scatter diagrams of the 3-m (blue points) vs 2.1-m hull (orange points) $\sigma_p$ percent differences between concurrent NDBC and CDIP data, when compared to CDIP sea state data for the Great Lakes NDBC 45001 and CDIP 230 (left) and Pacific Ocean NDBC 46029 and CDIP 179 (right). 3-m (dashed) vs 2.1-m (solid) hull locally weighted scatterplot smoothing (LOWESS; red) regressions highlight trends. Both plots include a dotted grey zero line.

A review of the $\sigma_p$ comparison statistics show similar results for the 2.1-m hull and 3-m hull data vs concurrent CDIP DWR data (Table 2.3). However, these less than desired results are to be expected as regression models only explain between 5 – 36 % of the variation within the directional spreading datasets ($R^2_{GreatLakes} \approx$ 30-36 % and $R^2_{PacificOcean} \approx 5 - 6$ %). Figure 2.11 shows directional spreading in the Great Lakes, illustrating a larger deviation in spread in smaller wave conditions, with a smaller deviation as wave height increases. This is to be expected in the Great Lakes local wind-dominated wave climate, where wave directions are highly variable in low wave height conditions. This trend is not as evident in the Pacific due to the swell-dominated wave climate, where swell is always present, even in low wave height conditions, and therefore showcase a more controlled directional wave spread. In both cases, NDBC's peak frequency directional spread is larger than CDIP, as there is a positive bias in the NDBC spread versus the CDIP spread. Although this bias is far more consistent within the range of $H_{m0}$ found within the Pacific Ocean data. The range of directional spread deviation appears independent to the

$H_{m0}$, but reviewed sample data that include consistently higher $H_{m0}$ are needed to definitely conclude this determination.

These results highlight that although the significant wave height and average wave period parameters show a significant improvement with the use of the 2.1-m hull, the directional parameters do not appear to be improved by the smaller hull size. To further understand these directional results, the directional spectral datasets produced by these test sites were interrogated by WavEval methodology to isolate variance in the directional wave frequency data.

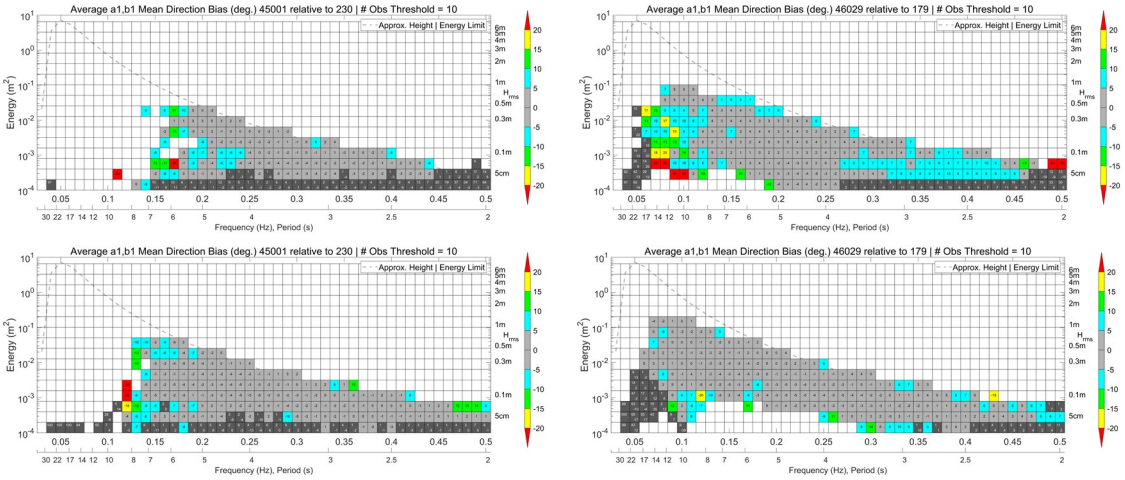


Figure 2.12. One month of CDIP DWR versus NDBC 3-m hull (top; August 2017 for the Great Lakes and August 2019 for the Pacific Ocean) and 2.1-m hull data (bottom; September 2020 for the Great Lakes and June 2021 for the Pacific Ocean) a1, b1 mean direction bias (in degrees) per CDIP frequency bands. Colours represent bias values, where grey = ± 0-5˚; blue = ± 5-10˚; green = ± 10-15˚; yellow = ± 15-20˚; and red = > ± 20˚. White bins indicate no comparable data.

As with the previously described wave height WavEval methodology, evaluations compared bias and RMSEs as a function of wave frequency and energy per frequency bin for mean wave direction and directional spread (Figure 2.12; Figure 2.13; Chapter 2's Appendix Figure 2.15 and Figure 2.16). One month's worth of 3-m hull (August 2017 for the Great Lakes and August 2019 for the Pacific Ocean) and 2.1-m hull data (September 2020 for the Great Lakes and June 2021 for the Pacific Ocean) were subset with their concurrent, co-located CDIP DWR data samples for testing.

Bearing in mind the distance between the NDBC and CDIP buoys (Great Lakes: 3 nm; Pacific Ocean: 7nm), and the Great Lakes seasonal temporal variability (August 2017 vs September 2020), the NDBC data vs concurrent CDIP DWR data (Figure 2.12) average $a_1$ and $b_1$ mean direction bias show a definitive improvement across all of the frequency bands for both 2.1-m hull deployment sites. Within Figure 2.12, very few 0.18 – 0.485 Hz frequency bins return bias results that are above ± 10 ˚ (NDBC directional accuracy tolerance; NDBC, 2003; NDBC, 2017), with a decrease from 9 % to 5 % of the bins recording bias above 5 ° in the Great Lakes, and a drop of 28 % to 14 % of the frequency bins reporting bias above 5 ° in the Pacific Ocean (Figure 2.12).

The Great Lakes 2.1-m hull low frequency mean directional bias appears similar to the 3-m hull data, which is attributable to the small 3 nm spatial difference between buoys, as well as the wind-driven directional wave climate (Figure 2.12). Notice that higher than 20 ˚ bias occurs in the low frequency bins (< 0.18 Hz) in the Great Lakes samples and the 3-m hull Pacific Ocean samples, caused by the lack of resolvable energy in the low frequency samples and the handling of low frequency data between the two sources (Figure 2.12). However, these high bias values are not present in the Pacific Ocean sites 2.1-m hull low frequency data, meaning that the NDBC 2.1-m hull data are able to confidently mirror the nearby (7 nm) CDIP DWR mean directional data (Figure 2.12).

Mean wave directional RMSE, with bias removed (Chapter 2's Appendix 2.2.6.1: Figure 2.15), appears similar in the Pacific Ocean site data, with approximately 69 % and 62 % of the energy across frequency bins (0.18 – 0.50 Hz) exhibiting RMSE between 0 and 20˚ for the 3-m and 2.1- hull data, respectively. RMSE results (Chapter 2's Appendix 2.2.6.1: Figure 2.15) remain similar between the 3-m and 2.1-m hull deployments within the Great Lakes (with most frequency bins bias between 0 – 20 ˚ between 0.18 – 0.50 Hz), with an increase in bias in the lower frequency bins (< 0.18 Hz). However, as mentioned this is due to spatial variability and the handling of low frequency energy between the two sources. Both bias and RMSE results are greater than the NDBC directional accuracy limits of ± 10 ˚ (NDBC, 2003; NDBC, 2017).

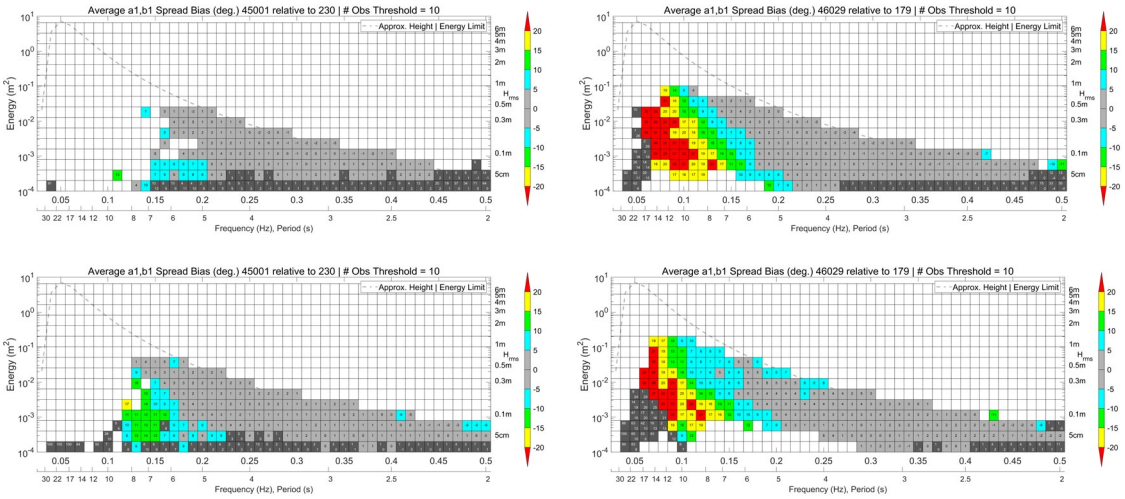


Figure 2.13. One month of CDIP DWR versus NDBC 3-m hull (top; August 2017 for the Great Lakes and August 2019 for the Pacific Ocean) and 2.1-m hull data (bottom; September 2020 for the Great Lakes and June 2021 for the Pacific Ocean) average $a_1$, $b_1$ spread bias (in degrees) per CDIP frequency bands. Colours represent bias values, where grey = ± 0-5 °; blue = ± 5-10 °; green = ± 10-15 °; yellow = ± 15-20 °; and red = > ± 20 °. White bins indicate no comparable data.

Considering mean directional spread of the directional Fourier coefficients, $a_1$ and $b_1$, for the NDBC data vs concurrent CDIP DWR data (Figure 2.13) shows a similar bias across the frequency bands for the 3-m and 2.1-m data. As before, the majority of the bins with higher bias value above 10 ° are detected in the frequencies below 0.18 Hz (Figure 2.13). This is consistent with our previous low frequency noise discussions, indicating an improved 2.1-m hull signal to noise ratio. As before, RMSE with bias removed comparisons (Chapter 2's Appendix 2.2.6.1: Figure 2.16) shows a slight improvement in low frequencies at the Pacific Ocean site but otherwise results remain stable (0 – 10 ° between 0.18 – 0.485 Hz) between the 3-m and 2.1-m hull deployment data for the time period reviewed. The Great Lake RMSE results are similar, but with higher low frequency RMSE values of 10 – 15 ° between 0.18 – 0.22 Hz (Chapter 2's Appendix 2.2.6.1: Figure 2.16). Of note is the increased amount of data for comparison in the lower frequencies within the 2.1-m hull dataset vs the earlier 3-m hull dataset, suggesting improvement in data return as the 2.1-m hull buoy is sensing an increase in low frequency energy that is above the NDBC low-frequency filter threshold, supporting the conclusion that the 2.1-m

hull buoy has an improved signal-to-noise ratio with the new 2.1-m hull. However, of note is that the reviewed Great Lakes data are temporally representing summer vs fall seasons, where the fall September data incorporates more energetic storm systems that inject low frequency energy into the wave conditions.

Overall, NBDC 2.1-m hull directional data shows a slight improvement over the previous 3-m hull deployment data. However these data still do not appear to confirm the advertised NDBC directional accuracy limits of ± 10 ˚ (NDBC, 2003; NDBC, 2017). The new NDBC 2.1-m hull directional data accuracy is consistent with, if not slightly better than, the previous standard NDBC 3-m hull directional data, remaining consistent with previous NDBC directional data evaluations (Hall et al., 2018a, 2018b; Jensen et al., 2021).

### *2.2.5 Conclusions*

Overall, the above results show that the lighter and smaller, newly operational NDBC 2.1-m hull produces significant wave height and average wave period data that more accurately compares with co-located and concurrent CDIP DWR data (improved goodness of fit results) than the previous, heavier and larger NDBC 3-m hull. The NDBC 2.1-m hull directional evaluation results remain consistent with previous NDBC 3-m hull directional wave data comparisons, allowing these authors to infer that hull size does not impact NDBC directional data estimates.

Interestingly the NDBC 2.1-m hull exhibits an improved signal-to-noise ratio, especially in the lower frequency spectral range, allowing for increase in energy retention in these frequencies. This improvement has particular relevance to USACE wave development in modelling scenarios, as swell wave development is of constant importance with regards to energy directed at coastal structures. Additionally, the NDBC 2.1-m hull provides improved high frequency spectral results above 0.25 Hz within the short seas and wind chop wave component regions. These results are extremely relevant to USACE estimates of the long-term U.S. wave climate, a significant risk assessment consideration in all coastal research studies. Therefore improvements within the accuracy of both NDBC bulk

and spectral data allow for the wave community's confidence in the wave measurements utilized as boundary conditions to drive nearshore wave model technologies and model improvements, as well as the wave measurements used as validation in wave models.

Future tasks include a review of the soon to be commissioned NDBC Ocean Wave Linux (OWL) system, which is a wave sensor under development at NDBC to replace their obsolete, legacy DDWM wave measurement system. Additionally, a repeat of these evaluations should be undertaken once NDBC has deployed additional 2.1-m hulls in a broader range of wave climates, especially higher wave heights, and time allows for larger 2.1-m hull data sample sizes.

Ultimately, independent evaluations of new wave measurement technologies and instrumentation are vital for the continued development and improvement of modelling capabilities, which are essential for the protection and resilience of coastal communities and structures around the world. We have also provided a template consisting of methods, tests and graphical presentations to follow for future intra-measurement evaluations. Regardless of their use, reliable and consistent wave measurements form the back-bone of all coastal related studies. Therefore evaluation considerations such as the data reviewed here are required to retain high confidence throughout the work flows, from data collection agencies, to model development and risk management estimates, to basic and applied research applications that aim to save lives along our coastlines.

### *2.2.6 Chapter 2 Appendix*

**Appendix 2.2.6.1: Spectral RMSE analysis results**

Spectral RMSE analysis results of a month of CDIP DWR versus NDBC 3-m hull (top in all of the plot sets; August 2017 for the Great Lakes and August 2019 for the Pacific Ocean) and 2.1-m hull data (bottom in all of the plot sets; September 2020 for the Great Lakes and June 2021 for the Pacific Ocean). Colours represent RMSE values as indicated by the legends. Plots were created using WavEval Wave Spectra Comparison Tool, v2.0.

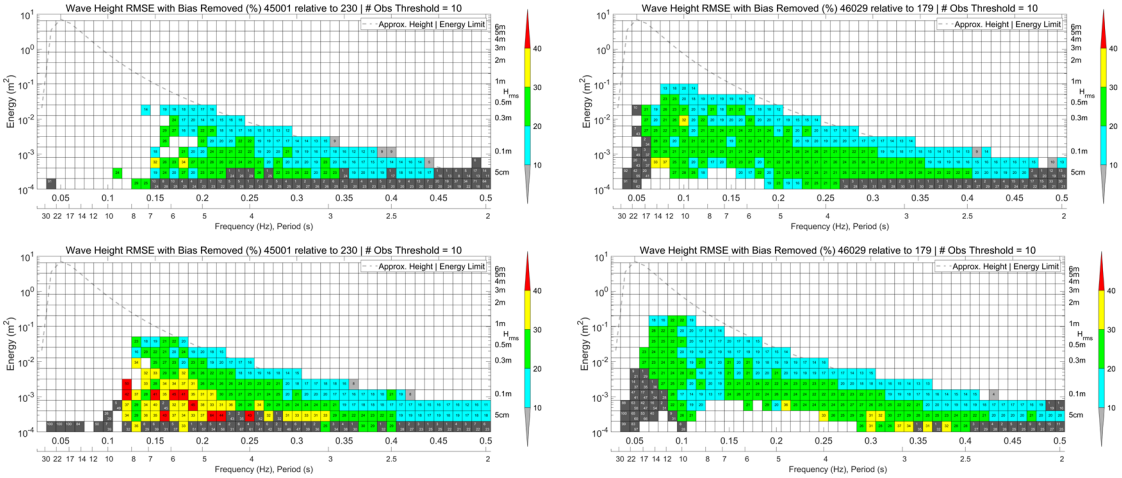


Figure 2.14. Wave height RMSE (in %), with bias removed, binned per CDIP frequency bands. Colours represent categorised RMSE values, where grey = ± 0-10 %; blue = ± 10-20 %; green = ± 20-30 %; yellow = ± 30-40 %; and red = > ± 40 %. White bins indicate no comparable data.

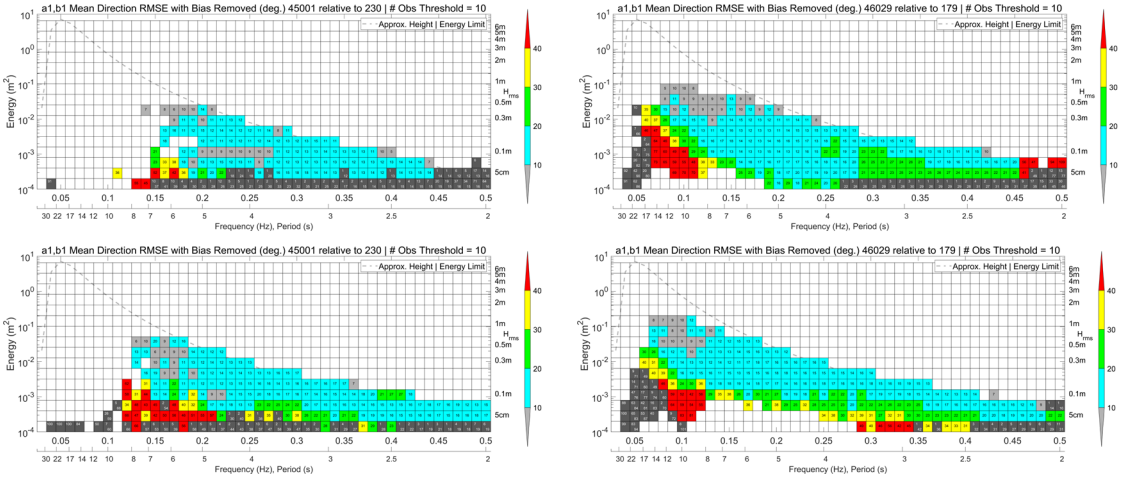


Figure 2.15. $a_1$, $b_1$ mean direction RMSE, with bias removed (in degrees), per CDIP frequency bands. Colours represent categorised RMSE values, where grey = ± 0-10 °; blue = ± 10-20 °; green = ± 20-30 °; yellow = ± 30-40 °; and red = > ± 40 °. White bins indicate no comparable data.

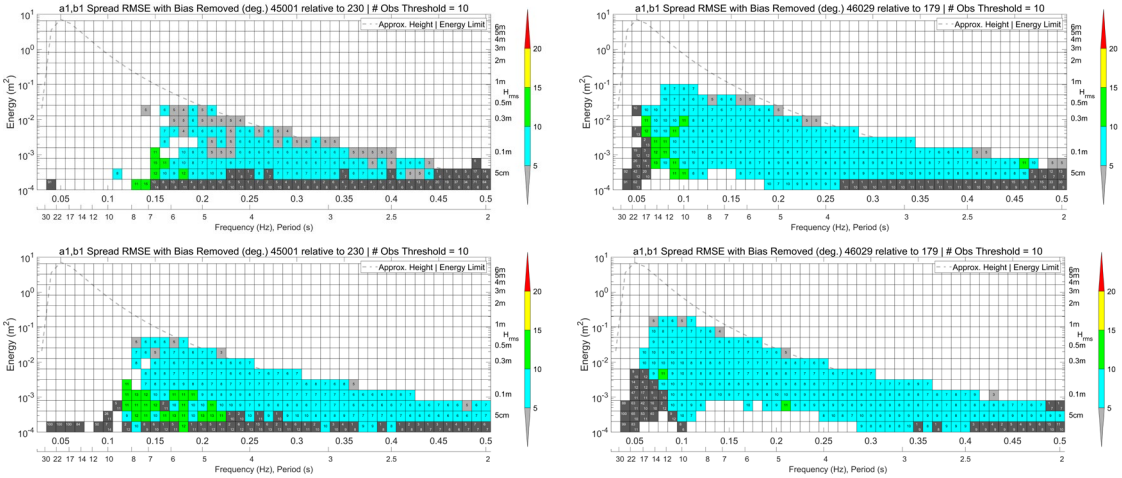


Figure 2.16. Average $a_1$, $b_1$ spread RMSE, with bias removed (in degrees), per CDIP frequency bands. Colours represent categorised RMSE values, where grey = ± 0-5 °; blue = ± 5-10 °; green = ± 10-15 °; yellow = ± 15-20 °; and red = > ± 20 °. White bins indicate no comparable data.

## Appendix 2.2.6.2: Average wave period and directional peak spreading exceedance results

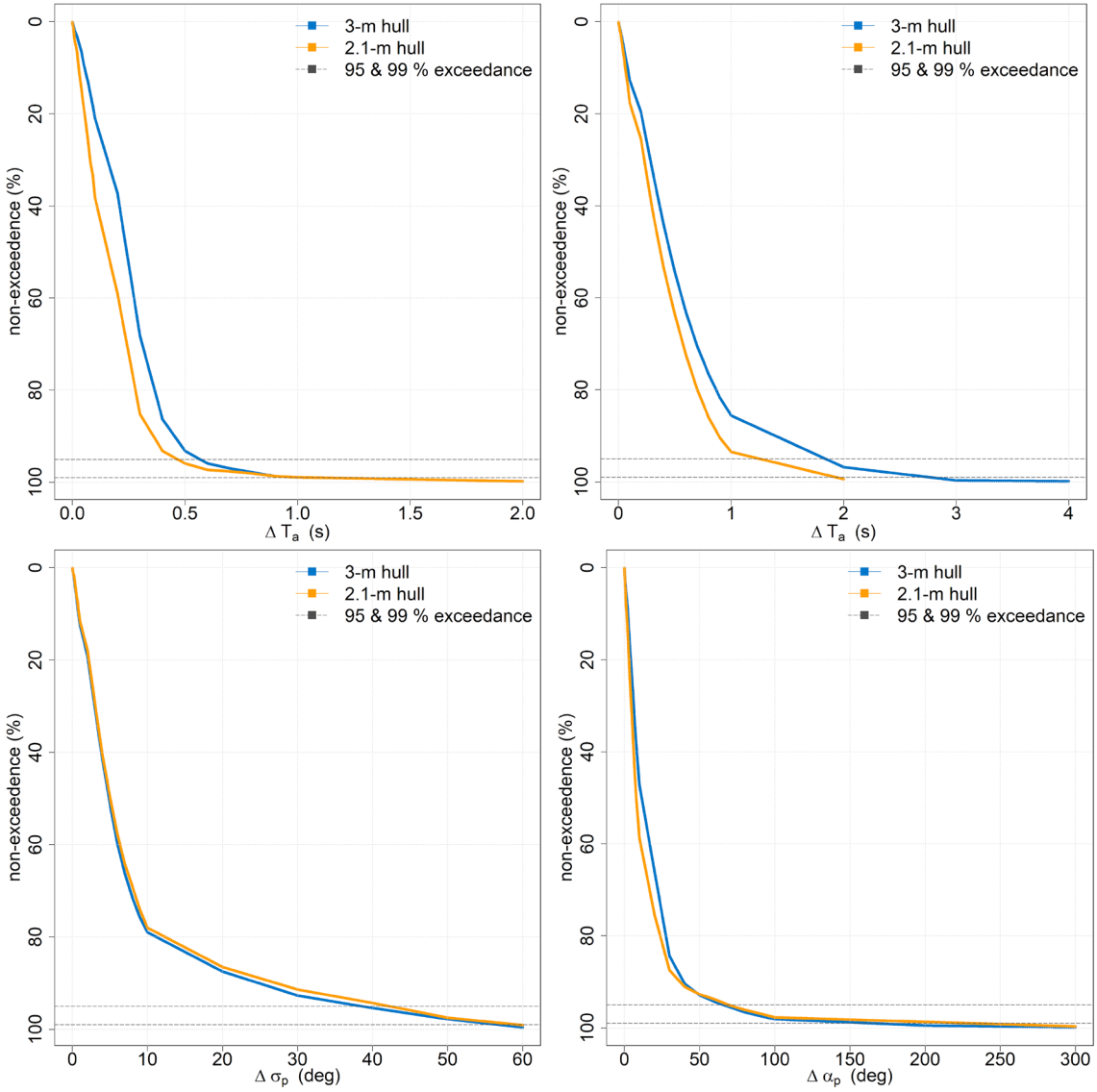


Figure 2.17. Exceedance curve for the absolute difference in $T_a$ (top) and $\sigma_p$ (bottom) between the 3-m vs 2.1-m hulls and their concurrent DWR data at the Great Lakes NDBC station 45001 (left) and Pacific Ocean NDBC station 46029 (right). The grey dotted lines represent the 95 % and 99 % exceedance limits.

## 2.3 Discussion and Conclusion

To summarise intercomparisons of NDBC wave measurement systems, Hall et al. (2018b) explored the accuracy of the lighter in weight NDBC 3-m foam hull that currently augments the NDBC 3-m aluminium hull fleet that NDBC routinely deploys. They determined that the 3-m foam hull produces bulk wave parameters that are consistent in accuracy with previous NDBC measurements, and within NDBC accuracy limits when compared to a nearby reference CDIP DWR.

Additionally, Jensen et al., 2021, undertook a five year FLOSSIE project to test wave sensor compatibility. They showed that various historically deployed NDBC and ECCC wave instrumentation, processing protocols and NDBC 6-m NOMAD hull produced statistical consistency within bulk wave parameters and spectral frequencies up to 0.35 Hz.

Within this chapter, Hall et al. (2022b) explored the accuracy of wave measurements collected with the now operational NDBC 2.1-m hull. This work shows a Pearson correlation improvement in significant wave height and average wave period between the NDBC 2.1-m hulls and collocated and concurrent DWR's from those data collected during the earlier NDBC 3-m hull deployments. Directional evaluations remain unchanged. Spectrally, an improved signal-to-noise ratio is observed during the NDBC 2.1-m hull deployments, suggesting an increase in energy retention across the wave swell spectral frequencies.

Of note within all of the above studies was the determination that the NDBC directional data are not within NDBC accuracy limits of ± 10 ˚. Additionally, the above studies that investigated wave energy densities noticed that the NDBC data deviates from the reference CDIP DWR data in the higher frequencies above 0.35 Hz. While these frequency ranges are vital with respect to model wave generation and satellite validations of sea surface roughness, they are not vital to the investigation of wave power, and will therefore not hinder this research.

Therefore, these bodies of work prove the hypothesis that these wave measurement systems are comparable for wave studies. Hence these data are used within the next chapter to explore possible biases that are introduced by different wave measurement systems across long-term time series. Of particular interest is possible discontinuities between the larger NDBC 12-m, 10-m and 6-m hulls and the smaller NDBC 3-m and 2.1-m hulls.

Chapter 3

# 3. Is it possible to correct for bias between different wave measurement systems to produce homogeneous long-term time series records?

## Preface:

This chapter offers methodologies to correct for discontinuities between wave measurement systems to allow for the homogeneous comparisons of wave time series data. Portions of this chapter have been published in the following peer-reviewed journals. The chapter has been laid out in this format:

**Hall, C. & Jensen, R.E. 2022.** United States Army Corps of Engineers Coastal and Hydraulics Laboratory Quality Controlled, Consistent Measurement Archive. *Scientific Data*. http://dx.doi.org/10.1038/s41597-022-01344-z

The methodology for further correction of discontinuities within the NDBC time series data is extracted from **Hall, C., Jensen, R.E., & Wang, D.W. 2022**. Wave Power Trends along the U.S. Coastline: In situ Measurements and Model Hindcasts Estimates. *Ocean Dynamics*. https://doi.org/10.1007/s10236-022-01515-x

This chapter addresses the second key question listed in Section 1.3.2.

### 3.1 Introduction

As shown within this literature review, numerous measurement and model studies and programs rely on the accuracy of NDBC wave and meteorological data. Unfortunately, a number of these studies have highlighted inconsistencies within these NDBC time series

datasets that possibly skew results, even when corrections are applied (e.g. Gemmrich et al., 2011; Young et al., 2011; Livermont et al., 2015; Livermont et al., 2017; Young and Ribal, 2019; Hall and Jensen, 2021).

These issues are due to two factors: inconsistencies within NDBC archive protocols, and NDBC instrumentation and platform technological advancements over the decades. The following chapter discusses these issues and offers a viable methodology to remove these known discontinuities within the datasets.

## 3.2 United States Army Corps of Engineers Coastal and Hydraulics Laboratory Quality Controlled, Consistent Measurement Archive

*The following work is published in Hall & Jensen (2022a): 'United States Army Corps of Engineers Coastal and Hydraulics Laboratory Quality Controlled, Consistent Measurement Archive', as cited at the top of this chapter.*

### *3.2.1 Abstract*

The US Army Corps of Engineers (USACE) utilises the National Oceanic and Atmospheric Administration (NOAA) National Data Buoy Center (NDBC) buoy measurements for validation of their wave models and within coastal applications. However, NDBC data are accessible via multiple archives; each with their own source-specific storage, metadata, and quality control protocols, which result in inconsistencies in the accessible data. Therefore, USACE has developed an independent, quality controlled, consistent (QCC) Measurement Archive that captures the best available NDBC observations with verified metadata. This work details the methodology behind this USACE QCC Measurement Archive; showcasing improvements in data quality via geographical location and wave parameter examples. Note that this methodology only removes known erroneous data, it does not verify data quality from an alternate source. This self-describing, USACE QCC Measurement Archive therefore provides a database of consistently stored, geographically QA/QC'd NDBC data and metadata.

### *3.2.2 Background & Summary*

One of the U.S. Army Corps of Engineers (USACE) missions is to oversee operations and maintenance activities in the coastal waters of the U.S. These activities include sediment transport, hardened structures, harbour navigability, climate resilience and coastal protection, all of which require knowledge and assessment of the wave climate. For practical assessments, USACE wave related technologies require accurate and homogeneous wave measurements from in situ observational platforms.

To that end, USACE sponsored an investigation into uncertainty errors in the wave measurement systems that are used for evaluating products such as their Wave Information Study (WIS), a wave hindcast effort that serves as the basis for resolving the U.S. wave climate. Of particular interest are measurement errors that may compromise wave model evaluations. These errors may be indistinguishable from wind forcing or wave model deficiencies, and may transfer into other USACE wave and coastal applications.

One source of validation data is the National Oceanic and Atmospheric Administration (NOAA) National Data Buoy Center (NDBC) in situ buoy meteorological and wave measurements. As of 2022, NDBC publishes their data via two different streams: real time and historical. The real time data feed undergoes broad, automated QA/QC protocols (NDBC, 2009) to meet emergency management and forecasting agency latency commitments that require swift publication to the Global Telecommunication System (GTS). These 'Real Time Data' files are also published within individual station pages on the NDBC website as tabular files that are continually updated and cover the last forty-five days (e.g. https://www.ndbc.noaa.gov/station_realtime.php?station=41009).

Once latency commitments are met, NDBC manually QA/QC's (NDBC, 2009) these data and stores them within station specific 'Historical Data' text files on their website on a monthly basis (e.g. https://www.ndbc.noaa.gov/station_history.php?station=41009). As per NOAA requirements, NDBC archives their data on a monthly basis in the official NOAA archives, which are found at the National Center for Environmental Information

(NCEI; https://www.ncei.noaa.gov/access/marine-environmental-buoy-database/). NDBC collates their website data annually and copy these data, in a Unidata's Network Common Data Form (netCDF) format, for storage on the NDBC Distributed Oceanographic Data Systems framework (DODS; https://dods.ndbc.noaa.gov/thredds/catalog/data/catalog.html). Essentially, the NDBC website and the DODS may be considered as a single source of NDBC historical data that are stored in different formats.

Over the decades, the NDBC data have experienced technological advances in instrumentation and archival storage. While NDBC has invested in minimising instrumentation effects on its datasets (Teng and Timpe, 1995; Teng et al., 2007; Riley and Bouchard, 2015), these various archives present their own set of specific storage procedures that influence data quality. These influences augment measurement discontinuities that are detectable within observation wave time series data (Gemmrich et al., 2011; Young et al., 2011; Livermont et al., 2015 and 2017; Ribal and Young, 2019), which were previously attributed to instrumentation or platform exchanges.

Therefore USACE undertook a thorough examination of the differences between these two NDBC and official NOAA archives at NCEI resources. The detected differences are detailed within a USACE Coastal and Hydraulics Engineering Technical Note (Hall and Jensen, 2021). In essence, the published NDBC website data, sourced from the in-house NDBC database that are subjected to manual NDBC QA/QC procedures (NDBC, 2009), presents a consistent, uniform formatting of historical variables and nomenclature. However the NDBC website data do not contain any metadata (geographical coordinates, instrumentation or software versioning information) that provide context to collection conditions. The official NOAA archive at NCEI, stored in netCDF format on the NCEI server, does contain those station, buoy and instrument metadata.

Unfortunately, since the implementation of the netCDF archiving process at NDBC in 2011, the NDBC data that are sourced for storage at NCEI are extracted from the automatically QA/QC'd NDBC Real Time Data stream. The automated NDBC QA/QC

process flags suspect data but only removes communication transmission errors and total sensor failures (NDBC, 2009). Suspect data flagged during automated NDBC QA/QC require manual inspection before data removal (NDBC, 2009). Therefore data quality issues not detected by the automated NDBC QA/QC protocols (such as gust wind values where wind speed and direction are not available, as well as directional data exceeding 360 ˚), including errors introduced by the NDBC netCDF data file construction process (such as duplicated data that are 5 – 10 seconds apart and erroneous wave frequency bands), are retained within the official NOAA archives of NDBC data at NCEI.

Due to USACE's data consistency and metadata requirements, these NDBC archive errors (Hall and Jensen, 2021) necessitated the development of an in-house USACE procedure that combined data from these archives to retain the manually QA/QC'd data and attached the required metadata. This procedure developed a best available, quality controlled and consistent measurement archive (herewith called the USACE QCC Measurement Archive) with accurately described metadata. The self-describing USACE QCC Measurement Archive is actively updated on an annual basis and stored on the USACE Coastal and Hydraulic Laboratory (CHL) Data server, accessible to both the USACE and the public (https://chldata.erdc.dren.mil/thredds/catalog/catalog.html). It is the methodology that created the NDBC portion of this USACE QCC Measurement Archive that is described in this manuscript.

### *3.2.3 Methods*

As NDBC publish their historical and real time in situ wave and meteorological data in multiple online locations, USACE developed a methodology to combine these data sources and develop a unique USACE QCC Measurement Archive that is fully self-describing. This required merging the manually quality controlled data that are stored on the NDBC website with the lower quality netCDF data with metadata files for the same stations that are stored at NCEI. The NOAA DODS source was not included as those data are exact copies of what is found within the NDBC historical station pages.

As mentioned, the NDBC website historical station pages contain the cleanest data that has been subjected to manual QA/QC by NDBC Mission Control data analysts. Data collected during service periods (when the buoys were physically on board ships for maintenance) were removed during the manual QA/QC, and are typically not present within the NDBC website data. However this data source contains no metadata other than date and time. This lack of metadata allows for the erroneous inclusion of unidentifiable data from historical time periods where the moored buoys were adrift (inaccurate wave readings, wind, temperature etc.). Additionally, although NDBC switched to a redundant meteorological sensor paradigm during the last decade, only single variable values are available per time stamp per station on the NDBC website. This is because NDBC toggles the release of primary and secondary sensor data to ensure that the highest quality data are published. However, the NDBC website contains no associated metadata indicating when these data release switches occur and hence instrumentation usage is indeterminable. Users often need these sensor details, for example wind sensor height above sea level to extrapolate wind speed at additional heights above the moored buoy. The NDBC website also does not store uncorrected non-directional spectral energy estimates ($c_{11}^{m}$).

Conversely, the NDBC netCDF data stored at NCEI includes metadata such as time-stamped GPS positions, instrumentation metadata, data quality flags (NDBC, 2009), and data release flags (indicating which data were released to the real time stream). These GPS positions allow for the identification of data that was collected while NDBC moored buoys were adrift. For ease of data source identification, these NDBC netCDF files stored at NCEI will be referred to as NCEI netCDF data below. However, readers should remember that these are all NDBC data, with time-paired values that are collected from the same, unique sensor.

This NCEI netCDF data source also includes both the primary and secondary redundant meteorological sensor outputs, with metadata, as well as uncorrected non-directional spectral energy estimates ($c_{11}^{m}$). These primary and secondary sensor variables are only found within these NCEI netCDF datasets. However, since 2011, these netCDF data are pulled from the NDBC real-time data stream, which is only subjected to automated

QA/QC protocols that flag but do not remove suspect data (NDBC, 2009). Prior to 2011, the NDBC data were stored in an encoded Trusted Data Format (TDF), but these data were converted into netCDF format in early 2020.

Of note is that the NCEI netCDF structures differ for data stored before and after the 2011 switch to netCDF file usage. Throughout the historical netCDF dataset, the netCDF file structures contain non-uniform netCDF formats that are dependent on the data collected during file-specific time periods. Additionally, the pre-2011 netCDF files contain a nominal, fixed deployment position that is repeated for each date/time stamp within the datasets. Furthermore, these pre-2011 netCDF files contain erroneous spectral wave frequency bands that are not included in the NDBC website datasets (and do not match any wave instrumentation frequencies that NDBC has historically deployed). Both formats include instrumentation metadata that are not only inconsistent throughout the years, but within individual netCDF file's group attributes.

Therefore, to mitigate these identified data source issues (Hall and Jensen, 2021), the USACE QCC Measurement Archive process utilized a methodology (Figure 3.1) that combines each dataset's advantages to develop a best available historical NDBC measurement dataset. For example, the GPS data included within the post-2011 NCEI netCDF files were used to detect data that fell outside a reasonable radius of the moored buoy. Conversely, the NDBC website data were used to isolate which primary or secondary sensor data were released to the public – achieved by matching the individual NDBC variable values to the equivalent primary or secondary NCEI netCDF values, therefore identifying the correct netCDF metadata. Additional outlier QA/QC variable checks, station and metadata verification (provided by literature reviews and historical NDBC buoy deployment log books) allowed for the development of a best available, self-described USACE QCC Measurement Archive.

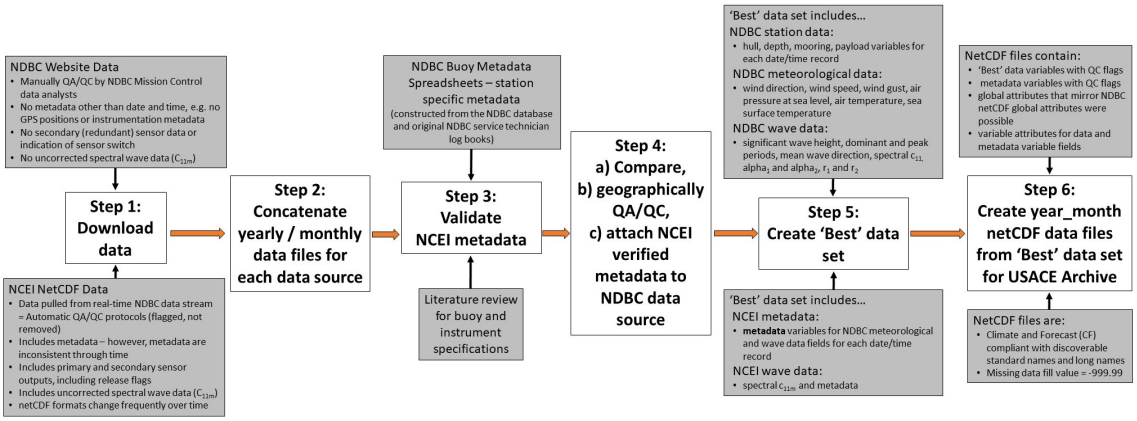


Figure 3.1. Flowchart of the USACE QCC Measurement Archive methodology. This flowchart outlines input data sources, station and metadata verification, selected 'best' data sets and output netCDF files.

The USACE QCC Measurement Archive methodology process consists of two phases. The first phase of the project processes the historical data, while a second phase annually appends newly available data to the historical database. The data archive routine involves a six step process (Figure 3.1) for each buoy station: (1) download, (2) concatenation, (3) metadata verification, (4) comparison, geographical QA/QC and metadata attachment, (5) best dataset selection, and (6) netCDF data file creation. Finally these netCDF files are uploaded to the buoy section of the USACE CHL Data server.

These steps were automated using scripts developed in R software (R Core Team, 2021). Where necessary, each script was subset to handle the particular idiosyncrasies (Hall and Jensen, 2021) of the NDBC and NCEI netCDF data archives. To process all of the historical NDBC data (1970 - 2021), steps two to five in phase one required ~ 400k cpu hours at the Department of Defense (DOD) Supercomputing Resource Center.

The following steps outline the methodologies utilized within this USACE QCC Measurement Archive development. For more detailed information, please see the USACE QCC Measurement Archive Standard Operating Procedure (SOP) document that is stored in the Archive GitHub (https://github.com/CandiceH-CHL/USACE_QCC_measurement_archive.git).

1. Step 1: **Download**. Historical NDBC data for all NDBC stations are downloaded from the NDBC website and the NCEI archives. Source-specific archive download links are listed in the USACE QCC Measurement Archive SOP. Data from the storage specific files types (detailed below) are extracted for concatenation in step 2.

   The NDBC website stores data in zipped yearly and monthly files as standard meteorological (stdmet), spectral wave density (swden), spectral wave ($alpha_1$) direction (swdir), spectral wave ($alpha_2$) direction (swdir2), spectral wave ($r_1$) direction (swr1), and spectral wave ($r_2$) direction data (swr2). These files require unzipping. Included within the NDBC stdmet datasets are collected meteorological and bulk wave data in the following structure: wind direction (˚), wind speed (m/s), wind gusts (m/s), significant wave height (m), dominant wave period (seconds), average wave period (seconds), mean wave direction (˚), air pressure at sea level (hPa), air temperature (˚C), water temperature (˚C), dew point temperature (˚C), visibility (miles) and tide (ft). Visibility and tide are no longer collected by NDBC, and are disregarded.

   The NCEI website stores monthly NDBC files per year in netCDF format. All available data and metadata are extracted from these netCDF files. These files contain the same NDBC data as listed above, but also include additional wave spectral parameters such as uncorrected spectral energy wave data ($c_{11}^{m}$), spectral wave co- and quad-spectra, and four wave data quality assurance parameters that are produced by the NDBC wave processing procedure (NDBC, 2003).

   The NCEI netCDF file formats differ significantly before and after January 2011. After January 2011, these netCDF structures varied throughout the years as NDBC buoy structures and netCDF creation procedures changed. Each format requires format-specific code to extract the data from the variable fields.

For example, the pre-2011 netCDF files consistently contain all variables directly within the main file directory. However, the post-2011 netCDF files are structured by 'payload', with subset sensor fields (e.g. 'anemomenter_1'), which in turn have their own subset variable fields (e.g. wind_speed, 'wind_direction') with associated quality control and release flags. Therefore users have to navigate through the payload and sensor subfields to discover the variable data with their associated metadata.

Importantly, these 'payload' fields do not always refer to the on-board computer system that serves the sensor suites, e.g. NDBC's Automated Reporting Environmental System[13] (ARES), but also delineate between sensor suites with available primary and secondary sensor data (e.g. 'payload_1', 'payload_2'). Conversely these primary and secondary sensor data (e.g. 'air_temperature_1' and 'air_temperature_2') may be subset within a single 'payload'. Of note is that these multiple payloads often contain duplicated data.

These 'payload' fields are also important when extracting data captured by NDBC Self-Contained Ocean Observations Payloads (SCOOP), as these netCDF files resemble the physical structure of the buoy stations with their modular sensor assembly. For example, the NCEI netCDF July 2020 data file for station 41009 includes 5 payload subsections. 'payload_1' contains an 'anemometer_1' sensor suite, which contains subset wind variables and data flags; 'barometer_1', with subset air pressure variables and flags; and a 'gps_1' sensor suites, with subset lat, lon variables, etc. 'payload_2' contains a second 'anemometer_1', 'barometer_1', 'gps_1', 'air_temperature_sensor_1', and 'humidity_sensor_1' suites. Payload 3 contains a single 'gps_1' fields (lat and lon variables with flags), while payloads 4 and 5 house 'wave_sensor_1' and 'ocean_temperature_sensor_1' sensor suites, respectively, both with their own 'gps_1' data. In this example, 'payload_1' represents an R.M. Young sensor, while 'payload_2' is listed as a MetPak Weather Station instrument in the netCDF sensor suite attributes.

NDBC is in the process of redesigning these netCDF file formats to be more user friendly. However, they do not plan to reformat their archive datasets. For more details on the NDBC and NCEI netCDF file formats and code extraction descriptions, please see the USACE QCC Measurement Archive SOP within the Archive GitHub.

2. Step 2: **Concatenation**. This step merges each yearly and monthly data files to produce a single time series of concatenated stdmet data, and time series files for each individual spectral wave variable. The concatenated stdmet data format mirrors the NDBC website data formats. To handle the NDBC data, this step allows for the management of differing yearly file formats and spectral frequencies; the concatenation of multiple date and time columns into one field; and the removal of redundant date, time and tide columns in stdmet data. This step allocates the spectral data into the standard NDBC 38 frequencies (old wave sensors), and 47 frequencies (new wave sensors). Finally, this step converts the NDBC $r_1$ and $r_2$ values to their correct units (NDBC $r_1$ and $r_2$ data are scaled by 100 to reduce storage requirements, so these data should be multiplied by 0.01).

   To handle the NCEI data, this step allows for the concatenation of stdmet data to create a dataset that matches the NDBC website data nomenclature. This step also removes data that were flagged as erroneous by automated NDBC QA/QC protocols. As unit standards vary between the NCEI and NDBC website archives, this step converts the NCEI netCDF pressure units to match the NDBC units (Pa to hPa), and converts the air, water and dew point temperatures from Kelvin to degree Celsius to match NDBC data. This step also performs outlier QA/QC, where it removes zero (‘0’) wind gust values when no wind speed values are present; direction values greater than 360 ˚; obvious variable outliers; and duplicated netCDF data points that are ~5-10 seconds apart. To handle the erroneous netCDF spectral frequency data, the code advances through the spectral

data and matches the available spectral frequency data to the appropriate 38 frequencies (old wave sensors) or 47 frequencies (new wave sensors).

3. Step 3: **Verify metadata**. This step is applied solely to the NCEI netCDF data files to validate the netCDF metadata with NDBC-sourced, buoy specific metadata spreadsheets. These metadata spreadsheets were constructed from the NDBC database and original NDBC service technician log books, and provide accurate station and sensor information. Scripts verify or insert missing hull type, payload and mooring type; and verify or insert missing instrument processing systems (for wave data only), instrumentation names and sensor deployment heights. If none are available, metadata fields are augmented with pre-set hull-specific instrumentation specifications that were sourced from online references (for hull-specific instrumentation specifications, please see the USACE QCC Measurement Archive SOP).

4. Step 4: **Compare, geographically QA/QC and attach metadata**. *Compare*: Although these data originate from the same sensor, storage protocols resulted in different time stamps for each within their various archives. This step compares the NDBC and NCEI sourced data by matching the datasets by nearest date and time (to the minute), after which geographical data are appended to the NDBC datasets.

   As the NDBC data are manually QA/QC'd and do not contain data collected during buoy maintenance operations, these data were considered as a date/time reference to quality control the fixed positions of the pre-2011 netCDF datasets. In other words, if data were present within the NCEI dataset, but not within the NDBC dataset, those NCEI data records were removed.

   Of interest are the datasets within the NCEI netCDF files that pre-date any data published on the NDBC website. These data are likely from sensor and processing tests conducted during deployments that were intentionally not released to the

public. These early data are included in the USACE QCC Measurement Archive but have quality control (QC) flags that rate them as unreliable. For more information on these earlier datasets, please reference the technical note on utilising NDBC data, ERDC/CHL CHETN-I-100 (Hall and Jensen, 2021).

*Geographically QA/QC*: Each dataset is filtered to remove GPS positions and associated data that are not within a one (1) degree radius (~60 nautical miles) of the NDBC station watch circles (the surface area through which a buoy can travel while tethered to specific location by a mooring). This radius allows for fluctuations in NDBC deployment locations over the decades, as tests showed that radii of less than one degree significantly removed viable data (see Figure 3.2 in the Technical Validation section). Users may wish to further filter their specific datasets to remove additional data points that are outside their target deployment locations; a task now easily achievable with the fully-described, verified metadata included within this USACE QCC Measurement Archive (Hall and Jensen, 2022a).

Two methods are used to geographically QA/QC these data: 1) a sorted table of value occurrences to find the most common latitude and longitude positions (using the assumption that the buoy held its correct station for the majority of its life cycle); 2) a manual confirmation and insertion of the primary station locations that were sourced from NDBC buoy specific metadata spreadsheets. This manual step was relevant for buoys that did not consistently hold their stations due to high vandalism rates or strong currents.

*Assign metadata*: Once the data are geographically QA/QC'd, this step assigns verified metadata (from step 3) to the NDBC stdmet datasets as follows. Station-specific hull type, water depth, payload and mooring type are appended to the NDBC stdmet datasets from the NDBC-sourced, buoy specific metadata spreadsheets. These NDBC Buoy Metadata Spreadsheets and the verified NCEI netCDF metadata are then used to assign the correct primary or secondary sensor

designation, which includes metadata such as instrument processing systems (for waves) and instrumentation information (names, deployment heights etc.), to the NDBC stdmet datasets by matching the time paired NDBC variable values with the exact NCEI values.

5. Step 5: **Create best dataset**. This step selects a combination of the geographically QA/QC datasets that were created in step 4 above. These best available, self-describing datasets (Figure 3.1) include:
   - NDBC website wind direction, wind speed, wind gust, air pressure at sea level, air temperature, sea surface temperature, significant wave height, dominant and peak periods, mean wave direction, spectral $c_{11}$, $alpha_1$, $alpha_2$, $r_1$, $r_2$, with their now fully-described, verified metadata.
   - NCEI netCDF spectral $c_{11}^{m}$. These data are retained within the USACE QCC Measurement Archive to allow for bulk wave parameter re-calculations without the influences of NDBC shore-side processing protocols.
   - Verified station metadata obtained from the NDBC Buoy Metadata Spreadsheets.
   - NCEI netCDF data for the above variables that pre-date the NDBC datasets (where applicable).

6. Step 6: **Create netCDF data files**. This step creates monthly netCDF NDBC data files that collate all of the best available data variables that were selected in step 5 above. For easy access by the USACE and user community, these month-long netCDF data files are stored on the USACE CHL Data Server and are updated annually. A static copy of the historical data (1970 - 2021) is located within the USACE Knowledge Core Library Datasets (Hall and Jensen, 2022a).

### *3.2.4 Data Records*

The static USACE QCC Measurement Archive is stored within the USACE Knowledge Core Library Datasets (Hall and Jensen, 2022a; http://dx.doi.org/10.21079/11681/43121). The archive includes 141 NDBC stations that have collected data from 1970 through 2021 (where available). Measurement data are stored in monthly netCDF files. For months where all data were available, these monthly, self-describing netCDF files contain 13 station variables and metadata fields, 41 wave data and metadata fields (either 47 or 38 spectral frequency bands), and 28 meteorological data and metadata fields. Metadata are fully described within the variable attributes, including flag number descriptions and metadata source references. All netCDF files contain global attributes that detail general NDBC collection information, World Meteorological Organization (WMO) ID's and other NDBC station-specific metadata. All netCDF files are Climate and Forecast (CF) compliant with discoverable standard names, and standard missing data fill values of -999.99.

Station metadata variables include time, depth, depthFlag, hull, hullFlag, latitude, latitudeFlag, longitude, longitudeFlag, mooring, mooringFlag, payload, payloadFlag

Wave data and metadata include:

- waveHs (with associated data Flag, Metadata, MetadataFlag)
- waveTm (data Flag, Metadata, MetadataFlag)
- waveTp (data Flag, Metadata, MetadataFlag)
- meanWaveDirection (data Flag, Metadata, MetadataFlag)
- waveFrequencies_47
- waveEnergyDensity_47Frequencies (data Flag, Metadata, MetadataFlag)
- waveEnergyDensityUncorrected_47Frequencies (data Flag, Metadata, MetadataFlag)
- waveAlpha1_47Frequencies (data Flag, Metadata, MetadataFlag)
- waveAlpha2_47Frequencies (data Flag, Metadata, MetadataFlag)
- waveR1_47Frequencies (data Flag, Metadata, MetadataFlag)
- waveR2_47Frequencies (data Flag, Metadata, MetadataFlag)
- waveFrequencies_38
- waveEnergyDensity_38Frequencies (data Flag, Metadata, MetadataFlag)
- waveEnergyDensityUncorrected_38Frequencies (data Flag, Metadata, MetadataFlag)
- waveAlpha1_38Frequencies (data Flag, Metadata, MetadataFlag)

- waveAlpha2_38Frequencies (data Flag, Metadata, MetadataFlag)
- waveR1_38Frequencies (data Flag, Metadata, MetadataFlag)
- waveR2_38Frequencies (data Flag, Metadata, MetadataFlag)

Meteorological data and metadata include:

- windDirection (data Flag, Metadata, MetadataFlag)
- windGust (data Flag, Metadata, MetadataFlag)
- windSpeed (data Flag, Metadata, MetadataFlag)
- surfaceAirPressure (data Flag, Metadata, MetadataFlag)
- surfaceAirTemperature (data Flag, Metadata, MetadataFlag)
- surfaceDewPointTemperature (data Flag, Metadata, MetadataFlag)
- surfaceSeaTemperature (data Flag, Metadata, MetadataFlag)

An active USACE QCC Measurement Archive is located within a buoy section on the CHL Data server and is updated annually.

### *3.2.5 Technical Validation*

Most data users assume the accuracy of the quality controlled NDBC datasets. Few confirm the geographical position of the data prior to use and rely on outlier checks to identify bad data. However, NDBC only posts the most recent deployment location on their website for each moored buoy site, and does not list historical deployment positions. While NCEI netCDF files do contain hourly GPS data (where available), these datasets also include erroneous wave data that were collected while the buoys are adrift and data that were flagged, but not removed during automated NDBC QA/QC procedures. These wave data are inaccurate as NDBC moored buoy wave data processing algorithms (NDBC, 2003) (e.g. hull response amplitude operators) are not designed to resolve for buoy pitch, roll and heave estimates while untethered to the sea floor, a fundamental component in estimating wave height.

Figure 3.2 showcases examples of geographical position importance when evaluating NDBC data accuracy. Green track lines and points within the maps and time series plots encapsulate data within an acceptable distance of the deployment location, with red track lines and points highlighting those outside the moored buoy watch circle. Importantly, the time series plots in Figure 3.2 showcase how the significant wave height ($H_s$) data reported

while the buoy was adrift (red points within the time series data) appears within reasonable ranges and are not easily identifiable as suspect. Hence a liberal geographical limit was placed on the USACE QCC Measurement Archive that removed data exceeding a one degree radius (~ 60 nautical miles) of the median geographical position of the station. This intentionally substantial buffer (~120 nautical miles in total) allows for fluctuating NDBC deployment locations over the decades, as highlighted by the four sites of high density green data points within Station 41001's GPS positions (Figure 3.2, bottom right map). As the USACE QCC Measurement Archive contains fully verified geographical positions for each data point, users may now easily refine these individual stations for their specific time period and deployment location of interest.

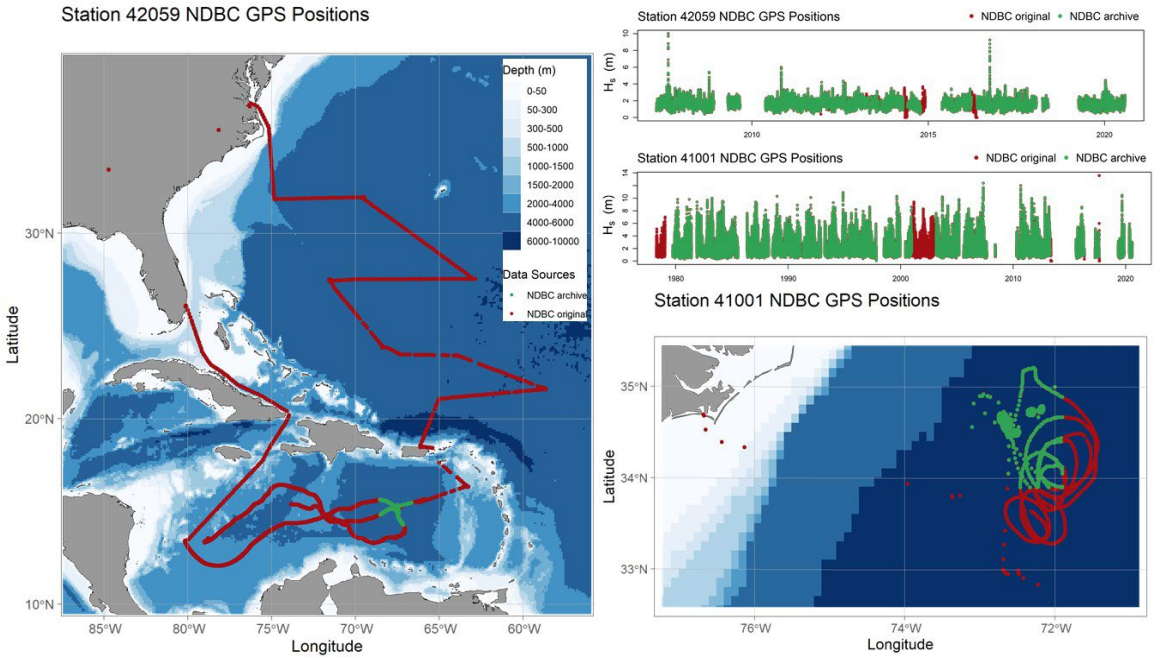


Figure 3.2. NDBC Stations 42059 (left map) and 41001 (bottom right map) buoy locations before and after geographically QA/QC of the buoy recorded GPS data. Map plots showcase the recorded buoy movement along the ship track (left map) and while the buoy was adrift (right map), while time series plots of the concurrent significant wave height (m) showcase the data collected while the buoys were both on and off their deployed mooring station (i.e. during ship transit and while adrift). In all plots, green points and track lines represent data within a one degree radius of the deployment location (mooring station), while red points and track lines indicate data recorded while outside of that target location.

Reviewing the USACE QCC Measurement Archive on a wave spectral level, Figure 3.3 shows mean wave energy density ($c_{11}$) across the spectral frequency from the NDBC and NCEI data sources for NDBC station 44014 during 2017. The pre-QA/QC *all* $c_{11}$ data are represented by light blue triangles for the NDBC data source, and pink triangles for the NCEI data source (note that the pink triangles are overshadowed by the post-QA/QC $c_{11}$ dark blue squares in Figure 3.3). These non-QC'd datasets show very little agreement in Figure 3.3, which clearly highlights the errors in the NCEI netCDF wave spectral data as these spectral data are duplicates of time-paired data from the same, unique sensor.

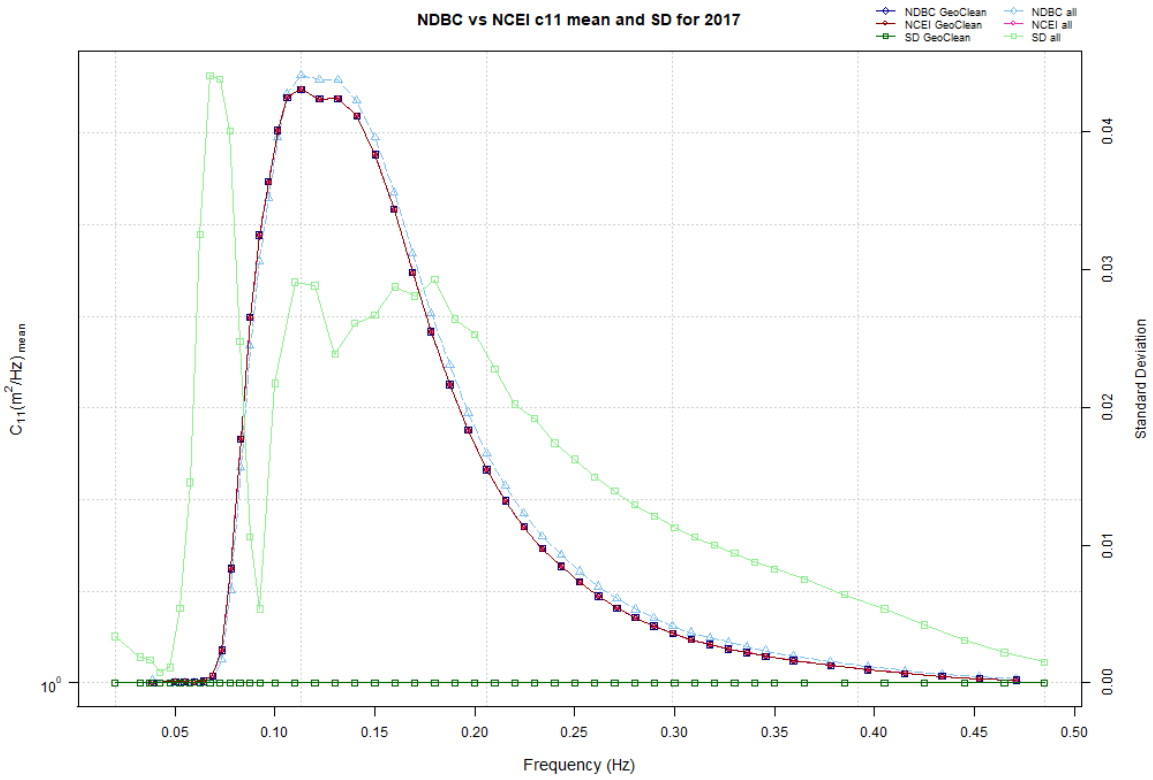


Figure 3.3. Mean spectral wave energy density ($c_{11}$) from NDBC and NCEI data sources for NDBC station 44014 for the year 2017. The geographically cleaned (*GeoClean*) post-QA/QC $c_{11}$ are represented by dark blue squares for the NDBC data source, and red squares for the NCEI data source. The pre-QA/QC *all* $c_{11}$ data are represented by light blue triangles for the NDBC data source, and pink triangles for the NCEI data source (where the pink triangles are overshadowed by the post-QA/QC *GeoClean* NDBC blue squares). Measured on the right axis, standard deviations are represented by light green squares for the pre-QA/QC *all* NDBC and NCEI standard deviations, and dark green squares for the post-QA/QC *GeoClean* NDBC and NCEI standard deviations.

After the removal of the erroneous geographical data and outliers, a review of the geographically cleaned (*GeoClean*) post-QA/QC $c_{11}$ data from the NDBC (dark blue squares) and the NCEI data sources (red squares) show agreement in that they overlay each other across the spectral frequencies. Additionally, standard deviations between the pre-QA/QC (light green squares) and post-QA/QC (dark green squares) NDBC and NCEI data show a vast improvement after geographical and outlier checks with the post-QA/QC $c_{11}$ standard deviations remaining at zero.

In summary, these typical example evaluations showcase the validity of this USACE QCC Measurement Archive process on the quality of the NDBC meteorological and oceanographic data. Note that this methodology only removes known errors and does not verify data quality from an alternate source. However, this validation and verification work allows for confidence in the NDBC data sourced from the USACE QCC Measurement Archive. Ultimately, this self-describing, consistent USACE QCC Measurement Archive provides measurement data with verified metadata for the accurate evaluation of historical U.S. coastal conditions, which are essential for USACE risk assessment studies, coastal flooding, wave applications, and coastal engineering efforts.

### *3.2.6 Usage Notes*

For code reviews, users should reference the USACE QCC Measurement Archive SOP document that is stored on the Archive GitHub (https://github.com/CandiceH-CHL/USACE_QCC_measurement_archive.git). This document details the USACE QCC Measurement Archive R code suite that was developed during this work. This R code suite is fully open access and is version controlled. If users plan to reproduce this study, please note that steps two to five in phase one (processing the 1970 – 2020 historical NDBC data) utilized ~400k high performance computing cpu hours.

Users developing their own quality controlled NDBC Measurement Archive should reference the technical note on utilising NDBC data, ERDC/CHL CHETN-I-100 (Hall and Jensen, 2021), which fully details the NDBC website and NCEI stored NDBC netCDF

data idiosyncrasies that were discovered during this process. For example, different netCDF file extractions codes are required to handle the multiple NCEI netCDF storage formats. NDBC is in the process of redesigning their present netCDF file format to be more user friendly, but do not plan to edit their archived data. This methodology is structured to handle future NDBC netCDF format changes with minimal code edits.

Additionally, the NCEI netCDF archive routinely contains monthly data that are separated into multiple files with non-sequential suffixes (D1 - $D_n$). These multiple monthly files indicate that the station was serviced during that month and the data separated to capture the change in instrumentation in the netCDF file metadata. Another note is the similar variable nomenclature that is employed within the NCEI NetCDF files that introduce duplicate data rows if not accounted for, for example: extracting the GPS variable, 'lon', from the netCDF files will also capture 'solar_radiation_sensor_1_ longwave_radiation' data where available. Please see Appendix E in the technical note on utilising NDBC data, ERDC/CHL CHETN-I-100 (Hall and Jensen, 2021), for a list of these similar variable names.

Data archive idiosyncrasies include the use of various column header nomenclature within the historical NDBC website over the decades (please see Appendix D: ERDC/CHL CHETN-I-100 for these changes). Station-specific idiosyncrasies also occur, such as the NDBC website data for station 41009 that has large periods of duplicate NDBC hourly records with no minute information (required manual insertion of minute data as these rows were determined to be unique). The NCEI netCDF data files had similar inaccurate records: for example, the September 2012 netCDF data file for station 41009 contains 2334 10-second continuous wind data fields, 2334 QC flag fields, but only 777 release flag fields. The netCDF files also contain spurious variable place holders that hold no data.

Additionally, while the NDBC website data contain the two sets of wave spectral frequency bands that represent the historically deployed wave instrumentation, the NCEI stored NDBC netCDF files contain multiple sets of wave spectral frequency bands that do not match the NDBC data (please see Appendix F: ERDC/CHL CHETN-I-100 (Hall and

Jensen, 2021) for a list of these erroneous frequencies). Data encased within these non-conforming frequencies bands were treated carefully to only extract the real spectral estimates from amongst the inaccurate wave frequency bands and values.

Finally, data of dubious quality require identification and removal via date/time comparisons with the manually QA/QC'd data, geographical QA/QC and metadata verification. These checks include obvious outlier and erroneous data corrections, including the removal of directional values greater than 360 °; wind gust data that were present when wind speed values were not available; and duplicated netCDF data points that are ~5-10 seconds apart.

## 3.3 Correcting for discontinuities in NDBC time series data

*This section of work is published in Hall, Jensen & Wang (2022a): 'Wave Power Trends along the U.S. Coastline: In situ Measurements and Model Hindcasts Estimates', as cited at the top of this chapter.*

### *3.3.1 Data and Methodology*

Over the decades, NDBC have developed and refined new moored buoy platforms, sensors, processing protocols and modelling algorithms to improve quality in their wave measurements while responding to increasing demands for providing long-term, high-quality, continuous observational data (Earle et al., 1984, 1999; Steele et al., 1985, 1992; NDBC, 2003; Riley et al., 2011; Riley and Bouchard, 2015). However, these data are known to contain discontinuities within the long time series data, which many have identified and attempted to correct (e.g. Gemmrich et al., 2011; Young et al., 2011; Livermont et al., 2015; Livermont et al., 2017; Young and Ribal, 2019; Hall and Jensen, 2021). This work offers a definitive solution to mitigate these discontinuities.

### *3.3.2 Moored NDBC buoy data*

Moored buoy data were collated from the USACE QQC Measurement Archive (Hall and Jensen, 2022b), stored on the USACE CHL Thredds Server (USACE, 2022). Multiple works have comprehensively described NDBC's collection methodology, applied calibration techniques and processing protocols for non-directional and directional wave measurements (e.g. Earle et al., 1984, 1999; Steele et al., 1985, 1992; NDBC, 2003; Riley et al., 2011; Riley and Bouchard, 2015).

Although NDBC has predominantly used the same wave parameter definitions and equations throughout its history, shore side quality control procedures and collection platforms have advanced through the decades. For example, NDBC has historically used different wave instrumentation (detailed within Chapter 4's Appendix 4.6.2) that record spectral wave energy estimates across two frequency band ranges (NDBC, 2003), a 38-band wave spectrum (0.300-0.400 Hz) and a 47-band wave spectrum (0.0325-0.485 Hz). The bandwidth is a constant 0.01 Hz for the 38-band wave spectrum. However, the bandwidths of the 47-band wave spectrum are 0.005 Hz, 0.01 Hz and 0.02 Hz for low, middle, and high frequency regions, respectively (detailed within Chapter 4's Appendix 4.6.2, NDBC, 2003, 2018b, Teng et al., 2009).

With the increase in range and bandwidth variations of the now standard 47-band wave spectrum in the 2000's (instrumentation replacement times differ across NDBC stations due to the variable maintenance schedules), the wave energy is displayed in different frequency bands between older systems and newer systems. Therefore, to account for the variations in wave energy distribution across the spectrum that would result from these different frequency ranges, available NDBC data that were collected using the 38-band wave spectrum were linearly interpolated to match the current NDBC standard 47-band wave spectrum (Chapter 4's Appendix 4.6.3), thereby reassigning captured wave energy within comparable frequency bands. This interpolation ensures that all of the following buoy station wave height, periods and power estimates were calculated from wave energy across consistent frequencies throughout the evaluated time periods.

Once these frequencies were interpolated where necessary, bulk wave parameters were calculated from the now consistent NDBC non-directional spectral frequency *E(f)* (*C11(f)* in NDBC nomenclature) to mitigate for possible variance from changing shore-side processing protocols. Significant wave height was calculated as $H_{m0} = 4\sqrt{m_0}$ . $m_0$ is the variance of the wave displacement time series acquired during the wave acquisition period: $m_0 = \sum_{fl}^{fu}(S(f).d(f))$, "where the summation of spectral density, *S(f)*, is over all frequency bands, from the lowest frequency $f_l$ to the highest frequency, $f_u$, of the nondirectional wave spectrum and *d(f)* is the bandwidth of each band'; NDBC, 2018a). Dominant wave period, or peak wave period, as defined as $T_p = \frac{1}{f_p}$ (NDBC, 2003), where $f_p$ represents the peak frequency band.

These frequency interpolations and subsequent recalculations of the NDBC bulk parameters identified that one of the culprits that contribute to the often discussed NDBC data discontinues (Gemmrich et al., 2011; Young et al., 2011; Livermont et al., 2015, 2017; Young and Ribal, 2019) is the historical use of these varying wave spectrum ranges. This observation is evident in the NDBC station 41009 $T_p$ time series data (Figure 3.4, top plot), where the switch between 38-band and 47-band wave spectrum usage adds more frequency bands in the low frequency range of the wave spectrum and thus reduces the number of expected dominant $T_p$ value shifts on October 4th, 2003 (as identified using the USACE QCC Measurement Archive). However, the bottom plot in Figure 3.4 visibly shows how the linear interpolation of the 38-band wave spectrum to 47 frequency bands and recalculation of peak wave period alleviates this impact, removing obvious discontinuities in this NDBC data record.

Another instrumentation change at NDBC station 41009 (Figure 3.4) occurred on October 4th, 2003: a switch from the Value Engineered Environmental Payload (VEEP) to the Acquisition and Reporting Environmental System (ARES) payload (as identified within the USACE QCC Measurement Archive), lending obscurity to the above statement that $T_p$ discontinuities are caused by different wave spectrum usage.

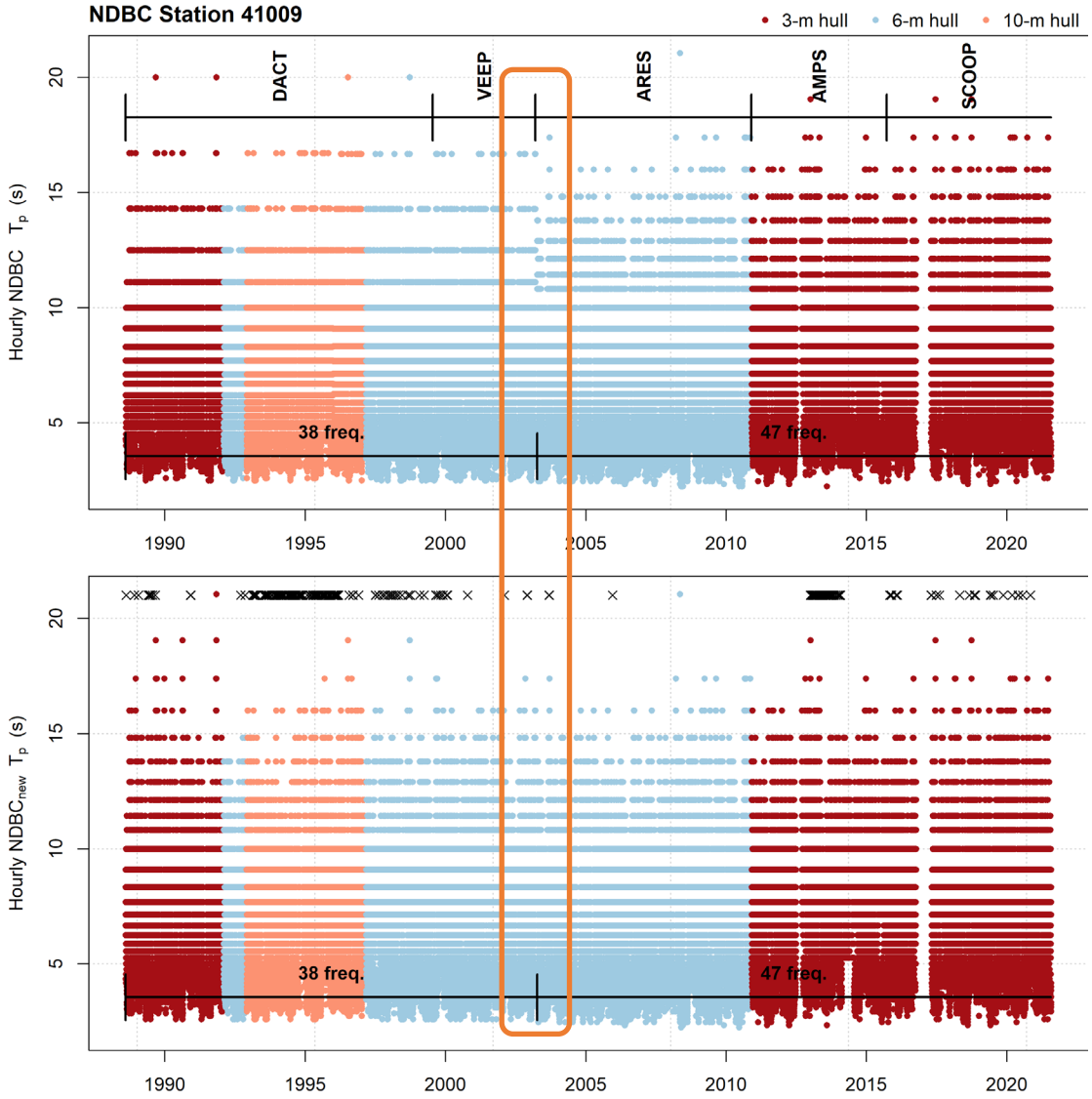


Figure 3.4. Published NDBC hourly $T_p$ (top) vs calculated hourly NDBC $T_p$ (bottom) for NDBC station 41009, with orange boxes highlighting variations in peak period. Colours represent deployed hull types. Historical timelines highlighting the use of verified payload type (payload acronyms are described in Chapter 4's Appendix 4.6.2) and frequency bands are shown for Station 41009. Mooring type and depth were constant for the full station deployment history. Black crosses indicate where original, hourly NDBC data are available to augment missing data within the recalculated dataset.

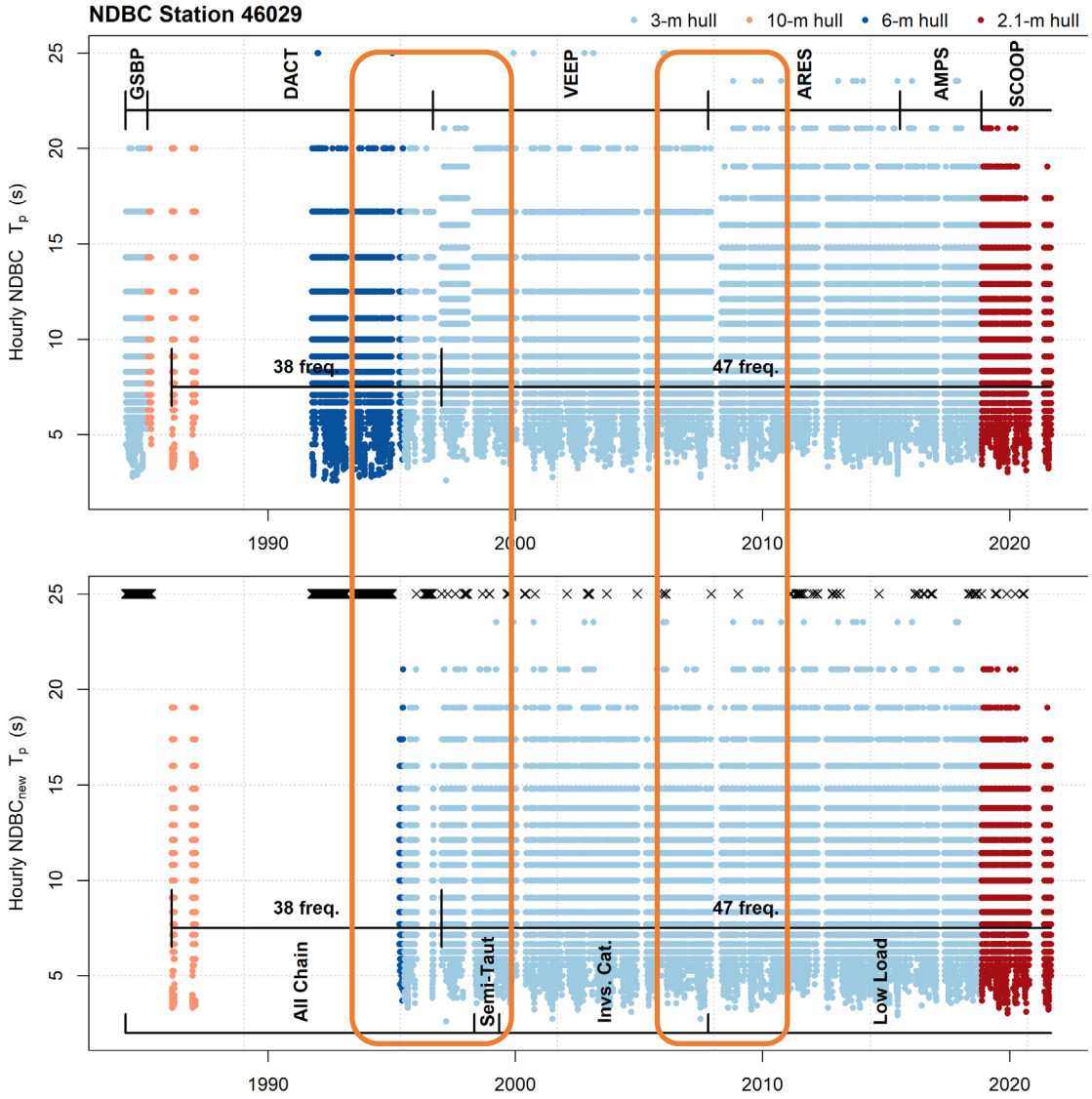


Figure 3.5. Published NDBC hourly $T_p$ (top) vs calculated hourly NDBC $T_p$ (bottom) for NDBC station 46029, with orange boxes highlighting variations in peak period. Colours represent deployed hull types. Timelines highlighting the usage of verified payload type (payload acronyms are described in Chapter 4's Appendix 4.6.2), mooring and frequency bands are shown for Station 46029. Black crosses indicate where original, hourly NDBC data are available to augment missing data within the recalculated dataset.

Figure 3.5 showcases an example of NDBC instrumentation shifts that affected the NDBC calculated $T_p$ at station 46029, where variations are evident between the 38-band and 47-band wave spectrum on January 3rd, 1997; with a random variation in $T_p$ that is not associated with an instrumentation or system change a few months later (possibly a shore-side processing change); and between the VEEP and ARES payload switch on October 21st, 2007 (as identified within the USACE QCC Measurement Archive). Figure 3.5 indicates that the expected dominant $T_p$ value shifts with the frequency band change in 1997, but not with the earlier switch from the Data Acquisition and Control Telemetry (DACT) payload to the VEEP on September 1st, 1996. Therefore this wave spectral frequency correction utilised within this work decreases variations within the peak period, regardless of deployed NDBC instrumentation or applied shore-side processing protocols, successfully removing discontinuities in the NDBC data records used within this work.

Apart from minimal outlier removal, no other quality control of the calculated bulk parameters was necessary. This chapter therefore provides the first published methodology to mitigate NDBC discontinuities discussed by others using NDBC data.

Of note is that data gaps (indicated by black crosses within the bottom plots in Figure 3.4 and Figure 3.5) show hourly time periods where no verified spectral wave data were available for recalculation. For these instances of missing hourly spectral data and where the original hourly NDBC datasets did contain bulk parameter values (Hall and Jensen, 2021; Hall and Jensen, 2022b), the original NDBC bulk parameter values were inserted into the newly calculated datasets to minimise data gaps. In light of the availability of these spectral data, the minimal offsets that were introduced by augmenting the recalculated datasets with these older NDBC data (that were calculated using the 38-band wave spectrum) are deemed acceptable for this work.

*(As the above subsection is extracted from Hall, Jensen & Wang (2022a): 'Wave Power Trends along the U.S. Coastline: In situ Measurements and Model Hindcasts Estimates' journal paper that is showcased in chapter 4, the appendices referenced in the above section are listed at the end of chapter 4.)*

## 3.4 Discussion and Conclusion

This chapter highlights archival inconsistencies that were discovered within the various NDBC archives. This chapter details how these data were corrected by geographically quality controlling the data, removing data that were recorded during instrumentation servicing, and with the application of a secondary measurement QC procedure. These data were further improved by appending station, buoy and instrument-specific metadata to each measurement value, ultimately creating the most comprehensive NDBC archive that is currently available - the USACE QCC Measurement Archive.

While this clean archive removed a significant portion of the inconsistencies with the time series data, additional discontinuities remained that required investigation. Tests show that the majority of these discontinuities are caused by the historical deployment of wave instruments that use different spectral frequency ranges. To correct for this, the older wave spectral data that were collected across 38 frequency bands were interpolated to match the currently deployed 47 frequency bands, in an effort to redistribute the wave energy across consistent frequency bands.

The recalculation of the bulk wave parameters from these now matching wave spectral frequencies results in a substantial improvement within the time series data continuity. Therefore this methodology provides a consistent, uniform wave time series data set for use within the following wave power trend analyses. This chapter proves that it is possible to correct for bias between different wave measurement systems and to produce homogeneous long-term time series records.

## Chapter 4

# 4. Is wave power increasing over time?

## Preface:

This chapter investigates whether wave power along the U.S. coastline is increasing over time. This chapter has been published in the following peer-reviewed journal, and is included within this chapter in the Ocean Dynamics journal format:

**Hall, C., Jensen, R.E. & Wang, D.W. 2022**. Wave Power Trends along the U.S. Coastline: In situ Measurements and Model Hindcasts Estimates. *Ocean Dynamics*. https://doi.org/10.1007/s10236-022-01515-x

This chapter addresses the third key question listed in Section 1.3.3.

*This section of work is published in Hall, Jensen & Wang (2022a): 'Wave Power Trends along the U.S. Coastline: In situ Measurements and Model Hindcasts Estimates', as cited above.*

**Wave Power Trends along the U.S. Coastline: In situ Measurements and Model Hindcasts Estimates**

### 4.1 Abstract

Observational data are successfully assessed to investigate wave power (wave energy flux per unit of wave-crest) trends within four coastal regions around the US, a parameter that is deemed vital to those responsible for coastal protection and community resilience. This study tests for shifting observational inter-annual wave power trends using a newly developed, unique, United States Army Corps of Engineers Quality Controlled Consistent

Measurement Archive, and offers a viable methodology to remove documented observational time series data discontinuations. This study is one of the first to show spatially and temporally comparative observational and model wave power results, providing new information on the accuracy of model wave power estimates, while showcasing in situ wave power trends at 29 sites around the U.S. coastline. Overall, the majority of the eastern Pacific Ocean and Hawaii wave power trends are downward, with mixed slope wave power trends apparent within the Atlantic Ocean and Gulf of Mexico. Observational and model results are similar with respect to timing, but not magnitude, of wave power peaks in long term inter-annual trends, with the moored buoy data presenting smaller wave power ranges for two (eastern Pacific Ocean and Hawaii) of the four regions. Additionally, the detection of a noticeable variability in the wave power trend direction within each region suggests that site specific wave power trends should not be generalised to represent a large region. This work demonstrates that observational data are essential in local and regional wave climate studies to accurately estimate wave power for coastal planners and engineers.

## 4.2 Introduction

Wave power measures the transport of wave energy (wave energy flux per unit of wave-crest) that is critical for shoreline evolution. Huppert et al. (2020) showed that wave power is a good predictor of how fast or slow a rocky coastline in Hawaii will erode, while Suzuki and Yoshiaki (2018) demonstrated that medium-term shoreline fluctuation is a direct result of wave power influence. Leonardi et al. (2015) postulate that variations in background or mean wave power over the long-term appear to have a greater effect on salt marsh erosion than short-term extreme wave conditions. Therefore, the background wave climate and associated long term inter-annual wave power trends are critically important for engineers to design, protect and fortify our coastal infrastructure (USACE, 2002).

There has been a substantial effort to analyse the impact of extreme storm events and the wave heights that affect our coastlines (Massey et al., 2011; Cialone et al., 2015; Gravens et al., 2018; Massey 2019). As multiple studies show that wave heights are increasing over

time (Allan and Komar, 2000; Komar and Allan, 2007; Menéndez et al. 2008; Ruggiero et al., 2010; Young et al., 2011; Bertin et al., 2013; Panchang et al., 2013; Storlazzi et al., 2015; Jabbari et al., 2021), then it stands to reason that the power of the waves hitting our coastlines is increasing. Monitoring events and/or peak conditions from a storm might not track mean coastal damage or climate trends sufficiently, as a modest event lasting hours or days could have a larger impact on a coastline than a fast moving extreme event. For instance, Panchang et al. (2013) and Appendini et al. (2018) found that although maximum significant wave height did not increase significantly in their independent Gulf of Mexico studies, the frequency of larger waves did. Therefore, with the added scaling effects of larger waves (with larger waves, the wavelength and period must increase), the use of only one variable (height) may lead to inaccurate results. These results necessitate an understanding of the background wave climate for determining the baseline stress levels on a coastline.

Wave data from hindcast wave models provides coverage in both space and time for long-term wave climate studies, while in-situ wave data from moored buoys are often lacking due to the cost of long-term deployment and maintenance. As a result, previous studies have investigated global and local wave power using wave hindcast model outputs (Furuichi et al., 2008; Dobrynin et al., 2012; Soares et al., 2014; Reguero et al., 2015; Kamranzad et al., 2016; Mentaschi et al., 2017; Ulazia, et al., 2017; Mudelsee, 2019; Reguero et al., 2019; Ahn and Neary, 2020). Few studies have strictly used moored buoy observation data to calculate wave power to investigate trends, due to the lack of consistent data over time (e.g. Saha et al., 2010; Reguero et al., 2019), as well as instrumentation and processing discontinuity uncertainties within observation time series data (e.g. Gemmrich et al., 2011; Young et al., 2011; Livermont et al., 2015, 2017; and Young and Ribal, 2019).

Recently the United States Army Corps of Engineers (USACE) developed a self-describing Quality Controlled and Consistent (QCC) Measurement Archive (Hall and Jensen, 2022b) that collates historical moored buoy measurements from online NOAA National Data Buoy Center sources, removes data points from periods when the buoys were adrift or undergoing maintenance, and verifies all available metadata from in-house

NDBC sources for each historical data point. As this study uses these geographically cleaned data and verified metadata from the newly developed USACE QCC Measurement Archive (Hall and Jensen, 2022b), it confidently identifies instrumentation and system changes that occurred throughout the history of NDBC study sites. These verified metadata enable this study to be the first to offer a viable methodology to remove the observational time series data discontinuations that were highlighted by previous studies (Gemmrich et al., 2011; Young et al., 2011; Livermont et al., 2015, 2017; and Young and Ribal, 2019). Additionally, this study tests for interannual and interdecadal trends in wave power using measurement data that are interpolated for missing values and detrended for seasonality (to isolate trend shifts), allowing for a continuous time series of moored buoy data with no gaps and or background seasonality variance bias.

As USACE now has two unique wave data resources, the USACE QCC Measurement Archive and a long-term Wave Information Study (WIS) model hindcasts, these resources enable this unique wave climate study that uses wave data from a model and moored buoys for wave power trend validation and comparisons. Hence this work compares long-term in situ wave power time series trends and calculations with collocated and concurrent wave model estimates of wave power, allowing for (1) the examination of long-term trend of in-situ wave power time series of wave buoy data and (2) the validation of spatially and temporally comparable WIS model estimates.

The paper is organised as follows. Section 2 describes the data used within this work, and provides a method for handling in situ observational calculations and discontinuities, before removing seasonality from data signals and outlining definitive statistical analyses. In Section 3, evaluations of the collated and concurrent observational and model wave power trends and estimates are discussed, with an overall summary in Section 4.

## 4.3 Data and Methodology

This work uses the National Oceanic and Atmospheric Administration (NOAA) National Data Buoy Center (NDBC) wave data as they provide one of the longest time series of

observational wave data that currently exists. This work develops the first set of wave power values that are calculated from the most accurate NDBC data to date: the newly developed USACE Quality Controlled Consistent Measurement Archive (Hall and Jensen, 2022b).

Wave power estimates from collated and concurrent USACE WIS datasets are used for comparative trend purposes to evaluate methodologies used within this work. The NOAA National Hurricane Center storm records and three NOAA teleconnection climate indices are included to provide context during interpretation of the observed moored buoy wave power trends.

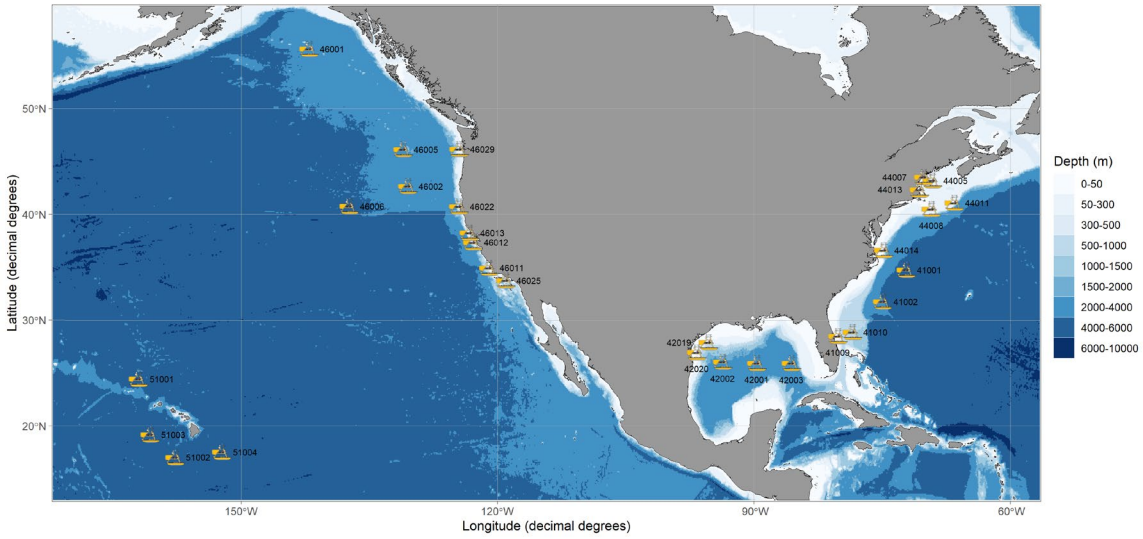


Figure 4.1. NDBC and WIS study sites.

Review sites are chosen to include a wide variety of wave environments (Figure 4.1). West coast and open ocean swell wave environments with large fetch potentials are represented by eastern Pacific Ocean and Hawaiian time series data. Locally generated wind sea conditions with localised extreme events are showcased by Atlantic Ocean and Gulf of Mexico data. Great Lakes data that would represent locally generated wind sea conditions are ignored due to the short, summer season deployment periods of these ice-prone winter regions, which are thus riddled with large gaps in the winter wave records that cannot be

supplemented. Sites were selected with deployment lengths of 30 years or longer, and deployment locations in waters that are deep enough to negate possible shallow water shoaling effects on wave power estimates. Chapter 4's Appendix 4.6.1 details the reviewed NDBC and WIS sites, including their water depths and lengths of record.

All data manipulation and analyses were performed using R software (R Core Team, 2021; RStudio Team, 2021).

### *4.3.1 Wave power calculations*

As per Resio et al. (2003), wave power (wave energy flux per metre of wave-crest length in kW/m) is calculated from $H_{m0}$ (m) and $T_p$ (s) as $P \approx \frac{\rho g^2}{64\pi} H_{m0}^2 T_p$, where "$\rho$ is the density of water (998 kg/m$^3$) and $g$ is the acceleration of gravity (9.81 m/s$^2$)" (Resio et al., 2003:72) for deep water waves (where water depth is greater than half the wavelength). Given the site-specific depths under review and wavelengths of the representative values for $T_p$, the deep water wave power equation is considered appropriate for this work (see Appendix 4.6.1).

The Resio et al. (2003) defined fresh water density constant was retained within this work due to the unavailability of the precise estimate of sea water density at each buoy location through specific regions, years and seasons. Therefore maintaining this Resio et al. (2003) constant across all stations negates the regionally variable effects of sea water density within this work. After validation, the wave_energy function in the R software waver package (Marchand and Gill, 2018), which uses the Resio et al. (2003) equation, is used to calculate wave power.

These wave power calculations require $H_{m0}$ and $T_p$ from the NDBC and WIS datasets. However, prior to those calculations, the NDBC moored buoy data are prepared as follows.

### *4.3.2 Moored NDBC buoy data*

Moored NDBC buoy data were prepared as described in section 3.4.2 above.

*NDBC buoy data gap interpolation*

To investigate the temporal behaviour of the wave power at each site, a continuous time series is required for the following seasonal decomposition of wave power estimates, 90$^{th}$ percentile analyses, trend analyses and context comparison with climate indices. However, interpolation across large data gaps causes over-smoothing of the missing data, primarily over gaps at the start of the datasets. Therefore, NDBC datasets were subset to disregard large gaps from the early years to remove bias from the final interpolations.

Using an interpolation function within the R software package, *oce* (Kelley, 2018; Kelley et al., 2021), the remaining subset of data were interpolated over time to replace missing values. The function interpolates the data using the Barnes algorithm (Koch et al., 1983), which allows for the handling of sparse data periods and provides an objective interpolation of data using a multi-pass scheme. The Barnes algorithm performs bilinear interpolations between two values, after which the actual corrected value is calculated as the sum of the weighted averages from the two passes across the dataset (Koch et al., 1983).

For computational efficiency, the hourly datasets were aggregated to daily mean datasets. Comparisons between the interpolations of hourly versus aggregated daily mean data showed no loss in data integrity, with the aggregated daily means reducing the need for interpolation of the daily values. Aggregation to daily mean values also removes diurnal and possible tidal effects from the datasets. Therefore aggregated daily mean values are used with confidence within these next analyses.

These interpolations were applied to all NDBC stations, with results for NDBC station 46001 from 1980 – 2021 showcased in Figure 4.2, which depicts the mean daily wave power (top plot) and interpolated mean daily wave power (bottom plot) in logarithmic scale.

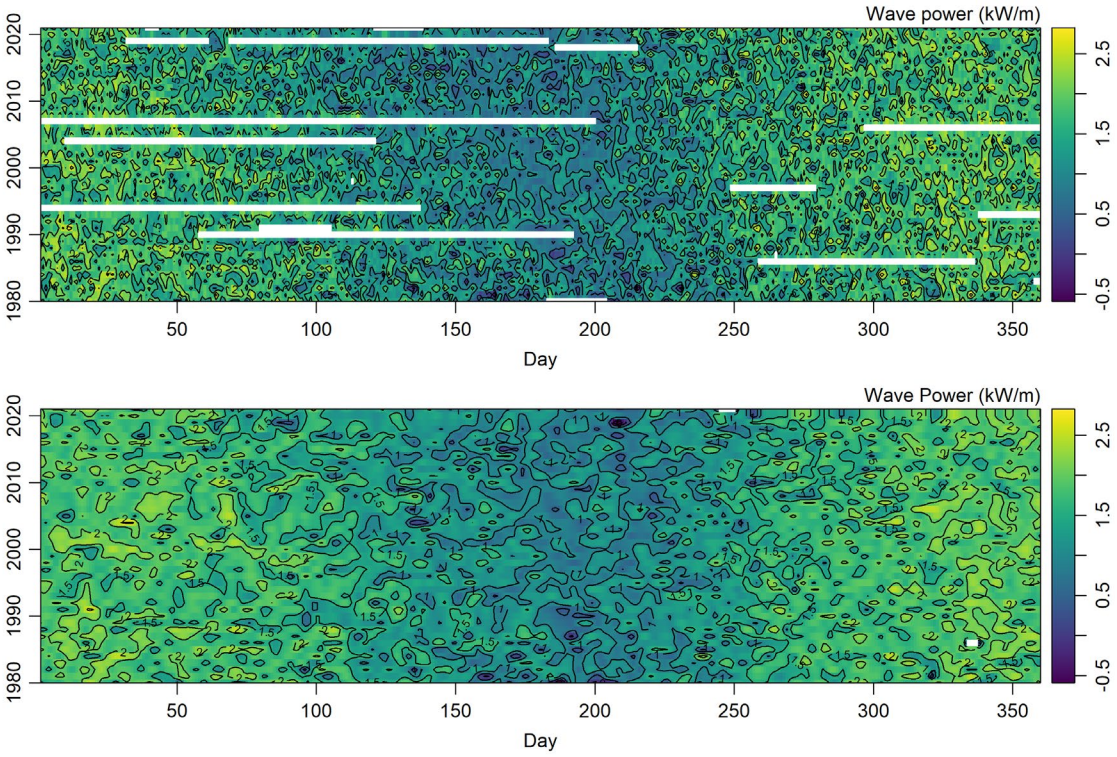


Figure 4.2. Heatmaps of mean daily wave power (top) and interpolated mean daily wave power (both in kW/m and on a $\log_{10}$ scale) for NDBC station 46001 from 1980 - 2021.

Although Figure 4.2 shows the equivalency of the interpolated data (bottom plot) with the original data (top plot), in the final time series data only the missing data within the datasets are augmented with the newly interpolated values. This practice allows for the creation of a continuous dataset that retains the integrity of the original data as much as possible. Henceforth, these new NDBC datasets that are recalculated from the consistent NDBC spectral data, and augmented with interpolated values to replace missing data, are referred to as NDBC data. These recalculated and interpolated hourly NDBC $H_{m0}$ and $T_p$ data are used within the wave power calculations. These hourly wave power data are then aggregated to provide mean daily wave power datasets prior to interpolation of the missing data gaps.

### *4.3.3 WIS model estimates*

These continuous, consistent observational wave power datasets that are created using this methodology are compared to collocated and concurrent USACE WIS wave estimates. The WIS effort was established to provide long-term wave estimates along all US coasts, including the Great Lakes, to fulfil the USACE coastal zone operations and project maintenance needs that require assessments of localised wave climates (USACE, 2020b). As wave climate information is scarce due to the lack of temporal and spatial point source measurements at coastal USACE locations, WIS generates "hindcast wave estimates (height, wave period, and direction) and directional spectral estimates for pre-selected output locations" (USACE, 2020b). Many of these sites are intentionally collocated with the NDBC buoy locations for validation of WIS wave estimates against wave measurements, which forms an essential part in confirming confidence in the model results.

This study inverses this model-measurement relationship by comparing these wave power measurement trends against the collocated and concurrent WIS wave power estimates. These WIS wave power estimates may be used as reference datasets within this work as they are uniformly calculated from WIS wave parameters that are computed using a consistent set of wind fields, modelling technology and general input parameters that are run on a set grid system.

WIS uses the WAVEWATCH III® (WW3DG, 2019) model for the Pacific and Atlantic Ocean and the WAM model (Komen et al., 1994) for the Western Alaska region and the Gulf of Mexico (USACE, 2020b). Importantly, the inclusion of these different wave models denotes that a number of different spectral frequency bands (wave model frequency bands are listed in Chapter 4's Appendix 4.6.3) are used within the calculation of wave bulk parameters. As shown in the section above, the calculation of $H_{m0}$ and $T_p$ wave parameters relies heavily on energy distribution across the spectral frequency range. As the frequency ranges differ both between the NDBC and WIS datasets and between WIS regions, the bulk parameters used in the calculation of wave power differ in value,

resulting in an offset between the comparative wave power estimates. Hence, while trends between WIS and NDBC wave power estimates are expected to mirror each other, the magnitude of the resultant wave power will not. Without recalculating WIS $H_{m0}$ and $T_p$ wave parameters used in calculations of WIS wave power (beyond the scope of this work), this offset still allows for the use of WIS estimates as a reference to evaluate the estimated NDBC wave power trends over time.

### *4.3.4 Removing seasonal effects*

A seasonal component is evident within the estimated wave power across the four regions. Therefore, the data require removal of the seasonal component to isolate changing trend signals over time. Ultimately non-detrended and seasonally detrended daily mean wave power (kW/m) results for each region are evaluated within this work to detect changing trends over time and the importance of seasonality to the overall wave climate.

Three seasonal detrending techniques were tested to determine the most appropriate detection of variable seasonality for this application: the classical decompose method (Kendall and Stuart, 1983); a Trigonometric seasonality, Box-Cox transformation, ARMA errors, Trend and Seasonal components (TBATS) model (De Livera et al., 2011); and a Seasonal and Trend decomposition using Loess (STL) method (Cleveland et al., 1990).

The classical *decompose* function from the base R software *stats* package allows for the selection of both additive and multiplicative decomposition techniques, where additive ($y_t = S_t + T_t + R_t$) and multiplicative ($y_t = S_t \times T_t \times R_t$) decomposition techniques ($y_t$ refers to the data at period $t$, $S_t$ the seasonal component, $T_t$ is the trend-cycle component and $R_t$ the remainder, Hyndman and Athanasopoulos, 2018) are applied to the data to identify which model best suits the seasonality (day of the week, day of the month, month of the year, season or annual) of the time series data. However, classical decomposition assumes an annually repeated seasonal component and is not robust to short term

deviations from the norm (Hyndman and Athanasopoulos, 2018), which may smooth and hide an increase in storm seasonality or intensity over time. Additionally, classical decomposition does not extend trend analyses to the tails of the datasets.

To account for the complex seasonality that is crucial for these long periods of environmental time series data, an exponential smoothing state space TBATS model (*tbats* function: using day, month, and year seasonal parameters) in the *forecast* package (Hyndman et al., 2021) were applied to the time series, as the model allows for seasonality changes over the period of record. Next, a STL method, which uses an additive decomposition technique to address shifts in seasonal components, outliers and change rates that reduce possible model overfitting (Hyndman and Athanasopoulos, 2018) was tested. The R software *forecast* package offers two STL model methods: a user defined *stl* function, and a more robust *mstl* function (mSTL) that handles multiple seasonality.

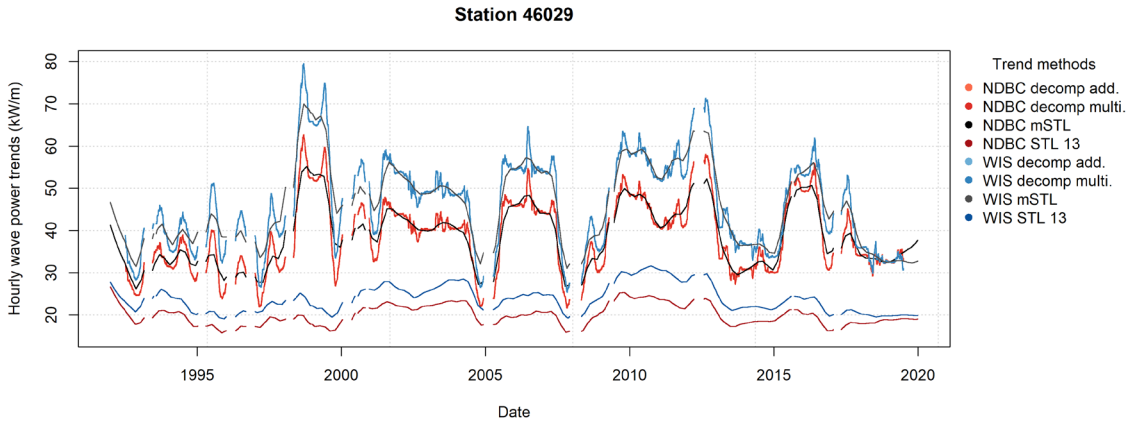


Figure 4.3. Decomposition methods for hourly wave power time series for Station 46029.

To minimise variability in test results, the various decomposition methods were applied to hourly and aggregated daily mean datasets with minimal data gaps and rigorously scrutinised. Figure 4.3 provides an example (Station 46029) of the wave power trends obtained from the different decomposition methods tested on the hourly data within this work. Of interest is that the classical *decompose* additive and multiplicative techniques

returned identical trends (the NDBC and WIS additive decomposition trend lines are hidden below their associated multiplicative decomposition trend lines in Figure 4.3). The manual STL model (*stl* function; abbreviated as STL 13 due to the use of a user-defined seasonal window = 13 in Figure 4.3) under predicted trends. The mSTL trend models (black and grey in Figure 4.3) appear robust enough to capture trend cycles without overfitting the model.

Therefore, the *mstl* (multiple STL) function, which uses Friedman's "super smoother" algorithm (Friedman, J. H., 1984a, 1984b) to capture the mean, was chosen as the best method to detrend multiple seasonal periods from the data (parameters: seasonal window=13, trend cycle window = auto) as it allows for a gradual change in possible trend cycles over time without overfitting the model. Additionally, unlike the classical decomposition methods, the mSTL function captured trend estimates across the full tails of the time series.

Of interest is that Figure 4.3 clearly depicts the magnitude of the offsets between the NDBC and WIS wave power estimates (by approximately 10-20 kW/m at Station 46029) as expected from the use of the non-uniform NDBC and WIS spectral ranges for bulk parameter calculations. However, WIS and NDBC decomposition trends are in agreement within Figure 4.3, as within all of the reviewed sites, highlighting the accuracy of the methodology used within this work, as well as the use of WIS as a stable reference for wave climate analyses.

A second methodology check that relied on these trend analyses was an evaluation of the possible loss of data integrity during aggregation of the hourly data into daily mean datasets. A review of the NDBC and WIS hourly vs aggregated daily mean decomposition trends showed no loss of data integrity. However, of interest is that the daily mean trends align more consistently with temporal-associated climate index regression trends than the hourly data, allowing for extra confidence in utilising these aggregated daily mean datasets for these wave power trend analyses.

### *4.3.5 Climate indices*

In an effort to interpret the peaks and troughs in the general wave power trends observed within this work, teleconnection climate indices are incorporated for the Pacific and Atlantic Ocean regions. Teleconnection patterns are a "recurring and persistent, large-scale pattern of pressure and circulation anomalies that spans vast geographical areas" (CPC, 2008) that can occur over months and years, providing an independent source of the long-term variability of the global atmospheric circulation. "Teleconnection patterns reflect large-scale changes in the atmospheric wave and jet stream patterns, and influence temperature, rainfall, storm tracks, and jet stream location/ intensity" (CPC, 2008). Hence, trends in these climate indices provide context as to whether the wave power trends echo these climate trends after the removal of seasonal effects, or whether the wave power trends are only directly related to wind driven storm events.

Three climate indices are reviewed: the El Niño/Southern Oscillation (ENSO), a periodic fluctuation in sea surface temperature and air pressure that affects global weather (PSL, 2021; NCEI, 2021a), and two basin-specific indices: the longer-lived Pacific Decadal Oscillation (PDO) Index that affects the Pacific Basin ocean temperatures and sea level pressures (NCEI, 2021b), and the North Atlantic Oscillation (NAO) index of sea-level pressure. The NAO affects the intensity and location of storm tracks and the North Atlantic jet stream, and is "based on the surface sea-level pressure difference between the Subtropical (Azores) High and the Subpolar Low" (NCEI, 2021c).

Odérix et al. (2020) reviewed four ENSO products and determined that the Multivariate ENSO Index Version 2 (MEI.v2) index is the product of choice to investigate global wave power. The MEI indices, which represent both oceanic and atmospheric variables, were sourced from the NOAA Physical Sciences Laboratory (PSL, 2021). The PDO indices (Mantua, 2002) were sourced from the NCEI PDO database (NCEI, 2021b), and are based on NOAA's extended reconstruction of SSTs (ERSST Version 5). The NAO indices were

also sourced from the NCEI NAO database (NCEI, 2021c), and are based on the "NAO loading pattern to the daily anomaly 500 millibar height field over 0-90°N" (NCEI, 2021c).

### *4.3.6 Statistical evaluations*

The following goodness of fit statistical analyses tested the relationship amongst and between the various moored buoy test sites and WIS model estimations. Relationships between the co-located NDBC and WIS are assessed by Pearson correlation coefficients ($r = \frac{\sum xy}{\sqrt{\sum x^2 \sum y^2}}$; Zar, 1984), with coefficients = 1 implying a perfect fit.

Linear regressions evaluate the trends of the datasets ($Y_i = a + bX_i$, with *X* representing the independent variable, *Y* the dependent variable, *a* the intercept, and *b* the slope; Zar, 1984). The curve of the data are showcased by locally weighted scatterplot smoothing (LOWESS) regressions as $(\sum_k w(x_k)G(x_k)(y_k - a - bx_k)^2$ for $k$ = 1,…,*N*, with calculation of the robust weighting functions, $w(x_k)G(x_k)$ and regression smoothing, $y_k - a - bx_k$, for each data point (Cleveland, 1979).

Descriptive statistics mean [$\underline{X} = \frac{\sum x}{n}$ , where $n$ is the size of the sample $x$], median [$Med(X) = X_{(n+1)/2}$, if $n$ is odd; $Med(X) = \frac{X_2 + X_{(n/2)+1}}{2}$ if $n$ is even], 90$^{th}$ and 99$^{th}$ percentile [$X = \underline{X} + Z\sigma$, where $\sigma$ represents the standard deviation and Z = 1.282 for 90$^{th}$ quantile and 2.326 for the 99$^{th}$ quantile] are used to investigate wave power intensity at each site over the reviewed time period (Zar, 1984). Standard error is computed as $SE = \frac{\sigma}{\sqrt{n}}$ (Zar, 1984).

## 4.4 Trends in Wave Power

### *4.4.1 Regional correlations between NDBC and WIS wave power estimates*

Correlations between the NDBC and WIS wave power estimates test the concurrent and collated use of these datasets for comparative wave power trend analyses. Figure 4.4 shows the Pearson correlation coefficients ($r$) of the NDBC and WIS seasonally detrended, daily mean wave power estimates for all sites across the reviewed regions. As expected, correlation coefficients (0.95, 0.78, 0.92 and 0.93 for daily mean wave power for the eastern Pacific Ocean, Hawaiian Island, Gulf of Mexico and Atlantic Ocean sites, respectively) between the NDBC and WIS data show good agreement for all regions apart from the Hawaiian sites (Figure 4.4).

This drop in correlation agreement within the Hawaiian sites is due to the lower efficiency of WIS to predict low wave conditions within the trade winds (Jensen, 2022, pers. comms., USACE WIS Principle Investigator). This is because WIS estimates wave conditions from large mesoscale wind conditions within that region, while Hawaii wave conditions are driven by localised weather systems that affect model estimates (Stopa et al., 2011; Li et al., 2021). During mixed wind seas and swells, WIS tends to select the swell period over the wind seas period, resulting in an overestimation of the wave power estimates compared to the measurements (Jensen, 2022, pers. comms.). Additionally, these Hawaii results only represent two buoy sites (northwest and south of the Hawaiian Islands, which in the latter case is in a sheltered region), reducing any normalisation that would be introduced by additional locations; in essence amplifying the variability signal observed at only these two specific sites. Overall, comparisons between the NDBC and WIS data at the Hawaii sites still reflect the overestimation trends observed within the eastern Pacific Ocean data comparisons, just to a greater degree.

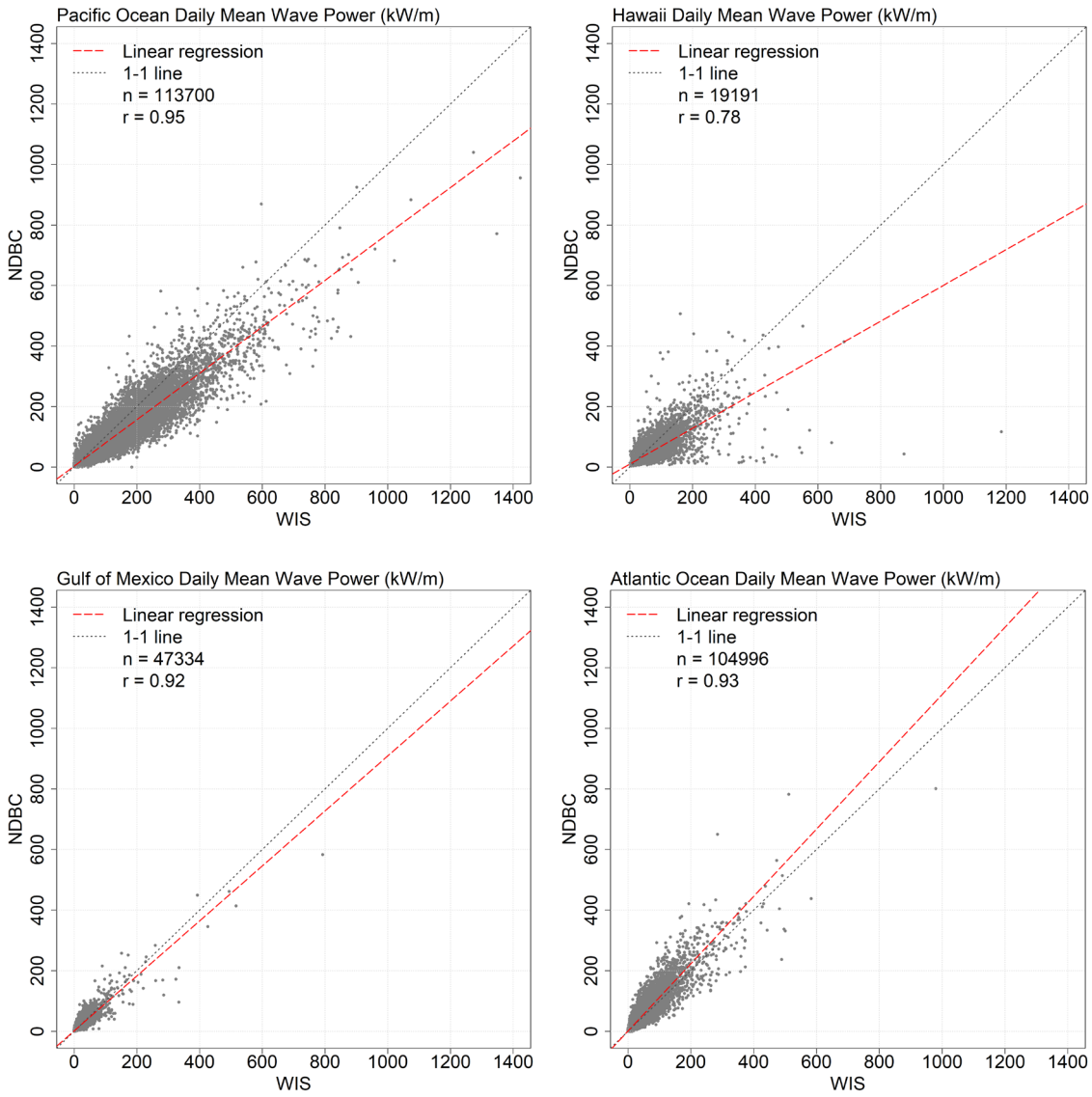


Figure 4.4. Scatter diagrams depicting the correlations between the NDBC vs WIS seasonally detrended, daily mean wave power (kW/m) for each region. Dashed red lines indicate linear regressions, with sample size and Pearson correlation coefficients (r) listed in the top right corner. All plots include a dotted grey 1-1 line for reference.

Another heterogeneity component between the two data sources may be the coupling effects of wave-current interaction that are reported in NDBC wave measurements (Wang et al., 1994; Steele, 1997). NDBC does not rectify the net effects of surface currents within wave measurements, while WIS estimates do not contain a current component, adding to variance between the two datasets. However, these current interactions are beyond the scope of this work, and are therefore disregarded within these comparisons.

Overall, the largest daily mean wave power values were calculated for the eastern Pacific Ocean and the Hawaiian sites. Lower daily mean wave power values register at the Atlantic Ocean sites, with the lowest daily mean wave power values estimated for the Gulf of Mexico region (Figure 4.4). The Atlantic Ocean WIS sites under-estimate wave power when compared to collocated and concurrent NDBC wave power values, while WIS appears to be over-estimating wave power within the eastern Pacific Ocean, Gulf of Mexico sites, and as expected, within the Hawaiian sites (Figure 4.4). However, even with these over- and under-estimates of wave power across the reviewed regions, the offsets between the NDBC and WIS decomposition trends still appear constant over time for each site (Figure 4.3).

### *4.4.2 Eastern Pacific Ocean wave power*

Data collected at ten eastern Pacific Ocean NDBC moored buoy sites shows maximum hourly (with seasonal effects included) intra-site wave power ranges between 416.16 kW/m (number of observations [n] = 12766) at NDBC 46025 to 1249.94 kW/m (n = 10307) at NDBC station 46022 (Table 4.1). The maximum hourly wave power at NDBC station 46025 is consistent with the expected lower wave power within the Southern California Bight, which is sheltered from North Pacific storms events, and the Channel Islands, which are not directly exposed to South Pacific and Southern Ocean swell events (Figure 4.1, NDBC 46025). In contrast, a high maximum hourly wave power at NDBC station 46022 is observed in the open waters offshore of Eel River near Eureka, California (NDBC 46022).

Table 4.1. Eastern Pacific Ocean hourly wave power (kW/m) descriptive statistics for each site (displayed from North to South) for the reviewed 40-year period

| Station | Median | Mean | 90th Percentile | 99th Percentile | Max. | Number of Obs. | Std. Deviation | Std. Error |
|---|---|---|---|---|---|---|---|---|
| NDBC 46001 | 25.47 | 48.29 | 117.14 | 307.12 | 893.12 | 13920 | 63.96 | 0.54 |
| WIS 46001 | 25.93 | 52.41 | 131.27 | 357.38 | 961.37 | 13346 | 72.19 | 0.62 |
| NDBC 46005 | 27.79 | 54.22 | 131.04 | 353.56 | 1135.07 | 12253 | 74.07 | 0.67 |
| WIS 46005 | 34.97 | 68.79 | 169.15 | 426.77 | 1153.04 | 11322 | 90.34 | 0.85 |
| NDBC 46029 | 19.05 | 38.41 | 93.48 | 273.02 | 651.12 | 8939 | 53.34 | 0.56 |
| WIS 46029 | 23.03 | 46.00 | 110.64 | 315.02 | 894.02 | 8612 | 61.91 | 0.67 |
| NDBC 46002 | 27.51 | 51.41 | 121.84 | 341.47 | 1067.81 | 11263 | 68.68 | 0.65 |
| WIS 46002 | 34.05 | 64.90 | 157.53 | 408.10 | 1772.31 | 10931 | 86.08 | 0.82 |
| NDBC 46006 | 30.89 | 60.84 | 147.65 | 406.40 | 1206.18 | 9821 | 83.07 | 0.84 |
| WIS 46006 | 38.03 | 74.14 | 180.72 | 479.54 | 1562.52 | 9516 | 99.76 | 1.02 |
| NDBC 46022 | 24.31 | 40.98 | 94.32 | 253.76 | 1249.94 | 10307 | 52.22 | 0.51 |
| WIS 46022 | 31.51 | 51.66 | 117.06 | 296.59 | 789.64 | 9781 | 59.30 | 0.60 |
| NDBC 46013 | 20.00 | 32.29 | 72.17 | 171.97 | 674.46 | 12446 | 37.02 | 0.33 |
| WIS 46013 | 24.29 | 39.87 | 89.28 | 215.97 | 595.46 | 12073 | 44.40 | 0.40 |
| NDBC 46012 | 18.89 | 30.33 | 68.30 | 168.19 | 611.87 | 11681 | 34.60 | 0.32 |
| WIS 46012 | 22.95 | 36.06 | 79.13 | 186.07 | 604.47 | 11109 | 38.71 | 0.37 |
| NDBC 46011 | 17.61 | 28.37 | 62.71 | 162.93 | 602.95 | 12449 | 33.54 | 0.30 |
| WIS 46011 | 22.79 | 37.34 | 83.90 | 209.78 | 601.29 | 11875 | 42.62 | 0.39 |
| NDBC 46025 | 5.56 | 8.21 | 15.63 | 46.98 | 416.16 | 12766 | 10.48 | 0.09 |
| WIS 46025 | 4.51 | 7.59 | 15.06 | 52.76 | 381.65 | 12226 | 11.88 | 0.11 |

Moored buoys are notorious for breaking adrift from their moorings during extreme weather events, compromising any wave data collected while untethered from the sea floor (Eulerian moored buoy data processing algorithms are not designed for Lagrangian movement). Therefore, of particular interest is the loss of viable maximum wave heights and periods (the building blocks of wave power) that may be recorded during these storm events. Hence, in the absence of true maximums, 90$^{th}$ and 99$^{th}$ percentile wave power values provide a more reliable comparison of wave power intensity across the individual NDBC stations. Note that this loss of viable maximum wave heights and periods are not a consideration for the WIS hindcast estimates. Therefore the WIS 90$^{th}$ and 99$^{th}$ percentile wave power estimates are expected to be higher than those observed at the NDBC sites. Within the reviewed eastern Pacific Ocean buoy sites (Table 4.1), NDBC station 46006 is subjected to the highest 90$^{th}$ and 99$^{th}$ percentile wave power due to its exposed, offshore, open ocean position (water depth: 4347 m; 600 nm west of Eureka, California, U.S.).

A review of the suspect maximum recorded values and more reliable 90$^{th}$ and 99$^{th}$ percentiles across the individual eastern Pacific Ocean stations (Table 4.1) highlights a significant increase in wave power intensity caused by a few passing storm events. Similar wave power differences are evident in the variance between the median and mean values across the individual stations (Table 4.1), highlighting that the majority (median) of the wave power occurring at each site is lower than the mean. This again showcases the effects of storm events with standard deviations that are higher than both the median and mean wave power estimates. For example, NDBC station 46001 experienced mean hourly wave power of 48.29 kW/m across its lifetime, with a higher standard deviation of 63.96 kW/m, while the median wave power values at that site were far less at 25.47 kW/m (Table 4.1). These results indicate that the wave power distribution is highly skewed by a few intense storms. Standard errors across the datasets remain low overall (Table 4.1), allowing for confidence in the estimated wave power values.

Of note is that Table 4.1 clearly highlights the offset between WIS and NDBC hourly wave power estimates, where 99$^{th}$ percentile WIS wave power estimates are consistently higher for all of the sites. The maximum wave power is only higher for WIS sites across the northern sites (stations 46001 – 46006). This pattern reverses for the southern sites (stations 46022 – 46025), where maximum wave power is consistently lower than the NDBC estimates (Table 4.1).

After removal of seasonal effects, NDBC daily mean wave power trends within the eastern Pacific Ocean show agreement across the sites, with the majority of the sites remaining with 20 – 82 kW/m (Figure 4.5), and only NDBC station 46025 (which is sheltered behind islands in Southern California near Santa Monica) returning a mean daily wave power trend that oscillates around 10 kW/m (Figure 4.5). Four significant peaks in 1997, 2006, 2015 and 2016 reflect the large number of tropical cyclones (depressions, storms and hurricanes), with 19, 21, 22 and 22 storms in those years, respectively (Chapter 4's Appendix 4.6.4), as recorded by the NOAA National Hurricane Center (NHC) for 1995-2021 (NHC, 2022).


Figure 4.5. NDBC wave power trends and overall linear regressions for the eastern Pacific Ocean (top plot), with concurrent LOWESS regressions of the reference PDO and ENSO indices for trend context (bottom plot).

Peaks in these linear regression trends appear to follow trends in both PDO and ENSO LOWESS regressions (Figure 4.5), where the peaks in wave power that are evident in 1987 are associated with both the PDO and ENSO peaks. However, the ENSO peak in 1992 appears aligned with the wave power peaks observed in Stations 46012 and 46013, while the wave power peaks at Stations 46005 and 46002 match the PDO peak in 1993 (Figure 4.5). Similar differences are observed within the 1982 - 1984 years, where NDBC 46011 and 46012 wave power trends appear to peak in time with the ENSO index, while Stations 46013 and 46005 wave power trends align with the peak in the PDO index. Therefore both of these climate indices provide valuable context to the observed eastern Pacific Ocean wave power trends, especially in the absence of NHC storm counts for these earlier years.

Table 4.2. Eastern Pacific Ocean 40-year regression trends for each site (displayed from North to South) for non-detrended and seasonally detrended daily mean wave power (kW/m). Significant trends per year are indicated in bold (p-value < 0.05)

| Station | Wave Power Trends (kW/m /yr.) | Wave Power slope (kW/m /day) | Wave Power intercept (kW/m) | NDBC / WIS Pearson Correlation Coefficient | Seasonally detrended wave power trends (kW/m /yr.) | Seasonally detrended wave power slope (kW/m /day) | Seasonally detrended wave power intercept (kW/m) | Seasonally detrended NDBC / WIS Pearson Correlation Coefficient | Number of samples |
|---|---|---|---|---|---|---|---|---|---|
| NDBC 46001 | **-0.173** | -0.00047 | 53.715 | 0.93 | **-0.176** | -0.00048 | 53.721 | 0.91 | 14611 |
| WIS 46001 | **-0.105** | -0.00029 | 55.288 | | **-0.107** | -0.00029 | 55.264 | | |
| NDBC 46005 | -0.036 | -0.00010 | 57.391 | 0.95 | -0.029 | -0.00008 | 57.200 | 0.93 | 14611 |
| WIS 46005 | **-0.117** | -0.00032 | 74.518 | | **-0.107** | -0.00029 | 74.230 | | |
| NDBC 46029 | -0.071 | -0.00019 | 43.374 | 0.91 | -0.069 | -0.00019 | 43.291 | 0.87 | 10228 |
| WIS 46029 | **-0.221** | -0.00061 | 55.934 | | **-0.216** | -0.00059 | 55.751 | | |
| NDBC 46002 | **-0.161** | -0.00044 | 57.045 | 0.95 | **-0.170** | -0.00047 | 57.181 | 0.93 | 14285 |
| WIS 46002 | **-0.149** | -0.00041 | 70.019 | | **-0.161** | -0.00044 | 70.198 | | |
| NDBC 46006 | **-0.158** | -0.00043 | 64.290 | 0.96 | **-0.140** | -0.00038 | 63.646 | 0.94 | 13880 |
| WIS 46006 | **-0.256** | -0.00070 | 80.829 | | **-0.232** | -0.00063 | 79.986 | | |
| NDBC 46022 | **-0.255** | -0.00070 | 48.108 | 0.94 | **-0.249** | -0.00068 | 47.873 | 0.91 | 13515 |
| WIS 46022 | **-0.292** | -0.00080 | 59.778 | | **-0.285** | -0.00078 | 59.504 | | |
| NDBC 46013 | -0.040 | -0.00011 | 34.207 | 0.94 | -0.032 | -0.00009 | 33.975 | 0.92 | 13867 |
| WIS 46013 | **-0.106** | -0.00029 | 43.619 | | **-0.096** | -0.00026 | 43.330 | | |
| NDBC 46012 | **0.204** | 0.00056 | 24.608 | 0.93 | **0.213** | 0.00058 | 24.326 | 0.92 | 14245 |
| WIS 46012 | **0.113** | 0.00031 | 32.338 | | **0.124** | 0.00034 | 31.944 | | |
| NDBC 46011 | **-0.077** | -0.00021 | 32.018 | 0.94 | **-0.067** | -0.00018 | 31.706 | 0.92 | 14245 |
| WIS 46011 | **-0.170** | -0.00047 | 43.906 | | **-0.157** | -0.00043 | 43.490 | | |
| NDBC 46025 | **-0.055** | -0.00015 | 10.125 | 0.89 | **-0.050** | -0.00014 | 9.980 | 0.88 | 13515 |
| WIS 46025 | **-0.064** | -0.00018 | 9.782 | | **-0.059** | -0.00016 | 9.605 | | |

As expected, linear regression trends vary across the spectrum of eastern Pacific Ocean NDBC sites (Figure 4.5) as each site experiences different environmental forcing. NDBC station 46022 shows the greatest (downward) wave power trend across the stations (Table 4.2), which is expected as that site also exhibits the maximum wave power (Table 4.1).

Of note is the difference in statistical significance between the collocated and concurrent NDBC and WIS wave power trends for the reviewed sites. All but three sites (70 %) show statistically significant trends (p-value less than 0.05) across the eastern Pacific Ocean NDBC stations for both the non-detrended and seasonally detrended daily mean wave power, while all WIS sites estimated significant trends (Table 4.2). However, all sites exhibited an acceptable NDBC-WIS Pearson correlation coefficient of 0.87 or higher (Table 4.2).

In summary, these trend results show agreement with some previous wave trend estimates in slope but are not unanimous in magnitude. For example, Reguero et al. (2015) used the WaveWatchIII model to calculate eastern Pacific Ocean wave power trends of 0.5 kW/m/year (28 years of data), while Wu et al. (2018) projected wave power trends of -0.2 kW/m/year (32 years of data) that are more in agreement with our results. Of note is that these results are estimated across 1.0˚ x 1.0˚ and 1.5˚ x 1.0˚ resolution eastern Pacific Ocean model grids, respectively, so are not comparable in magnitude to the discrete wave power trends per year calculated at each site within this work. Results that are comparable are the eastern Pacific Ocean buoy results within Ahn and Neary (2020) that show an inter-annual mean total wave power of -0.13 kW/m/yr. (30 years of data) for NDBC buoy 46026, which, possibly due to the use of different wave power calculations, is only comparable in slope to the nearby NDBC buoy 46012 (0.20 and 0.21 kW/m/yr. for the non-detrended and seasonally detrended wave power, respectively) reviewed within this work (Table 4.2). Interestingly, Ahn and Neary (2020) results are more closely aligned with the magnitude of WIS wave power results of 0.11 and 0.12 kW/m/year for the non-detrended and seasonally detrended data, respectively, although trend slopes still differ (Table 4.2).

### *4.4.3 Hawaii wave power*

Travelling westwards into the open Pacific Ocean waters, Table 4.3 describes the wave power environment at the Hawaiian island review sites. Only four sites around the Hawaiian Island chain met the study parameters of deployment lengths of 30 years or longer. Additionally, NDBC stations 51003 and 51004 do not have corresponding WIS grid points for reference.

Table 4.3. Hawaiian Island hourly wave power (kW/m) descriptive statistics for each site (displayed from North to South) for the reviewed 36-year period

| Station | Median | Mean | 90th Percentile | 99th Percentile | Max. | Number of Obs. | Std. Deviation | Std. Error |
|---|---|---|---|---|---|---|---|---|
| NDBC 51001 | 22.99 | 37.09 | 76.56 | 224.81 | 706.59 | 9488 | 43.34 | 0.44 |
| WIS 51001 | 28.71 | 47.56 | 102.29 | 276.67 | 2212.66 | 8944 | 59.52 | 0.63 |
| NDBC 51003 | 20.13 | 27.26 | 53.19 | 119.46 | 321.38 | 11467 | 23.05 | 0.22 |
| NDBC 51004 | 23.97 | 30.10 | 55.37 | 109.81 | 391.32 | 9732 | 22.11 | 0.22 |
| NDBC 51002 | 23.38 | 29.32 | 53.89 | 107.37 | 259.18 | 10510 | 20.84 | 0.20 |
| WIS 51002 | 25.76 | 33.39 | 63.97 | 128.59 | 371.11 | 9919 | 25.21 | 0.25 |

The reviewed Hawaiian Island sites show the same maximum versus 90th and 99th percentile variability in wave power intensity (Table 4.3) that was observed within the eastern Pacific Ocean sites. WIS site 51001 shows an exorbitant maximum of 2212.66 kW/m (n = 8944) that does not correspond to the maximum wave power of 706.59 kW/m (n = 9488) identified at the collocated and concurrent NDBC station 51001 (Table 4.3).

NDBC station 51001 (Figure 4.1) shows significantly higher values for 90th – 99th percentile and maximum wave power than the other Hawaiian sites, highlighting its unique location to the north of the Hawaiian Island chain with exposure to north Pacific storm swells. The rest of the reviewed Hawaiian sites fall within the southern lee of the island chains, receiving wave signals from swells originating from distant Southern Ocean storms. Again storm swell effects are evident in the standard deviations for each site across the 36 year review timeframe, with NDBC station 51001 showing a standard deviation (43.34 kW/m) of approximately twice its median wave power estimate (22.99 kW/m; Table 4.3). This pattern is far less evident in the southern sites, with median and standard deviations within relative agreement (Table 4.3). Again, standard errors remain low across the reviewed sites (Table 4.3).


Figure 4.6. NDBC wave power trends and overall linear regressions for Hawaii (top plot), with concurrent LOWESS regressions of the reference PDO and ENSO indices for trend context (bottom plot).

This offset in northern versus southern wave power values are echoed within the overall trends of the time series data (Figure 4.6), where mean daily wave power for NDBC station 51001 registers higher (30 – 50 kW/m) than the rest of the Hawaiian sites (20 – 40 kW/m). The peak in mean daily wave power during 1997 (Figure 4.6) mirrors the nine tropical cyclones that were recorded by the NHC within the Central Pacific Ocean during that year (Chapter 4's Appendix 4.6.4). Similarly, the 2015 peak in wave power reflects the five tropical cyclones listed by the NHC (Chapter 4's Appendix 4.6.4) for the region. Again, trends in the wave power (kW/m) show a temporal agreement with the PDO and ENSO LOWESS regression trends, where both climate trends match peaks in NDBC 51002 and 51003 wave power in 1987, and again in 1997 and 2010 (Figure 4.6). The peaks in the PDO index appear reflected within the 1993 peaks in wave power at NDBC station 51004, and the 2001 peaks across all of the reviewed NDBC sites (Figure 4.6). A smaller peak in

2012 is evident in wave power at Station 51004 that coincides with a peak in the ENSO index (Figure 4.6), justifying the use of both climate indices to provide context to the Hawaiian Island sites.

The disagreement in NDBC and WIS wave trends for site 51001 are clearly evident in the low 0.78 and 0.67 Pearson correlation coefficients for non-detrended and seasonally detrended data, respectively (Table 4.4). These results show that all trends, both non-detrended and seasonally detrended data, are downward at the Hawaiian sites (Table 4.4), indicating that wave power has decreased slightly over the reviewed 36-year time period. Again, trend statistical significance (p-value less than 0.05) appears independent of seasonal effects, with 100 % of the reviewed sites showing a downward trend in wave power over the 36-year time period (Table 4.4). These results agree in slope but are not comparable in magnitude (with -1.16 and -1.15 kW/m/yr. for non-detrended and seasonally detrended wave power) with Ahn and Neary's (2020) recent 30 year review, which estimated an inter-annual mean total wave power of -0.25 kW/m/year for NDBC station 51001.

Table 4.4. Hawaiian Island 36-year regression trends for each site (displayed from North to South) for non-detrended and seasonally detrended daily mean wave power (kW/m). Significant trends per year are indicated in bold (p-value < 0.05)

| Station | Wave Power Trends (kW/m /yr.) | Wave Power slope (kW/m /day) | Wave Power intercept (kW/m) | NDBC / WIS Pearson Correlation Coefficient | Seasonally detrended wave power trends (kW/m /yr.) | Seasonally detrended wave power slope (kW/m /day) | Seasonally detrended wave power intercept (kW/m) | Seasonally detrended NDBC / WIS Pearson Correlation Coefficient | Number of samples |
|---|---|---|---|---|---|---|---|---|---|
| NDBC 51001 | **-0.163** | -0.00045 | 42.647 | 0.78 | **-0.145** | -0.00040 | 42.073 | 0.67 | 12784 |
| WIS 51001 | **-0.495** | -0.00136 | 61.867 | | **-0.470** | -0.00129 | 61.029 | | |
| NDBC 51003 | **-0.195** | -0.00053 | 34.077 | - | **-0.185** | -0.00051 | 33.744 | - | 13392 |
| NDBC 51004 | **-0.210** | -0.00057 | 37.369 | - | **-0.198** | -0.00054 | 36.949 | - | 11566 |
| NDBC 51002 | **-0.171** | -0.00047 | 34.373 | 0.83 | **-0.166** | -0.00045 | 34.183 | 0.76 | 12784 |
| WIS 51002 | **-0.143** | -0.00039 | 37.025 | | **-0.132** | -0.00036 | 36.664 | | |

### *4.4.4 Atlantic Ocean wave power*

Results show less wave power within the northwest Atlantic Ocean than in the eastern Pacific Ocean, with a maximum hourly intra-site wave power range between 384.47 kW/m (n = 9453) at NDBC station 44014, to 906.36 kW/m (n = 10132) at NDBC station 41002 (Table 4.5). NDBC station 44011, which is subjected to frequent Nor'easter storms, appears the most energetic over the reviewed 40-year period, with 90$^{th}$ and 90$^{th}$ percentiles measuring 59.01 and 199.88 kW/m, respectively.

Of note is that the mean and median wave power values recorded within the Atlantic Ocean are approximately five times lower than those observed within the eastern Pacific Ocean. These results are due to the difference in storm systems that affect the two areas, as well as the position of the buoys relative to the open ocean within each region, both affecting the $T_p$ values that feed into the wave power estimations.

Table 4.5. Atlantic Ocean hourly wave power (kW/m) descriptive statistics for each site (displayed from North to South) for the reviewed 40-year period

| Station | Median | Mean | 90$^{th}$ Percentile | 99$^{th}$ Percentile | Max. | Number of Obs. | Std. Deviation | Std. Error |
|---|---|---|---|---|---|---|---|---|
| NDBC 44007 | 2.02 | 5.60 | 12.18 | 60.72 | 414.61 | 13015 | 13.66 | 0.12 |
| WIS 44007 | 1.63 | 3.97 | 9.16 | 38.22 | 161.92 | 12410 | 7.89 | 0.07 |
| NDBC 44005 | 4.99 | 12.79 | 29.87 | 117.54 | 411.43 | 10805 | 24.06 | 0.23 |
| WIS 44005 | 3.53 | 8.49 | 20.41 | 74.22 | 328.98 | 10506 | 15.38 | 0.15 |
| NDBC 44013 | 1.34 | 5.13 | 10.57 | 66.97 | 496.36 | 10895 | 14.94 | 0.14 |
| WIS 44013 | 0.93 | 3.11 | 6.89 | 36.40 | 196.61 | 10355 | 8.12 | 0.08 |
| NDBC 44011 | 9.88 | 24.00 | 59.01 | 199.88 | 751.05 | 9490 | 40.54 | 0.42 |
| WIS 44011 | 7.75 | 18.53 | 44.81 | 152.90 | 980.83 | 9202 | 34.11 | 0.36 |
| NDBC 44008 | 7.34 | 17.93 | 43.22 | 162.33 | 744.55 | 11316 | 32.59 | 0.31 |
| WIS 44008 | 6.22 | 14.58 | 35.07 | 126.79 | 634.79 | 10728 | 26.63 | 0.26 |
| NDBC 44014 | 4.97 | 11.58 | 26.58 | 107.64 | 384.47 | 9851 | 20.99 | 0.21 |
| WIS 44014 | 5.09 | 10.66 | 23.33 | 89.45 | 384.45 | 9453 | 18.85 | 0.19 |
| NDBC 41001 | 10.45 | 23.62 | 57.39 | 188.39 | 604.43 | 9729 | 38.83 | 0.39 |
| WIS 41001 | 9.26 | 20.17 | 47.94 | 154.49 | 648.88 | 9440 | 33.05 | 0.34 |
| NDBC 41002 | 8.72 | 18.69 | 42.99 | 149.27 | 906.36 | 10132 | 32.62 | 0.32 |
| WIS 41002 | 8.64 | 16.84 | 37.43 | 121.11 | 959.39 | 9937 | 29.52 | 0.30 |
| NDBC 41010 | 6.49 | 12.86 | 28.23 | 100.88 | 557.85 | 10322 | 22.35 | 0.22 |
| WIS 41010 | 7.39 | 13.34 | 29.00 | 90.53 | 518.32 | 9828 | 21.23 | 0.21 |
| NDBC 41009 | 3.71 | 7.71 | 17.43 | 59.91 | 428.99 | 11091 | 13.96 | 0.13 |
| WIS 41009 | 5.52 | 9.65 | 20.73 | 61.82 | 345.55 | 10597 | 13.81 | 0.13 |

Standard deviations across a number of the reviewed Atlantic sites are generally comparable to the 90$^{th}$ percentile wave power estimates, and not the median or mean wave power calculations (Table 4.5). These results are due to the locally generated wind sea wave conditions with localised extreme events that are experienced at these sites. Standard errors across the reviewed sites remain low (Table 4.5), again allowing for confidence in these calculations.

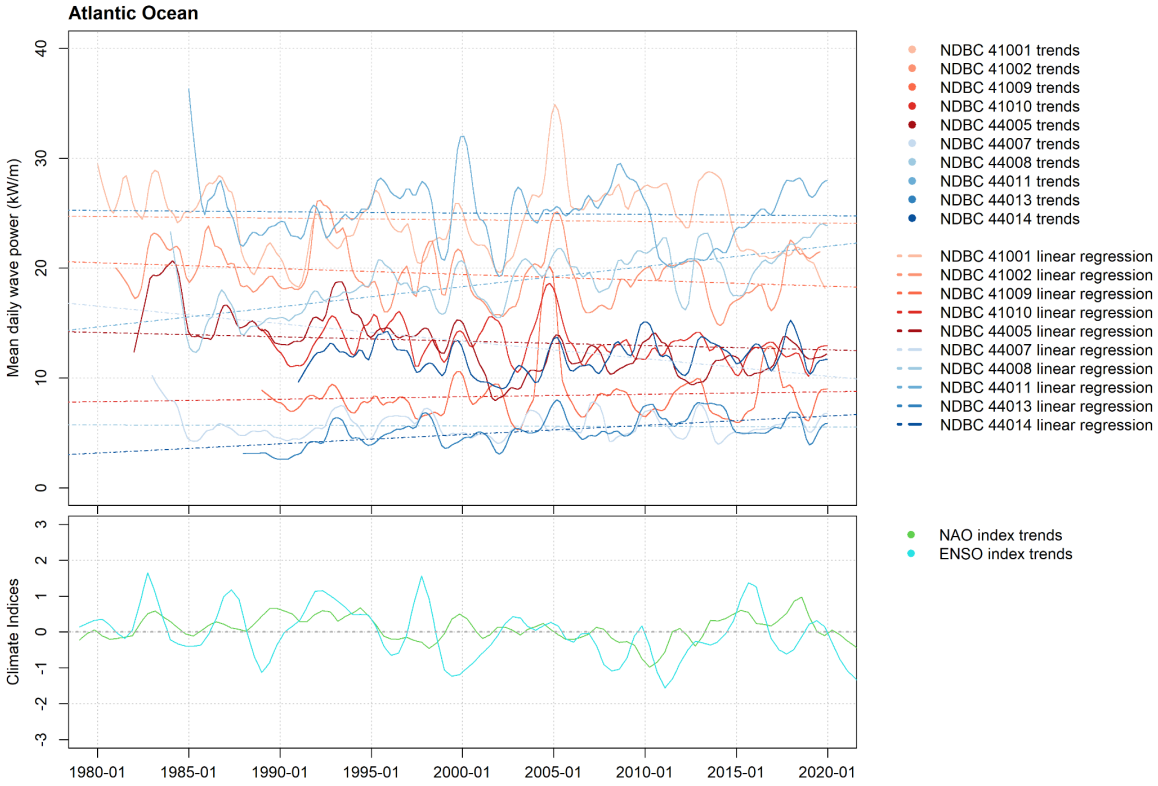


Figure 4.7. NDBC and WIS wave power trends for the Atlantic Ocean, with concurrent LOWESS regressions of the reference NAO and ENSO indices for trend context (bottom plot).

As at the eastern Pacific Ocean sites, linear regression trends within the Atlantic Ocean vary across the spectrum of NDBC sites (Figure 4.7) with environmental forcing variations. After removal of seasonal effects, NDBC daily mean wave power trends (ranging from 5 to 35 kW/m) within the Atlantic Ocean show agreement in mean daily wave power peaks and troughs, if not wave power magnitude, across each site (Figure 4.7).

These trends appear to follow trends in both NAO and ENSO LOWESS regressions, where peaks are evident within both climate indices and NDBC stations 44005, 41001 and 41002 between 1982 and 1984 (Figure 4.7). Trends in wave power peaks at NDBC stations 41001 and 41002 correspond to NAO peaks in 1989, while peaks at all but one of the NDBC stations match the NAO peak in 1999 (Figure 4.7). Peaks in wave power at NDBC stations 44008, 44011, 41001 and 41002 appear aligned with a peak in ENSO trends in 1986-1987, with all NDBC stations showing a peak in line with the ENSO peak in the 1998 timeframe, and again in 2015 (Figure 4.7).

Of interest is the universal peak in wave power across the NDBC stations within 2005 that does not correspond to a peak in the NAO or ENSO indices (Figure 4.7). This peak, however, clearly reflects the extremely active 2005 hurricane season that the Atlantic Ocean experienced (Chapter 4's Appendix 4.6.4), where the NHC recorded 31 tropical cyclones for the area. This seasonal intensity is only matched within the Atlantic Ocean by the recent 2020 hurricane season, which, unfortunately, is not fully captured within our dataset (Figure 4.7). However, the 1995, 2003, 2010, 2011 and 2019 hurricane seasons all registered 20 or more storm events (NHC, 2022; Chapter 4's Appendix 4.6.4), which are echoed in the trend peaks within Figure 4.7.

The overarching objective of these plots is to notice that a number of NDBC stations are showing an upward linear regression trend across the 40-year reviewed period (Figure 4.7), deviating from the previous, almost universal downward linear regression trends observed within the eastern Pacific Ocean. In fact, four (NDBC stations 41009, 44008, 44013 and 44014) of the ten Atlantic sites show upward trends for both seasonal and seasonally detrended trends over the time period (Figure 4.7; Table 4.6), which are consistent with Ahn and Neary's (2020) Atlantic moored buoy inter-annual mean total wave power of 0.02 kW/m/year for NDBC station 44025 (a site not reviewed within this study due to a deployment period of less than 30 years). Interestingly, NDBC stations 44008 (0.175 kW/m/yr.) and 44011 (-0.025 kW/m/yr.), both situated on the coastal shelf in relatively close proximity (Figure 4.1), return opposite non-detrended wave power trend results (Table 4.6).

Table 4.6. Atlantic Ocean 40-year regression trends for each site (displayed from North to South) for non-detrended and seasonally detrended daily mean wave power (kW/m). Significant trends per year are indicated in bold (p-value < 0.05)

| Station | Wave Power Trends (kW/m /yr.) | Wave Power slope (kW/m /day) | Wave Power intercept (kW/m) | NDBC / WIS Pearson Correlation Coefficient | Seasonally detrended wave power trends (kW/m /yr.) | Seasonally detrended wave power slope (kW/m /day) | Seasonally detrended wave power intercept (kW/m) | Seasonally detrended NDBC / WIS Pearson Correlation Coefficient | Number of samples |
|---|---|---|---|---|---|---|---|---|---|
| NDBC 44007 | -0.007 | -0.00002 | 5.855 | 0.91 | -0.005 | -0.00001 | 5.791 | 0.91 | 13515 |
| WIS 44007 | **0.043** | 0.00012 | 2.647 | | **0.044** | 0.00012 | 2.611 | | |
| NDBC 44005 | **-0.165** | -0.00045 | 18.332 | 0.93 | **-0.159** | -0.00044 | 18.144 | 0.91 | 13867 |
| WIS 44005 | -0.001 | 0.00000 | 8.803 | | 0.002 | 0.00000 | 8.698 | | |
| NDBC 44013 | **0.083** | 0.00023 | 2.370 | 0.95 | **0.084** | 0.00023 | 2.329 | 0.95 | 11689 |
| WIS 44013 | **0.072** | 0.00020 | 0.721 | | **0.073** | 0.00020 | 0.708 | | |
| NDBC 44011 | -0.025 | -0.00007 | 25.764 | 0.95 | -0.012 | -0.00003 | 25.382 | 0.94 | 12784 |
| WIS 44011 | **0.164** | 0.00045 | 14.024 | | **0.173** | 0.00048 | 13.727 | | |
| NDBC 44008 | **0.175** | 0.00048 | 13.081 | 0.94 | **0.184** | 0.00050 | 12.817 | 0.93 | 13150 |
| WIS 44008 | **0.209** | 0.00057 | 8.608 | | **0.216** | 0.00059 | 8.398 | | |
| NDBC 44014 | 0.028 | 0.00008 | 10.901 | 0.94 | 0.028 | 0.00008 | 10.936 | 0.93 | 10593 |
| WIS 44014 | **0.091** | 0.00025 | 7.533 | | **0.089** | 0.00025 | 7.605 | | |
| NDBC 41001 | -0.028 | -0.00008 | 25.276 | 0.92 | -0.015 | -0.00004 | 24.870 | 0.91 | 14564 |
| WIS 41001 | 0.029 | 0.00008 | 19.595 | | **0.038** | 0.00010 | 19.294 | | |
| NDBC 41002 | **-0.060** | -0.00016 | 21.254 | 0.92 | **-0.053** | -0.00015 | 21.040 | 0.91 | 14094 |
| WIS 41002 | **0.102** | 0.00028 | 14.286 | | **0.108** | 0.00030 | 14.114 | | |
| NDBC 41010 | -0.038 | -0.00010 | 14.511 | 0.93 | **-0.039** | -0.00011 | 14.543 | 0.92 | 11323 |
| WIS 41010 | **0.094** | 0.00026 | 10.508 | | **0.092** | 0.00025 | 10.555 | | |
| NDBC 41009 | 0.026 | 0.00007 | 7.496 | 0.95 | 0.022 | 0.00006 | 7.623 | 0.95 | 11323 |
| WIS 41009 | **0.139** | 0.00038 | 5.688 | | **0.135** | 0.00037 | 5.796 | | |

All but three NDBC stations show upward trends that are statistically significant (p-value less than 0.05), with all of the WIS sites estimating upward trends for wave power that is seasonally detrended (Table 4.6). As expected with the offset in wave power, a higher number of WIS sites return significant trends; however, all sites exhibited a good NDBC-WIS Pearson correlation coefficient of 0.91 or higher (Table 4.2). No site specific correlations for latitudinal (North to South) or longitudinal (East to West) wave power trends were detected.

### *4.4.5 Gulf of Mexico wave power*

Of the reviewed regions and even with its famous hurricane prone reputation, the Gulf of Mexico sites capture the least amount of wave power overall, with hourly maximums ranging from a low of 144.89 kW/m (n = 8659) at NDBC station 42019, to a high of 664 kW/m (n = 11941) at NDBC station 42003 for the 39-year review period (Table 4.7). However, a large portion of the wave power is captured within the 99$^{th}$ percentile, which reaches a Gulf of Mexico maximum of 59.84 kW/m (n = 13146) at NDBC station 42002 (Table 4.7). Within this region, median hourly wave power values are predominantly lower than the other regions, ranging between 2.29 kW/m (n = 11941) at NDBC station 42003 (even though this station exhibits the highest maximum wave power within the region) to 4.02 kW/m (n = 9097) at NDBC station 42020 (Table 4.7).

Table 4.7. Gulf of Mexico hourly wave power (kW/m) descriptive statistics for each site (displayed from North to South, then West to East) for the reviewed 39-year period

| Station | Median | Mean | 90$^{th}$ Percentile | 99$^{th}$ Percentile | Max. | Number of Obs. | Std. Deviation | Std. Error |
|---|---|---|---|---|---|---|---|---|
| NDBC 42019 | 3.52 | 6.46 | 15.29 | 42.65 | 144.89 | 8659 | 9.17 | 0.10 |
| WIS 42019 | 2.61 | 5.49 | 13.17 | 38.70 | 407.63 | 8037 | 9.87 | 0.11 |
| NDBC 42020 | 4.02 | 7.06 | 16.27 | 45.03 | 233.45 | 9097 | 10.29 | 0.11 |
| WIS 42020 | 3.28 | 5.37 | 12.17 | 32.01 | 72.18 | 2237 | 6.42 | 0.14 |
| NDBC 42002 | 3.34 | 7.40 | 18.04 | 59.84 | 310.63 | 13146 | 12.75 | 0.11 |
| WIS 42002 | 2.73 | 6.45 | 15.28 | 57.42 | 266.75 | 12428 | 12.28 | 0.11 |
| NDBC 42001 | 2.36 | 6.08 | 14.47 | 55.04 | 461.48 | 12394 | 12.73 | 0.11 |
| WIS 42001 | 2.02 | 5.51 | 13.14 | 50.48 | 365.26 | 12118 | 12.06 | 0.11 |
| NDBC 42003 | 2.29 | 5.87 | 13.92 | 50.05 | 664.00 | 11941 | 13.14 | 0.12 |
| WIS 42003 | 1.44 | 4.65 | 10.77 | 45.50 | 736.67 | 11272 | 13.61 | 0.13 |

These results are due to the smaller Gulf of Mexico body of water, where the background wave climate is predominantly composed of locally generated wind sea conditions, and minimal swells entering into the system through the Yucatan Channel or Florida Straits. NDBC station 42003 (Figure 4.1) is the closest reviewed station to these channels to the Atlantic Ocean, and is situated within the location of the oscillating Gulf Loop Current (Maul, 1977; Oey et al., 2005). NDBC stations 42020 and 42019 (Figure 4.1) are on the continental shelf in the shadow of the US land mass that reduces open water area for local wind-wave development, which explains their minimal wave power values, although they are exposed to easterly and south-easterly wind-wave growth. NDBC station 42001 and 42002 (Figure 4.1) are subjected to Loop Current eddies that break away from the main Loop Current and propagate westwards (Maul, 1977; Oey et al., 2005), introducing wave energy into the system via non-linear wave-current interaction (Romero et al, 2017).

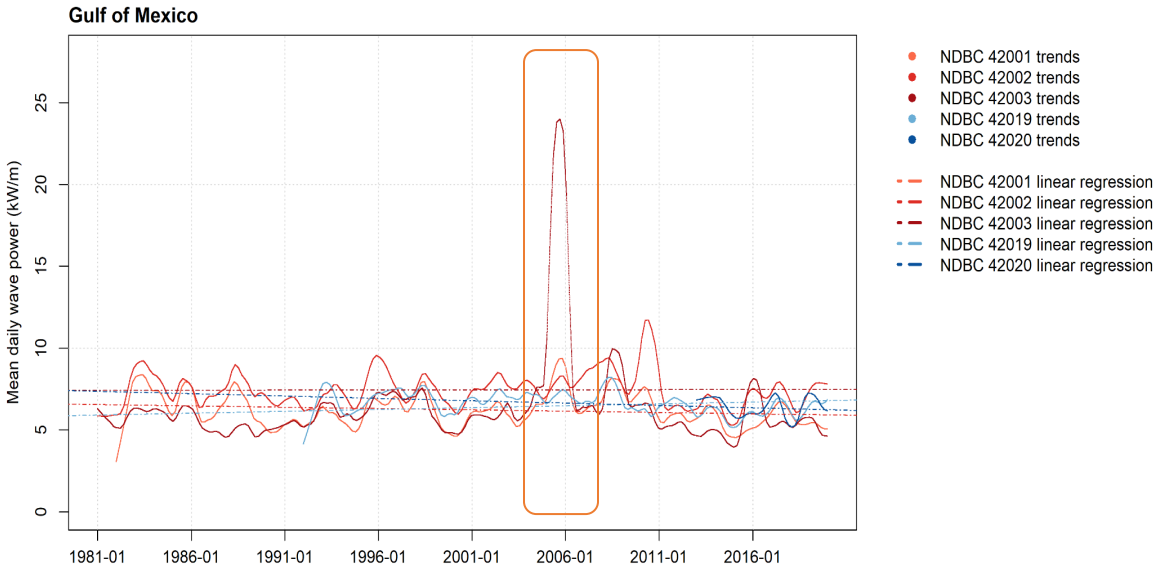


Figure 4.8. NDBC and WIS wave power trends for the Gulf of Mexico. Peaks within the wave power trends did not appear similar to trends within the climate indices, and so are not included. The dramatic peak experienced during 2005 at NDBC station 42003 represents the increase in wave power as Hurricane Katrina moved over the buoy (orange box).

These various land and oceanographic influences on the wave climate within the Gulf of Mexico are evident in the mean daily wave power trends and linear regression trends over time (Figure 4.8). However, significant hurricane events, Hurricane Katrina (August 2005; Knabb, 2005); Hurricane Rita (September 2005; NHC, 2022); and Hurricane Wilma (October 2005; NHC, 2022), passed over NDBC station 42003 with enough wave power to ensure their signals are represented in the seasonally detrended mean daily wave power (orange box in Figure 4.8). Here the mean daily seasonally detrended wave power reaches 24 kw/m, far exceeding the background mean daily wave power trends that range within 5 – 12 kW/m for that (then, prior to 2020) record-breaking 2005 hurricane season (Figure 4.8). Of note is that the data signal evident for September 2005 is interpolated NDBC data, as the mooring at NDBC Station 42003 failed during Hurricane Katrina (August 28$^{th}$, 2005), before NDBC redeployment in October 6$^{th}$, 2005. These results provide yet another validation of the data methodology applied for these analyses.

Table 4.8. Gulf of Mexico 39-year regression trends for each site (displayed from North to South) for non-detrended and seasonally detrended daily mean wave power (kW/m). Significant trends per year are indicated in bold (p-value < 0.05)

| Station | Wave Power Trends (kW/m /yr.) | Wave Power slope (kW/m /day) | Wave Power intercept (kW/m) | NDBC / WIS Pearson Correlation Coefficient | Seasonally detrended wave power trends (kW/m /yr.) | Seasonally detrended wave power slope (kW/m /day) | Seasonally detrended wave power intercept (kW/m) | Seasonally detrended NDBC / WIS Pearson Correlation Coefficient | Number of samples |
|---|---|---|---|---|---|---|---|---|---|
| NDBC 42019 | **-0.030** | -0.00008 | 7.705 | 0.86 | **-0.029** | -0.00008 | 7.678 | 0.85 | 10228 |
| WIS 42019 | **0.027** | 0.00007 | 4.576 | | **0.027** | 0.00008 | 4.545 | | |
| NDBC 42020 | -0.022 | -0.00006 | 7.455 | 0.93 | -0.022 | -0.00006 | 7.467 | 0.92 | 2557 |
| WIS 42020 | 0.091 | 0.00025 | 1.453 | | 0.090 | 0.00025 | 1.460 | | |
| NDBC 42002 | 0.000 | 0.00000 | 7.436 | 0.90 | 0.001 | 0.00000 | 7.409 | 0.89 | 14245 |
| WIS 42002 | 0.014 | 0.00004 | 6.140 | | 0.014 | 0.00004 | 6.150 | | |
| NDBC 42001 | -0.018 | -0.00005 | 6.782 | 0.93 | **-0.016** | -0.00005 | 6.744 | 0.93 | 13880 |
| WIS 42001 | 0.014 | 0.00004 | 5.237 | | 0.014 | 0.00004 | 5.219 | | |
| NDBC 42003 | 0.022 | 0.00006 | 5.684 | 0.97 | 0.023 | 0.00006 | 5.657 | 0.97 | 14245 |
| WIS 42003 | 0.030 | 0.00008 | 4.520 | | 0.030 | 0.00008 | 4.514 | | |

The lower background wave power estimates are echoed within the non-detrended and seasonally detrended daily mean wave power regression trends in Table 4.8, where only one NDBC station (42019) shows both a statistically significant non-detrended (-0.030 kW/m/yr.; n = 10228) and seasonally detrended (-0.029 kW/m/yr.) trend, and only one NDBC station (42001) shows a significant seasonally detrended trend (-0.016 kW/m/yr.; n = 13880). These results show the benefits of reviewing variability between non-detrended and seasonally detrended wave power trends. Of note is that these smaller wave power trends show relative agreement in magnitude but not trend with Ahn and Neary's (2020) NDBC station 42040 inter-annual mean total wave power results of 0.04 kW/m/year.

Overall, of the five reviewed Gulf of Mexico NDBC stations, three stations returned downward mean power trends, and two stations returned upward trends per year (Table 4.8), regardless of seasonality. NDBC and WIS trends and slopes differ at all the sites, with downward or neutral trends per year for NDBC measurements and upward trends from WIS collocated locations. However, all sites exhibited reasonable NDBC-WIS Pearson correlation coefficients of 0.85 or higher (Table 4.8), even with the varying directional slope trends.

### *4.4.6 Regional 90$^{th}$ percentile wave power*

For coastal engineering and planning purposes (Forte et al., 2012), the non-detrended 90$^{th}$ percentile wave power results were annually aggregated across each region to isolate maximum values within the Atlantic Ocean, Gulf of Mexico, eastern Pacific Ocean and Hawaii (Figure 4.9). These results show that those considering baseline wave power conditions within the eastern Pacific Ocean should expect the maximum 90$^{th}$ percentile of non-detrended for season wave power values to range between 414– 1937 kW/m (n = 43 years), with standard errors (SE) from 45 to 175 kW/m, respectively across the eastern Pacific Ocean NDBC stations (Figure 4.9, top plot). Within the Atlantic Ocean, non-detrended for season wave power values are less intense, with maximum 90$^{th}$ percentile values ranging between 312 – 1551 kW/m (SE: 21 – 196 kW/m; n = 42 years) across the

NDBC sites (Figure 4.9, top plot). Moving further down the scale in wave power intensity, the Hawaiian NDBC sites (Figure 4.9, top plot) show a maximum 90$^{th}$ percentile of non-detrended for season wave power values that range between 180 – 803 kW/m (SE: 12 – 171 kW/m; n = 37 years). Finally, the least intense reviewed wave power region, the Gulf of Mexico NDBC sites (Figure 4.9, top plot), have recorded maximum 90$^{th}$ percentile of non-detrended for season wave power values that range between 66 – 934 kW/m (SE: 3 – 148 kW/m; n = 41 years). Interestingly, the 2005 Gulf of Mexico hurricane season is represented as above the norm within the annual maximum 90$^{th}$ percentile (Figure 4.9).

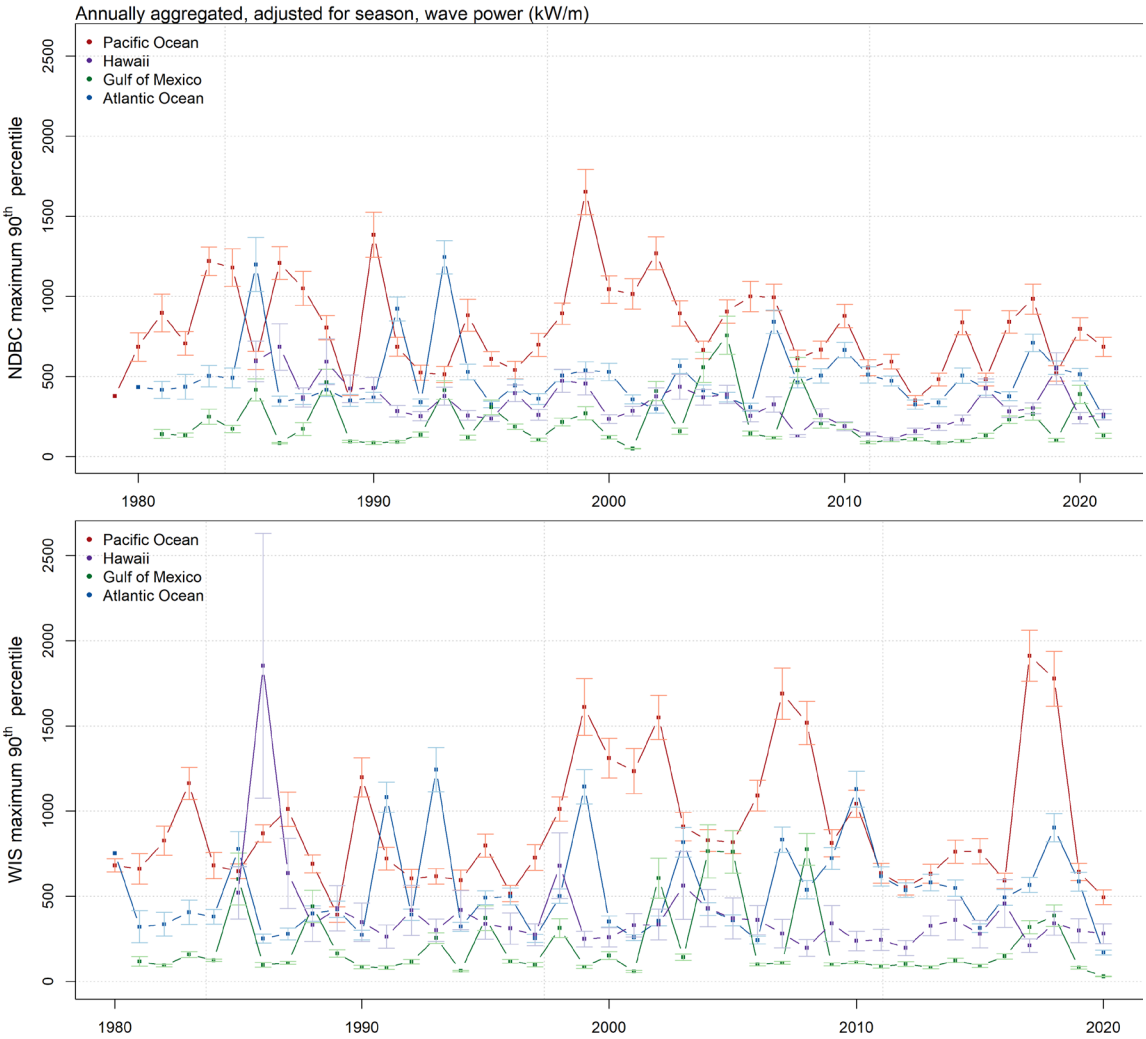


Figure 4.9. Spatial and temporal variability in annually aggregated, non-detrended, maximum NDBC (top plot) and WIS (bottom plot) 90$^{th}$ percentile wave power (kW/m) across the Atlantic Ocean, Gulf of Mexico, eastern Pacific Ocean and Hawaii, with error bars representing the standard error.

WIS non-detrended for season, maximum 90$^{th}$ percentile wave power shows a larger range of 471 – 2311 kW/m (SE: 45 – 206 kW/m; n = 41 years) for the eastern Pacific Ocean sites, 240 – 1492 kW/m (SE: 20 – 155 kW/m; n = 41 years) for the Atlantic Ocean sites, 252 – 2200 kW/m (SE: 64 – 922 kW/m; n = 36 years) for the Hawaiian sites, and 47 – 923 kW/m (SE: 5 – 188 kW/m; n = 40 years) for the Gulf of Mexico sites. As before, NDBC and WIS wave power estimates show agreement in the peaks over time, but magnitude differences between the two dataset persist within these results.

The spatial and temporal variability between the NDBC and WIS wave power estimates are evidenced by higher WIS wave power ranges for the eastern Pacific Ocean and Hawaiian Island sites, and comparable maximum 90$^{th}$ percentile wave power ranges for the Atlantic and Gulf of Mexico sites. Apart from the Hawaiian sites, standard errors appear relatively similar between the NDBC and WIS wave power ranges. The annual maximum 90$^{th}$ percentile per region has a tendency to overshadow the individual buoy results, necessitating the calculation of site specific wave power estimates for accurate assessments. However, while the investigation of wave power potential at individual sites requires a localised wave climate study for accurate planning and engineering purposes, these overall baseline wave power estimates will assist in initial project design and development within each of the four regions.

## 4.5 Summary

In summary, buoy measurement data can be used to calculate wave power trends over time. Additionally, moored buoy wave power data are comparable with wave model wave power estimates; both showing that wave power trends are not increasing over time as appreciably as significant wave heights. Overall, the majority of the eastern Pacific Ocean and Hawaii wave power trends are downward, with mixed slope wave power trends apparent within the Atlantic Ocean and Gulf of Mexico. As there is a noticeable variability in the trend direction within each reviewed region, site specific trends should not be generalised to represent a large region.

Wave power estimates differ from region to region due to area specific wave generation and propagation, with the eastern Pacific Ocean ranking as more energetic of the regions with respect to wave power. After ranking by maximum wave power, 60 % of the top ten stations are located along the eastern Pacific Ocean coastline. The Atlantic Ocean registers as the second most energetic coastline within these reviewed sites, with Hawaii logging in at third place. The Gulf of Mexico contains the least amount of wave power within these regions, although the Gulf of Mexico wave power trends clearly highlight extreme weather events that affect the region.

The higher wave power values that are observed within the eastern Pacific Ocean are attributed to the swell-dominated, longer $T_p$ and higher $H_{m0}$ conditions that those sites are exposed to. These conditions form from a combination of North Pacific storms that pass through between autumn and spring, as well as the southern swells from the South Pacific and Southern Ocean that penetrate the region within the summer months. The Atlantic Ocean experiences lower $T_p$ conditions due to a predominant wave climate of local wind seas with following swells from Nor'easters. For the southern North Atlantic Ocean locations (south of Cape Hatteras), tropical cyclone activity is evident in spatially variable wave power values that are a factor of five lower than those observed within the eastern Pacific. Within the Hawaiian region, the northern versus southern sites showed a difference in wave power magnitude (higher in the north), highlighting the effect of the northern site's exposure to north Pacific storm swells, while the rest of the reviewed Hawaiian sites experienced central Pacific and Southern Ocean swell signals. While the Gulf of Mexico records the lowest wave power values across the four reviewed regions due to its wind sea conditions and smaller area, the net impact of extreme events (i.e. tropical storms and hurricanes) is evident within the background wave power estimates.

Overall, all of the reviewed regions produced daily mean wave power trends that show associations with extreme tropical weather events that were recorded by the NHC (1995 – 2021). Peaks in wave power trends throughout the eastern Pacific Ocean, Hawaiian and Atlantic Ocean sites appear to follow trends in both concurrent and variable PDO, NAO

and ENSO LOWESS regressions. However, correlation does not infer causation and without in-depth analyses into the relationships between these wave power trends and the reviewed climate indices, no definitive results are available here.

Finally, as the majority of wave power trend analyses and coastal engineering wave climate risk assessments are performed using wave model datasets, one of the objectives of this work was to quantitatively assess the differences between these model and observational data sources. Results show significant differences between the NDBC moored buoy and wave model wave power results that highlight the importance of using site specific results to investigate wave power within regions. These NDBC and WIS differences may be due to the different spectral-band frequency ranges that are used to calculate the bulk wave parameters required for these wave power calculations. They also highlight the importance of using wave power over individual bulk parameters to evaluate the performance of WIS modelling technology. As this is the first study to use wave power as a metric to evaluate wave model results, there is reason for additional investigation to identify potential deficiencies in wind forcing or modelling technology.

In conclusion, moored buoy data are successfully accessed to investigate wave power trends within four coastal regions around the US. While observational and model results are relatively similar, the moored buoy data presents smaller wave power ranges for two of the four regions, suggesting that observational data are essential in local wave climate studies to ensure accurate estimates for coastal planners and engineers.

## 4.6 Chapter 4 Appendix

Appendix 4.6.1: NDBC and associated WIS Stations, water depth and length of record

| Eastern Pacific Ocean | | | | Atlantic Ocean | | | |
|---|---|---|---|---|---|---|---|
| NDBC | | | Corresponding WIS Point | NDBC | | | Corresponding WIS Point |
| Station | # years | Depth (m) | | Station | # years | Depth (m) | |
| 46001 | 42 | 4054 | ST46001 | 41001 | 42 | 4486 | ST41001 |
| 46002 | 42 | 3455 | ST46002 | 41002 | 42 | 3759 | ST41002 |
| 46005 | 42 | 2852 | ST46005 | 41009 | 32 | 42 | ST41009 |
| 46006 | 41 | 4323 | ST46006 | 41010 | 32 | 890 | ST41010 |
| 46011 | 40 | 464.8 | ST46011 | 44005 | 41 | 176.8 | ST44005 |
| 46012 | 40 | 208.8 | ST46012 | 44007 | 38 | 49 | ST44007 |
| 46013 | 39 | 123.4 | ST46013 | 44008 | 38 | 68.9 | ST44008 |
| 46022 | 38 | 419 | ST46022 | 44011 | 36 | 91.1 | ST44011 |
| 46025 | 38 | 890 | ST46025 | 44013 | 36 | 64.6 | ST44013 |
| 46029 | 36 | 131 | ST46029 | 44014 | 30 | 47 | ST44014 |
| Gulf of Mexico | | | | Hawaii | | | |
| NDBC | | | Corresponding WIS Point | NDBC | | | Corresponding WIS Point |
| Station | # years | Depth (m) | | Station | # yrs. | Depth (m) | |
| 42001 | 42 | 3194 | ST42101 | 51001 | 39 | 4895 | ST81310 |
| 42002 | 42 | 3088 | ST42102 | 51002 | 36 | 4948 | ST81301 |
| 42003 | 42 | 3265 | ST42103 | 51003 | 36 | 1987 | - |
| 42019 | 30 | 83.5 | ST42019 | 51004 | 36 | 5183 | - |
| 42020 | 30 | 84.1 | ST42020 | | | | |

Appendix 4.6.2: Historical NDBC Payloads and Wave Measurement Systems

NDBC Payloads (NDBC, 2003)

| | |
|---|---|
| GSBP | General Service Buoy Payload |
| MARS | Multifunction Acquisition and Reporting System |
| DACT | Data Acquisition and Control Telemetry |
| VEEP | Value Engineered Environmental Payload |
| AMPS | Advance Modular Payload System |
| ARES | Acquisition and Reporting Environmental System |
| SCOOP | Self-Contained Ocean Observing Payload |

Historical NDBC Wave measurement systems and sampling information (NDBC, 2003, 2018b; Teng et al., 2009)

| Wave Sensor | Record Length | Sampling rate | Number of Frequency Bands | Frequency Range | Frequency Band Width |
|---|---|---|---|---|---|
| Wave Data Analyzer (WDA) | 20 min (1200 s) | 1.50 Hz | 38 | 0.02 Hz to 0.50 Hz | 0.01 Hz |
| Wave Analyser (WA) | 20 min (1200 s) | 2.56 Hz | 38 | 0.03 Hz to 0.40 Hz | 0.01 Hz |
| Digital Wave Analyzer (DWA) | 20 min (1200 s) | 2.00 Hz | 38 | 0.00 Hz to 0.50 Hz | 0.01 Hz |
| Magnetometer Only Directional Wave Analyzer (DWA-MO) | 20 min (1200 s) | 2.00 Hz | 38 | 0.03 Hz to 0.40 Hz | 1.00 Hz |
| Wave Processing Module (WPM) | 40 min (2400 s) | 1.7066 Hz | 47 | 0.0325 – 0.4850 Hz | 0.020 Hz (noise band): 0.010 Hz bandwidth<br>0.0325 – 0.0925 Hz: 0.005 Hz bandwidth<br>0.1000 – 0.3500 Hz: 0.010 Hz bandwidth<br>0.3650 – 0.485 Hz: 0.020 Hz |
| Directional Wave Processing Module (DWPM) | 20 min (1200 s) | 1.7066 Hz | 47 | 0.0325 – 0.4850 Hz | 0.020 Hz (noise band): 0.010 Hz bandwidth<br>0.0325 – 0.0925 Hz: 0.005 Hz bandwidth<br>0.1000 – 0.3500 Hz: 0.010 Hz bandwidth<br>0.3650 – 0.485 Hz: 0.020 Hz |
| Non-Directional Wave Processing Module (NDWPM) | 20 min (1200 s) | 1.7066 Hz | 47 | 0.0325 – 0.4850 Hz | 0.020 Hz (noise band): 0.010 Hz bandwidth<br>0.0325 – 0.0925 Hz: 0.005 Hz bandwidth<br>0.1000 – 0.3500 Hz: 0.010 Hz bandwidth<br>0.3650 – 0.485 Hz: 0.020 Hz |
| Digital Directional Wave Module (DDWM) | 20 min (1200 s) | 1.7066 Hz | 47 | 0.0325 – 0.4850 Hz | 0.020 Hz (noise band): 0.010 Hz bandwidth<br>0.0325 – 0.0925 Hz: 0.005 Hz bandwidth<br>0.1000 – 0.3500 Hz: 0.010 Hz bandwidth<br>0.3650 – 0.485 Hz: 0.020 Hz |

Appendix 4.6.3: Spectral frequency bands

NDBC: 38 frequency bands

| | | | | | | | | | |
|---|---|---|---|---|---|---|---|---|---|
| 0.0300 | 0.0400 | 0.0500 | 0.0600 | 0.0700 | 0.0800 | 0.0900 | 0.1000 | 0.1100 | 0.1200 |
| 0.1300 | 0.1400 | 0.1500 | 0.1600 | 0.1700 | 0.1800 | 0.1900 | 0.2000 | 0.2100 | 0.2200 |
| 0.2300 | 0.2400 | 0.2500 | 0.2600 | 0.2700 | 0.2800 | 0.2900 | 0.3000 | 0.3100 | 0.3200 |
| 0.3300 | 0.3400 | 0.3500 | 0.3600 | 0.3700 | 0.3800 | 0.3900 | 0.4000 | | |

NDBC: 47 frequency bands

| | | | | | | | | | |
|---|---|---|---|---|---|---|---|---|---|
| 0.0200 | 0.0325 | 0.0375 | 0.0425 | 0.0475 | 0.0525 | 0.0575 | 0.0625 | 0.0675 | 0.0725 |
| 0.0775 | 0.0825 | 0.0875 | 0.0925 | 0.1000 | 0.1100 | 0.1200 | 0.1300 | 0.1400 | 0.1500 |
| 0.1600 | 0.1700 | 0.1800 | 0.1900 | 0.2000 | 0.2100 | 0.2200 | 0.2300 | 0.2400 | 0.2500 |
| 0.2600 | 0.2700 | 0.2800 | 0.2900 | 0.3000 | .03100 | 0.3200 | 0.3300 | 0.3400 | 0.3500 |
| 0.3650 | 0.3850 | 0.4050 | 0.4250 | 0.4450 | 0.4650 | 0.4850 | | | |

WIS WAVEWATCH III® 29 frequency bands: Pacific and Atlantic Ocean

| | | | | | | | | | |
|---|---|---|---|---|---|---|---|---|---|
| 0.0350 | 0.0385 | 0.0424 | 0.0466 | 0.0512 | 0.0564 | 0.0620 | 0.0682 | 0.0750 | 0.0825 |
| 0.0908 | 0.0999 | 0.1098 | 0.1208 | 0.1329 | 0.1462 | 0.1608 | 0.1769 | 0.1946 | 0.2141 |
| 0.2355 | 0.2590 | 0.2849 | 0.3134 | 0.3447 | 0.3792 | 0.4171 | 0.4588 | 0.5047 | |

WIS WAM frequency bands: 28 Western Alaska and Gulf of Mexico

| | | | | | | | | | |
|---|---|---|---|---|---|---|---|---|---|
| 0.0314 | 0.0345 | 0.0380 | 0.0418 | 0.0459 | 0.0505 | 0.0556 | 0.0612 | 0.0673 | 0.0740 |
| 0.0814 | 0.0895 | 0.0985 | 0.1083 | 0.1192 | 0.1311 | 0.1442 | 0.1586 | 0.1745 | 0.1919 |
| 0.2111 | 0.2323 | 0.2555 | 0.2810 | 0.3091 | 0.3400 | 0.3740 | 0.4114 | | |

Appendix 4.6.4: Annual counts of US NHC and Central Pacific Hurricane Center Annual Tropical Cyclones per year (sourced from NHC, 2022)

| Year | Atlantic Ocean | Eastern Pacific Ocean | Central Pacific Ocean |
|---|---|---|---|
| 1995 | 20 | 11 | 1 |
| 1996 | 13 | 12 | 2 |
| 1997 | 9 | 19 | 9 |
| 1998 | 14 | 15 | 3 |
| 1999 | 16 | 14 | 3 |
| 2000 | 19 | 19 | 4 |
| 2001 | 17 | 17 | 4 |
| 2002 | 14 | 16 | 5 |
| 2003 | 21 | 16 | 2 |
| 2004 | 16 | 16 | 3 |
| 2005 | 31 | 16 | 3 |
| 2006 | 10 | 21 | 5 |
| 2007 | 17 | 15 | 2 |
| 2008 | 17 | 18 | 1 |
| 2009 | 11 | 20 | 3 |
| 2010 | 21 | 12 | 1 |
| 2011 | 20 | 13 | 0 |
| 2012 | 19 | 17 | 0 |
| 2013 | 15 | 18 | 3 |
| 2014 | 9 | 21 | 2 |
| 2015 | 12 | 22 | 5 |
| 2016 | 16 | 22 | 1 |
| 2017 | 19 | 20 | 0 |
| 2018 | 16 | 25 | 1 |
| 2019 | 20 | 21 | 1 |
| 2020 | 31 | 21 | 0 |
| 2021 | 13 | 14 | 0 |

## Chapter 5

# 5. General Discussion and Concluding Remarks

## Preface:

Overall, this work showcases a comprehensive methodology for accomplishing a wave power climate study that uses long-term modelled and observational wave data with viable data quality assurance practices. However, prior to wave power trend evaluations, this study first carried out an often neglected but essential task of data quality assurance of observational wave data. These quality control practices focussed on (a) data comparability of multiple wave measurement systems due to buoy hull (hardware) difference; and (b) data homogeneity of long-term archiving due to software differences.

This chapter collates the work that supports confidence in observational wave measurement data and the resultant wave power trends over time. Section **5.1** reviews the statistical comparisons that showcase confidence in different wave instrumentation platforms (key question 1), while section **5.2** showcases how discontinuities in the NDBC wave time series data are removed (key question 2). Section **5.3** overviews the analyses that calculate wave power and inspect wave power trends over time (key question 3). Section **5.3** also showcases the essential utilisation of observational wave power results over model results when considering wave power trends, due to the variance between the measurement and model wave power results.

### 5.1 Key question 1: Are measurements from different wave measurement systems comparable?

As detailed within the literature review, confidence in the quality and consistency of moored buoy wave measurement is essential for model and satellite validation and calibration purposes; as well as wave climate research required for coastal resilience,

protection, navigation and planning. Therefore, chapter 2 investigated whether wave measurements from different wave measurement systems were comparable.

While many studies have investigated legacy NDBC wave measurement systems (Earle et al., 1984; 1985; Teng and Timpe, 1995; O'Reilly et al., 1996; Earle et al., 1999; Teng et al.; 2007; Crout et al., 2008; Teng et al., 2009; Bender et al., 2010; Riley et al., 2011; Jensen et al., 2015; Riley and Bouchard, 2015; Bouchard et al., 2016; 2017; 2018; Hall et al., 2018b; Bouchard and Jensen, 2019; Riley et al., 2019; and Jensen et al. 2021), none have reviewed the newly operational NDBC 2.1-m hull. Therefore, chapter 2 reviews the earlier work listed above, before describing the first published results of the performance of the newly operational NDBC 2.1-m hull.

Chapter two's evaluations tested the correlations between both the test NDBC 2.1-m hulls and the previously deployed legacy NDBC 3-m hulls with their respective reference CDIP DWR datasets, in search of an improvement in 2.1-m hull versus DWR correlations. Statistical performance was evaluated between two non-directional (significant wave height, $H_{m0}$, and average wave period, $T_a$) and two directional (mean wave direction at peak frequency, $\alpha_p$, and peak directional spread, $\sigma_p$) bulk wave parameters. To remove agency data processing bias, the study dove deeper to review energy density comparisons on a spectral level (mean spectral wave energy density, $C_{11}$, and mean acceleration spectra, $C_{11}^m$).

These spectral evaluations showcased an improvement in the 2.1-m hull vs DWR bias and RMSE values compared to those obtained from the earlier 3-m hull and DWR comparison. The NDBC 2.1-m hulls show an improved signal-to-noise ratio, indicating that the 2.1-m hull is introducing less hull and sensor noise into the spectral signals, which allows for an increase in energy retention in the lower frequency spectral range.

To explore these improvements more thoroughly, this work recalculated wave component datasets (forerunners, long swell, short swell, long seas, short seas, wind chop) from the mean spectral wave energy density ($C_{11}$). NDBC 2.1-m hull improvements were detected

within the short seas and wind chop components for all regions, with improvements in Great Lakes short swell and long seas, and Pacific Ocean forerunners and wind chop.

Overall, these analyses proved that wave measurements reported from the NDBC 2.1-m hulls showed an increase in significant wave height and average wave period accuracy, based on a nearby reference DWR, when compared to the previously collected NDBC 3-m hull wave data. While no definitive improvements were detected within the directional data estimates, these data retained the same accuracy levels as the earlier hull.

Therefore, this work confirms improvements in both NDBC bulk and spectral data accuracy with the deployment of the newly operational 2.1-m hull. As the 2.1-m buoy is to be the future operational NDBC platform, it was timely that this work was initiated at the initial stages rather than be faced with data uncertainties in the future. Both these and the previous NDBC evaluation results provide confidence for the wave community's use of NDBC wave data to drive wave model technologies for coastal studies.

Hence this work, in combination with previous NDBC data reviews, proves that measurements from different wave systems are comparable, satisfying the objective of key question 1.

## 5.2 Key question 2: Is it possible to correct for bias between different wave measurement systems to produce homogeneous long-term time series records?

With the proof that different wave measurement systems are comparable, chapter 3 discusses known inconsistencies within the NDBC wave time series data (Gemmrich et al., 2011; Young et al., 2011; Livermont et al., 2015, 2017; Young and Ribal, 2019; Hall and Jensen, 2021), and offers a viable methodology to remove these discontinuities (key question 2).

A primary suspect that introduces inconsistencies into the NDBC time series data is the historical NDBC archiving process. To date, historical NDBC data are archived in three primary locations: 1) The NDBC website (as zipped text files); 2) The official NOAA archives (as netCDF files), which are found at the NCEI; and 3) The NDBC DODS framework. As the DODS data are duplicates of those stored on the NDBC website, they were ignored within this work. However, issues stem from the differing handling procedures between the NDBC and NCEI archived datasets. While the NDBC website houses the most accurate, manually QC'd data, these data do not have any associated metadata, meaning that users are unable to link critical GPS positions, instrumentation information or quality control flags to these data. The NDBC data within the NCEI archives do contain this associated metadata, but unfortunately these data are sourced from the real-time NDBC data feed, which is not manually QC'd. Therefore these lower quality data have the essential metadata, but not the quality control. Adding to these NCEI archive issues are a number of handling errors that are introduced during the creation of these netCDF files. The differences between these two archives, including netCDF creation issues, are detailed within Hall and Jensen (2021).

Therefore, users that require the most accurate data and associated metadata would need to extract information from both archival sources and work through the known issues to create a clean dataset with matching metadata. Chapter 3 showcases the work that was undertaken to do just that, combining these two historical NDBC website and NCEI archive datasets to develop the best available, self-describing, quality controlled and consistent NDBC measurement archive: the USACE QCC Measurement Archive. The data archive routine involved a six step process for each historical buoy station: (1) data download and extraction from both archives; (2) individual archive dataset concatenation to create time series files of all available variables; (3) NCEI sourced metadata verification using an independent metadata index provided by NDBC; (4) data concatenation of the two datasets by date and time for comparison to a) remove data that were collected during service visits, b) geographically QA/QC the matching data to remove data collected while the buoys were adrift, and c) attach metadata to the merged, best available dataset; (5) extract the best historical, self-describing dataset for each station; and (6) create Thredds

netCDF data files for each year and month per station. This process required 400k high performance supercomputer computational processor unit hours, and these final netCDF files were transferred over to the USACE CHL Data Server for public access.

Ultimately, this USACE QCC Measurement Archive provides a database of consistently stored, QA/QC data with verified metadata. Of note is that this methodology is only able to remove erroneous data that are easily identifiable within QC protocols, as these data could not be verified for quality due to a lack of nearby reference datasets.

Although this USACE QCC Measurement Archive removed a number of inconsistencies within the NDBC time series data, issues were still present. Therefore, work continued with the investigation into whether the use of changing instrumentation and platforms over the decades was introducing discontinuities into the time series data.

As this is the first time that verified metadata are available for an NDBC dataset, the NDBC time series data from the USACE QCC Measurement Archive were reviewed to investigate whether instrumentation changes affected the homogeneity of the data. These comparisons showed that discontinuities within the time series data were visually evident within the $T_p$ records. These discontinuities were often associated with changes in the discretization of the frequency bands defining the spectrum between the deployed wave instrumentation.

NDBC has historically recorded spectral wave energy estimates across two frequency band ranges, a 38-band and a 47-band wave spectrum. Therefore the non-directional data collected using the earlier 38-band wave spectrum were linearly interpolated across the now standard 47 frequencies, redistributing the captured energy across analogous frequency ranges. Once these data were converted, bulk wave parameters were recalculated from the now consistent NDBC non-directional spectral wave density data, $C_{11}$, using NDBC standard algorithms for $H_{m0}$, $T_a$, and $T_p$.

Not only did this frequency interpolation and uniform recalculation remove the discontinuities within the time series datasets that were associated with the shifting wave frequency ranges, this methodology removed inconsistencies that were associated with payload shifts. In one case (Station 46029), this methodology corrected a shift in the $T_p$ that did not appear to be caused by any recorded metadata, so this methodology may also correct for undetectable processing adjustments or earlier NDBC algorithm changes.

Overall, this methodology of a) using the new USACE QCC Measurement Archive with verified metadata, b) interpolating the wave frequency ranges to redistribute the wave energy across consistent frequency bands, and c) recalculating the bulk wave parameters using uniform algorithms, removed the identified discontinuities within the NDBC time series data.

Chapter 3 details a viable methodology that proves that it is possible to remove the observational NDBC time series discontinuities to generate homogeneous datasets, satisfying the objective of key question 2. Any attempt to look at long-term wave trends without validated, consistent data could potentially lead to erroneous conclusions.

## 5.3 Key question 3: Is wave power increasing over time?

As shown in the literature review and chapter 4, the majority of wave power estimates are assessed from a wave model due to the lack of consistent, long term observational datasets that contain few data gaps. However, with the creation of the quality controlled, uniform time series datasets within chapter 3, this work is the first to develop an observational wave time series dataset that provides the same coverage in time and space as available hindcast wave models.

This study tested for shifting observational inter-annual wave power trends at sites within the North Pacific Ocean, Hawaiian Islands, Gulf of Mexico and North Atlantic Ocean. These results were validated with statistical comparisons to collocated and concurrent,

reference WIS hindcast wave power trends. Both teleconnection climate indices (ENSO, PDO and NAO) and NHC extreme weather event records were incorporated to provide context to the peaks and troughs evident within the wave power trends.

This wave power work required consistent NDBC and WIS $H_{m0}$ and $T_p$ time series data to calculate wave power as per Resio et al. (2003). To generate this coherent observational time series data, this work used the frequency-interpolated and recalculated $H_{m0}$ and $T_p$ from the new USACE QCC Measurement Archive that were developed in chapter 3. To handle gaps within the time series data, missing values were interpolated across the datasets, although interpolated values were only inserted when missing to retain the integrity of the original data. These datasets were then detrended for seasonality using a verified multiple STL methodology to remove background seasonality variance bias and isolate interannual and interdecadal trends.

Non-detrended and seasonally detrended daily mean wave power results showed that typically the eastern Pacific Ocean and Hawaii wave power trends slope downwards, while wave power trends vary in slope direction within the Atlantic and Gulf of Mexico. As wave power trend directions were variable within each reviewed region, site specific wave power trends should not be generalised to represent a large region.

Observational and model results show similar trends, but differ in magnitude, within wave power peaks and troughs in long term inter-annual comparisons. Of note is that the moored buoy data presents lower wave power ranges for two (eastern Pacific Ocean and Hawaii) of the four regions than those that are detected within the model trends. However, peaks in observational wave power trends do echo peaks within climate indices trends (ENSO, PDO and NAO) and NHC extreme weather events. While extreme weather events affect the mean daily wave power trends, a direct link between the climate indices and wave power requires more in depth investigations.

For coastal engineering purposes, regional non-detrended 90$^{th}$ percentile wave power results were annually aggregated to isolate maximum values within the regions. These regional results highlighted the previously detected NDBC and WIS wave power spatial and temporal variability with higher WIS wave power ranges for the eastern Pacific Ocean and Hawaiian Island sites, and comparable maximum 90$^{th}$ percentile wave power ranges for the Atlantic and Gulf of Mexico sites. Apart from the Hawaiian sites, standard errors were consistent between the NDBC and WIS wave power ranges.

In summary, this study is one of the first to show spatially and temporally comparative observational and model wave power results, providing new information on the accuracy of model wave power estimates, while showcasing in situ wave power trends at 29 sites around the U.S. coastline. This work also highlights the consequences of estimating wave power from regional studies, as wave power trends varied in direction within neighbouring sites, and annual maximum 90$^{th}$ percentile per region overshadow the individual site wave power results.

Therefore, chapter 4 details a viable methodology to interpolate missing observational data and remove background seasonality variance bias to estimate accurate interannual and interdecadal wave power trends. NDBC observational and WIS model non-detrended and seasonally detrended daily mean wave power and regional 90$^{th}$ percentile wave power trends are compared for equivalency. These results highlight the variable trends in wave power at each reviewed site, satisfying the objective of key question 3.

## 5.4 Key Question Summaries

In summary, this dissertation is one of the first to show spatially and temporally comparative observational and model wave power results, providing new information on the accuracy of model wave power estimates. This work showcases in situ wave power trends at 29 sites around the U.S. coastline in connection with proven data quality assurance practices. This work also highlights the consequences of estimating wave power

from regional studies, as wave power trends varied in slope direction within neighbouring sites, and regionally grouped annual maximum 90$^{th}$ percentiles obscured the variability of individual site wave power results.

Chapter 2 shows that measurements from different wave measurement systems are comparable (key question 1), while chapter 3 provides a methodology for developing homogeneous long-term NDBC observational wave time series records (key question 2). In chapter 4 these homogeneous wave time series records are corrected for missing values and detrended for season, allowing for the determination of whether interannual and interdecadal wave power is increasing over time (key question 3).

Therefore, the results in chapter 4 show that wave power trends are site-specific, varying in trend direction and magnitude at each reviewed site. These results indicate that the hypothesis that wave power trends are increasing over time should be rejected (key question 3). This wave power variability within each region suggests that site specific wave power trends should not be generalised to represent a large region. Ultimately this work demonstrates that observational data are essential in local wave climate studies to accurately estimate wave power for sediment transport studies, recreational and commercial coastal development, offshore exploration, and climate resiliency planning and research.

## 5.5 Advantages, limitations, challenges and future work

One limitation of key question one's platform investigation is that we can only test wave measurement systems that are available now. Additionally, developing QC methods for any wave measurement systems (NDBC or non-NDBC) without having collocated comparison of nearby reference data relies on self-examination. However, once new equipment is evaluated, measurements between systems may be compared for confidence in the time series data. Therefore identifying and quantifying instrumentation differences will benefit all wave measurement users.

Additionally, it is critical to assess the quality of new wave measurement systems at the initial stages going toward 'fully operational' rather than playing catch up after years of data being archived and used. As new instruments and platforms are continually introduced into the measurement arena, intercomparison studies are never complete, requiring future data quality evaluations to determine the accuracy of newly available measurements. Evaluations should be repeated within different wave regimes and span all four seasons at least once during examination.

A challenge with key question one's 2.1-m hull evaluation methodology is the question of whether a DWR is the best choice as a relative reference, even though they were the only co-located wave recorders to our test sites. Magnusson et al. (1999) suggested that the semi-Lagrangian DWR's "broaden the crests and sharpens the troughs so that the skewness become[s] negative" (Magnusson et al., 1999:158). Although Magnusson et al. (1999) suggest a correction for these skewness offsets, Magnusson et al. (2021) compared a non-directional DWR against wave radar and laser technologies, and determined that their positive DWR comparisons to the laser "adds credibility to the JCOMM/DBCP recommendation to use the Datawell as a common reference" (Magnusson et al., 2021:909). Additionally, as both the NDBC buoys and DWR are moored platforms, both exhibit a quasi-Lagrangian movement around their tethers, allowing for a satisfactory apples to apples comparison of their data quality.

A major advantage of the work performed in response to key question two is that, with support from NDBC, our community now has access to a quality controlled, consistently stored historical measurement archive (the USACE QCC Measurement Archive) that provides the best version of NDBC data with verified metadata for future studies. As NDBC provides one of the longest available time series of meteorological and wave observations, their data are globally utilised for the validation and calibration of models and satellites, as well as coastal management and climate resiliency research.

The methodology constructed during this archive process is adaptable for all future NDBC data and data storage structures. However, this USACE QCC Measurement Archive presently only contains NDBC data. Observational ocean data are collected by numerous other agencies, including long-term altimeter wave data, many of which present more challenging standardisation, quality controls and metadata issues than those detected within the NDBC data sources. For complete standardisation, these datasets should be added to the USACE QCC Measurement Archive.

Additionally, the analysis methods and results for the wave QC methodology utilised within Chapter 2 and 3 are relevant to the NDBC buoy wave operation. These NDBC implemented in-house QC practices have been developed and operated for years. Therefore, it is conceivable that long-term wave data collections by other agencies may not have the same level of QC and thus may require additional work prior to the work we have presented here.

However, this USACE QCC Measurement Archive allowed for the calculation of the most consistent wave power trends to date. A significant advantage of the wave power trends estimated within this work is proof that a single point source of wave power cannot be used to predict wave power across a region, as wave power estimates are spatially variable. Previous box or regional interpretations of model and measurement wave power estimates should be reconsidered before use in local wave climate studies as they lead to simplification of a complex problem.

Another important result of the wave power trends work is the evidence that the WIS wave model produces the same peaks and troughs in the wave power trends, but not in wave power magnitude. This offset proves how critical observational data are for not only both local wave climate and coastal resilience studies, but also for model and satellite validations and calibrations.

As the WIS model is only validated against bulk parameters, the future validation and calibration of WIS estimates from a compound variable such as wave power may improve the WIS validation process, providing better WIS estimates. However, as wave power defined by Resio (2003) is linearly dependent on wave period and the square of the significant wave height, it seems as though the problem of isolating what is the cause of the magnitude differences would be complicated by the interplay between height and period, and not singularly on a height error or period error alone.

Delving deeper into the improvement of these WIS estimates using wave power, future work involves the calculation of wave power from wave spectral data, and not the bulk parameters used within this work. The use of spectral wave data to calculate wave power will allow for the interpolation of the presently miss-matched frequency ranges between the observational and model non-directional spectral data. Although this spectral wave power calculation methodology is not expected to reduce the full scale of the current WIS versus NDBC buoy wave power magnitudes, it should provide quantitative offsets to allow for an implementation of a bias correction to WIS wave power estimates.

Additionally, the use of wave power algorithms (Liakatas et al., 2017) that require the full spectrum of wave data introduces directionality into the wave power estimates, showcasing how much wave power is directed towards the shore and how much is lost out to sea. Therefore, with a sufficient number of moored buoy wave power data points, WIS wave power estimates may be re-scaled to accurately estimate wave power trends at each grid point, providing a full picture of the wave power resource within a region. These techniques should also be applied to test other wave model technologies.

Of note is that these analyses specifically used deep water sites to negate tidal or shoaling effects of waves. Therefore, it would be useful to broaden this study using more coastal sites, knowing that depth-dependent mechanisms and local conditions (i.e. bathymetry) will have a dramatic effect on the results. Future work should investigate the effect of coastal bathymetry and other causes on the variation of wave power trends, before

applying the deep-water wave predictions to the near-shore wave power trend predictions that are so pertinent to localised coastal resilience works.

Within the coastal engineering realm, the Kamphius (1991) equation for the transport rate of underwater mass (longshore sediment transport) incorporates wave height, peak wave period parameters (essentially wave power), and the wave angle at breaking. With a 10% uncertainty in wave height and period, the longshore sediment transport uncertainty would be ~39%, not including the uncertainty in the wave direction. Therefore accurate wave height, period and wave power estimates are essential for coastal engineering and development, as any uncertainty errors impact coastal resilience mitigations methods exponentially.

Additionally, this work provides a baseline for understanding extremal analyses of wave power, which estimates 50 and 100 year wave events. However, these extremal analyses are based on maximum wave power values, not direction and duration of wave power events. Therefore calculating directional wave power from spectral wave energy may quantify uncertainties within presumed structure stabilities and sediment transportation.

Finally, this work provides the framework for future investigations into the connection of the global climate changes and near-shore wave power trend within and outside US coastal waters. Therefore, the methodologies and analyses showcased within this dissertation are not wave power specific, and can be applied to any long term observational variable around the globe.

## 5.6 Executive Summary

Overall, this study showcases a complete and systematic approach to conducting a wave power climate study with the use of both long-term modelled and observational wave data in connection with data quality assurance practices. This work showcases intercomparisons between multiple wave collection platforms, allowing for the continued

use of NDBC wave data regardless of deployed instrumentation. Additionally, this work offers a viable methodology for removing known discontinuities within the NDBC data to provide a continuous, consistent time series of historical data.

This ability to construct a continuous, historical time series of observational data provides a solid methodology for the use of observations in prediction studies, including wave power trends. This work has provided independent point source wave power estimates and trends for multiple sites within the U.S. zone of responsibility. It has identified offsets in magnitude between observational and WIS wave power estimates, and provided a wave power baseline for future work to re-scale WIS datasets. Finally, future work that calculates directional wave power estimates from observational spectral wave data, will allow for the determination of incidental wave power striking the coast, which is critical for coastal construction and resilience.

Although these platform intercomparisons, consistent datasets, observational and model wave power trends are U.S. specific, the methodologies developed within this work are applicable to observational datasets in any region. The limiting factors to any continuous, historical time series of observational data are only the period of record themselves. Therefore, a continuous and sufficient spatial, temporal and fiscal investment in ocean observational measurement systems and agencies is critical for the continued support of climate and ocean studies – essential information for future resilient coastlines.

# References


Alliance for Coastal Technologies (ACT). 2007. ACT Wave Sensor Technologies. Proceedings of a Workshop held by the Alliance for Coastal Technologies, March 7-9, 2007, St. Petersburg, FL. Available: https://www.act-us.info/Download/Workshops/2007/USF_NDBC_Wave/act_wr07-03_wave_sensor.pdf [2021, January 31]

Alliance for Coastal Technologies (ACT). 2012. Waves Measurement Systems Test and Evaluation Protocols in Support of the National Operational Wave Observation Plan. Proceedings of a Workshop held by the Alliance for Coastal Technologies, February 22-24, 2011, St. Petersburg, FL. Available: http://www.act-us.info/Download/Workshops/2012/USFUM_Wave_Measurement [2021, January 31]

Allan, J.C. & Komar, P.D. 2000. Spatial and temporal variations in the wave climate of the North Pacific. *EOS.* 81(47).

Allan, J.C. & Komar, P.D. 2006. Climate controls on U.S. West Coast erosion processes. *Journal of Coastal Research*. 22 (3):511–529. https://doi.org/10.2112/03-0108.1

Ahn, S. & Neary, V.S. 2020. Non-stationary historical trends in wave energy climate for coastal waters of the United States. *Ocean Engineering*. 216(108044). https://doi.org/10.1016/j.oceaneng.2020.108044

American Meteorological Society (AMS). 2021. *Glossary of Meteorology: wave celerity*. Available: https://glossary.ametsoc.org/wiki/Wave_celerity [2021, January 31].

Appendini, C.M., Hernández-Lasheras, J., Meza-Padilla, R. & Kurczyn, J.A. 2018. Effect of climate change on wind waves generated by anticyclonic cold front intrusions in the Gulf of Mexico. *Climate Dynamics*. 51:3747–3763. https://doi.org/10.1007/s00382-018-4108-4

Ardhuin, F., Collard, F. & Chapron, B. 2004. Wave Spectra From ENVISAT's Synthetic Aperture Radar In Coastal Areas, *International Society of Offshore and Polar Engineers*. https://www.onepetro.org/conference-paper/ISOPE-I-04-319

Ardhuin, F., Brandt, P., Gaultier, L., Donlon, C., Battaglia, A., Boy, F., Casal, T., Chapron, B., Collard, F., Cravatte, S., Delouis, J-M., De Witte, E., Dibarboure, G., Engen, G., Johnsen, H., Lique, C., Lopez-Dekker, P., Maes, C., Martin, A., Marié, L., Menemenlis, D., Nouguier, F., Peureux, C., Rampal, P., Ressler, G., Rio, M-H., Rommen, B., Shutler, J.D., Suess, M., Tsamados, M., Ubelmann, C., van Sebille, E., van den Oever, M & Stammer, D. 2019a. SKIM, a Candidate Satellite Mission Exploring Global Ocean Currents and Waves. *Frontiers in Marine Science*. 6 (209):1-8. https://doi.org/10.3389/fmars.2019.00209

Ardhuin, F., Stopa, J.E., Chapron, B., Collard, F., Husson, R., Jensen, R.E., Johannessen, J., Mouche, A., Passaro, M., Quartly, G.D., Swail, V. & Young, I. 2019b. Observing Sea States. *Frontiers in Marine Science.* 6. https://doi.org/10.3389/fmars.2019.00124

Arinaga, R. & Cheung, K. 2012. Atlas of global wave energy from 10 years of reanalysis and hindcast data. *Renew Energy*. 39:49–64. http://dx.doi.org/10.1016/j.renene.2011.06.039

Babanin, A.V, Rogers, W.E., de Camargo, R., Doble, M., Durrant, T., Filchuk, K., Ewans, K., Hemer, M., Tim Janssen,T., Kelly-Gerreyn, B., Machutchon, K., McComb, P., Qiao, F., Schulz, E., Skvortsov, A., Thomson, J., Vichi, M., Violante-Carvalho, N., Wang, D., Waseda, T., Williams, G. & Young, I.R. 2019. Waves and Swells in High Wind and Extreme Fetches, Measurements in the Southern Ocean. *Frontiers in Marine Science*. 6(361). http://dx.doi.org/10.3389/fmars.2019.00361

Bacon, S., & Carter, D.J.T. 1991. Wave climate changes in the North Atlantic and North Sea. *International Journal of Climatology*. 77:545-558. https://doi.org/10.1002/joc.3370110507

Bender, L.C., Guinasso, N.L., Walpert, J.N. & Howden, S.D. 2010. A Comparison of Methods for Determining Significant Wave Heights – Applied to a 3 m Discus Buoy during Hurricane Katrina. *Journal of Atmospheric and Oceanic Technology*. 27(6):1012-1028. https://doi.org/10.1175/2010JTECHO724.1

Bertin, X., Prouteau, E. & Letetrel, C. 2013. A significant increase in wave height in the North Atlantic Ocean over the 20th century. *Global and Planetary Change*. 106:77–83. http://dx.doi.org/10.1016/j.gloplacha.2013.03.009

Bouchard, R.H., Jensen, R.E. & Riley, R.E. 2016. Project FLOSSIE: Marine Data Stewardship at the Waterline. *Conference: AGU Ocean Sciences 2016,* New Orleans, LA, USA.

Bouchard, R.H., Riley, R.R., LeBlanc, L.A., Vasquez, M., Robbie, M., Jensen, R.E., Bryant, M.A. & Fiorentino, L.A. 2017. Field Evaluation of the Wave Module for NDBC's New Self-Contained Ocean Observing Payload (SCOOP) on Modified NDBC Hulls. *1st International Workshop on Waves, Storm Surges, and Coastal Hazards, Liverpool, UK*.

Bouchard, R.H., Jensen, R.E., Montalvo, S., & Kamranzad, B. 2018. Finding NOMAD: An Examination of the Impacts of Changing Wave Systems on Long term Wave Measurements, *Proceedings of the American Geophysical Union Ocean Sciences Meeting 2018, Portland, OR, USA*. https://www.researchgate.net/publication/322765014_Finding_NOMAD_An_Examination_of_the_Impacts_of_Changing_Wave_Systems_on_Long-term_Wave_Measurements

Bouchard, R.H. & Jensen, R.E. 2019. Further Study on the Accuracy of NDBC Wave Measurements and Their Possible Impact on Wave Climate Trends. *Presentation for the 2nd International Workshop on Waves, Storm Surges, and Coastal Hazards*, 11 November 2019, Melbourne, Victoria, Australia

Brüning, C., Hasselmann, S., Hasselmann, K. & Lenhner, S. 1994. First evaluation of ERS-1 synthetic aperture radar wave mode data. *Global Atmosphere and Ocean Systems*. 2:61-98.

Bryant, M.A. & Jensen, R.E. 2017. Application of the nearshore wave model STWAVE to the North Atlantic coast comprehensive study. *Journal of Waterway, Port, Coastal, and Ocean Engineering*. 143(5): 04017026. https://doi.org/10.1061/(ASCE)WW.1943-5460.0000412

Carter, D. J.T. & Draper, L. 1988. Has the northeast Atlantic become rougher? *Nature*. 332:494. https://doi.org/10.1038/332494a0

Cavaleri, L., Abdalla, S., Benetazzo, A., Bertotti, L., Bidlot, J., Breivik, O., Carniel, S., Jensen, R.E., Portilla-Yandun, J., Rogers, W.E., Roland, A., Sanchez-Arcilla, A., Smith, J., Staneva, J., Toledo, Y., van Vledder, G., van der Westhuysen, A.J. 2018. Wave modelling in coastal and inner seas. *Progress in Oceanography*. 167:164-233.

Chapron, B., Johnsen, H. & Garello, R. 2001. Wave and wind retrieval from SAR images of the ocean. *Annales Des Télécommunications*. 56:682–699. https://doi.org/10.1007/BF02995562

Cialone, M.A., Massey, T.C., Anderson, M.E., Grzegorzewski, A.S., Jensen, R.E., Cialone, A., Mark, D.J., Pevey, K.C., Gunkel, B.L., McAlpin, T.O., Nadal-Caraballo, N.C., Melby, J.A., Ratcliff, J.J. 2015. North Atlantic Coast Comprehensive Study (NACCS) Coastal Storm Model Simulations: Waves and Water Levels. *ERDC/CHL TR-15-14. Vicksburg, MS: U.S. Army Engineer Research and Development Center* https://apps.dtic.mil/sti/citations/ADA621343

Cleveland, W.S. 1979. Robust Locally Weighted Regression and Smoothing Scatterplots. *Journal of the American Statistical Association*. 74:829-836.

Cleveland, R.B., Cleveland, W.S., McRae, J.E., Terpenning, I.J. 1990. STL: A seasonal-trend decomposition procedure based on loess. *Journal of Official Statistics*. 6(1): 3–33. http://bit.ly/stl1990

Comola, F., Lykke Andersen, T., Martinelli, L., Burcharth, H.F. & Ruol, P. 2014. Damage pattern and damage progression on breakwater roundheads under multidirectional waves. *Coastal Engineering*. 83:24-35. https://doi.org/10.1016/j.coastaleng.2013.09.004

Conathan, M., Buchanan, J. & Polefka, S. 2014. The Economic Case for Restoring Coastal Ecosystems. *Center for American Progress and Oxfam America*, Washington, D.C.

Cooley, J.W. & Tukey, J.W. 1965. An Algorithm for the Machine Calculation of Complex Fourier Series. *Mathematics of Computation*. 19(90):297–301. www.jstor.org/stable/2003354

Copernicus. 2017. *News and Events: New Satellite Wave Product*. Copernicus Marine Service. Available: https://marine.copernicus.eu/new-satellite-based-wave-product-released/ [2020, June 26].

Cornett, A.M. 2008. A global wave energy resource assessment. *Proceedings of The Eighteenth International Offshore and Polar Engineering Conference, Vancouver, Canada, July 2008*. ISOPE-I-08-370:1–9.

Crout, R.L., Hervey, R.V. & Bouchard, R.H. 2008. Operational field test and evaluation of NDBC's compact ocean observing system, configured for ocean wave, meteorological, and ocean current profiling measurements. *Proceedings of the 12th Conference on IOAS-AOLS, AMS*. https://ams.confex.com/ams/88Annual/techprogram/paper_135170.htm

Currin C.A., Chappell W.S. & Deaton, A. 2010. Developing alternative shoreline armoring strategies: The living shoreline approach in North Carolina. Puget Sound Shorelines and the Impacts of Armoring. *Proceedings of a State of the Science Workshop, May 2009. Shipman, H., Dethier, M.N., Gelfenbaum, G., Fresh, K.L., Dinicola, R.S.,* Eds. *US Geological Survey, Reston, VA*. 91-102. https://pubs.usgs.gov/sir/2010/5254/pdf/sir20105254_chap10.pdf

Dahl, T.E. & Stedman, S.M. 2013. Status and trends of wetlands in the coastal watersheds of the Conterminous United States 2004 to 2009. *U.S. Department of the Interior, Fish and Wildlife Service, and NOAA National Marine Fisheries Service*.

Data Buoy Cooperation Panel (DBCP). 2019. *DBCP Task Team on Wave Measurement (TT-WM)*. Joint Technical Commission for Oceanography and Marine Meteorology. Available: http://www.jcomm.info/WET [2020, July 01]

Data Buoy Cooperation Panel (DBCP). 2020. *DBCP Task Team on Wave Measurement (TT-WM): Terms of Reference for Task Team on Wave Measurement*. Joint Technical Commission for Oceanography and Marine Meteorology. Available: https://www.jcomm.info/index.php?option=com_oe&task=viewGroupRecord&groupID=420 [2020, July 01]

Datawell BV. 2020. Datawell BV Buoy Products. Available: https://www.datawell.nl/Products/Buoys.aspx [2020, June 26].

Davies, J.L. 1980. *Geographical Variation in Coastal Development*. 2nd edition, London: Longman.

Davies, J.L. 1982. *Wave environments*. Beaches and Coastal Geology. Encyclopedia of Earth Sciences Series. Springer, New York, NY. https://doi.org/10.1007/0-387-30843-1_491

De Livera, A.M., Hyndman, R.J., Snyder, R.D. 2011. Forecasting Time Series With Complex Seasonal Patterns Using Exponential Smoothing. *Journal of the American Statistical Association*. 106(496). https://doi.org/10.1198/jasa.2011.tm09771

Dean, R. & Dalrymple, R. 1991. Water wave mechanics for engineers and scientists. *Advanced series on ocean engineering. World Scientific, Singapore*. ISBN 9810204205.

Dee, D.P., Uppala, S.M., Simmons, A.J., Berrisford, P., Poli, P., Kobayashi, S., Andrae, U., Balmaseda, M.A., Balsamo, G., Bauer, P., Bechtold, P., Beljaars, A.C.M., van de Berg, L., Bidlot, J., Bormann, N., Delsol, C., Dragani, R., Fuentes, M., Geer, A.J., Haimberger, L., Healy, S.B., Hersbach, H., Hólm, E.V., Isaksen, L., Kållberg, P., Köhler, M., Matricardi, M., McNally, A.P., Monge-Sanz, B.M., Morcrette, J.-J., Park, B.-K., Peubey, C., de Rosnay, P., Tavolato, C., Thépaut, J. -N. & Vitart, F. 2011. The ERA-Interim reanalysis: configuration and performance of the data assimilation system. *Quarterly Journal of the Royal Meteorological Society.* 137(656):553-597. https://doi.org/10.1002/qj.828

Delft University of Technology. 2020. SWAN: *User Manual SWAN Cycle III version 41.31A*. Available: http://www.swan.tudelft.nl/ [2020, June 26].

Dobrynin, M., Murawksy, J. & Yang, S. 2012. Evolution of the global wind wave climate in CMIP5 experiments. *Geophysical Research Letters*. 39(L18606). https://doi.org/10.1029/2012GL052843

Earle, M.D. & Bishop, J.M. 1984. *A Practical Guide to Ocean Wave Measurement and Analysis*. Endeco Inc., Marion, MA.

Earle, M.D., Steele, K.E. & Hsu, Y.L. 1984. Wave Spectra Corrections for Measurements of Hull-Fixed Accelerometers. *OCEANS 1984*: 725-730. https://doi.org/10.1109/OCEANS.1984.1152234

Earle, M.D., Steele, K.E. & Wang, D.W.C. 1999. Use of advanced directional wave spectra analysis methods. *Ocean Engineering*. 26:1421-1434, https://doi.org/10.1016/S0029-8018(99)00010-4

Ellingson, S.W. 2020. 6.1: Phase and Group Velocity. *Virginia Polytechnic & State University, Virginia Tech Libraries' Open Education Initiative*. Available: https://phys.libretexts.org/Bookshelves/Electricity_and_Magnetism/Book%3A_Electromagnetics_II_(Ellingson)/06%3A_Waveguides/6.01%3A_Phase_and_Group_Velocity [2021, February 22]

Emanuel, K.A. 2005. Increasing destructiveness of tropical cyclones over the past 30 years. *Nature.* 456:686-688. https://www.nature.com/articles/nature03906

Emanuel, K. 2013. Downscaling CMIP5 climate models shows increased tropical cyclone activity over the 21st century. *PNAS* .110(30):12219-12224. https://doi.org/10.1073/pnas.1301293110

Eslinger, D. 2014. Hurricane Tracks: Past + Present = Future? *International Best Track Archive for Climate Stewardship (IBTrACS), NOAA Digital Coast GeoZone*, U.S. National Oceanic and Atmospheric Administration. Available: https://geozoneblog.wordpress.com/2014/05/23/hurricane-tracks-past-present-future/ [2021, March 13].

European Centre for Medium-Range Weather Forecasts (ECMWF). 2012. *Ocean waves at ECMWF*. Available: https://www.ecmwf.int/sites/default/files/elibrary/2012/14556-ocean-waves-ecmwf.pdf [2020, June 26].

European Centre for Medium-Range Weather Forecasts (ECMWF). 2020. *Ocean Wave Model – ECWAM*. Available: https://confluence.ecmwf.int/display/FUG/2.2+Ocean+Wave+Model+-+ECWAM [2020, June 26].

Extremes of Weather: Horrifying hurricanes. 2004. *The Canadian Atlas*. 14 March. Available: http://www.canadiangeographic.com/atlas/themes.aspx?id=weather&sub=weather_phenomena_hurricanes&lang=En [2021, March 14]

Fagherazzi, S. 2014. Coastal processes: Storm-proofing with marshes. *Nature Geoscience*. 7:701–702. https://doi.org/10.1038/ngeo2262

Fitzpatrick, R. 2016. Gravity Waves in Deep Water. *Online Teaching: Professor of Physics. The University of Texas at Austin*. Available: https://farside.ph.utexas.edu/teaching/336L/Fluidhtml/node148.html [2020, July 01].

Forte, M.F., Hanson, J.L., Hagerman, G. 2012. North Atlantic wind and wave climate: Observed extremes, hindcast performance, and extratropical recurrence intervals. *Oceans 2012*:1-10. https://doi.org/10.1109/OCEANS.2012.6404822

Friedman, J.H. 1984a. SMART User's Guide. Laboratory for Computational Statistics, *Stanford University Technical Report No.1*. https://apps.dtic.mil/sti/citations/ADA148262

Friedman, J.H. 1984b. A variable span scatterplot smoother. Laboratory for Computational Statistics, *Stanford University Technical Report No.5*. http://www.slac.stanford.edu/cgi-wrap/getdoc/slac-pub-3477.pdf

Furuichi, N., Hibiya, T., Niwa, Y. 2008. Model-predicted distribution of wind-induced internal wave energy in the world's oceans. *Journal of Geophysical Research*. 113(C09034). https://doi.org/10.1029/2008JC004768

Gemmrich, J., Thomas, B. & Bouchard, R. 2011. Observational changes and trends in northeast Pacific wave records. *Geophysical Research Letters*. 38(L22601). https://doi.org/10.1029/2011GL049518

Gravens, M.B. & Sanderson, D.R. 2018. Identification and Selection of Representative Storm Events from a Probabilistic Storm Data Base. ERDC/CHL CHETN-VIII-9. *U.S. Army Engineer Research and Development Center*, Vicksburg, MS. http://dx.doi.org/10.21079/11681/26341

Gulev, S.K. & Hasse, L. 1999. Changes of wind waves in the North Atlantic over the last 30 years. *International Journal of Climatology*. 19:1091-1117.

Gulev, S.K. & Grigorieva, V. 2004. Last century changes in ocean wind wave height from global visual wave data. *Geophysical Research Letters*. 31(L24302). http://dx.doi.org/10.1029/2004GL021040

Gulev, S.K. & Grigorieva, V. 2006. Variability of the Winter Wind Waves and Swell in the North Atlantic and North Pacific as Revealed by the Voluntary Observing Ship Data. *Journal of Climate*. 19(21):5667-5685. https://doi.org/10.1175/JCLI3936.1

Gunn, K. & Stock-Williams, C. 2012. Quantifying the global wave power resource. *Renew Energy*. 44:296–304.

Hall, C., Bouchard, R., Riley, R., Stewart, R., Wang, D. & DiNapoli, S. 2018a. Emerging National Data Buoy Center (NDBC) Wave Systems, *Conference: JCOMM DBCP-34 Meeting, Cape Town, South Africa*. https://www.researchgate.net/publication/328748840_Emerging_National_Data_Buoy_Center_NDBC_Wave_Systems

Hall, C., Bouchard, R.H. & Petraitis, D.C. 2018b. Wave module field evaluations between the NDBC's SCOOP on modified 3-m foam hulls and nearby operational systems. *Conference: OCEANS '18 MTS/IEEE* Charleston, SC. https://doi.org/10.1109/OCEANS.2018.8604855

Hall, C. & Jensen, R. 2021. Utilizing Data from the NOAA National Data Buoy Center. *ERDC/CHL CHETN-I-100. U.S. Army Corps of Engineers*. Engineering Research and Development Center, Vicksburg, MS. http://dx.doi.org/10.25607/OBP-1087

Hall, C. & Jensen, R.E. 2022a. USACE QCC NDBC Measurement Archive. *U.S. Army Engineer Research and Development Center Coastal and Hydraulics Laboratory (CHL) Knowledge Core Datasets*. http://dx.doi.org/10.21079/11681/43121

Hall, C. & Jensen, R. 2022b. United States Army Corps of Engineers Coastal and Hydraulics Laboratory Quality Controlled, Consistent Measurement Archive. *Scientific Data.* http://dx.doi.org/10.1038/s41597-022-01344-z

Hall, C., Jensen, R.E., & Wang, D.W. 2022a. Wave Power Trends along the U.S. Coastline: In situ Measurements and Model Hindcasts Estimates. *Ocean Dynamics*. https://doi.org/10.1007/s10236-022-01515-x

Hall, C., Jensen, R.E. & Wang, D.W. 2022b. Performance evaluation of the newly operational NDBC 2.1-m hull. *Journal of Atmospheric and Oceanic Technology*. https://doi.org/10.1175/JTECH-D-21-0172.1

Hanson, J.L., Tracy, B.A., Tolman, H.L. & Scott, R.D. 2009. Pacific hindcast performance of three numerical wave models. *Journal of Atmospheric and Oceanic Technology*. 26(8):1614-1633. https://doi.org/10.1175/2009JTECHO650.1

Harley, M.D., Turner, I.L., Kinsela, M.A., Middleton, J.H., Mumford, P.J., Splinter, K.D., Phillips, M.S., Simmons, J.A., Hanslow, D.J. & Short, A.D. 2017. Extreme coastal erosion enhanced by anomalous extratropical storm wave direction. *Scientific Reports*. 7(6033). https://doi.org/10.1038/s41598-017-05792-1

Hauser, D., Tison, C., Amiot, T., Delaye, L., Corcoral, N. & Castillan, P. 2017. SWIM: The First Spaceborne Wave Scatterometer. *IEEE Transactions on Geoscience and Remote Sensing*. 55(5):3000-3014. https://doi.org/10.1109/TGRS.2017.2658672

Hemer, M.A., Church, J.A. & Hunter, J.R. 2010. Variability and trends in the directional wave climate of the Southern Hemisphere. *International Journal of Climatology*. 30:475–491. https://doi.org/10.1002/joc.1900

Hristov, T.S., Miller, S.D. & Friehe, C.A. 2003. Dynamical coupling of wind and ocean waves through wave-induced air flow. *Nature: Letters to Nature*. 422:55-58.

Huppert, K.L., Perron, J.T., Ashton, A.D. 2020. The influence of wave power on bedrock sea-cliff erosion in the Hawaiian Islands. *Geology*. 48(5):499-503. https://doi.org/10.1130/G47113.1

Hubertz, J.M., Driver, D.B. & Reinhard, R.D. 1991. Wind Waves on the Great Lakes: A 32 Year Hindcast. *Journal of Coastal Research*. 7(4):945–967. https://www.jstor.org/stable/4297914

Hyndman, R.J. & Athanasopoulos, G. 2018. *Forecasting: principles and practice*. 2nd edition, OTexts: Melbourne, Australia. Available: https://otexts.com/fpp2/ [2022, January 06].

Hyndman, R., Athanasopoulos, G., Bergmeir, C., Caceres, G., Chhay, L., O'Hara-Wild, M., Petropoulos, F., Razbash, S., Wang, E. & Yasmeen, F. 2021. forecast: Forecasting functions for time series and linear models. *R package version 8.15*. https://pkg.robjhyndman.com/forecast/

Intergovernmental Oceanographic Commission (IOC). 2010. *PP-WET Steering Committee meeting*. Available: http://ioc-unesco.org/index.php?option=com_oe&task=viewEventRecord&eventID=445 [2020, July 01].

Integrated Ocean Observing System (IOOS). 2020a. *About Us*. Available: https://ioos.noaa.gov/about/about-us/ [2020, July 01].

Integrated Ocean Observing System (IOOS). 2020b. *Wave Observation (IOOS): The National Operational Wave Observation Plan*. Available: https://ioos.noaa.gov/ioos-in-action/waves/ [2020, July 01].

Integrated Ocean Observing System (IOOS). 2020c. *Manual for Real-Time Quality Control of In-Situ Surface Wave Data*. Available: https://ioos.noaa.gov/ioos-in-action/wave-data/ [2020, July 01].

Intergovernmental Panel on Climate Change (IPCC). 2014. *AR5 Climate Change 2014: Impacts, Adaptation, and Vulnerability*. Available: https://www.ipcc.ch/report/ar5/wg2/ [2020, June 26].

Intergovernmental Panel on Climate Change (IPCC). 2022: *Climate Change 2022: Impacts, Adaptation, and Vulnerability*. Contribution of Working Group II to the Sixth Assessment Report of the Intergovernmental Panel on Climate Change [H.-O. Pörtner, D.C. Roberts, M. Tignor, E.S. Poloczanska, K. Mintenbeck, A. Alegría, M. Craig, S. Langsdorf, S. Löschke, V. Möller, A. Okem, B. Rama (eds.)]. Cambridge University Press (in press). Available: https://www.ipcc.ch/report/sixth-assessment-report-working-group-ii/ [2022, April 04].

International Comprehensive Ocean-Atmosphere Data Set (ICOADS). 2019. International Comprehensive Ocean-Atmosphere Data Set. Available: https://icoads.noaa.gov/ [2020, June 26].

Jabbari, A., Ackerman, J.D., Boegman, L. & Zhao, Y. 2021. Increases in Great Lake winds and extreme events facilitate interbasin coupling and reduce water quality in Lake Erie. *Scientific Reports*. 11:5733 https://doi.org/10.1038/s41598-021-84961-9

Jensen, R.E., Swail, V., Lee, B. & O'Reilly, W.A. 2011. Wave measurement evaluation and testing. *12th International Workshop on Wave Hindcasting and Forecasting & 3rd Coastal Hazard Symposium*, Kohala Coast, Hawaii.

Jensen, R.E., Cialone, M.A., Chapman, R.S., Ebersole, B.A., Anderson, M. & Thomas, L. 2012. *Lake Michigan storm: Wave and water level modeling*. Report: ERDC/CHL TR-12-26, U.S. Army Engineer Research and Development Center, Vicksburg, MS.

Jensen, R.E, Swail, V.R., Bouchard, R.H., Riley, R.E., Hesser, T.J., Blaseckie, M. & MacIsaac, C. 2015. Field Laboratory for Ocean Sea State Investigation and Experimentation: FLOSSIE. *14th International Workshop on Wave Hindcasting and Forecasting & 3rd Coastal Hazard Symposium*, Key West, Florida.

Jensen, R.E., Cialone, A., Smith, J.M., Bryant, M.A. & Hesser, T.J. 2017. Regional Wave Modeling and Evaluation for the North Atlantic Coast Comprehensive Study. *Journal of Waterway, Port, Coastal, and Ocean Engineering*. 143(5): B4016001-1. https://doi.org/10.1061/(ASCE)WW.1943-5460.0000342

Jensen, R.E., Swail, V. & Bouchard, R.H. 2021. Quantifying wave measurement differences in historical and present wave buoy systems. *Ocean Dynamics*. 71:731-755. https://doi.org/10.1007/s10236-021-01461-0

Jinsong, Y., Weigen, H., Chenghu, Z. & Qingmei, X. 2004. Wave Height Estimation from SAR Imagery. *Chinese Journal of Oceanology and Limnology*. 22(2):157-161. https://doi.org/10.1007/BF02842587

Jinsong, Y., He, W., Xiaoyan, C., Rong, Z. & Weigen, H. 2008. A new method for significant wave height retrieval from SAR imagery. *Proceedings of the SPIE 7154, Microwave Remote Sensing of the Atmosphere and Environment*. VI(71540C). https://doi.org/10.1117/12.804856

Kamphuis, J.W. 1991. Alongshore sediment transport rate. Journal of Waterways, Port, *Coastal and Ocean Engineering*, ASCE. 117(6):624-641.

Kamranzad, B., Etemad-Shahidi, A. & Chegini, V. 2016. Sustainability of wave energy resources in southern Caspian Sea. *Energy*. 97:549-559

Kaihatu J.M. & Ananthakrishnan, P. 2016. Mechanics of Ocean Waves. *In: Springer Handbook of Ocean Engineering*. Dhanak M.R., Xiros N.I., Eds. Springer Handbooks. Springer, Cham. Online ISBN: 978-3-319-16649-0; Print ISBN: 978-3-319-16648-3

Kelley, D.E. 2018. *The oce Package*. In: Oceanographic Analysis with R. Springer, New York, NY. https://doi.org/10.1007/978-1-4939-8844-0_3

Kelley, D.E., Clark, C. & Layton, C. 2021. *oce: Analysis of Oceanographic Data*. https://cran.r-project.org/web/packages/oce/index.html

Kendall, M. & Stuart, A. 1983. *The Advanced Theory of Statistics*. Griffin. 3:410-414.

Kinsman, B. 1965. *Wind Waves: Their Generation and Propagation on the Ocean Surface*. Prentice-Hall, Englewood Cliffs, N.J. ISBN-10: 0139603441

Knabb, R.D., Rhome, J.R. & Brown, D.P. 2005. *Tropical Cyclone Report Hurricane Katrina*. U.S. National Oceanic and Atmospheric Administration, National Hurricane Center, National Data Buoy Center. https://www.nhc.noaa.gov/data/tcr/AL122005_Katrina.pdf

Koch, S.E., DesJardins, M. & Kocin, P.J. 1983. An interactive Barnes objective map analysis scheme for use with satellite and conventional data. *Journal of Applied Meteorology and Climatology*. 22:1487-1503. https://doi.org/10.1175/1520-0450(1983)022%3C1487:AIBOMA%3E2.0.CO;2

Kohler, C., LeBlanc, L. & Elliott, J. 2015. SCOOP – NDBC's New Ocean Observing System. *OCEANS 2015 - MTS/IEEE Washington*, 2015. 1-5. https://doi.org/10.23919/OCEANS.2015.7401834

Komar, P.D. & Allan, J.C. 2007. Higher Waves Along U.S. East Coast Linked to Hurricanes. *EOS*. 88(30):301–308. https://doi.org/10.1029/2007EO300001

Komen, G.K., Cavaleri, L., Donelan, M., Hasselmann, K., Hasselmann, S. & Janssen, P.A.E.M. 1994. *Dynamics and modelling of ocean waves*. Cambridge University Press. ISBN: 0 521 43291.

Kuik, A.J., van Vledder, G.Ph. & Holthuijsen, L.H. 1988. A Method for the Routine Analysis of Pitch-and-Roll Buoy Wave Data. *Journal of Physical Oceanography*. 18(7):1020-1034. https://doi.org/10.1175/1520-0485(1988)018%3C1020:AMFTRA%3E2.0.CO;2

Kushnir,Y., Cardone, V.J., Greenwood, J.G. & Cane, M.A. 1997. The recent increase in North Atlantic wave heights. *Journal of Climate*. 10(8):2107-2113. https://doi.org/10.1175/1520-0442(1997)010%3C2107:TRIINA%3E2.0.CO;2

Lang, N. 1987. The Empirical Determination of a Noise Function for NDBC Buoys with Strapped-Down Accelerometers. *OCEANS '87*, Halifax, NS, Canada, 1987. 225-228. https://doi.org/10.1109/OCEANS.1987.1160904

Leonardi, N., Ganju, N.K. & Fagherazzi, S. 2015. A linear relationship between wave power and erosion determines salt-marsh resilience to violent storms and hurricanes. *PNAS*. 113(1):64-68. https://doi.org/10.1073/pnas.1510095112

Li N., García-Medina G., Cheung K.F. & Yang Z. 2021. Wave energy resources assessment for the multi-modal sea state of Hawaii. *Renewable Energy*. 174:1036-1055. https://doi.org/10.1016/j.renene.2021.03.116

Liakatas, A., Galanis, G., Kalogeri, C. & Kallos, G. 2017. Wave power estimation by means of spectral wave models and satellite records. *Journal of Operational Oceanography*. 10(1):93-113. http://dx.doi.org/10.1080/1755876X.2017.1289011

Lin, L. & Resio, D. 2001. Improving wave hindcast information for the Great Lakes. *Ocean Wave Measurement and Analysis*. Edge, B.L. & Hemsley, J.M., Eds. ASCE. 650–660. https://ascelibrary.org/doi/pdf/10.1061/40604%28273%2967

Livermont, E.A., Miller, J.K. & Herrington, T.O. 2015. Trends and Changes in the NDBC Wave Records of the U.S. East Coast. *Proceedings of the 14th International Workshop on Wave Hindcasting and Forecasting & 5th Coastal Hazard Symposium*, FL, USA. http://waveworkshop.org/14thWaves/Presentations/B2_WAVES-Livermont%202015-%20In%20Situ-%2016-9.pdf

Livermont, E.A., Miller, J.K. & Herrington, T.O. 2017. Correcting for Changes in the NDBC Wave Records of the United States. *Proceedings of the 1st International Workshop on Waves, Storm Surges, and Coastal Hazards*, Liverpool, UK. http://waveworkshop.org/15thWaves/Presentations/A3.pdf

Longuet-Higgins, M.S., Cartwright, D.E. & Smith, N.D. 1963. Observations of the directional spectrum of sea waves using the motions of a floating buoy. *Ocean Wave Spectra*. Prentice-Hall, Englewood Cliffs, NJ.

Losada, I.J., Reguero, B.G., Méndez, F.J., Castanedo, S., Abascal, A.J. & Mínguez, R. 2013. Long-term changes in sea-level components in Latin America and the Caribbean. *Global and Planetary Change*. 104:34–50. http://dx.doi.org/10.1016/j.gloplacha.2013.02.006

Luther, M.E., Meadows, M., Buckley, E., Gilbert, S.A., Purcell, H. & Tamburri, M.N. 2013. Verification of Wave Measurement Systems. *Marine Technology Society Journal*. 47(5):104-116. https://doi.org/10.4031/MTSJ.47.5.11

Maciñeira, E. & Burcharth, H.F. 2008. Spatial damage distribution over cube armoured roundheads. *Proceedings of the 31st International Conference on Coastal Engineering*, Hamburg, Germany. 3449–3460. https://doi.org/10.1142/9789814277426_0286

Mackay, E.B.L. 2012. Resource Assessment for Wave Energy. *Comprehensive Renewable Energy*. 8:11–77 [Ch. 8.03] Oxford: Elsevier.

Magnusson, A.K., Donelan, M.A. & Drennan, W.M. 1999. On estimating extremes in an evolving wave field. *Coastal Engineering*. 36:147-163. https://doi.org/10.1016/S0378-3839(99)00004-6

Magnusson, A.K., Jensen, R. & Swail, V. 2021. Spectral shapes and parameters from three different wave sensors. *Ocean Dynamics*. 71:893-909. https://doi.org/10.1007/s10236-021-01468-7

Mantua, N.J. & Hare, S.R. 2002. The Pacific Decadal Oscillation. *Journal of Oceanography*. 58(1):35-44 https://link.springer.com/article/10.1023/A:1015820616384

Marchand, P. & Gill, D. 2018. *waver: Calculate Fetch and Wave Energy*. R package version 0.2.1. https://github.com/pmarchand1/waver

Masselink, G. & Hughes, M.G. 2003. *Introduction to coastal processes and geomorphology*. Oxford University Press. ISBN 9780340764107, 0340764104.

Massey, T.C., Wamsley, T.V. & Cialone, M.A. 2011. *Coastal Storm Modeling – System Integration*. ASCE 2011: Solutions to Coastal Disasters. https://ascelibrary.org/doi/pdf/10.1061/41185%28417%2910

Massey, T.C. 2019. ERDC'S Coastal Storm Modeling System: South Atlantic Coast Study. *Proceedings of the 2nd International Workshop On Waves, Storm Surges And Coastal Hazards*, Melbourne, Australia. http://waveworkshop.org/16thWaves/Presentations/JJ4%20Massey_CSTORM_Briefing_2019_WavesSurge_Australia.pdf

Maul, G. 1977. The Annual Cycle of the Gulf Loop Current: Part 1: Observations During a One-year Time Series. *Journal of Marine Research*. 35(1):29-47.

Maul, G. 2005. Wave Climate. In *Encyclopedia of Coastal Science. Encyclopedia of Earth Science Series*. Schwartz M.L., Ed. Springer, Dordrecht. https://doi-org.erdclibrary.idm.oclc.org/10.1007/1-4020-3880-1_342

Meadows, G.A., Meadows, L.A., Wood, W.L, Hubertz, J.M. & Perlin, M. 1997. The Relationship between Great Lakes Water Levels, Wave Energies, and Shoreline Damage. *Bulletin of the American Meteorological Society*. 78(4):675–684. https://doi.org/10.1175/1520-0477(1997)078<0675:TRBGLW>2.0.CO;2

Méndez, F.J., Menéndez, M., Luceño, A. & Losada, I.J. 2006. Estimation of the long-term variability of extreme significant wave height using a time-dependent peak over threshold (POT) model. *Journal of Geophysical Research*. 111(C07024). https://doi.org/10.1029/2005JC003344

Menéndez, M., Méndez, F.J., Losada, I. & Graham, N.E. 2008. Variability of extreme wave heights in the northeast Pacific Ocean based on buoy measurements. *Geophysical Research Letters*. 35(L22607). https://doi.org/10.1029/2008GL035394

Mentaschi, L., Vousdoukas, M.I., Voukouvalas, E., Dosio, A. & Feyen, L. 2017. Global changes of extreme coastal wave energy fluxes triggered by intensified teleconnection patterns. *Geophysical Research Letters*. 44:2416-2426. https://doi.org/10.1002/2016GL072488

Moebs, W., Ling, S.J. & Sanny, J. 2016. *Energy and Power of a Wave*. University Physics. Vol 1. Rice University, OpenStax. Available: https://openstax.org/books/university-physics-volume-1/pages/16-4-energy-and-power-of-a-wave [2021, February 20].

Moller, I., Kudella, M., Rupprecht, F., Spencer, T., Paul, M., van Wesenbeech, B.K, Wolters, G., Jensen, K., Bouma, T.J, Miranda-Lange, M. & Schimmels, S. 2014. Wave attenuation over coastal salt marshes under storm surge conditions. *Nature Geoscience*. 7:727-731. https://doi.org/10.1038/ngeo2251

Moghim, M.N. & Alizadeh, F. 2014. Hydraulic stability of reshaping berm breakwaters using the wave momentum flux parameter. *Coastal Engineering*. 83:56-64. http://dx.doi.org/10.1016/j.coastaleng.2013.10.008

Morim, J., Hemer, M., Wang, X.L., Cartwright, N., Trenham, C., Semedo, A., Young, I., Bricheno, L., Camus, P., Casas-Prat, M., Erikson, L., Mentaschi, L., Mori, N., Shimura, T., Timmermans, B., Aarnes, O., Breivik, O., Behrens, A., Dobrynin, M., Menendez, M., Staneva, J., Wehner, M., Wolf, J., Kamranzad, B., Webb, A., Stopa, J. & Andutta, F. 2019. Robustness and uncertainties in global multivariate wind-wave climate projections. *Nature Climate Change*. 9:711-718. https://doi.org/10.1038/s41558-019-0542-5

Mork, G., Barstow, S., Kabuth, A. & Teresa Pontes, M. 2010. Assessing the global wave energy potential. *In: ASME. Proceedings of OMAE2010. No. 20473. 29th international conference on ocean, off-shore mechanics and Artic Engineering*.

Mudelsee, M. 2019. Trend analysis of climate time series: A review of methods. *Earth-Science Reviews*. 190:310-322. https://doi.org/10.1016/j.earscirev.2018.12.005

Munk, W.H. 1951. Origin and generation of waves. *Proceedings 1st International Conference on Coastal Engineering*. Long Beach, California. ASCE. 1-4.

NOAA National Center for Environmental Information (NCEI). 2021a. *El Niño/Southern Oscillation (ENSO)*. U.S. National Oceanic and Atmospheric Administration. Available: https://www.ncdc.noaa.gov/teleconnections/enso/ [2021, December 29].

NOAA National Center for Environmental Information (NCEI). 2021b. *Pacific Decadal Oscillation (PDO)*. U.S. National Oceanic and Atmospheric Administration. Available: https://www.ncdc.noaa.gov/teleconnections/pdo/ [2021, December 29].

NOAA National Center for Environmental Information (NCEI). 2021c. *North Atlantic Oscillation (NAO)*. U.S. National Oceanic and Atmospheric Administration. Available: https://www.ncdc.noaa.gov/teleconnections/nao/ [2021, December 29].

NOAA National Centers for Environmental Prediction (NCEP). 2019. *WAVEWATCH III® Model*. Environmental Modeling Center. U.S. National Oceanic and Atmospheric Administration, National Weather Service, National Centers for Environmental Prediction. Available: https://polar.ncep.noaa.gov/waves/wavewatch/ [2020, June 26].

NOAA National Data Buoy Center (NDBC). 1996. Nondirectional and Directional Wave Data Analysis Procedure, *NDBC Technical Document 96-01, U.S. National Oceanic and Atmospheric Administration.* National Weather Service, National Data Buoy Center. https://www.ndbc.noaa.gov/wavemeas.pdf

NOAA National Data Buoy Center (NDBC). 2003. Nondirectional and Directional Wave Data Analysis Procedures. *NDBC Technical Document 03-01, Silver Springs. MD: U.S. National Oceanic and Atmospheric Administration*. National Weather Service, National Data Buoy Center.

NOAA National Data Buoy Center (NDBC). 2009. Handbook of Automated Data Quality Control Checks and Procedures. *NDBC Technical Document 09-02, Silver Springs. MD: U.S. National Oceanic and Atmospheric Administration*. National Weather Service, National Data Buoy Center. https://www.ndbc.noaa.gov/NDBCHandbookofAutomatedDataQualityControl2009.pdf

NOAA National Data Buoy Center (NDBC). 2010. *How are estimates of wind-seas and swell made from NDBC wave data?* U.S. National Oceanic and Atmospheric Administration, National Data Buoy Center. Available: https://www.ndbc.noaa.gov/windsea.shtml [2021, February 06].

NOAA National Data Buoy Center (NDBC). 2016. *At what heights are the sensors located on moored buoys?* U.S. National Oceanic and Atmospheric Administration, National Weather Service, National Data Buoy Center. Available: https://www.ndbc.noaa.gov/bht.shtml [2021, July 21].

NOAA National Data Buoy Center (NDBC). 2017. *What are the sensors' reporting, sampling, and accuracy readings?* U.S. National Oceanic and Atmospheric Administration, National Weather Service, National Data Buoy Center. Available: https://www.ndbc.noaa.gov/rsa.shtml [2020, July 17].

NOAA National Data Buoy Center (NDBC). 2018a. *How are significant wave height, dominant period, average period, and wave steepness calculated?* U.S. National Oceanic and Atmospheric Administration, National Weather Service, National Data Buoy Center. Available: https://www.ndbc.noaa.gov/wavecalc.shtml [2020, July 17].

NOAA National Data Buoy Center (NDBC). 2018b *Description of NDBC wave spectra*. U.S. National Oceanic and Atmospheric Administration, National Weather Service, National Data Buoy Center. Available: https://www.ndbc.noaa.gov/wavespectra.shtml [2022, January 25].

NOAA National Data Buoy Center (NDBC). 2018c. *How Are Spectral Wave Data Derived from Buoy Motion Measurements?* U.S. National Oceanic and Atmospheric Administration, National Weather Service, National Data Buoy Center. Available: https://www.ndbc.noaa.gov/wave.shtml [2020, August 01].

NOAA National Data Buoy Center (NDBC). 2020a. *Glossary of Terms for Detailed Wave Information*. U.S. National Oceanic and Atmospheric Administration, National Weather Service, National Data Buoy Center. Available: https://www.ndbc.noaa.gov/waveobs.shtml [2020, July 07].

NOAA National Data Buoy Center (NDBC). 2020b. *About Us*. U.S. National Oceanic and Atmospheric Administration, National Weather Service, National Data Buoy Center. Available: https://www.ndbc.noaa.gov/ndbc.shtml [2020, June 26].

NOAA National Data Buoy Center (NDBC). 2020c. *Measurement Descriptions and Units*. U.S. National Oceanic and Atmospheric Administration, National Data Buoy Center Available: https://www.ndbc.noaa.gov/measdes.shtml [2020, June 26].

NOAA National Data Buoy Center (NDBC). 2020d. *Moored Buoy Program*. U.S. National Oceanic and Atmospheric Administration, National Weather Service, National Data Buoy Center. Available: https://www.ndbc.noaa.gov/mooredbuoy.shtml [2021, August 08].

NOAA National Data Buoy Center (NDBC). 2022. *National Data Buoy Center website*. U.S. National Oceanic and Atmospheric Administration, National Weather Service, National Data Buoy Center. Available: https://www.ndbc.noaa.gov/ [2022, April 04].

NOAA National Hurricane Center (NHC). 2020. *NHC Marine Product Descriptions*. U.S. National Oceanic and Atmospheric Administration, National Weather Service, National Hurricane Center and Central Pacific Hurricane Center. Available: https://www.nhc.noaa.gov/abouttafbprod.shtml#WINDWAVE [2020, June 26].

NOAA National Hurricane Center (NHC). 2022. *2021 Atlantic Hurricane Season*. U.S. National Oceanic and Atmospheric Administration, National Weather Service, National Hurricane Center. Available: https://www.nhc.noaa.gov/data/tcr/index.php?season=2021&basin=atl [2022, January 30].

National Oceanic and Atmospheric Administration (NOAA). 2020. *Record-breaking Atlantic hurricane season draws to an end.* U.S. National Oceanic and Atmospheric Administration. Available: https://www.noaa.gov/media-release/record-breaking-atlantic-hurricane-season-draws-to-end [2020, November 24].

NOAA National Weather Service Climate Prediction Center (CPC). 2008. Northern Hemisphere Teleconnection Patterns. National Oceanic and Atmospheric Administration, Climate Prediction Center. Available: https://www.cpc.ncep.noaa.gov/data/teledoc/teleintro.shtml [2022, August 17].

NOAA National Weather Service (NWS). 2020. *Weather-Ready Nation: About Us*. U.S. National Oceanic and Atmospheric Administration, National Weather Service. Available: https://www.weather.gov/wrn/about [2020, June 26].

NOAA Physical Sciences Laboratory (PSL). 2021. *Multivariate ENSO Index Version 2 (MEI.v2)*. U.S. National Oceanic and Atmospheric Administration. Available: https://www.psl.noaa.gov/enso/mei [2021, December 29].

O'Reilly, W.C., Herbers, T.H.C., Seymour, R.J. & Guza, R.T. 1996. A Comparison of Directional Buoy and Fixed Platform Measurements of Pacific Swell. *Journal of Atmospheric and Oceanic Technology*. 13:231-238.

Odériz, I., Silva, R., Mortlock, T.R. & Mori, N. 2020. El Niño-Southern Oscillation Impacts on Global Wave Climate and Potential Coastal Hazards. *Journal of Geophysical Research: Oceans*. 125(e2020JC016464). https://doi.org/10.1029/2020JC016464

Oey, L.Y., Ezer, T. & Lee, H.C. 2005. Loop Current, Rings and Related Circulation in the Gulf of Mexico: A Review of Numerical Models and Future Challenges. In: Circulation in the Gulf of Mexico: Observations and Models, Sturges W, Lugo-Fernandez A (Eds.). *Geophysical Monograph Series*. 161:31-56.

Ortiz-Royero, J.C. & Mercado-Irizarry, A. 2008. An intercomparison of SWAN and WAVEWATCH III models with data from NDBC-NOAA buoys at oceanic scales. *Coastal Engineering Journal*. 50(01):47-73 https://doi.org/10.1142/S0578563408001739

Panchang, V., Kwon Jeong, C. & Demirbilek, Z. 2013. Analyses of Extreme Wave Heights in the Gulf of Mexico for Offshore Engineering Applications. ASME. *Journal of Offshore Mechanics and Arctic Engineering*. 135(3), 031104. https://doi.org/10.1115/1.4023205

Pierson, W.J., Neumann, G. & James, R.W. 1955. *Practical methods for observing and forecasting waves by means of wave spectra and statistics*. U.S. Navy Hydrographic Office Pib. 603.

Plant, W.J. & Zurk, L.M. 1997. Dominant wave directions and significant wave heights from synthetic aperture radar imagery of the ocean. *Journal of Geophysical Research*. 102(C2):3473-3482. https://doi.org/10.1029/96JC03674

Pleskachevsky, A., Jacobsen, S., Tings, B. & Schwarz, E. 2019. Estimation of sea state from Sentinel-1 Synthetic aperture radar imagery for maritime situation awareness. *International Journal of Remote Sensing*. 40(11); 4104-4142. https://doi.org/10.1080/01431161.2018.1558377

Pramudya, F.S., Pan, J. & Devlin, A.T. 2019. Estimation of Significant Wave Height of Near-Range Traveling Ocean Waves Using Sentinel-1SAR Images. *IEEE Journal of Selected Topics in Applied Earth Observations and Remote Sensing*. 12(4):1067-1075. https://doi.org/10.1109/JSTARS.2019.2902566

R Core Team. 2021. *R: A language and environment for statistical computing*. R Foundation for Statistical Computing, Vienna, Austria. https://www.R-project.org/.

Rascle, N. & Ardhuin, F. 2013. A global wave parameter database for geophysical applications. Part 2: model validation with improved source term parameterization. *Ocean Model*. 70:174-188.

Reguero, B.G., Menéndez, M., Méndez, F.J., Mínguez, R. & Losada, I.J. 2012. A Global Ocean Wave (GOW) calibrated reanalysis from 1948 onwards. *Coastal Engineering*. 65:38-55. https://doi.org/10.1016/j.coastaleng.2012.03.003

Reguero, B.G., Losada I.J. & Méndez, F.J. 2015. A global wave power resource and its seasonal, interannual and long-term variability. *Applied Energy*. 148:366-380. https://doi.org/10.1016/j.apenergy.2015.03.114

Reguero, B.G., Losada I.J. & Méndez, F.J. 2019. A recent increase in global wave power as a consequence of oceanic warming. *Nature Communications*. 10(205):1-14. https://doi.org/10.1038/s41467-018-08066-0

Reynolds, R.W., Smith, T.M., Liu, C., Chelton, D.B., Casey, K.S. & Schlax, M.G. 2007. Daily high-resolution-blended analyses for sea surface temperature. *Journal of Climate*. 20:5473-5496. https://doi.org/10.1175/2007JCLI1824.1

Resio, D.T., Bratos, S.M. & Thompson, E.F. 2003. Meteorology and Wave Climate, Chapter II-2. *Coastal Engineering Manual*. US Army Corps of Engineers, Washington DC.

Ribal, A. & Young, I.R. 2019. 33 years of globally calibrated wave height and wind speed data based on altimeter observations. *Scientific Data*. 6(77):1-15. https://doi.org/10.1038/s41597-019-0083-9

Riley, R., Teng, C., Bouchard, R., Dinoso, R. & Mettlach, T. 2011. Enhancements to NDBC's Digital Directional Wave Module. *OCEANS '11 MTS/IEEE KONA*, Waikoloa, HI, 2011. 1-10. https://doi.org/10.23919/OCEANS.2011.6107025

Riley, R. & Bouchard, R.H. 2015. An Accuracy Statement for the Buoy Heading Component of NDBC Directional Wave Measurements. *The Twenty-fifth International Ocean and Polar Engineering Conference*, Kona, Hawaii, USA, June 2015. Paper Number: ISOPE-I-15-497.

Riley, R., Hall, C., Stewart, R., DiNapoli, S. & Wang, D.W. 2019. NDBC OWL wave system development, *Conference: 2019 IEEE/OES Twelfth Currents, Waves, Turbulence Measurements and Applications Workshop* (CWTMA). https://doi.org/10.1109/CWTM43797.2019.8955248

Rogers, W.E., Hwang, P.A. & Wang, D.W. 2002. Investigation of Wave Growth and Decay in the SWAN Model: Three Regional-Scale Applications. *Journal of Physical Oceanography*. 33:366-389. https://doi.org/10.1175/1520-0485(2003)033%3C0366:IOWGAD%3E2.0.CO;2

Rogers, W.E. & Wang, D.W.C. 2006. Directional Validation of Wave Predictions. *Journal of Atmospheric and Oceanic Technology*. 24:504-520. https://doi.org/10.1175/JTECH1990.1

Rogers, W.E., Dykes, J.D. & Wittmann, P.A. 2014. US Navy global and regional wave modeling. *Oceanography*. 27(3):56–67. http://dx.doi.org/10.5670/oceanog.2014.68

Rogowski, P., Merrifield, S., Collins, C., Hesser, T., Ho, A., Bucciarelli, R., Behrens, J. & Terrill, E. 2021. Performance Assessments of Hurricane Wave Hindcasts. *Journal of Marine Science and Engineering*. 9(7),690. https://doi.org/10.3390/jmse9070690

Romero, L., Lenain, L. & Melville, W.K. 2017. Observations of Surface Wave–Current Interaction. *Journal of Physical Oceanography*. 47(3):615-632. https://doi.org/10.1175/JPO-D-16-0108.1

RStudio Team. 2021. *RStudio: Integrated Development for R. RStudio, Inc.*, Boston, MA. http://www.rstudio.com/

Ruggiero, P., Komar, P.D. & Allan, J.C. 2010. Increasing wave heights and extreme value projections: The wave climate of the U.S. Pacific Northwest. *Coastal Engineering*. 57(5):539-552. https://doi.org/10.1016/j.coastaleng.2009.12.005

Rusu, L. & Guedes Soares, C. 2012. Wave energy assessments in the Azores islands. *Renewable Energy*. 45:183-196. https://doi.org/10.1016/j.renene.2012.02.027

Sallenger, A.H., Doran, K.S. & Howd, P.A. 2012. Hotspot of accelerated sea-level rise on the Atlantic coast of North America. *Nature Climate Change*. 2:884-888. https://doi.org/10.1038/nclimate1597

Saha, S., Moorthi, S., Pan, H., Wu, X., Wang, J., Nadiga, S., Tripp, P., Kistler, R., Woollen, J., Behringer, D., Liu, H., Stokes, D., Grumbine, R., Gayno, G., Wang, J., Hou, Y., Chuang, H., Juang, H.H., Sela, J., Iredell, M., Treadon, R., Kleist, D., Van Delst, P., Keyser, D., Derber, J., Ek, M., Meng, J., Wei, H., Yang, R,. Lord, S,. van den Dool, H., Kumar, A., Wang, W., Long, C,. Chelliah, M., Xue, Y., Huang, B., Schemm, J., Ebisuzaki, W., Lin, R., Xie, P., Chen, M., Zhou, S., Higgins, W., Zou, C., Liu, Q., Chen, Y., Han, Y., Cucurull, L., Reynolds, R.W., Rutledge, G. & Goldberg, M. 2010. The NCEP Climate Forecast System Reanalysis. *Bulletin of the American Meteorological Society*. 91(8):1015-1058. https://doi.org/10.1175/2010BAMS3001.1

Scripps Institute of Oceanography Coastal Data Information Program (CDIP). 2020. *Introduction to CDIP*. Available: https://cdip.ucsd.edu/m/about/ [2020, June 26].

Scripps Institute of Oceanography Coastal Data Information Program (CDIP). 2021a. *Parameter File Description*. Available: https://cdip.ucsd.edu/themes/cdip?pb=1&d2=p70&u2=s:155:st:1:v:product_descriptions&u3=p_desc:pm_format [2021, August 26].

Scripps Institute of Oceanography Coastal Data Information Program (CDIP). 2021b. *Wave Component Definitions*. Available: https://cdip.ucsd.edu/themes/cdip?tz=UTC&r=999&un=1&pb=1&u2=ibc:1&d2=p6 [2021, August 26]

Scripps Institute of Oceanography Coastal Data Information Program (CDIP). 2021c. *Products: ASTORIA CANYON, OR – 179*. Available: https://cdip.ucsd.edu/m/products/?stn=179p1 [2021, May 24].

Scripps Institute of Oceanography Coastal Data Information Program (CDIP). 2022. *Wave Buoy Station*. Available: https://cdip.ucsd.edu/m/deployment/station_view/ [2022, April 04].

Seymour, R.J. 2011. Evidence for Changes to the Northeast Pacific Wave Climate. *Journal of Coastal Research*. 27(1):194-201. https://doi.org/10.2112/JCOASTRES-D-09-00149.1

Shao, W., Zhang, Z., Li, X. & Li, H. 2016. OceanWave Parameters Retrieval from Sentinel-1 SAR Imagery. *Remote Sensing*. 8(9), 707. https://doi.org/10.3390/rs8090707

Short, A.D. 1999. *Handbook of Beach and Shoreface Morphodynamics*. Chichester: John Wiley and Sons. ISBN: 978-0-471-96570-1

Short A.D. 2005. Wave Environments. *In: Encyclopedia of Coastal Science*. Schwartz M.L., Eds. Encyclopedia of Earth Science Series. Springer, Dordrecht. https://doi.org/10.1007/1-4020-3880-1_345. Online ISBN 978-1-4020-3880-8; Print ISBN 978-1-4020-1903-6

Sigal, M.J. & Chalmers, R.P. 2016. Play It Again: Teaching Statistics With Monte Carlo Simulation. *Journal of Statistics Education*. 24(3):136-156. https://doi.org/10.1080/10691898.2016.1246953

Soares, C.G., Bento, A.R., Gonçalves, M., Silva, D. & Martinho, P. 2014. Numerical evaluation of the wave energy resource along the Atlantic European coast. *Computers and Geosciences*. 71:37-49. https://doi.org/10.1016/j.cageo.2014.03.008

Sopkin, K.L., Stockdon, H.F., Doran, K.S., Plant, N.G., Morgan, K.L.M., Guy, K.K. & Smith, K.E.L. 2014. Hurricane Sandy: Observations and Analysis of Coastal Change. *US Geological Survey Open-File Report 2014–1088*. https://doi.org/10.3133/ofr20141088

Steele, K.E., Lau, J.C & Hsu, Y.L. 1985. Theory and Application of Calibration Techniques for an NDBC Directional Wave Measurements Buoy. *IEEE Journal of Oceanic Engineering.* 10(4):382-396. https://doi.org/10.1109/JOE.1985.1145116

Steele, K.E., Teng, C. & Wang, D.W.C. 1992. Wave Direction Measurements Using Pitch-Roll Buoys. *Ocean Engineering*. 19:349-375. https://doi.org/10.1016/0029-8018(92)90035-3

Steele, K.E. 1997. Ocean current kinematic effects on pitch–roll buoy observations of mean wave direction and nondirectional spectra. *Journal of Atmospheric and Oceanic Technology*. 14(2):278-291. https://doi.org/10.1175/1520-0426(1997)014<0278:OCKEOP>2.0.CO;2

Stopa, J.E., Cheung, K.F., Chen, Y.L. 2011. Assessment of wave energy resources in Hawaii. *Renewable Energy*. 36(2):554-567. https://doi.org/10.1016/j.renene.2010.07.014

Stopa, J.E. & Cheung, K.F. 2014. Intercomparison of wind and wave data from the ECMWF Reanalysis Interim and the NCEP Climate Forecast System Reanalysis. *Ocean Modelling*. 75:65-83. https://doi.org/10.1016/j.ocemod.2013.12.006

Stopa, J.E. & Mouche, A. 2016. Significant wave heights from Sentinel-1 SAR: Validation and applications. *Journal of Geophysical Research*, 122(3):1827-1848. https://doi.org/10.1002/2016JC012364

Stopa, J.E., Ardhuin, F., Babanin, A. & Zieger, S. 2016. Comparison and validation of physical wave parameterizations in spectral wave models. *Ocean Modelling*, 103:2-17. https://doi.org/10.1016/j.ocemod.2015.09.003

Storlazzi, C.D., Elias, E.P.L., Berkowitz, P. 2015. Many Atolls May be Uninhabitable Within Decades Due to Climate Change. *Scientific Reports*. 5:14546. https://doi.org/10.1038/srep14546

Stutz, M.L. & Pilkey, O.H. 2011. Open-ocean barrier islands: Global influence of climatic, oceanographic, and depositional settings. *Journal of Coastal Research*. 27(2): 207-222. https://doi.org/10.2112/09-1190.1

Suzuki, T. & Kuriyama, Y. 2014. The effects of offshore wave energy flux and longshore current velocity on medium-term shoreline change at Hasaki, Japan. *Coastal Engineering Journal*. 56(2), 1450007-1. https://doi.org/10.1142/S0578563414500077

Swail, V., Jensen, R.E., Lee, B. Turton, J., Thomas, J., Gulev, S., Yelland, M., Etala, P., Meldrum, D., Birkemeier, W., Burnett, W. & Warren, G. 2009. Wave measurements, needs and developments for the next decade. *Proceedings of the OceanObs'09: Sustained Ocean Observations and Information for Society Conference* (Vol. 2), Venice, Italy, September 21-25, 2009. http://waveworkshop.org/11thWaves/Papers/Swail_etal_Wave%20Measurements.pdf

Temmerman, S., Meire, P., Bouma, T.J., Herman, P.M.J., Ysebaert, T. & De Vriend, H.J. 2013. Ecosystem-based coastal defence in the face of global change. *Nature*. 504:79-83. https://doi.org/10.1038/nature12859

Teng, C., & Timpe, G.L. 1995. Field Evaluation of the Value-Engineered 3-meter Discus Buoy. *Proceedings: Challenges of Our Changing Global Environment, OCEANS '95 MTS/IEEE*, San Diego, California, USA. 1:316-322. https://doi:10.1109/OCEANS.1995.526789

Teng, C., Mettlach, T., Chaffin, J., Bass, R., Bond, C., Carpenter, C., Dinoso, R., Hellenschmidt, M. & Bernard, L. 2007. National Data Buoy Center 1.8-meter Discus Buoy, Directional Wave System, *Proceedings of the MTS/IEEE Oceans 2007* Conference, Vancouver, Canada https://ieeexplore.ieee.org/stamp/stamp.jsp?tp=&arnumber=4449298

Teng, C., Bouchard, R., Riley, R., Mettlach, T., Dinoso, R. & Chaffin, J. 2009. NDBC's digital directional wave module. *OCEANS 2009*, Biloxi, MS. Print ISSN: 0197-7385:1-8. https://doi.org/10.23919/OCEANS.2009.5422386

Thomas, M.H.B. 1982. The estimation of wave height from digitally processed SAR imagery. *International Journal of Remote Sensing*. 3(1):63-68. https://doi.org/10.1080/0143116820894838

Thomson, J., Fan, Y., Stammerjohn, S., Stopa, J., Rogers, W.E., Girard-Ardhuin, F., Ardhuin, F., Shen, H., Perrie, W., Shen, H., Ackley, S., Babanin, A., Liu, Q., Guest, P., Maksym, T., Wadhams, P., Fairall, C., Persson, O. & Bidlot, J. 2016. Emerging trends in the sea state of the Beaufort and Chukchi seas. *Ocean Modelling*. 105:1-12. https://doi.org/10.1016/j.ocemod.2016.02.009

Tolman, H.L. & the WAVEWATCH III® Development Group. 2014. *User Manual and System Documentation of WAVEWATCH III® version 4.18*. Technical Note 316, NOAA/NWS/NCEP/MMAB, 282 pp. + Appendices.

Thorpe, S.A. 2001. Wave Generation by Wind. *Encyclopedia of Ocean Sciences*. Steele, J.H., Eds. Academic Press. 3191-3193. https://doi.org/10.1006/rwos.2001.0069

Ulazia, A., Penalba, M., Ibarra-Berastegui, G., Ringwood, J. & Saénzde, J. 2017. Wave energy trends over the Bay of Biscay and the consequences for wave energy converters. *Energy*. 141:624-634. https://doi.org/10.1016/j.energy.2017.09.099

US Army Corps of Engineers (USACE). 2002. *U.S. Army Corps of Engineers Coastal Engineering Manual – Part II*. CECW-CE EM1110-2-1100. https://www.publications.usace.army.mil/LinkClick.aspx?fileticket=BL4oDlcbwvc%3d&tabid=16439&portalid=76&mid=43544

US Army Corps of Engineers (USACE). 2020a. *Field Research Facility, Coastal & Hydraulics Laboratory*. U.S. Army Corps of Engineers (ERDC). Available: http://www.frf.usace.army.mil/ [2020, June 26].

US Army Corps of Engineers (USACE). 2020b. *Wave Information Studies*. U.S. Army Corps of Engineers (ERDC). Available: http://wis.usace.army.mil/; http://wis.usace.army.mil/wis_documentation.html [2020, June 26].

US Army Corps of Engineers (USACE). 2022. *Coastal and Hydraulics Laboratory Data Server Website*. Engineer Research and Development Center (ERDC). https://chldata.erdc.dren.mil/.

U.S. Census Bureau. 2013. *Beach Nourishment: A Guide for Local Government Officials*. Office of Coastal Management, Digital Coast U.S. National Oceanic and Atmospheric Administration. Available: http://coast.noaa.gov/archived/beachnourishment/html/human/law/index.htm [2020, June 26].

U.S. Census Bureau. 2019a. *American Community Survey Five-Year Estimates.* Office of Coastal Management, Digital Coast U.S. National Oceanic and Atmospheric Administration. Available: https://coast.noaa.gov/digitalcoast/data/acs.html [2020, June 26].

U.S. Census Bureau. 2019b. *Total Economy (Coastal).* Office of Coastal Management, Digital Coast U.S. National Oceanic and Atmospheric Administration. Available: https://coast.noaa.gov/digitalcoast/data/coastaleconomy.html [2020, June 26].

U.S. Federal Government. 2019. *Coastal Erosion*. U.S. Climate Resilience Toolkit Available: https://toolkit.climate.gov/topics/coastal-flood-risk/coastal-erosion [2020, June 26].

University of South Florida (USF). 2005. *Waves in the Ocean*. Exploring Florida: A Social Studies Resource for Students and Teachers. Produced by the Florida Center for Instructional Technology, College of Education, University of South Florida. Available: https://fcit.usf.edu/florida/teacher/science/mod2/waves.html [2021, February 06].

Van Nieuwkoop, J.C.C., Smith, H.C.M., Smith, G.H. & Johanning, L. 2013. Wave resource assessment along the Cornish coast (UK) from a 23-year hindcast dataset validated against buoy measurements. *Renewable Energy*. 58:1-14. http://dx.doi.org/10.1016/j.renene.2013.02.033

Vinent, O.D & Moore, L.J. 2014. Barrier island bistability induced by biophysical interactions. *Nature Climate Change*. 5:158-162. https://doi.org/10.1038/NCLIMATE2474

Wang, D.W., Liu, A.K., Peng, C.Y. & Meindl, E.A. 1994. Wave-current interaction near the Gulf Stream during the surface wave dynamics experiment. *Journal of Geophysical Research*. Oceans. 99(C3):5065-5079. https://doi.org/10.1029/93JC02714

Wang, D.W., Mitchell, D.A., Teague, W.J., Jarosz, E. & Hulbert, M.S. 2005. Extreme Waves Under Hurricane Ivan. *Science*. 309(5736):896. https://doi.org/10.1126/science.1112509

The WAVEWATCH III Development Group (WW3DG). 2019. *User manual and system documentation of WAVEWATCH III R version 6.07*. Tech. Note 333, NOAA/NWS/NCEP/MMAB, College Park, MD, USA, 465 pp. +Appendices. https://raw.githubusercontent.com/wiki/NOAA-EMC/WW3/files/manual.pdf

Wu, L., Qin, J., Wu, T. & Li, X. 2018. Trends in global ocean surface wave characteristics as represented in the ERA-Interim wave reanalysis for 1979–2010. *Journal of Marine Science and Technology*. 23:2-9. https://doi.org/10.1007/s00773-017-0450-1.

x-engineer. 2021. *Control Systems: The principle of superposition.* x-engineer.org, Engineering Tutorials. Available: https://x-engineer.org/graduate-engineering/ signals-systems/control-systems/the-principle-of-superposition/ [2021, May 24].

Yang, X., Li, X., Nunziata, F. & Mouche, A. Eds. 2018. *Ocean Remote Sensing with Synthetic Aperture Radar*. Ocean Remote Sensing with Synthetic Aperture Radar, Printed Edition of the Special Issue Published in Remote Sensing. ISBN 978-3-03842-720-9 (Pbk); ISBN 978-3-03842-719-3 (PDF). https://doi.org/10.3390/books978-3-03842-719-3

Yang, J & Zhang, J. 2019. Validation of Sentinel-3A/3B Satellite Altimetry Wave Heights with Buoy and Jason-3 Data. *Sensors*. 19:1-14. https://doi.org/10.3390/s19132914

Young, I.R. & Holland, G.J. 1996. *Atlas of the Oceans: Wind and Wave Climate*. 1st ed. New York: Elsevier. ISBN-13: 978-0080425191; ISBN-10: 0080425194

Young, I.R. & Verhagen, L.A. 1996. The growth of fetch limited waves in water of finite depth. Part 1. Total energy and peak frequency. *Coastal Engineering*. 29:47-78. https://doi.org/10.1016/S0378-3839(96)00006-3

Young, I.R., Zieger, S. & Babanin, A.V. 2011. Global Trends in Wind Speed and Wave Height. *Science*. 332:451-455. https://doi.org/10.1126/science.1197219

Young, I.R. & Ribal, A. 2019. Multiplatform evaluation of global trends in wind speed and wave height. *Science.* 364:548-552. https://www.science.org/doi/epdf/10.1126/science.aav9527

Zang, K. & Leatherman, S. 2011. Barrier Island Population along the U.S. Atlantic and Gulf Coasts. *Journal of Coastal Research*. 27(2):356-363. https://doi.org/10.2112/JCOASTRES-D-10-00126.1

Zar, J.H. 1984. *Biostatistical analysis*. 2nd ed., Prentice-Hall, Englewood Cliffs, New Jersey. ISBN 0-13-077925-3

Zieger, S., Babanin, A.V., Rogers, W.E. & Young, I.R. 2015. Observation-based source terms in the third-generation wave model WAVEWATCH, *Ocean Modelling*. 96:2-25. http://dx.doi.org/10.1016/j.ocemod.2015.07.014

# Appendix

## Appendix A1. Wave Generation, Measurement and Processing Overview

This overview provides a comprehensive overview of wave theory and subsequent NDBC data collection, including wave generation and the impacts of wave environments and wave climates within the reviewed North Pacific Ocean, Gulf of Mexico and the North Atlantic Ocean. This wave theory overview provides context to the subsequent literature review.

### *A1.1 Wave Types and Generation*

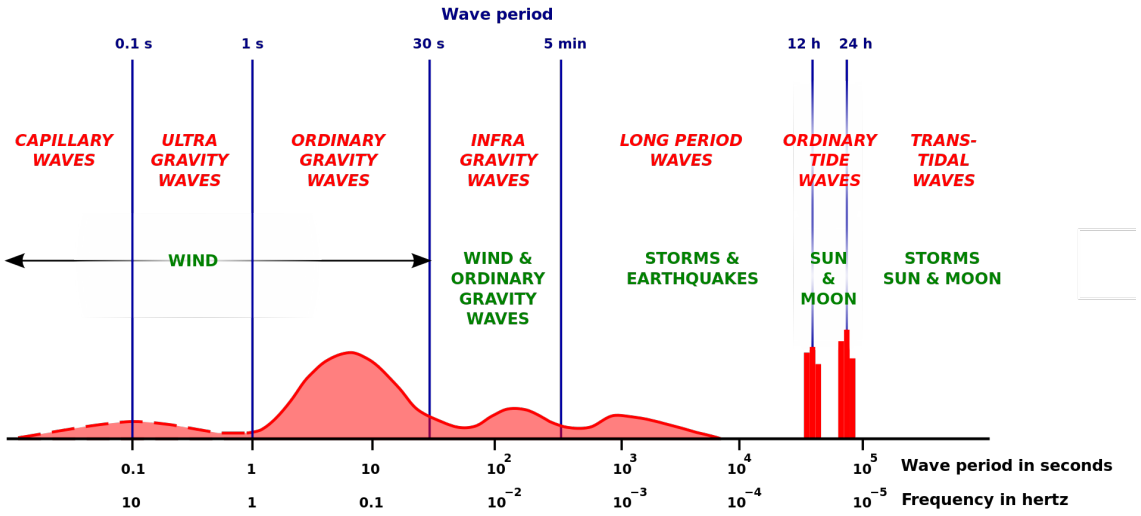


Figure A1.1. Classification of the spectrum of ocean waves according to wave period (modified by Mikhail Ryazanov from Figure 1 in Munk, 1950).

One usage of wave period/frequency and length characteristics is to allow for the identification of different wave types (Figure A1.1). As mentioned, the focus of this work are the wind seas and swell waves that range from 0.2 to 30 second periods (Figure A1.1), and comparable wavelengths of a few centimetres (cm) to hundreds of metres (m).

While Figure A1.1 showcases the classes of waves as defined by their respective wavelength or period, Figure A1.2 depicts how Figure A1.1's wave classes are formed through differences in fetch (horizontal distance that winds can blow without interruption or directional deviation) and dispersion (rate at which waves of different wavelengths travel at different phase speeds). Working from left to right in Figure A1.2, capillary waves are formed from the parallel component of wind friction (called wind stress) as small perturbations on the surface waters. As these capillary waves continue to accept energy or momentum from the atmosphere, they grow into "ripples and short, choppy waves. With increased wind velocity, duration, and fetch", "more energetic (higher), longer waves are generated" (Kaihatu and Ananthakrishnan, 2016:26), which are called wind seas (Figure A1.2). These locally-forced winds disperse from their origin in different directions and speeds as groups or wave trains. Of note, winds blowing over land-locked bodies of water, such as the U.S. Great Lakes, wave conditions are dominated by local wind-seas with limited swell.

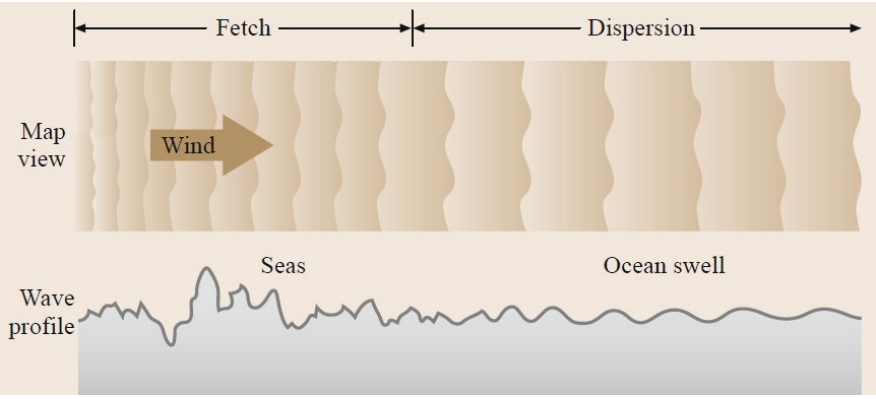


Figure A1.2. Wind forcing over the ocean surface generates capillary waves, which evolve into chop, wind waves and eventually fully developed seas (Reprinted from Kaihatu and Ananthakrishnan, 2016).

When these wind sea waves have grown to the point where they travel faster than the local wind speeds (i.e. their phase speed exceeds the wind speed), and therefore no longer accept momentum from the winds, they are termed swell waves (Figure A1.2). Well-developed ocean swell waves are therefore typically generated by winds or storms that are some distance away, and groups of swell waves usually arrive at a shore location from the same

direction (e.g. Thorpe, 2001; Hristov et al., 2003; Short, 2005; Kaihatu and Ananthakrishnan, 2016). For example, swells from storms in the Southern Ocean radiate into all major ocean basins (Babanin et al., 2019). Storms in different locations form swell waves that may meet at the shoreline from different directions, creating cross sea wave conditions.

### *A1.2 Wave Spectra and Statistics*

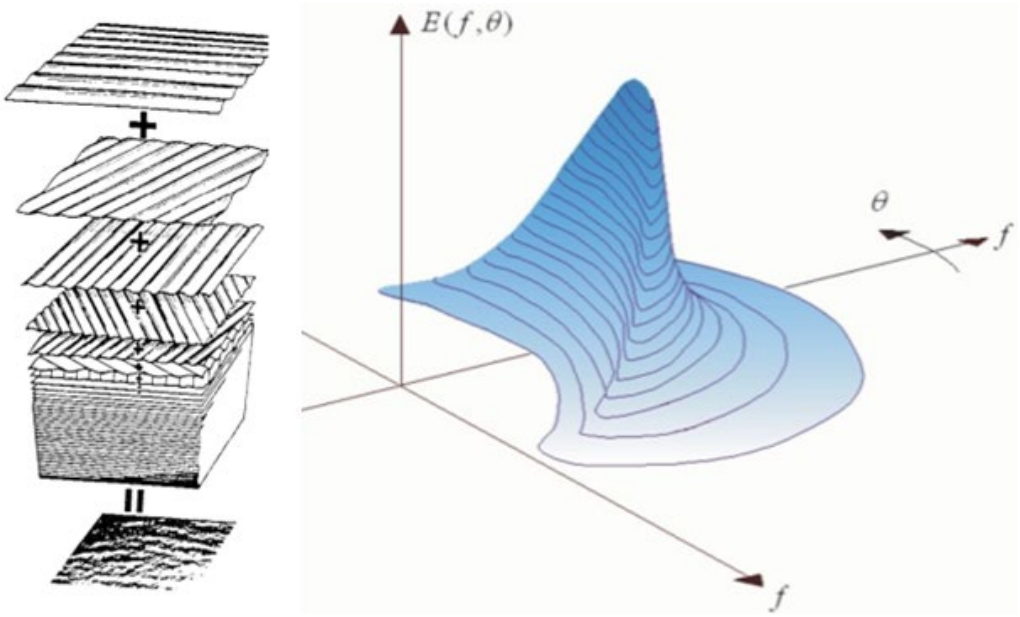


Figure A1.3. Decomposed sea surface and energy distribution across frequencies. The irregular surface of the sea can be decomposed into a number of individual wave components (left; Pierson et al., 1955). The distribution of wave energy among these frequency ($f$) and direction ($\theta$) components is the Wave Spectrum $E(f, \theta)$ (right; adapted from ECMWF, 2020).

However, "the open ocean sea surface is generally chaotic because it is a superposition of many different waves, with different wavelengths and heights" (Kaihatu and Ananthakrishnan, 2016:24). Therefore, these ocean surfaces display many different oscillatory motions at different frequencies from multiple directions, which can be decomposed into a number of individual wave components (Figure A1.3, left), each with their own unique height, period and direction. To represent the irregular and random nature of the ocean surface, individual wave trains are often reduced down to unique

forms, known as regular waves, which are considered to have a single wavelength (frequency) and height (amplitude). The assumption governing the result of an irregular free surface is based on the linear superposition principle, which states that "for all linear systems, the net response caused by two or more stimuli is the sum of the responses that would have been caused by each stimulus individually" (x-engineer, 2021).

Therefore, to measure an ocean surface that is comprised of waves with different periods (frequencies) and heights (displacement amplitudes) that travel from multiple directions, spectral analysis techniques are used to deconstruct the irregular free surface into a number of frequency ($f$) dependent sinusoidal components and propagation directions ($\theta$), hence moving from a time domain to a frequency domain (Figure A1.3, right). This methodology is based on the Longuet-Higgins et al. (1963) technique that utilises cross-spectral analysis to identify individual wave components of a random sea. Longuet-Higgins et al. (1963) estimated the wave components from a time series of displacement and the slope of the sea surface. Cooley and Tukey's (1965) addition of using fast Fourier transform (FFT) algorithms to calculate the Fourier transforms (efficiently decomposes periodic functions into sinusoidal components) of these displacement data, allowed wave researchers to speed up the computation process for a near-real time understanding of the true state of the sea.

As this dissertation focuses on in situ wave observations from moored buoys (in wave frequencies from 0.0325 – 0.4850 Hz), the overarching methodology to estimate the wave components from the displacement and slope of the sea surface is discussed here. NDBC, for instance, use symmetric discus hulls that allow for the collection of "acceleration, angular rate and magnetic flux density each along three orthogonal axes of the buoy hull" (Hall et al., 2018a:2).

Therefore, NDBC's wave measurement systems typically measure buoy acceleration, not buoy heave (NDBC, 2003). "Estimates based on buoy acceleration are converted to estimates based on wave elevation (displacement)" (NDBC, 2003:8). To do this, NDBC calculates five frequency-dependent parameters: vertical displacement, $c_{11}(f)$; two

directional functions, $\theta_1(f)$ and $\theta_2(f)$; and two spreading functions, $r_1(f)$ and $r_2(f)$ (which are defined by NDBC [2020c] as the nondimensional "first and second normalised polar coordinates of the Fourier coefficients").

Using the Fourier transform methodology (Longuet-Higgins et al., 1963; Cooley and Tukey, 1965; Earle and Bishop, 1984; Steele et al., 1985; and Steele et al., 1992), NDBC transforms the raw times series data (x and y) of acceleration, pitch, roll and yaw to into Power Spectral Density (PSD) and cross-spectral density (CSD) estimates (NDBC, 2003).

The PSD (acceleration spectra *S* for the raw times series *xy*) evaluations for the $j^{th}$ segment are given by:

$$S_{xx}(j, M\Delta f) = \frac{X^*(j,M\Delta f)\, X(j,M\Delta f)}{L\Delta t} \quad (1)$$

$$= \frac{|X(j,m\Delta f)|^2}{L\Delta t} \quad (2)$$

where L is the record or data segment length, M is the number of frequencies, Δf is the frequency interval and X is the complex conjugate of X" (NBDC, 2003:4-6).

Cross-spectral density evaluations for the $j^{th}$ segment are given by:

$$S_{xy}(j, M\Delta f) = \frac{X^*(j,M\Delta f)\, Y(j,m\Delta f)}{L\Delta t} \quad (3)$$

$$= C_{xy}(j, M\Delta f) - iQ_{xy}(j, M\Delta f) \quad (4)$$

where $C_{xy}$ is the co-spectral density (co-spectrum), $Q_{xy}$ is the quadrature spectral density (quadrature spectrum), and X and Y are frequency domain representations of the time series, x and y (NBDC, 2003:6).

Steele et al. (1985, 1992), Kuik et al. (1988) and NDBC (2003) clearly describe the myriad of statistical theories associated with nondirectional and directional wave data analysis procedures, including the statistical calculations for estimating the co- and quad spectra. For brevity, those equations will not be repeated here. Of importance is NDBC's use of the following sub and superscript conventions, as they are used in following equations:

1 = wave elevation/displacement (heave after sensor and hull-mooring response corrections)

2 = east-west wave slope (directional tilt after sensor and hull-mooring response corrections)

3 = north-south wave slope (directional tilt after sensor and hull-mooring response corrections)

m = "spectral or cross-spectral estimate based on a measured time series that is not corrected for the effects of noise, hull-mooring responses, or sensor responses" (NDBC, 2003:7-8).

This "directional Fourier series approach provides the directional Fourier coefficients, $a_n$ and $b_n$, in the following truncated Fourier series" (NDBC, 2003:8):

$$S(f,\theta) = \frac{a_0}{2} + \sum_{n=1}^{2}[a_n \cos(n\theta) + b_n \sin(n\theta)] \quad (5)$$

which can also be written as:

$$S(f,\theta) = c_{11}(f)\, D(f,\theta) \quad (6)$$

where the non-directional wave spectra are calculated as:

$$c_{11} = \pi a_0 \quad (7)$$

and the directional spreading function (Kuik et al., 1988) is given by:

$$D(f,\theta) = \frac{1}{\pi}\left(\frac{1}{2} + r_1 \cos[\theta - \theta_1] + r_2 \cos[2(\theta - \theta_2)]\right) \quad (8)$$

As mentioned, the co- and quad spectral estimates are converted into directional Fourier coefficients. There are multiple methods to calculate directional Fourier coefficients, $a_n$ and $b_n$ that are dependent on how the wave sensor measures change (heave/displacement vs acceleration etc.). The following describes directional Fourier coefficient calculations for near-vertical acceleration, pitch, roll and azimuth time series data (NDBC, 2003:9).

$$a_0 = \frac{C_{11}}{(2\pi f)^4 \pi} \quad (9)$$

$$a_1 = \frac{Q_{12}}{(2\pi f)^2 k\pi} \quad (10)$$

$$b_1 = \frac{Q_{13}}{(2\pi f)^2 k\pi} \quad (11)$$

$$a_2 = \frac{(C_{22} - C_{33})}{k^2 \pi} \quad (12)$$

$$b_2 = \frac{2C_{23}}{k^2 \pi} \quad (13)$$

The spreading functions ($r_n$) and directional functions ($\theta_n$) are estimated using the calculated Longuet-Higgins directional Fourier coefficients (Longuet-Higgins et al., 1963) as follows:

$$r_1 = \frac{1}{a_0}(a_1^2 + b_1^2)^{\frac{1}{2}} \quad (14)$$

$$r_2 = \frac{1}{a_0}(a_2^2 + b_2^2)^{\frac{1}{2}} \quad (15)$$

$$\theta_1 = \tan^{-1}(b_1, a_1) \quad (16)$$

$$2\theta_2 = \tan^{-1}(b_2, a_2) \quad (17)$$

These methodologies allow for the measurement of the distribution of the non-directional and directional energy over diverse frequencies (typically 0.02 – 0.5 Hz) in the combined wave system at that particular instance and location.

### *A1.3 NDBC Wave Parameters*

As data sourced from NDBC comprises the majority of the data under investigation within this work, NDBC wave parameter definitions are described here. NDBC classifies significant wave height ($H_{m0}$ in metres) as the "average of the highest one-third of all of the wave heights during the 20-minute sampling period", whereas dominant wave period ($T_p$ in seconds) is the "period with the maximum wave energy" (NDBC, 2020c). Average wave period ($T_m$ in seconds) is defined as the average inverse frequency of "all the waves during the 20-minute period", while mean wave direction ($\theta$ in degrees) is the direction of the dominant wave period, in degrees from true North (NDBC, 2020c).

NDBC calculated these bulk parameters from buoy wave sensor transmitted messages that contain the spectral wave density data ($c_{11}$) and four Fourier directional parameters for spectral wave direction data ($alpha_1$, $alpha_2$, $r_1$, and $r_2$) for each frequency bin (historically 0.030 – 0.400 Hz and 0.020 – 0.485 Hz). NDBC parameter definitions and methodologies are detailed within Steele et al. 1985; NDBC 2009; NDBC 2018a, 2018c, and 2020c.

NDBC (2003, as derived from Steele et al., 1985) calculates wave displacement spectral density $c_{11}$ [$m^2$/Hz] from uncorrected acceleration spectral density $c_{11}^m$ [$(m/s^2)^2$/Hz] as:

$$c_{11}(f) = \frac{c_{11}^m(f)}{R_{hH}(2\pi(f)^2)^2} \tag{18}$$

However, hull response correction ($R_{hH}$) is assumed insignificant (i.e., a perfect wave following buoy where $R_{hH} = 1$), allowing for

$$c_{11} = \frac{c_{11}^m}{(2\pi(f))^4} \tag{19}$$

For their accelerometer-based directional wave measurement systems, NDBC adapts equations (36) and (37) from Steele et al. (1985) to calculate mean and principal wave directions ($alpha_1(f)$ and $alpha_2(f)$, respectively) from the angle for each frequency band (NDBC, 2003). NDBC also accounts for known sensor effects (static over time) and hull-mooring responses (including wave depth effects) by investigating hull amplitude responses, $R_h$ (Steele et al., 1985, 2003).

From these wave displacement spectral densities, the spectral significant wave height ($H_{m0}$) is defined by NDBC (2018a) as:

$$H_{m0} = 4\sqrt{m_0} \tag{20}$$

"where $m_0$ is the variance of the wave displacement time series acquired during the wave acquisition period" (NDBC, 2018a), also defined as the zeroth moment of the frequency spectrum. "However, since wave displacement time series are not returned from NDBC's wave measurement systems, variance is calculated using the nondirectional wave spectrum according to the following relationship" (NDBC, 2018a):

$$m_0 = \sum_{f_l}^{f_u}(S(f) \times d(f)) \tag{21}$$

"where the summation of spectral density, *S(f)*, is over all frequency bands, from the lowest frequency $f_l$ to the highest frequency, $f_u$, of the nondirectional wave spectrum and *d(f)* is the bandwidth of each band" (NDBC, 2018a).

$T_p$ is calculated by NDBC (2018a) as the reciprocal of the peak frequency, $f_p$:

$$T_p = {}^{1}/_{\mathrm{f_p}} \tag{22}$$

$T_m$ is represented by NDBC (2018a) as:

$$T_m = \sqrt{{}^{\mathrm{m_0}}/_{\mathrm{m_2}}} \tag{23}$$

where the second moment, $m_2$, is calculated by NDBC (2018a) as:

$$\mathrm{m_2} = \sum_{\mathrm{f_l}}^{\mathrm{f_u}} (\mathrm{S(f)} \times \mathrm{d(f)} \times \mathrm{f^2}) \tag{24}$$

$\mathrm{Alpha_1}$ and $\mathrm{alpha_2}$, representing mean and principal wave directions, respectively (NDBC, 1996; 2020c), are calculated using the Longuet-Higgins Fourier Coefficients (Longuet-Higgins et al., 1963) as:

$$\mathrm{alpha_1} = 270.0 - \arctan(\mathrm{b_1}, \mathrm{a_1}) \tag{25}$$

$$\mathrm{alpha_2} = 270.0 - (0.5 \times \arctan(\mathrm{b_2}, \mathrm{a_2}) + \{0.\,\mathrm{or}\,180.\}) \tag{26}$$

In summary, at the time of this dissertation, NDBC publishes the five spectral parameters ($c_{11}$, $\mathrm{alpha_1}$, $\mathrm{alpha_2}$, $\mathrm{r_1}$ and $\mathrm{r_2}$), and uses $c_{11}$ and $\mathrm{alpha_1}$ to estimate and publish four bulk wave parameters ($H_{m0}$, $T_p$, $T_m$, and $\theta_m$), on an hourly basis.

### *A1.4 Wave Power*

This dissertation builds on these published spectral data to estimate and test a hypothesis that wave power (wave energy flux per metre of wave-crest length in kW/m) is increasing over time. For irregular waves, the energy transported by a wave can be calculated by its amplitude (height) and frequency (period) (Moebs et al., 2016). "The total mechanical energy of the wave is the sum of its kinetic energy and potential energy" (Moebs et al., 2016); when summed for deep water waves, as:

$$E = \frac{\rho g A^2}{2} \tag{27}$$

where $\rho$ is the density of water, $g$ is the gravitational acceleration, and $A$ is the amplitude of the wave, or half of the wave height (Komen et al., 1994, Eq. 1.52:16).

To calculate the power of a wave, the amount of energy transported by the group velocity of waves is calculated. A deep water dispersion relationship, $\omega = (gk)^{1/2}$ (Fitzpatrick, 2016, Eq. 11.23) yields a group velocity ($C_g$) equation (adapted from Ellingson, 2020, Eq. 6.1.5):

$$C_g = \frac{\Delta\omega}{\Delta k} = nC \tag{28}$$

Hence total wave power (in horsepower units) during that sampling period can be calculated with the following equation (Kinsman, 1965, pp. 154)

$$P = EC_g = \frac{\rho g^2 A^2}{4\omega} = \frac{\rho g^2 T H^2}{32\pi} \tag{29}$$

For deep water waves (water depth > ½ wavelength), Resio et al. (2003) calculates wave power from $H_{m0}$ (m) and $T_p$ (s) as:

$$P = \frac{\rho g^2}{64\pi} H_{m0}^2 T_p \tag{30}$$

where water density $\rho$ = 998 kg/m$^3$, and gravitational acceleration, $g$ = 9.81 m/s (Resio et al., 2003).

This dissertation utilises these equations to convert published spectral data at predetermined locations into bulk parameters for the calculation of wave power time series datasets. Trends in these wave power estimates are ultimately tested to determine if power is significantly increasing in the wave systems over time.